TIDAL ENERGY SITE CHARACTERISATION AT THE FALL OF WARNESS, EMEC, UK

ENERGY TECHNOLOGIES INSTITUTE REDAPT MA1001 (MD3.8)

September 2015 - Version 3.1 (Draft)

v4.0
Updated December 2016

Brian G. Sellar and Duncan R.J. Sutherland
Institute for Energy Systems
School of Engineering
University of Edinburgh
http://redapt.eng.ed.ac.uk

Acknowledgements

This work was funded by the Energy Technologies Institute (ETI).

The authors wish to thank the ETI and the project consortium members: Tidal Generation Ltd, Alstom Ocean Energy, DNV-GL Renewable Advisory, EDF, E.ON, Plymouth Marine Laboratory and the European Marine Energy Centre (EMEC). This large, expensive and complex marine-based project could not have been completed without the sustained dedication and collaborative approach of the team.

The authors wish to thank the University of Edinburgh's School of Engineering and the Engineering and Physical Sciences Research Council (EPSRC) for their financial support beyond the completion of the ReDAPT project which has allowed further analysis and re-analysis of the extensive data-sets. This work is ongoing.

Nomenclature

Symbol	Term	Units
	Coefficients	
c_i	Integral sub-range coefficient	-
c_L	Lift coefficient	-
c_p	Power conversion efficiency coefficient	-
c_v	Structure function coefficient	-
	Latin Symbols	
A	Area	m^2
c	Phase velocity or celerity	ms^{-1}
C	Speed of sound	ms^{-1}
D	Structure function	m^2s^{-2}
D_h	Hydraulic diameter	m
E_{TKE}	Turbulent kinetic energy	m^2s^{-2}
f	Frequency	Hz
F_L	Lift Force	N
f_{s-max}	Frequency associated with spectral peak	Hz
f_d	Doppler shifted frequency	Hz
f_{pulse}	Pulse carrier frequency	Hz
g	Acceleration due to gravity	ms^{-2}
h	Height above seabed	m
H	Wave height	m
H_m	Mean wave height	m
H_{m0}	Significant wave height	m
I	Turbulence intensity	%
k	Wave number	m^{-1}
K	Number of lags used to compute PSD	-
N	Number of points in FFT	-
P	Power	W
R	Autocorrelation coefficient	-
s	Wave Steepness	-
S	Power spectral density	$m^2s^{-2}Hz^{-1}$
S_ω	Spectral (variance) density	m^2s
S_f	Spectral (variance) density	m^2
$S_{f\,\theta}$	Directional spectral density	$m^2s\,deg^{-1}$
t	time	s
T_{02}	Average wave period	s
T_e	Energy period	s
T_m	Mean wave period	s
T_{Stat}	Period of stationarity	s
u_{h1} & u_{h2}	Horizontal Velocity relative to ADCP	ms^{-1}
u_{v1}	Vertical Velocity relative to ADCP	ms^{-1}
u	Instantaneous velocity in the x direction	ms^{-1}
$\overline{u}$	Mean velocity in the x direction	ms^{-1}

u'	Velocity fluctuation about the mean in the x direction	ms^{-1}
v	Instantaneous velocity in the y direction	ms^{-1}
$\overline{v}$	mean velocity in the y direction	ms^{-1}
v'	Velocity fluctuation about the mean in the y direction	ms^{-1}
w	Instantaneous velocity in the z direction	ms^{-1}
$\overline{w}$	Mean velocity in the z direction	ms^{-1}
w'	Velocity fluctuation about the mean in the z direction	ms^{-1}
x	Vector associated with axial or stream-wise measurements	-
y	Vector associated with transverse or lateral measurements	-
Y	Spectral periodogram	$\mathrm{ms}^{-1}\mathrm{Hz}^{-1}$
z	vector associated with vertical measurements and height above seabed	-
	Greek and Other Symbols	
α	Wave amplitude	m
β	Beam inclination angle	$\circ$
ϵ	Turbulent kinetic energy dissipation rate	$\mathrm{J\,kg}^{-1}\mathrm{s}^{-1}$
η	Surface elevation	m
θ	Heading angle	$\circ$
θ_{1p}	Directional angle of waves	$\circ$
λ	Wave length	m
μ	Dynamic viscosity	$\mathrm{m}^2\mathrm{s}$
ρ	Density	$\mathrm{kg\,m}^{-3}$
σ^2	Variance of velocity	$\mathrm{m}^2\mathrm{s}^{-2}$
σ_{1p}	Directional speed of waves?	$\circ$
τ_{vw}	Vertical-streamwise Reynolds stress tensor	Pa
Υ	Temporal lag	s
ϕ	Pitch angle	$\circ$
ψ	Roll angle	$\circ$
ω	Angular frequency	rad^{-1}
ℓ	Integral lengthscale	m
$\Im$	Integral timescale	s

All units are Système International (SI)

Abbreviations

Acronym	Definition
ADV	Acoustic Doppler Velocimeter
API	Application Interface
AST	Acoustic Surface Tracking
AWAC	Acoustic Wave And Current sensor
BDM	Bayesian Direct Method
BEM	Blade-Element Momentum
C-ADP	Converging-beam Acoustic Doppler Profiler
CFD	Computational Fluid Dynamics
D-ADP	Diverging-beam Acoustic Doppler Profiler
DEEP-Gen	Deepwater Economic Energy Prototype Generator
DIWASP	Directional Wave Spectra Toolbox
DNVGL	Det Norske Veritas - Germanischer Lloyd
EDF	Électricité de France
EMEC	European Marine Energy Centre
EMEM	Extended Maximum Entropy Method
ENU	East North Up
ESIP	Edinburgh Subsea Instrument Platform
ETI	Energy Technologies Institute
FFT	Fast Fourier Transform
FoW	Fall of Warness
GPS	Global Positioning System
GSM	Global System for Mobile communications
GUI	Graphical User Interface
HDD	Hard Disk Drive
HF	High Frequency
KML	Keynvor MorLift
LES	Large Eddy Simulation
MEM	Micro-ElectroMechanical
MWL	Mean Water Level
O & M	Operation and Maintenance
PTP	Precision Time Protocol
PCMCIA	Personal Computer Memory Card International Association
PG	Pressure Gauge
PSD	Power Spectral Density
PUV	Pressure/U-velocity/V-velocity
QC	Quality Control
RANS	Reynolds Averaged Navier-Stokes
RDI	RD Instruments
ReDAPT	Reliable Data Acquisition Platform for Tidal
RF	Radio Frequency
ROV	Remotely Operated Vehicle
SBD	Single Beam Dopler
SEM	Synthetic Eddy Method
SUV	Surface/U-velocity/V-velocity

TCP/IP	Transmission Control Protocol/Internet Protocol
TEC	Tidal Energy Converter
TI	Turbulence Intensity
TKE	Turbulent Kinetic Energy
TRN	Test Request Notice
UoE	University of Edinburgh
WACSIS	Wave Crest Sensor Intercomparison Study
WAFO	Wave Analysis for Fatigue and Oceanography
WLR	Water Level Recorder
WoV	Wave-Orbital Velocities

List of Figures

List of Tables

Contents

Chapter 1

Executive Summary

This twelve page summary seeks to provide a short introduction to the ReDAPT project, to set the individual work-packages in context - thus highlighting the level of inter-dependency between project partners' activities - and to provide a summary of the main findings of the University of Edinburgh's field measurement campaign and subsequent data analysis. Section 2 provides an introduction to the field of site characterisation for tidal energy sites. Section 3 reports on the analysis conducted from site measurements for the EMEC Fall of Warness test site specifically. Section 4 discusses the integration and operation of sensor systems and outlines lessons-learned and recommendations for future site surveys.

1.1 ReDAPT within the ETI Marine Programme

The Reliable Data Acquisition Platform for Tidal energy (ReDAPT) project was commissioned and co-funded by the Energy Technologies Institute (ETI) under their Marine Programme whose central objective is to accelerate the development and deployment of commercially viable marine energy technologies that will:

- Make a material contribution to the future UK energy system
- Deliver significant greenhouse gas emissions reductions
- Contribute to the delivery of long-term energy security in the UK

Specifically, their Marine Programme seeks to contribute to the delivery of marine energy cost reduction and performance improvements in line with the ETI Marine Energy Roadmap.

1.2 The ReDAPT Project

ReDAPT is led by Alstom and includes the University of Edinburgh (UoE), DNV-GL Renewable Advisory, EDF Energy, E.ON, Tidal Generation Ltd., Plymouth Marine Laboratory and the European Marine Energy Centre (EMEC). The project centres around a commercial scale (1MW) tidal turbine developed by Alstom deployed at EMECs Tidal Test Site with the aim of producing a comprehensive suite of data on turbine operation, the flow field and the interaction between the two. ReDAPT is a four year programme intended to provide information to the Tidal Industry to facilitate rapid growth. Specific goals include:

- Accelerate development of tidal energy industry
- Successful deployment and operational testing of a 1MW system at EMEC, delivering substantial learning to the acceleration of commercial product roll-out
- Data, insights and lessons learned are recognised as key reference materials and are used by the industry, e.g. Device performance
- Environmental monitoring and resource assessment
- Industry certification standards and protocols informed by ReDAPT outcomes

- Increase confidence in tidal turbine technologies
- Validation and industry acceptance of tidal flow/machine models

A complete list of released project outputs can be found in Annex I.

1.3 Modelling Work Package (MD)

Specific to the "Modelling" (MD) work package, validation of engineering tools forms a core project outcome through comparison of predicted to experienced loads *under measured environmental conditions*. This document reports upon these field measurements of tidal currents and waves; data that enables the validation of engineering tools whilst also forming the basis of an in-depth site characterisation study.

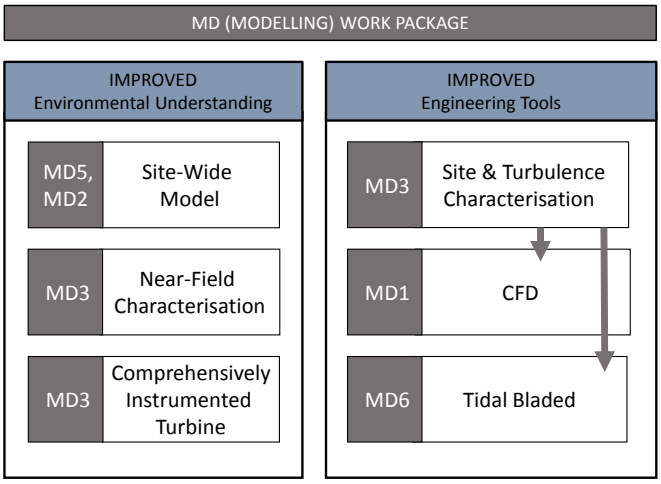

Figure 1.1: MD (Modelling) Work Package Activities with sub-package labels MD1-MD6.

Within the modelling work package, led by EDF, numerical modelling work was undertaken by E.ON, DNV-GL and the University of Manchester. MD1 involved cutting-edge numerical simulation of the Alstom 1MW tidal turbine in turbulent flows [7,8]. MD5 involved the construction and validation of a model of the wider Fall of Warness, Orkney site [9,10] and incorporated both an existing EMEC dataset and new UoE field measurements as part of MD2. These current profiles were used in the model build and model validation phase of MD5. MD6 involves the validation - through comparison to field and machine data - of the GLGH Tidal Bladed software which seeks to capture environmental and turbine characteristics in a desktop application [11–13].

1.4 Field Measurement Work Package (MD3)

This section outlines the objectives and acceptance criteria associated with the University of Edinburgh's MD3 work-package.

1.4.1 Objectives of ReDAPT Work Package MD3

The objective of the University of Edinburgh's MD3 sub-project work package is to design and conduct a data acquisition campaign to increase understanding of the flow conditions in the nearfield of a tidal stream turbine and to increase confidence in flow measurement and analysis methods.

1.4.2 Outline of Activities of MD3

Activities centre on near-field flow characterisation where near-field is defined herein as up to 10 rotor diameters range from the turbine. Three primary activities were originally identified with a fourth added during project review:

- Site mean-flow and turbulence characterisation
- Acquisition, processing and dissemination of data for the validation of the ReDAPT numerical models
- Recommendations for monitoring parameters and equipment type
- Additional: Provision of data in a format suitable for archival and access by the Industry

1.4.3 Acceptance Criteria of MD3

The contracted description of work can be found below.

1. Procure, test and calibrate the Acoustic Doppler Profiler (ADP) instrument system, including power, foundations, data logging and retrieval system. (MD3.2)
2. Design and construct appropriate flexible support structures.
3. Interim turbulence characterisation activity outlined (MD3.4)
4. Perform multiple measurement campaigns with the instruments, analysing the data and improving the the turbulence characterisation. (MD3.15)
5. Provide a final report including characterisation of the near field flow, a sensitivity analysis, assumptions and estimate of confidence. (**MD3.8**)

1.4.4 Acceptance Criteria of MD3.8

The contracted acceptance criteria for MD3.8 is listed below.

1. Report describing a method by which robust descriptions of flow parameters incident to a tidal device can be generated using multiple high-resolution current profilers.
2. These flow parameters will inform the inflow conditions to both the MD CFD modelling and MD Engineering Tools activities

1.5 MD3.8 Summary of Findings

1.5.1 Tidal Site Characterisation - Overview

Tidal sites are energetic and complex systems featuring turbulent flows, surface water waves, varying bathymetry and never-constant mean-flow conditions - to name a few aspects of their character. Tidal site characterisation in the context of this work has been driven by the immediate requirements of tidal turbine developers i.e., providing information on the flow impressing upon a commercial scale tidal turbine. The specification for this information is in turn driven by the data input requirements of the engineering tools used by device designers and operators, namely simulations using Computational Fluid Dynamics and other modelling techniques. Other site characterisation works would likely focus on alternative aspects of the flow.

Whilst the authors believe that fundamental research effort is required to (i) understand the interaction of tidal flows and wave fields and (ii) better understand what is driving the multi-faceted features of the flow, a detailed characterisation of this tidal site has been achieved. Furthermore, this characterisation has enabled better validation of cutting edge simulations and allows for comparison of the *modelled* machine loads - under representative input conditions - to the loads *measured* during turbine operation.

Due to the volume of data collected, the resource required to sustain the duration of data campaigns and moreover the multiple variants of data sets returned by both established and prototype instruments operating across a wide variety of configurations much further analysis could be carried out. Analysis will continue beyond this final report at the University of Edinburgh working with existing and new partners. Areas of further work is outlined at the end of this summary.

1.5.2 Instrumentation

Instrumentation technology and availability developed during the course of the project. Equipment is now available, offering definitive advantages for tidal site characterisation, that was not available at project commencement and the procurement stage. In the latter stages of ReDAPT some of these advances were trialled and will be reported upon in subsequent publications. However, ReDAPT did have access to an exceptional set of tools including: tried and tested four beam Diverging Acoustic Doppler Profilers (D-ADPs) (or *ADCPs* as they are commonly referred to); three beam plus vertical D-ADPs of the *AWAC* variant and over twelve prototype single beam ADPs (SB-ADP) herein referred to as Single Beam Doppler devices (SBDs). These latter instruments offered the required flexibility and redundancy going into a multi-year turbine-interfaced measurement campaign.

Single Beam Acoustic Doppler Profiling (SB-ADP)

The Nortek AD2CP platform upon which their supplied Mark I prototype 1MHz SBDs operate is a useful tool when integrating ADP instrumentation with a commercial scale tidal turbine. Robust remote access to the instruments over TCP/IP communications (internet) is easily achieved and is accurate timing control through the use of an external broadcast Precision Time Protocol (PTP) clock. The inclusion at the request of the UoE of an Application Program Interface (API) exposes the instruments to control via MATLAB which allows for a high level of end-user control when required.

Acoustically, useful instrument range was found at this site to be limited to approximately 17m. This was increased to approximately 20m through upgraded power supplies and grounding methods. This profiling range was found to be suitable for inflow velocity assessment during periods of turbine non-generation. Whilst generating, particularly at rated power (which this turbine quickly ramps up to) the range is not sufficient to penetrate the region of upstream-affected flow.

The instruments sampling rate of 4Hz (recently increased to 16Hz) allows more of the frequency range of velocity spectra to be assessed compared to similar equipment at the time of use. Their small size simplified instrument integration with the turbine and instrumentation package frames.

The presence of a velocity bias (underestimation as compared to sea-bed mounted D-ADPs) of the order of 5% continues to be investigated.

Instrument reliability and feature set increased over the course of the project due to supplier provided firmware and software updates. Instruments were robust enough to survive prolonged (up to 3 months) deployments.

Diverging Beam Acoustic Doppler Profiling (D-ADP)

Two Teledyne RDI Workhorse Sentinel 600kHz were used during fifteen deployment campaigns. Data capture success was 93% with a single deployment failing due to a data writing error. The instruments performed well and captured seabed to surface profiles of velocity in 1m bins at various configured sample rates from 0.5Hz, 1Hz and 2Hz. By deploying at either side of the turbine in a pair a long-term reliable reference velocity was provided, enabling all subsequent analysis of turbine-mounted measurements and the generation of turbine power curves.

Being based on legacy computational platforms memory limitations of 4GB caused operational and logistics issues. Whilst planned, the retrofitting of enhanced data storage was not achieved although it would be a sensible and cost-effective step to continue their operation where longer deployments or higher sample rates lead to increased memory requirements. These instruments survived prolonged (3 months) deployments with no maintenance issues.

A next generation RDI device, The Sentinel 5 five beam D-ADP was not available at the time of project procurement.

A newly released D-ADP instrument, the 500kHz Nortek Signature 500 which features 5 beams and is based on their AD2CP platform was trialled as an ancillary instrument in one of the last ReDAPT deployments. The data will be analysed following completion of ReDAPT deliverables.

Converging Beam Acoustic Doppler Profiling (C-ADP)

Large scale converging ADPs with significantly smaller measurement volume than diverging beam instruments could offer new ways to measure flow and turbulence. A prototype system was trialled during core ReDAPT testing when the opportunity arose. Comparison of C-ADP to standard divergent D-ADP velocity measurements revealed sub-cm/s differences in velocity and order-of-magnitude reduction in realisable length-scale. C-ADP focal point measurements compared to a proximal single-beam reference showed excellent correlation and a 47% reduction in Doppler noise.

The dual functionality of the C-ADP as a profiling instrument with a high resolution focal point make this configuration a valuable advancement in underwater velocimetry enabling improved quantification of flow turbulence. Since waves are simultaneously measured - via profiled velocities, pressure measurements and surface detection - it is expected that derivatives of this system will be a powerful tool in wave-current interaction studies [4].

1.5.3 Deployment and Retrieval

Multiple deployment and recovery methods were used. Recommendations depend upon the range of deployment location from the turbine and other expensive seabed assets including cables or potential mooring configurations for any future operations.

Distant from turbine (>250m)

Deployments and recoveries of the type routinely employed by EMEC (and others) worked well. They involved local vessels with excellent site knowledge and reasonable day rates. Frames of approximately 600kg mass fabricated from stainless steel worked well. No ROV was required in their deployment or recovery as small buoys attached to side-attached clump weights with trailing ground lines could be used. Where buoys cannot be used acoustic release technologies can be used to bring markers and lifting attachments to the surface upon triggering. These were not required in this project.

Close to turbine (<250m)

Where more accurate positioning of the seabed frames was required (either due to test specification or risk to other assets) Remotely Operated Underwater Vehicles (ROV) proved useful whilst adding significant cost to the operations. Through the use of an ROV two seabed instrument packages, for example, were deployed approximately 45m from the turbine to within $\pm$ 5m.

In several deployments a line-attached hydraulically released shackle was successfully used to deploy the seabed frames leaving recovery-only to an ROV equipped vessel (the ROV can be piloted to attach a lifting shackle onto the frames single point lifting eye).

Visual inspection proved essential whether deployments were assisted by ROV (which have integrated cameras) or otherwise. Suitable cameras can be fabricated or rented (which in this case represented better value for money) and allow the frames to be repositioned following settling on uneven bathymetry.

Coordination of instrument deployment and retrieval with the turbine related activities in a dynamic marine environment was challenging and required flexible budgeting, working hours and co-operation between multiple project partners and suppliers.

Custom deployment frames were successfully designed to minimise frame movement on the seabed, provide adequate space for extended battery and communications housings and to allow the installation of experimental damped instrument gimbals to minimise pitch and roll of the instruments whilst allowing an initial settling to near-vertical upon deployment.

1.5.4 Instrumentation Platforms

Two major instrumentation platforms were designed and deployed. Through negotiation with the turbine developers two areas on the machine were assigned for use by UoE: an area at the top and rear of the nacelle and the back face of the turbine thruster unit to within approximately 0.5m of the outer edge. The two frames, Edinburgh Subsea Instrumentation Platform -1 (ESIP-1) and ESIP-2 (top and rear respectively) involved considerable design and fabrication work.

These glass-flake epoxy coated steel frames survived prolonged deployments in the marine environment, performed well, were amenable to adaptation and were relatively simple to detach and re-attach from the turbine. This importantly allowed maintenance work to be predominantly carried out on the ground at site.

1.5.5 Data Management

Data management was organised firstly internally between project partners (to allow data share between UoE and the MD and MC sub-packages) and then a plan for use by the wider community beyond ReDAPT developed. With hindsight it would have been more efficient to have incorporated Data Management into a central plan from the project start.

Instrumentation was controlled in real-time remotely by the University of Edinburgh and the data saved to the local servers on the EMEC, Eday substation. This was routinely downloaded over the limited bandwidth from this location and backed up to UoE Engineering dept. servers. Proprietary data was converted to a format that could be read by Matlab from within which all processing was carried out. In most cases this data had to be converted manually, albeit in batches.

Transferring, converting, pre-processing and sharing large volumes of varied data within a moving IT environment (operating systems becoming redundant, computers and HDDs failing) consumed a large amount of project time.

1.5.6 Data Archival

Environmental data has been uploaded to the UK Energy Research Centre's Energy Data Centre (UKERC-EDC) where it will be permanently archived. It has been converted to netcdf format and will be available for download from the beginning of October 2015. For further information please see the introductory material to the data and its formatting in [14] which is available to download at `http://redapt.eng.ed.ac.uk`.

The data comprises:

- Seabed mounted D-ADP (*ADCP*)

- Turbine mounted SB-ADP *(SBD)* data in multiple orientations where the instrumentation was in a stable configuration.
- Turbine mounted D-ADP *(AWAC)* data where instrumentation configuration is stable.
- Turbine mounted SB-ADP Long Range (CONT - Nortek Continental)

1.5.7 Site Characterisation within EMEC's Fall of Warness Tidal Test Site

A comprehensive site characterisation for the turbine deployment site within the Fall of Warness has been carried out across several years and all seasons. Mean flows and turbulence has been shown to vary significantly between Flood and Ebb tides. Of particular note are the differing velocity depth profile forms: being traditionally logarithmic on flood and featuring a parabolic shape during parts of the ebb cycle. The latter, due to its complex form, has consequences for the ongoing development of numerical modelling techniques and will be investigated further. Turbulence Intensity and Streamwise Lengthscales also vary significantly between tidal cycles and show intra-cycle dependency on flow acceleration. Importantly, the presence of waves is shown to clearly impact on all of these metrics.

An extensive range of metrics was specified at group level, targeted and largely delivered.

Metrics identified and secured:

- Mean Velocities - at mid-depth
- Mean Velocities - full depth profile
- Turbulence Intensity - at mid-depth
- Turbulence Intensity - full depth profile
- Lengthscale - at mid-depth
- Reynolds Stress - full depth profile
- TKE - at mid-depth
- Dissipation Rate - at mid-depth

Metrics identified and not secured at time of report:

- Secondary Lengthscales (variation with lengthscale in alternate axes)

Turbulence Intensity

Streamwise Turbulence Intensity in the **flood tide** and without the presence of any significant wave action was found to be 9.1% ± 1.9%. Applying noise correction techniques brings this value to 8.6% ± 2.0%.

Streamwise Turbulence Intensity in the **ebb tide** and without the presence of any significant wave action was found to be 7.3% ± 1.6%. Applying noise correction techniques brings this value to 6.7% ± 1.7%. Summaries are presented in Table 3.11.

Lengthscales

Streamwise Lengthscale in the **flood tide** and without the presence of any significant wave action was found to be $15.5m \pm 6.9m$ and displaying a log-normal distribution. Under the large wave conditions (featuring H_{m0} >1.6m) measured in storms of 2014 these values are shown to diminish to $12.6m \pm 6.9m$.

Streamwise Lengthscale in the **ebb tide** and without the presence of any significant wave action was found to be $8.6m \pm 4.4m$ and displaying a log-normal distribution. Under the large wave conditions (featuring H_{m0} >1.6m) measured in storms of 2014 these values are shown to diminish to $7.3m \pm 3.6m$.

For both flood and ebb data sets further analysis is required on wave-current interaction and its impact on reported metrics. This analysis is ongoing at UoE. Summaries are presented in Table 3.9 and 3.10.

Flow Direction

Flow direction when reported from uncorrected ADCP instrument headings shows large variation between deployments. A major proportion of heading error (which leads to flow direction misrepresentations) can be attributed to non-ideal on-board compass calibrations being carried out. However, post-processing of the ADCP data via an alignment technique with fixed instrumentation installed on the turbine (with known and changeable orientation in yaw) reveals that there remains differences in direction between deployments. New design of tests are required to probe these differences further. Data also indicates there is significant flow direction change at instrument separations of approximately 50-100m in the cross-channel direction.

Corrected headings for the **flood tide** are found to be $137° \pm 4°$.

Corrected headings for the **ebb tide** are found to be $318° \pm 5°$.

Flow directions above are reported as a mean above a threshold velocity magnitude. Flow direction, however, changes between the accelerating and decelerating phase of each tidal cycle. This spread in direction is wider for the flood tide (up to 30 °).

Flow Profile

Flow profiles for flood tides follow generally logarithmic form. The presence of waves was found to significantly affect these forms.

Flow profiles for ebb tides often feature parabolic form, whereby velocity decreases towards the surface from approximately mid-depth. Again, the presence of waves was found to significantly affect these forms. The prevalence of these complex depth profiles of velocity at other sites (and moreover the causes) should be further investigated.

Flow Twist

Flow "twist" was identified early in the project from visual plots of flow direction with depth and is particularly evident during periods of high acceleration and low flow speed in the tidal cycle. However, at speeds greater than 1ms^{-1} it was found not to exceed 5 degrees across the tides. As a parameter it should be assessed at other sites.

Waves

Waves were measured in a partially ad-hoc fashion throughout with mean flow and turbulence characterisation in the absence of waves the project focus. Large sets of initial flow data were acquired (intentionally) in the Orkney summer months during low wave activity and at a time when turbine and instrument platform commissioning were the highest priority. Towards the project close as sufficient data was collected to complete core tasks and as larger sea states increased in frequency instrument configurations were adapted to capture various wave parameters. Indeed, following completion of the ReDAPT data acquisition campaign, the UoE continued to support the remote operation of instruments and monitoring of the site.

Waves have been shown to significantly impact turbulence metrics including lengthscales, turbulence intensities and Reynolds stresses.

The interaction of waves with the flow is complex. Whilst typical and expected effects can be seen (longer wavelength, lower amplitude waves are measured during waves aligned with current for example) the extent of these modifications varies and can be severe. Impact is highly dependent on the combination of wave direction, wave period, tide type and flow velocity and direction. Uncertainties in these parameters make de-coupling of the two systems difficult. This is an area of ongoing investigation.

1.5.8 Recommendations and Guidance

The following brief summaries are primarily "lessons learned", gained from successes, failures and in-between experiences over the last four years.

Flow Measurement Instrumentation on Turbines

Integrating data collection with installed machinery is recommended. Advantages include real-time access to data (for site characterisation as well as turbine operational control), unlimited power supply and the ability to re-configure devices. Turbine's also provide mid-depth access to instruments with limited range or operating principles that mean they cannot achieve the same fidelity from the seabed.

A rationalised instrument set would include:

- ADP installed on horizontal axis TEC, forward facing.
- D-ADP installed on top of TEC to allow assessment of ambient flow including headings and waves
- Pressure gauges could play a useful role in the measurement of large wave conditions.[1]

Auxiliary Flow Measurement Instrumentation Platforms

Where possible auxiliary flow measurement stations / pods / platforms should be integrated into TEC projects and hard-wired to provide long term, reliable, real-time and consistent measurements. This type of setup would be particularly useful for power curve validation where both TEC and instruments need to function correctly and contemporaneously.

Aside from "hard-wired" considerations a rationalised seabed instrument set would include (*briefly summarised*):

- Essential: Upstream D-ADP positioned sufficiently far from the rotor plane to provide ambient inflow conditions. Recommendations exist in IEC TS 62600-201. This guidance is currently being used in an assessment of power-curve production and will be disseminated soon.
- Ideal: Multiple "time-synched" D-ADPs positioned on the mean particular tidal direction to allow wake investigation and potentially spatial correlation analysis

Upgraded Equipment

Enhanced seabed mounted instrumentation should be used (either customised in-house or by upgrading to latest generation systems) to remove trade-offs between instrument configuration (sample rate, data storage) and deployment duration.

[1] If only large, long wavelength waves are a concern a calibrated and properly post-processed pressure gauge system may suffice for wave measurement. This could be particularly useful if volume TEC arrays were implemented where multiple ADP units could prove too expensive and where wave directionality was important (due to the advantages of physical array-based measurements for wave directionalityy studies)

Sources of Equipment Failure

The dominant source of instrument failure was through corrosion of cable connectors, particularly on the power pins. This problem was less severe on larger series connectors (those >MCIL 8-way as are typically used). Upgraded grounding methods (by grounding instruments locally to seawater) appeared to reduce the problem although tests were not conducted in a controlled manner and a root cause was not identified.

Having instrument arrays connected effectively "in series" should be avoided where possible.

Remote, dedicated and turbine-operator independent power cycling is essential when operating equipment across networks. This is simple and inexpensive to implement.

Where prior testing cannot be undertaken remotely selectable paths to ground and/or remotely selectable power provision modes should be employed to assess instrument performance in the presence of varying levels of electrical noise.

Mechanical failures were all associated with galvanic corrosion across dissimilar materials. Mixed fastener systems (mixing the use, during assembly or maintenance, of A2 grade and A4 grade stainless steel machine screws and washers for example) failed on several occasions. Due to designed redundancy in fixings, impact was minimal.

Incorrectly wired electrical systems (leaving behind a stray single strand of a shield wire for example) caused two cases of connector failure - the connectors dissolved - and allowed water ingress into associated equipment.

Staged Data Processing

A staged and progressive data retrieval, conversion and analysis process is recommended. Whilst not always possible due to measurement campaigns being tied to the larger TEC project this would help the build up of large, complex data sets and allow early feedback to subsequent test campaigns. Also, where appropriate data should be shared as early as possible to allow input from interested parties whilst changes to methodology etc. can be implemented.

Data Handling: Begin With Headroom

Sufficient computational resources should be estimated *(and then increased)* and made available at project outset in terms of computational power and storage space to avoid backlogs, delays and forced relocations mid-way. Multi-core machines, solid-state disks and parallel computing significantly speeded up processing (and re-processing when operator mistakes were found) during this analysis.

Bench Testing Hardware and Software

Using prototype equipment (or standard equipment in new ways) without sufficient bench testing can lead to test failure. With real-time, hard-wired systems tests can be re-run but when co-ordinating tests with other project deliverables valuable opportunities and data events can be lost. For stand-alone systems it may be impossible to re-run the test.

Even once complete, in-house bench testing may not be able to simulate the complex system architecture of the fully deployed system e.g., different IP addresses, firewalls, operating systems etc. Additional commissioning time should be allowed as system complexity increases.

Ongoing Work and Opportunities for Immediate Collaboration

Following the authors' experiences on the ReDAPT project, currently ongoing efforts - in addition to improving provision of the metrics already presented - are focused on the following areas:

- Wave measurement techniques at tidal energy sites
- Enhanced deployment and retrieval methodologies for seabed deployed equipment and peripheral enhancements and modifications
- Wave-current interaction
- Lengthscale analysis, particularly sensitivity of lengthscale distributions to site conditions
- Advanced C-ADP

Closing Comments and Dissemination Plan

Due to the complexity and large volume of data collected - and the even larger number of research avenues that it opens - this report cannot fully address all the elements that are introduced (and of courses doesn't address those areas that were left out). It is hoped that it serves as an overview to the field of tidal site characterisation specifically for those likely to go on to delve deeper in order to eventually understand the loads that this environment will impart on tidal energy converters.

Environmental data has been archived and is available. The data is available as a "frozen" repository and a "living" in-use and updated set. These can be accessed from:

1. Permanent archive of data from snapshot at project end:
   http://data.ukedc.rl.ac.uk/simplebrowse/edc/renewables/marine/
2. Up-to-date data and in-use by researchers:
   http://redapt.eng.ed.ac.uk

As of 2016 analysis and dissemination is ongoing and collaborations between academia and industry are currently active.

Chapter 2

Tidal Site Characterisation

2.1 Introduction and Overview

Flow characterisation of a tidal energy site centres on gaining information on water velocity over a range of spatial and temporal scales suitably chosen to capture the key underlying fluid motions. These potentially include information varying across annual and seasonal time scales to fluctuations in velocity at timescales of seconds and below - with different scales of motion understood to have different effects on energy extraction devices [15]. Likewise, knowledge of spatial variation of flow parameters is required across a wide range, from orders of tens of blade diameters (for wake studies and array interaction for example) to variations of metres and below for investigations into blade fatigue. Ideally, 3D velocity information would be captured with high spatial densities of sub-metre resolution across the entire fluid domain of the turbine, at sample rates capable of measuring high frequency velocity fluctuations and for durations long enough to capture the characteristics of tidal cycles throughout the year. No instrument yet exists to provide these measurements. Identifying key velocity measurements and metrics that are obtainable, reliable and representative becomes the goal of any flow characterisation.

2.2 Background and Advantages of Tidal Energy

2.2.1 Tidal Industry Background

Amongst the first grid connected tidal turbines was the 300kW HS300 prototype built by Hammerfest (now Andritz Hydro) and was first installed in 2003 in Kvalsund in Finnmark, Norway. It has since been superseded by the HS1000 1MW commercial scale device, which had produced over 1.5GWh of electricity by the end of 2014 [16]. It is a single three-bladed rotor axial flow device based on a tripod support structure. Another early commercial ($\geq$ 1MW) scale grid connected tidal turbine was Seagen which was installed in Strangford Narrows (Northern Ireland) in June 2008. This 1.2 MW device employs two two-bladed rotors either-side of a surface piercing central pile. It had by the end of 2014 achieved over 8GWh of production [17]. Since then other tested or currently operational 1MW or greater rated-power devices include the Alstom DEEPGEN IV, the Open Hydro 'Open-Centre', the Atlantis 'AR1000' and the Voith turbines.

At the time of writing, consent had been granted to begin development of the first tidal array projects. These were: MeyGen in the Pentland Firth, Scottish Power Renewables' Sound of Islay project and France's Agency for Environment and Energy Management project in Raz Blanchard, Normandy, France. It is hoped that these projects will significantly drive forward the sector and reveal information regarding device-flow interactions that will help improve longer term economic viability.

2.3 Challenges to the Tidal Energy Sector

As an emerging industry the tidal energy sector has significant challenges to overcome before it can become cost competitive with established modes of electrical energy generation. These challenges include but are not limited to:

- Understanding the effects of multiple scales of turbulence
- Understanding the drivers of turbulent characteristics (such as surface roughness etc.)
- Optimisation of TKE designs to minimise fatigue loadings and maximise power extraction
- Effect of combined waves and currents
- Effect of array layouts (and device design appropriate for these arrays) to maximise power extraction
- Access to measurement technology to enable site characterisation of the flow for both long term (period of years) variation in resource and very short term (period of less than seconds) turbulence
- Bio-fouling
- Immature supply chain
- Minimising Operation and Maintenance (O & M) costs

2.3.1 Gaps in knowledge

The loading on devices at tidal stream sites are a complex combination of: mean flow, turbulence and directionally-dependent wave orbital effects. In operational tidal arrays, spatially and temporally varying wake-induced velocity variations will also be present. These fluctuations in flow velocity magnitude, direction and duration effect device loadings. One of the key differences between wind turbines and tidal turbines is that for atmospheric wind flow, the most energetic turbulent structures are not restricted by an upper boundary layer and thus the highest energy containing structures can be very large, tending towards 280 m as separation from the boundary increases [18]. In a tidal channel the turbulent structures are limited by the channel depth. However, the limited size of the eddies is offset by the increased fluid density, which increases the energy within the eddies. In addition, since turbine blade diameters are often close in scale to half the channel depth, the effect of turbulent structures of similar dimensions to the device on the loadings are an important factor and one that is not well understood. Finally, there is additional uncertainty over the effect of the smallest (dissipation) scales of the turbulence which are predicted to increase skin-friction drag and affect flow transition on blades [15, 19].

Significant engineering challenges and areas of ongoing research include:

- Characterising the resource across multiple spatial and temporal scales
- Determining maximum and fatigue-inducing design loads
- Understanding device-device interactions within tidal device arrays

Although the main drivers of the flow which make them a predictable resource are understood at site scale there remains uncertainty about local flow velocities and flow turbulence. The flow at site-scale is driven by local bathymetric features and coastline which can cause significant variation in flow over small (<100 m) scales [20].

Tidal Flow-Specific Considerations

Although much work has been done on the theory and measurement of turbulence particularly in the area of atmospheric flows there has been less focus specific to turbulence in tidal flows. Tidal channel regimes have several key differences compared with atmospheric regimes:

- Increased number of boundary layers. Much of the flow field of interest may be exposed to boundary layer effects e.g., seabed, sea surface, coastline.

- Turbulence and flow statistics may be sensitive to parameters other than the mean flow speed e.g., tide direction and bathymetry.
- Characterisation of the flow-field will require the consideration of the effects of a local wave-field.
- Securing good data on which to build models is more challenging.

2.4 Tidal Energy Site Characterisation

2.4.1 The Physics of Tidal Flow

The Moon and the Sun

Tides are the result of the bodies which exert the strongest gravitational forces on the Earth; the Moon and the Sun, pulling the earth and thus the fluids on the surface towards them. The earth rotates relative to the moon once every 12.42 hours [21]. The time varying forces applied to the seas result in tides composed of multiple harmonic constituents each with a magnitude and phase which vary spatially across the globe. As the Moon contributes the largest component of these forces on the earth this causes the largest of these constituents, the M2.

The effect of these constituents is site-specific based on the longitude of the site and the effect of the land bounding it. In order to resolve tidal constituents data must be collected over a period roughly equal to that of the constituent. Thus the longer the deployment the greater the number of constituents that can be resolved and the more accurate the long term predictions that are based on these harmonic analyses are. For further information on harmonic analysis conducted within ReDAPT refer to [11].

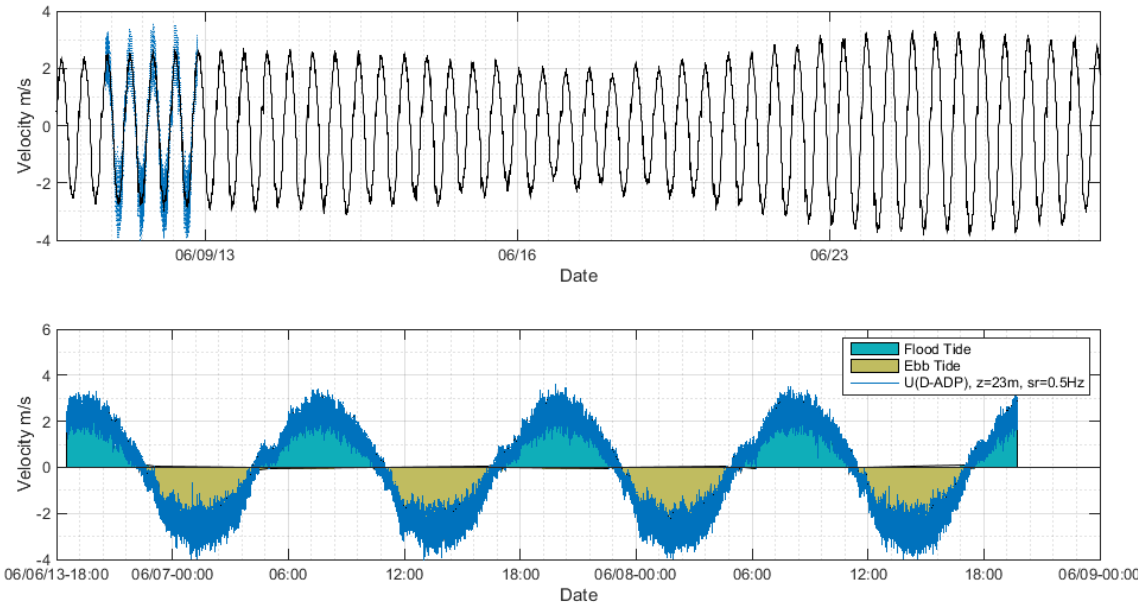

Figure 2.1: Tidal cycles (June 2013) from the Fall of Warness, Orkney showing defined Flood and Ebb tidal velocities. Streamwise flow velocity sampled at 0.5Hz (bottom) and averaged to 5 minutes (top).

Types of Tidal Site

Tidal sites applicable for energy extraction are generally defined as anywhere where flow velocities are sufficiently fast ($> 1\text{ms}^{-1}$) for extended periods of time. In order for these velocities to occur the tides must be constrained by landmasses which cause the flow to accelerate. There are several conditions that can facilitate these speeds and the first stage in site characterisation is to qualitatively define the types of site. There are 3 basic types of site: tidal basins, symmetrical (also referred to as rectilinear) bi-directional channels and asymmetrical bi-directional channels.

A tidal basin occurs where the tide flows into and out of a reservoir through a single narrow channel. Examples of this include Strangford Loch where Seagen is deployed and Digby Gut (along with other basins off the Bay of Fundy) in Nova Scotia. These sites are ideal as the narrow channels restrict the variability of flow angle thus they have very symmetrical flow directions for both tides.

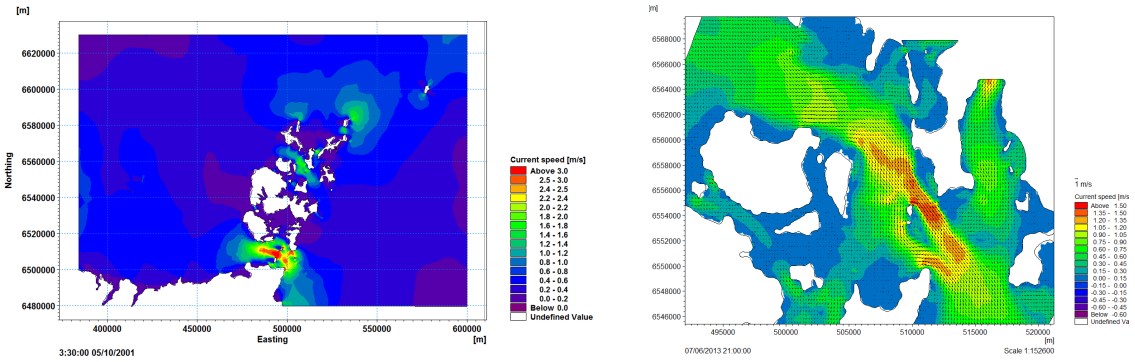

(a) Pentland Firth and Orkney waters

(b) Fall of Warness, Orkney

Figure 2.2: Typical Tidal Flow velocity plots for the Pentland Firth and Fall of Warness produced by UoE using MIKE 21 Flow model. [1, 2].

Examples of rectilinear flow include Admiralty Inlet in Puget Sound and the Fall of Warness Site in Orkney (see Figure 2.2) on which the core of this work reports. Rectilinear sites are desirable as turbines can be designed to be mounted in a fixed position, pitching the blades to capture the tides from both directions.

Sites with strong asymmetry in flood and ebb flow directions impact on the design of any installed TEC e.g., necessitating a turbine yawing capability. Additionally, the equality of the magnitudes of the Ebb and Flood flow speeds at a site impact design aspects. Sites such as Ramsey Sound and Stockholm Island off the coast of Wales exhibit flows of varying strength across flood and ebb [20, 22] where installed machines could require a power take off system that is efficient at a wide varying of flow speeds or where reduced power capture has been factored into the design optimisation.

Generating power

The complete systems through which tidal energy extraction devices convert the kinetic energy of a fluid to grid-specification electrical energy are complex and vary widely. It is important to underline the most basic principles which flow characteristics will affect. In the majority of devices a hydrofoil is employed, a surface which is designed to maximise the pressure difference across it, creating a force. The component of this force normal to the chord of the lifting surface is termed lift and the along-chord component termed drag. A basic example of this principle is illustrated in Figure 2.3. The equation for lift is:

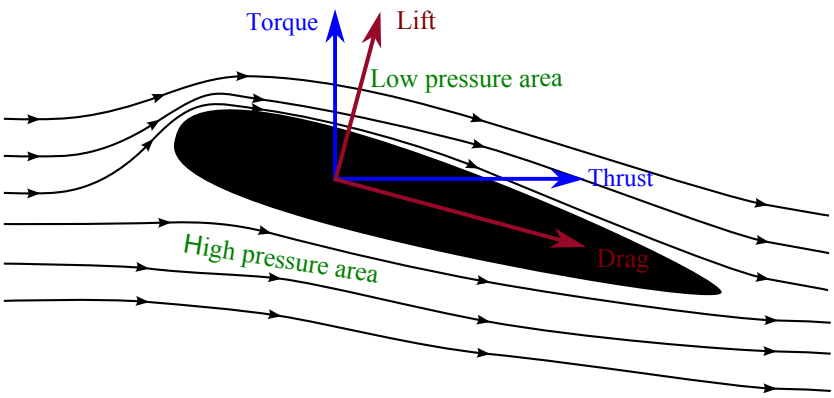

Figure 2.3: Basic principles of lift and drag

$$F_L = \frac{1}{2}\rho A c_L u^2 \tag{2.1}$$

where F_L is the lift force, ρ is the fluid density, A the platform surface area of the lift surface and c_L is the lift coefficient [23]. For wind and tidal turbines the resultant force of the lift and drag forces in the direction of rotation is termed torque and the force along the flow direction thrust. In the case of a turbine, the torque is used to power a generator (often via a gearbox). The lift and drag coefficients vary with angle of attack which is the resultant flow angle relative to the lifting surface. Thus the lift and drag forces are sensitive to both the magnitude and direction of the onset flow. The response of lifting surfaces to velocity fluctuations is complex and responds to fluctuations of different sizes and magnitudes in varying ways [19, 24]. Hence the need to characterise the turbulent flow at tidal sites.

The force required to overcome the initial inertia of the device is related to a minimum flow speed, known as a cut-in velocity. In order to optimise the generator design a rated power is selected which is related to a maximum rotational speed of the generator for the common flow speeds at the site. A rated velocity is the minimum flow velocity needed to achieve this. As with most wind turbine designs, techniques such as adjusting the blade angle are then employed to keep machine parameters within acceptable ranges (e.g., to maintain constant rotational speed at high flow velocities). The relationship of power extracted to inflow velocity under a specific turbine control strategy is referred to as a "Power curve". The optimum power curve is site specific, hence the need for accurate long term resource predictions to enable designers to tailor a device for a specific site.

The theoretical extractable power (P) from the flow is defined as:

$$P = \frac{1}{2}\rho A c_p u^3 \tag{2.2}$$

Where ρ is the fluid density, A the swept area of the device and c_p is the efficiency coefficient for the specific device. In *wind* power systems this has an upper limit, the Betz limit, of 0.593 [18]. In tidal power systems, due to channel constraints and the potential for high blockage ratios, this limit does not apply [25–27].

Turbulent Flow

Turbulent flows can be described, [3], as one which varies significantly and irregularly in both position and time". Generally this is found in flows whose Reynolds number is above 4000 [28]. The equation

of the Reynolds number, which is a ratio of the inertial to the viscous forces in a flow, is given as:

$$Re = \frac{\rho \overline{u} D_h}{\mu} \tag{2.3}$$

Where μ is the dynamic viscosity of the fluid and D_h is the hydraulic diameter which, for an open top rectangular cross section channel, is given as:

$$D_h = \frac{area}{perimeter} = \frac{2yz}{2z + y} \tag{2.4}$$

Here y is the channel width and z the depth [28]. A representative cut in speed for a commercial turbine of 1 ms^{-1}, a hydraulic diameter of 91m (representative of a rectangular cross-section tidal channel 1km wide and 50m deep) the Reynolds number would be 91×10^6.

The most basic explanation of the physical process which causes a flow to become turbulent is due to the water flowing over a rough surface in the seabed. This process can be conceptualised by the roughness of the boundary layer causing a gradient in the flow velocity - with the water slowest near the boundary - and this gradient causing the faster higher flow to 'spill over' the lower flow causing large turbulent eddies to form. These large eddies then transfer energy by frictional momentum transfer to smaller eddies down to the scale where viscous forces dissipate the kinetic energy to heat.

The rate at which large eddies transfer energy to smaller scales is captured in the dimensional analysis work of [29] and the minus five-thirds law according to:

$$E(k) = \alpha \epsilon^{2/3} k^{-5/3} \tag{2.5}$$

Where $E(k)$is the kinetic energy per unit mass per wavenumber, alpha is a constant, ϵ is the dissipation rate of kinetic energy and k is the wavenumber defined as:

$$k = \frac{2\pi f}{\overline{u}} \tag{2.6}$$

Where f is frequency and $\overline{u}$ is the mean velocity over a period of stationarity (T_{stat}) [29].

This region is part of what is known as the turbulent cascade and the -5/3 slope region is known as the inertial sub-range. The turbulent cascade covers all regions of turbulent motion and a diagram illustrating the various scales is presented in Figure 2.4. In tidal site analysis, there is uncertainty regarding the effect of the largest structures in the flow; how much kinetic energy they contain and what their impact on devices will be. It has been estimated that the scales of turbulence in tidal sites would be approximately one third the channel depth [30]. Studies by [31] of lengthscales have found an average streamwise integral lengthscale of approximately 17m for a 55m deep channel for a site (Admiralty Inlet) with flow speeds of 1.5 ms^{-1} which supports this estimate. In addition, the smaller scales of turbulence can also affect devices. In addition, the smaller scales of turbulence are thought to affect lift and drag of blades [15].

An additional important theory in turbulence measurements is that of the 'frozen field hypothesis' developed by Taylor [32]. It is an assumption that the largest turbulent structures evolve significantly slower than they are advected and thus the flow past a given point can be considered as a snapshot of the structure moving with velocity $\overline{u}$.

2.4.2 Site Characterisation as an Input to Numerical Models

Computational modelling can be used to predict the dynamics of turbulent flow (and in the presence of a wave field). Computational models exist for all scales of fluid motion from global oceanography

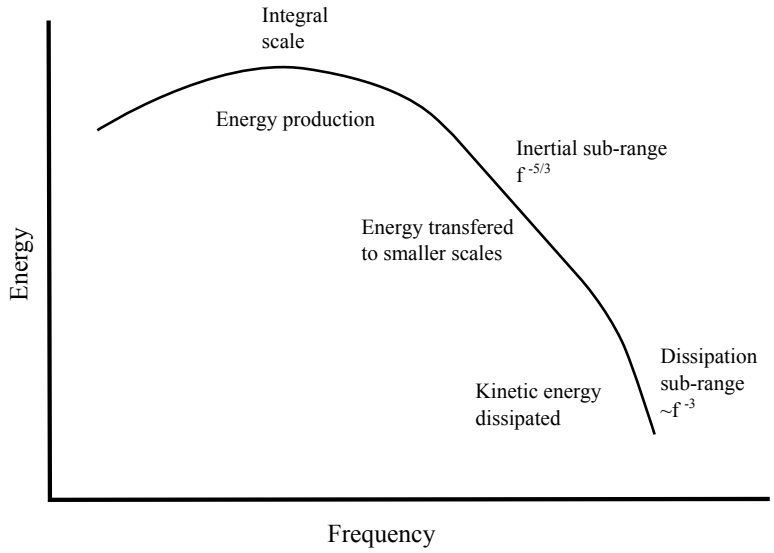

Figure 2.4: Illustration of the energy cascade highlighting the most important regions in tidal site characterisation. Adapted from [3].

models to Computational Fluid Dynamics (CFD) which resolve flows at tiny scales. The advantage of these models is that they don't require expensive site surveys and can be modified for any site and used for the prediction of resource, with the inclusion of energy extracting devices in the form of tidal turbines. However, these models require high quality field data for validation. Furthermore, data ideally would be available from a range of sites so that the driving factors for inter-site variation can be better understood. One of the fundamental goals of field velocity measurements (and the ReDAPT project) is to gather data suitable to improve the confidence in these models.

Numerical Modelling of Tidal Flows

Tidal flows are turbulent, exhibiting random motions across all dimensions. Whilst the equations to describe turbulent flows are known (the Navier-Stokes equations) the computational power required to model these flows across the entire scale of motion severely restricts a direct numerical approach (at present). Traditionally, extensive, expensive and careful experimentation has produced empirical formulae for simplified systems. As system complexity increases empirical methods become less realisable and/or reliable. In this regime, statistical methods can be applied to the Navier-Stokes equations to 'smooth' the fluctuations (turbulence) whilst maintaining a correct description of the averaged properties such as velocity. The averaging of the turbulence terms cannot be fully neglected however. In order to maintain conservation of energy in the system, information on the characteristics of turbulent motion needs to be injected in to the numerical simulations. The descriptions of these motions and the methods of inputting the information into the simulations are called "turbulence models". These models simulate the effect of turbulence on the behaviour of the mean properties of the flow. An introduction to the numerical modelling techniques used in ReDAPT can be found in the sections immediately below and in ReDAPT reports of MD1, MD5 and MD6 [7, 9–11]. Further reading can be found in [33–35].

> "Turbulence models can only give an approximate description, and, with a particular set of empirical constants, they are valid only for a certain flow or at most a range of

flows."

[36]

For reliable results consideration should be given to the following aspects of turbulence models:

- They need to be tailored for specific problems
- Their validity will likely be limited to specific types of flow or ranges of flows
- Extensive testing is required to have confidence in any extrapolations made
- Their associated computational expense increases with complexity

In order to build confidence in a selected turbulence model and numerical simulation, verification with measurements acquired in either or both the field and the laboratory may be required.

MD1 - Detailed Numerical Simulations

In order to increase confidence in the outputs of CFD techniques, confidence in the inputs to these numerical models must be established. CFD conducted as part of the MD sub-project within ReDAPT was based upon EDF's Code_Saturne [37]. This is an Open Source CFD code designed for efficient parallel computation of turbulent flow around and within complex geometries. The code includes a range of Reynolds Averaged Navier-Stokes (RANS) turbulence models and is widely used for Large Eddy Simulation (LES). The primary objective of the ReDAPT MD1 work was to compare numerical predictions of the characteristics of time varying load to measurements of time-varying loads on the TGL 1 MW turbine.

It is important that the inflow conditions are defined such that the spatial and temporal variation of the incident flow are representative of the conditions experienced by the DEEPGEN IV turbine.

Turbulent length scales are of particular significance to this work involving Large Eddy Simulation. The software component that handles the generation of inflow data to these simulations, in this case the Synthetic Eddy Method (SEM), can use turbulence length scales to create velocity fluctuations that are more representative of the modelled environment [38]. Since the outputs of an LES model are known to be sensitive to inflow conditions, it is important that the ambient flow-field is accurately modelled so that physical and modelled effects can be isolated. The University of Edinburgh worked with EDF and their partners to ensure that values of important inflow parameters can be measured or inferred to an acceptable level of confidence.

MD6 - Industry Design Tools

Sub-project MD6 aimed to improve confidence in DNV's Tidal Bladed tidal turbine design tool. Tidal Bladed, in order to give information on loads and performance of a particular tidal turbine, requires a description of the turbine (blades, rotor, drive train etc.) and a description of the environment (currents, waves, turbulence etc.). At present Tidal Bladed describes the environment in terms of vertical profiles of velocity and the turbulence intensity (from a prescribed location or 'point') and incorporates the effects of waves through measurements of traditional wave spectral parameters such as H_{m0}.

> "Very few measurements of the turbulence intensity of tidal currents and their spectral distribution are known. Especially for the spectral distribution, no standard models as used in the wind industry or for sea state description [waves] exist." [39].

Unsteadiness in the flow, which imparts loads on to the tidal turbine, will be the result of both wave kinematics and turbulent fluctuations in the tidal stream. Unlike the wave-field, the tidal-flow-field does not have standardised parametric models which can be used to characterise it. As

random variables are inherently unpredictable focusing on probabilistic characterisation is appropriate [3].

Statistical tools for measuring probability include:

- Probability density functions including joint probability techniques
- Probability distributions
- Correlations
- Variances
- Spectra

[3, 40].

The range of complexity of models or descriptions that can be built upon these tools is large and confidence in their use is generally reliant on large quantity of high quality experimental measurements.

2.4.3 The Presence of Waves

The significance of waves in the characterisation of a tidal site depends on multiple parameters including:

- Relative orientation of the local wind field to the tidal flow directions
- Length of water over which the wind can act (the fetch)
- Magnitude of the wind field
- Permeability of the channel to far-field (swell) waves
- Distribution of wave period and wave height
- Channel depth and spatial derivatives (sloping seabed etc.)
- Tidal flow velocity profile
- Time varying water depth/wavelength ratio (tidal range)

The characterisation of waves was not an original MD3 sub project goal and therefore a robust analysis is beyond the scope of this report. However, wave data has been acquired in parallel to ReDAPT data analysis and is currently being assessed. Where wave data is available for periods of core ReDAPT tests it has been incorporated - primarily to filter flow data into classified system states e.g., flows with underlying low, medium and high wave activity.

Linear wave theory is a well used tool in the study of ocean waves and their impact on marine structures, vessels and machines. It should be noted that the theory diverges from reality as ocean wave complexity and non-linearities increase making predictions of wave effect less reliable. In the presence of tidal currents modifications are required to analyses taking advantage of measurements of wave orbital velocity. Moreover, the underlying waves (and current) are physically modified with significant changes in observed wave period, height, steepness and orbital dynamics.

The are of wave-current interaction, both in the context of this work and in fundamental oceanography, requires further investigation and is being followed up by the project participants.

For further information on potential measurement techniques and analysis conducted to date see section 2.8 and 3.3 respectively.

2.5 Tidal Energy Site Characterisation: Metrics

Tidal site characterisation is often based on velocimetry techniques using acoustic Doppler-based sensors. These devices have the advantage over other technologies in that they measure remotely, hence measurements are not affected by the fluid flow around the sensor or their mounting structure.

By taking advantage of the known speed of sound and through precise control of timing, measurement of spatial profiles, such as the variation of velocity with depth can be achieved.

Characterisation work has historically focused on a set of transient metrics, a high level of confidence in which is crucial to device designers. This section introduces and defines these metrics which cover: mean flow properties, magnitude of turbulent fluctuations and scales of turbulent structures.

Early work on tidal site characterisation using D-ADP and C-ADP velocimetry include [41–43]. More recent works include [44–46].

2.5.1 Mean Flows: Depth Profiles

To estimate long term resource mean velocities should be collected and a harmonic analysis performed [47]. The flow measurement should either be at predicted hub height of a device or averaged over the probable rotor diameter. For early feasibility studies the two largest constituents are sufficient, but for an 'advanced' tidal project site assessment, a minimum of 3 months of continuous field data are required, in order to resolve 20 of the Harmonic Constituents. The longer period constituents are of up to 2191 hours and as they combine can cause variation in yield predictions over a period of years. Unfortunately most resource work is project specific and is therefore unpublished. This report does not include long term (project lifespan) characterisation or subsequent energy yield as the focus is on turbulence and parameter uncertainties arising from typical deployment methodologies.

Channel flows vary vertically as previously discussed thus flow measurements throughout the water column are required. The tidal industry uses a variety of curves to describe how the flow varies with depth, known as velocity depth profiles. Equation 2.7 gives the form of the relationship of velocity with depth ($u(z)$):

$$u(z) = \left(\frac{z}{H}\right)^{1/n} u_{z=0} \tag{2.7}$$

Where n is an approximate empirically calculated power normally in the range of 7 to 10 and H is the total depth.

It should be noted that equation 2.7 assumes no wind and wave driven surface effects or large scale bathymetric features which would be expected (and are shown herein) to significantly affect velocity depth profile.

2.5.2 Quantifying turbulence magnitude and structure

In order to derive subsequent turbulence metrics from velocity time-series a period of stationarity (T_{stat}) of the flow must be defined. All turbulence metrics require the assumption that the flow is statistically stationarity over the period over which the metric is being calculated. As real flows evolve throughout their cycles this period assignation can only be done in a statistical sense. [48] investigated a series of periods from 1 to 20 minutes before concluding that 5 minutes was the longest period that could be considered stable in terms of mean and variance. Although it should be noted that this result is based on measurements at only two locations and may be site specific. A study on the selection of a valid stationarity period was conducted for the FoW and 5 minutes was chosen as a pragmatic compromise to a system that is highly dynamic and has, by most definitions, a variable stationarity period. This work will be presented as part of a future publication.

Velocity Perturbations

As turbulence analysis involves analysis of fluctuations around the mean value $\overline{u}$ these must be defined. A velocity perturbation u'_n for a single velocity sample (n), is defined as [3]:

$$u'_n = \overline{u} - u_n \tag{2.8}$$

with the average perturbation being defined as:

$$u' = \sum_{n=1}^{T_{Stat}} u'_n \tag{2.9}$$

The same equations are used to define the transverse and vertical velocity perturbations v' and w'.

Signal Detrending

Analyses can be sensitive to the method used to estimate the representative mean of a signal particularly for dynamic systems and for those comprised of varied physical drivers (chaotic multi-scale eddies, pseudo-deterministic wave oscillations, periodic constituents etc.) Common methods of defining a mean value include constant-value detrending, linear and higher order polynomial detrending, pre-filtering data to remove known oscillations and moving average detrending. This is discussed further in section 3.2.10.

Turbulence Intensity

A metric commonly used to quantify the magnitude of turbulence is the Turbulence Intensity (I). This term is adopted from the wind industry as a measure of the magnitude of fluctuation as a percentage of the mean flow velocity. It is defined as the root-mean-square (rms) of the velocity perturbations divided by the mean velocity over a period of stationarity as given by:

$$I = \frac{\sqrt{\frac{1}{3}\langle u'^2 + v'^2 + w'^2 \rangle}}{\overline{u}} \times 100 \tag{2.10}$$

Where u', v and w' are the velocity perturbations along the three Cartesian vectors. Angled brackets are used to denote an average value. If the turbulence is assumed to be isotropic (i.e. equal in all directions) only a single velocity perturbation measurement is required [18]:

$$I_i = \frac{\sqrt{\langle u_i'^2 \rangle}}{\overline{u_x}} \times 100 \tag{2.11}$$

Where u'_i for the i^{th} Cartesian vector (i.e. $u'_y = v'$). Note that I is always normalised by the mean streamwise velocity component $\overline{u_x}$.

Reynolds Stresses

To quantify the driving forces that generate turbulence the standard metric set are the Reynolds stresses. First introduced by [49], they are a measure of the shear forces which generate the turbulent flow conditions, again calculated from velocity perturbations. They are defined by the Reynolds stress tensors, for example for the transport of the horizontal fluid momentum in the vertical:

$$\tau_{uw} = -\rho \langle u' w' \rangle \tag{2.12}$$

where τ_{uw} is the Reynolds stress tensor and ρ is the density of the fluid. These stresses are strictly defined as a matrix of three momentum components in the three Cartesian planes. The density term can be omitted (and often is in tidal site characterisation work) for a fluid where the variation in density in negligible [50].

Several previous tidal site characterisation studies have contained measurements of Reynold stress tensors including [43, 46, 51, 52]. Both [52] and [46] were conducted at EMEC with the former finding maximum streamwise-vertical tensors of 7 Pa at flow speeds of 2 ms^{-1} and the latter using results of peak flows (estimated at 3 ms^{-1}) found longitudinal Reynolds stresses of up to 12.7 Pa, highlighting an increase with mean flow speed, with vertical-transverse tensors generally having smaller values, with a maximum of 5.1 Pa. Both studies showed that the Reynolds stresses were at a maximum close to the seabed and decreasing towards the surface.

Integral Lengthscale

The integral lengthscale (ℓ) is defined qualitatively as the average size of the largest eddies in a turbulent flow [3]. There are several methods of estimating this value. A method that does not depend on the Frozen Field hypothesis is the Spatial Correlation method, where velocities at multiple points are measured at the same instant in time. The correlation coefficient is then calculated for a range of spatial separations or 'lags' via:

$$R(\Delta x) = \frac{\langle (u_x - \overline{u})(u_{x+\Delta x} - \overline{u}) \rangle}{\sigma_u^2} \tag{2.13}$$

Where $R(\Delta x)$ is the correlation coefficient,x is a location along the streamwise axis, Δx is a spatial separation and σ_u^2 is the variance of the velocity [3].

$$\ell_x = \sum_{\Delta x=0}^{R(\Delta x)=0} R(\Delta x)\, \mathrm{d}\Delta x \tag{2.14}$$

The integration is only performed on R values up to the first zero axis crossing as recommended by [53].

The drawback of this method is that the maximum spatial range must be ~ 7 times that of the desired lengthscale or the value calculated will be biased low [53]. [54] used this method and found streamwise lengthscales of $\sim 2m$ for a $9m$ deep channel.

A variation on this method utilises the timescale $\Im$ of turbulence which is calculated from the time based autocorrelation function given by:

$$R(\tau) = \frac{\langle (u_t - \overline{u})(u_{t+\tau} - \overline{u}) \rangle}{\sigma_u^2} \tag{2.15}$$

$$\ell_x = \overline{u} \cdot \Im = \overline{u} \cdot \sum_{\tau=0}^{R(\tau)=0} R(\tau)\, \mathrm{d}\tau \tag{2.16}$$

Assuming the largest turbulent structures are frozen as proposed by [32] the timescale multiplied by the mean velocity advecting the structures will yield the lengthscale as given in equation 2.16. The advantage of this method is that it is not restricted by range as long as the time-series is of suitable duration to accurately compute the auto-correlation function.

This method has been used by [31] where an ADV suspended in the chanel on a bouyant line was used to measure the velocities. The lengthscales for the fastest flow speeds were approximately 17m for a 55m deep channel 10.5m above the seabed at $\sim$1.5ms^{-1}.

Alternatively the integral lengthscale can be estimated by the maximum turning point of the power spectral density. The Power Spectral Density (PSD) uses a Fast Fourier Transform (FFT) of a de-trended statistically stationary velocity sample defined as:

$$Y(f) = \int_{-\infty}^{\infty} y(t) e^{-i2\pi f t} dt \tag{2.17}$$

Where $y(t)$ is a time series, f is the frequency, t is time and Y(f) spectral periodogram. This is then modified to give the PSD ($S(f)$) via :

$$S(f) = \frac{2}{(N+K)\Delta t} |Y(f)|^2 \tag{2.18}$$

Where N is the number of points in $Y(f)$, Δt is the period and K is the number of lags [55]. The maximum turning point of $S(f)$ represents the frequency at which there is most energy in the velocity, which is by definition the frequency of the integral lengthscale. Assuming the frozen field hypothesis, This can be stated as:

$$\ell = \frac{\overline{u}}{f_{S-max}} \tag{2.19}$$

Where the frequency $f_{S\,max}$ is the frequency corresponding to the maximum value of $S(f)$, to calculate the integral lengthscale ℓ. Integral lengthscale is also discussed in ReDAPT report [13].

Further Metrics

Further higher level turbulence metrics exist, however, due to time constraints and data volume these have not been thoroughly investigated at this point. These include the Turbulent Kinetic Energy, Turbulent Kinetic Energy Dissipation rate and the Structure Function.

An alternate expression for the magnitude of turbulence is the Turbulent Kinetic Energy (E_{TKE}) which is based on the standard kinetic energy equation. In the case of (E_{TKE}) no normalisation by $\overline{u}$ is carried out. The definition is given as [44]:

$$E_{TKE} = \frac{1}{2}\langle u_i'^2 \rangle \tag{2.20}$$

This relation also assumes isotropic turbulence.

[56] introduced the Structure function, $D(z,r)$ as a method to estimate the turbulent kinetic energy dissipation rate (ϵ). ϵ describes the rate at which the viscous forces in the flow transfer the kinetic energy to heat at the smallest scales of the turbulent cascade. The structure function which is a version of the two point spatial autocorrelation function with a point separation or lag (r), is given as:

$$D(z,r) = \overline{\left(u'(x) - u'(x+\Delta x)\right)^2} \tag{2.21}$$

Calculating $D(z,r)$ from Equation 2.21 for a range of r values allows the use of the calculation of ϵ:

$$D(z,r) = C_v^2 \epsilon^{2/3} r^{2/3} \tag{2.22}$$

where C_v is a constant. [44] showed that for a site in Puget Sound, ϵ could vary in order of magnitude from 10^{-6} Wm^{-3} at slack water to 10^{1} Wm^{-3} at peak flow velocities.

2.6 Site Characterisation: Flow Measulrement Technology

There are a wide variety of established techniques for measuring fluid velocities. This section introduces these techniques, the theory behind them and their main advantages and relative drawbacks. Acoustic Doppler-based sensors - which are used throughout this work - are discussed in more detail in Section 2.7.

2.6.1 Tide Gauge

A 'Tide Gauge' or water level meter, is a sensor which records surface elevation while averaging out variation due to waves. Sensors use a variety of technologies including pressure which are mounted on the seabed and radar which are mounted on the shore. If the cross section of the channel is known this elevation can be used to inform the average volume flowrate. It cannot give information about variation of flow with depth or any smaller scale motions.

ReDAPT utilised a MIDAS WLR Water Level Recorder based on a piezo-resistive cell with internal temperature compensation to provide pressure measurements with Precision: ±0.01 % FS and Resolution: 0.001 % FS.

The MIDAS WLR was deployed beyond the northern bounds of EMEC's Fall of Warness tidal site for around 30 days (27-7-2011 to 25-8-2011) in the Westray Firth at the location 59 °12.049'N 2 °56.049'W. The instrument collected data until 20-8-2011, when the memory was full. The data time series is shown in Figure 2.5.

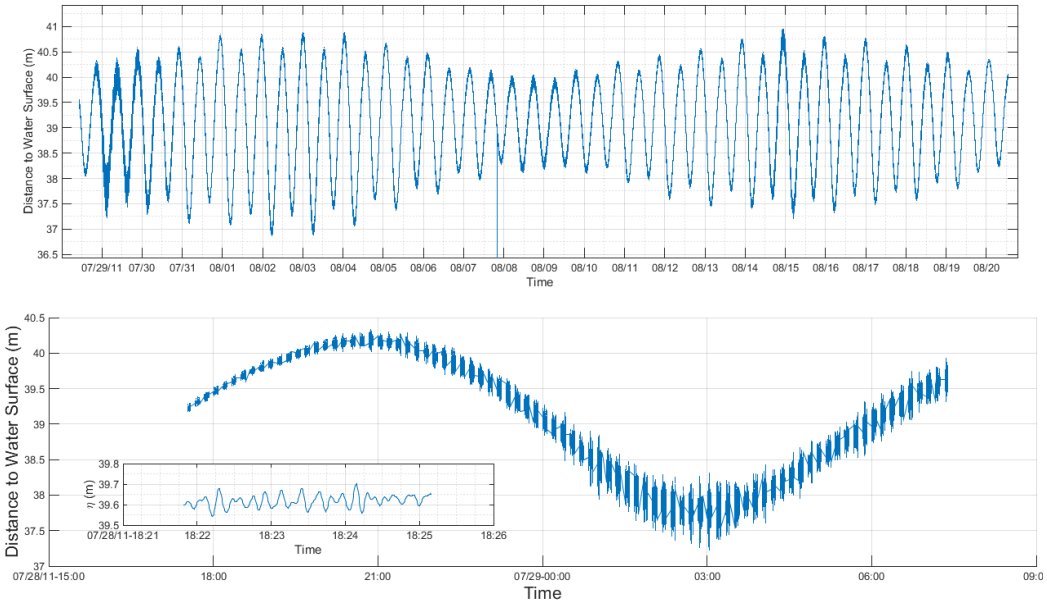

(a) Westray Tide Gauge Deployment

Figure 2.5: WLR Tide Gauge Deployment for MD2 showing(top) the full deployment and (bottom) one tidal cycle. Inset image shows raw data from the burst mode where wave action can be seen.

2.6.2 Piezo-electric Probes

A piezo-electric sensor is composed of a solid surface (often a ceramic) that generates an electrical charge when subjected to mechanical strain. As the pressure increases due to the dynamic pressure the

strain on the probe surface will increase creating a voltage. Multiple probes orientated at different angles can be used to measure the velocity fluctuations in multiple axes. One advantage of these devices is that the probe face can be very small allowing measurements of the smaller scales of turbulent flow, particularly as they can operate at sample rates of up to 200 Hz [57–60]. A drawback is that they do not measure the mean velocity thus a secondary sensor is required to give a reference flow velocity for these fluctuations. Similar devices can use a piezo-resistive strain gauge where a deformable diaphragm is strained by dynamic pressure. When attached to a Wheatstone bridge they can be calibrated to calculate the change in output voltage.

2.6.3 Electromagnetic induction sensors

As water (and in particular brackish water) has electrically conductive properties, it is able to influence magnetic fields [61]. Electromagnetic induction sensors use this effect by creating a magnetic field which, as the water flows through it, induces a potential difference by an amount directly proportional to the flow velocity perpendicular to the flux lines. Multiple electromagnetic fields can resolve fluid flows across multiple axes. The direction of the electro-magnetic fields generated by these devices is often alternated, inducing a voltage that also changes in polarity which counteracts interfering voltage effects. This technique has also been adapted for tidal velocity measurements, but are limited to a single point measurement at the location of the sensor. As an example, the Valeport 803 ROV Current Meter can measure at 16Hz with an accuracy of $0.01 \mathrm{ms}^{-1}$ [62]. Figure 2.6 shows data recorded in October 2014 by the Valeport current meter mounted on the DEEPGen IV turbine. In this example the turbine was orientated 90 degrees off of principal tidal direction as part of multiple UoE flow tests.

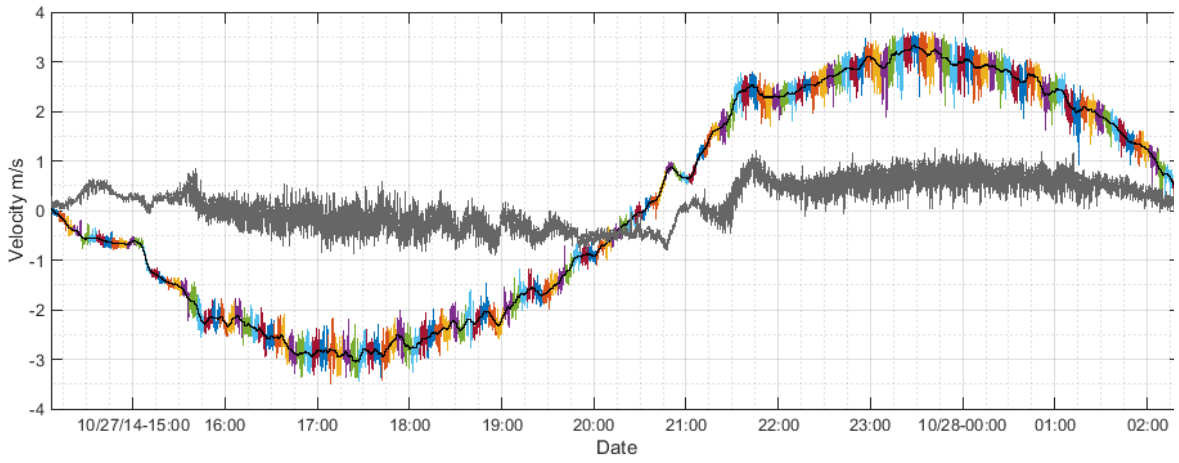

Figure 2.6: Velocity time series recorded by Valeport CM installed on ESIP-1. Streamwise velocity at 10Hz in 5 minute (colored) sections, Streamwise velocity 5 minute running average (black) and Transverse velocity at 10Hz (grey).

2.6.4 Further Techniques

Rotational anemometer/impeller

An adaptation in the tidal industry of the commonly used wind industry anemometer is to replace the rotating cups with an impeller mounted on a directional vane. For tidal applications it is a significant challenge to mount such a device in the appropriate part of the water column.

Hot wire/film

Hot wire anemometers use a heated wire which is cooled by convection as fluid flows over it. The resistance of the wire changes with temperature and the wire is installed in a Wheatstone bridge and calibrated such that the voltage output changes commensurately with flow velocity. Hot wire probes have been used in tidal turbulence analysis such as in work by [51]. However the sensor calibration can drift and it is only capable of measuring an single point without complex multi-wire solutions.

Differential pressure sensors

Most flow sensors work on Bernoulli's principle whereby a moving fluid will create a pressure that increases proportionally with the square-root of the velocity, assuming no changes to the ambient pressure. This is often measured by the difference between the pressure due to the fluid flow (the dynamic pressure) and the pressure of the stagnate flow (the static pressure). These devices are generally referred to as differential pressure gauges such as the Pitot tube, commonly used in the aerospace industry [63, 64].

2.6.5 Sensor Mounting Solutions

Tidal channel flows vary with separation from solid boundaries, where the frictional processes cause stresses which cause a velocity gradient [50]. With tidal channels being of the order of 50m deep flow sensors must be mounted $\sim$ 25m from either the sea surface or the seabed. In the absence of an existing superstructure in the channel to mount to, there are various solutions for taking measurements at the required depths. A selection of the most common solutions are presented : Seabed gravity frames, buoy suspended lines, boat mounted and sub-sea gliders.

Seabed gravity frames and boat mounted systems require instruments that can measure remotely to the mid-depth range. A gravity frame is a heavy non-buoyant structure designed such that the frictional force of the frame exceeds the drag force caused by the flow. Instruments are sometimes mounted in a two axis of rotation gimbals-set to allow them to sit horizontal on an uneven seabed. However, the trade off is that forces induced by the fluid (which is often very turbulent in the boundary layer) on the sensor can cause extreme pitching and tilting, thus the stiffness of gimbals (which can be affected by bio-fouling over long deployments) is important. The effect of small dynamic pitching and tilting on velocity measurements can be corrected for in post processing if they are accurately measured and are within acceptable ranges. Higher order metrics including Reynold Stresses may be more sensitive to these deviations than average velocities. Boat mounted sensors require correction for the boat's pitch, roll and yaw in a similar fashion but with the additional requirement of measuring and subtracting the boat velocity. Small boat designs can also be tethered to a mooring system and used as a stationary surface measurement platform.

A glider is a remotely operated underwater vehicle tailored to operate smoothly in high flow conditions. A buoy suspended line requires a gravity base as previously described as a tether point for a buoy which provides the up-force and resulting tension in a line to which measurement sensors can be mounted. An acoustic release can be employed to release the equipment without needing to retrieve the gravity base.

All these solutions (with the exception of a non-gimbaled gravity base) have multiple degrees of freedom for the sensor to move which is undesirable and will affect the velocity measurements. This is frequently achieved with a combination of tilt sensors, to measure the instrument's angle in the three rotational degrees of freedom and/or accelerometers to measure the speed of the sensor's movements in up to 6 degrees of freedom. This allows correction of the magnitude of the initial measurement and the direction of resolved velocity vectors where required.

(a) Screenshot of bathymetry at FoW, EMEC

(b) Recovery of ADCP from seabed using ROV

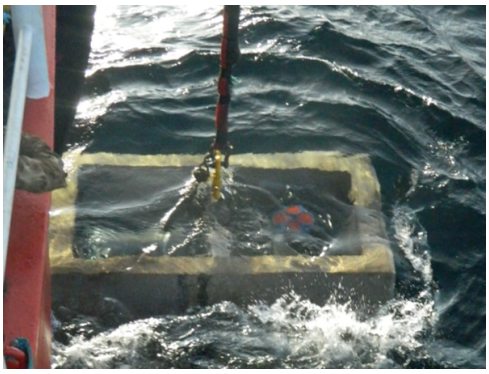

(c) Recovery of ADCP to vessel

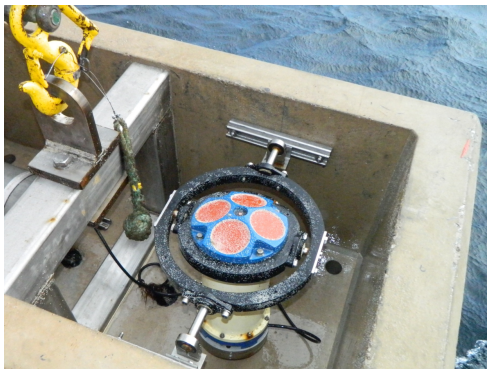

(d) ADCP following recovery. Signs of bio-fouling visible on transducers.

Figure 2.7: Images from ADCP July 2013 Recovery and Re-Deployment.

2.7 Sub-sea Acoustic Doppler-Based Velocity Sensors

Acoustic Doppler Velocimetry (ADV) techniques, particularly geometrically diverging configurations, are widely used in the field measurement of offshore flow velocities due to the relative ease of configuration and installation, unobtrusive flow measurements, as well as the ability to sample throughout the water column. Acoustic Doppler Profilers (ADP) have been successfully used to characterise the mean flow conditions and energy flux in several sites for TEC installations [22, 42, 65–67]. Conventional ADPs emit acoustic signals from a number of transducers (typically 1 to 5) installed on a single device. While a variety of beam configurations exist, in order to deduce a three-dimensional velocity measurement, these acoustic beams must be transmitted in at least three directions [68]. The beam directions are therefore necessarily diverging, typically at an angle of $20° - 30°$ from vertical. A conventional D-ADP is shown in Figures 2.8a and 2.7c . Because the velocity measurement of each beam is calculated from the Doppler shift resulting from the scattering of sound by suspended particles in the water the velocity component is measured in the direction of the beam itself.

Acoustic Doppler profilers are the most commonly used velocimeters in tidal channels as, unlike all the other technologies discussed, they can measure the flow remotely at a significant range from the device. This means they can be mounted upwards orientated on the seabed or downwards orientated from a vessel and provide mid-depth flow measurements.

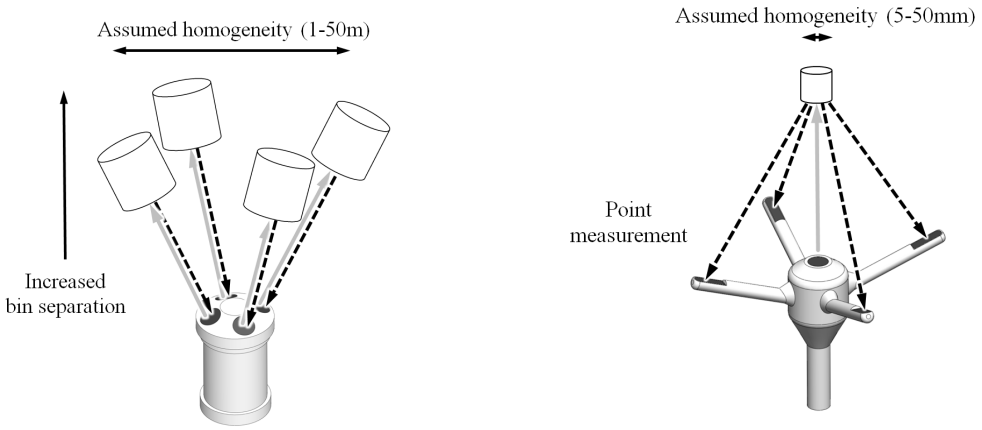

(a) ADP - Divergent Beams

(b) ADV - Convergent Beams

Figure 2.8: Comparison of beam directions for representative a) D-ADP and b) ADV instruments. The gray arrow in the direction of the sample volume represents the transmitted acoustic signal, and the dashed black arrow in the direction of the receiver represents the reflected signal [4].

2.7.1 Doppler Theory

A Doppler sensor has a transducer that transmits an ultrasonic pulse or 'chirp' into the water. The path of this pulse through the water is referred to as the 'beam'. As this chirp passes through the water it is reflected by particulate matter (of the order of 1-30mm in size) suspended in the water. The reflected signals from particulates are known as backscatter. As the reflected pulse is not reflected by the water itself, it is a key assumption that the particulates move with the same velocity as the water. At the end of transmitting the pulse, the transducer acts as a receiver and listens for the response from the reflections back along the beam axis. The reflected beam will be affected by an effect known as the Doppler shift whereby if the source of a wave is moving relative to an observer, the observed wave is compressed or expanded as a function of the velocity component along the observer's line of sight [5].

The change in frequency ratio is proportional to that of the flow speed relative to the speed of sound in that medium. The relation is given as:

$$f_d = f_{pulse}(u_{beam}/C) \tag{2.23}$$

Where f_d is the shifted frequency, f_{pulse} is the transmitted pulse frequency, u_{beam} is the fluid velocity along the beam axis and C is the speed of sound in the appropriate medium, in this case sea water. It is this frequency shift in the reflected signal that allows Doppler velocimeters to estimate the velocity along each beam.

2.7.2 Range Gating

The acoustic pulse will lose power as an inverse square of distance traversed through a medium. As the beam travels it will continuously be reflected (based on the encountered distribution of sound scattering particles) with pulses of decreasing strength returned to the transducer. This continuous returned signal has to be processed in sections in order that each section is representative of a small volume of water along the beam path. The receiving phase of the transmit-receive cycle is divided into even sections based on a fixed time period. This time period corresponds to the reflections from separate measurement volumes. Each of these volumes is referred to as a range bin. This process is illustrated in 2.9.

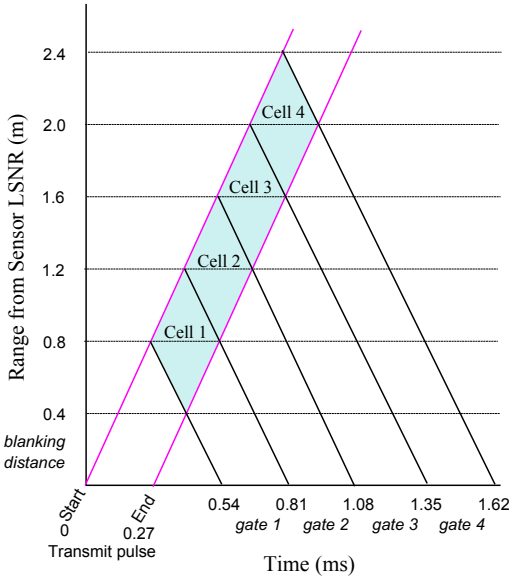

Figure 2.9: Example of range gating for a sensor with a bin size and blanking distance of 0.4m. Image adapted from [5].

This process is illustrated in Figure 2.9. The gap between the end of the transmitting of the pulse and the start of the first listening period is known as the 'blanking distance'. 2.9 shows that the cells are weighted towards the centreline of the measurement volume for a cell. In reality the beam will spread out with separation from the sensor (governed by acoustic frequency and transducer geometry and design) and thus measurement volumes increase with range.

2.7.3 Design Variations

Sensors can have single range bins up to hundreds of bins. The general design trade off is range versus resolution at the expense of increased random error. A lower frequency pulse will travel further through the water but requires larger cell sizes to process the received pulse without increasing noise. A higher frequency instrument can resolve very small spatial scales and has a lower random error associated with it, but the range can be limited to a few centimetres due to the increased attenuation rates of higher acoustic frequencies.

In addition to range, the main design variation is the number of transducers used. A single beam can only resolve one velocity component along the angle of the beam. With three beams three velocity vectors can be resolved, although many designs employ a fourth beam (for *tidal applications*) in order to generate an additional vertical velocity estimate. Having two measurement of the same velocity vector allows an error velocity to be calculated which is a good indicator of measurement quality. Additionally, a fourth angled beam can be used to provide redundancy in 3D velocity reconstruction where the returned data from a single beam is corrupted. Finally, for *wave applications* an additional vertical beam can be used to track the surface elevation.

Subsea Doppler sensors can be classified into two basic types: Diverging (Beam) Acoustic Doppler Velocimiters (D-ADV) and Converging (Beam) Acoustic Doppler Velocimeters (C-ADV). D-ADV typically provide range-gated Profiles (D-ADP) over short to long ranges employing three to five transducers, each of which act both as a transmitter and a receiver (see Figure 2.8a). They are able to resolve three velocity vectors and are available in configurations optimised for different range and accuracy trade offs: from 8Hz sample rate, 2 MHz pulse frequency over 1m range [69], to 1Hz sample rate, 190kHz pulse frequency over 300m [70]. The C-ADV has one transmitting and three to four receiving transducers around it, all angled to focus on a single measurement volume, generally

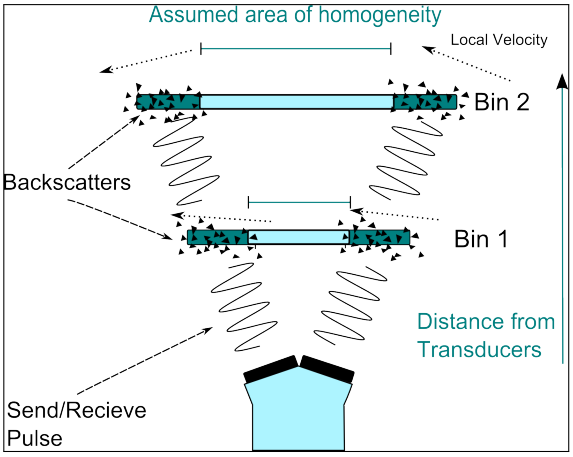

(a) Sketch showing assumed area of flow homogeneity on Divergent Acoustic Doppler Profiler (D-ADP) system.

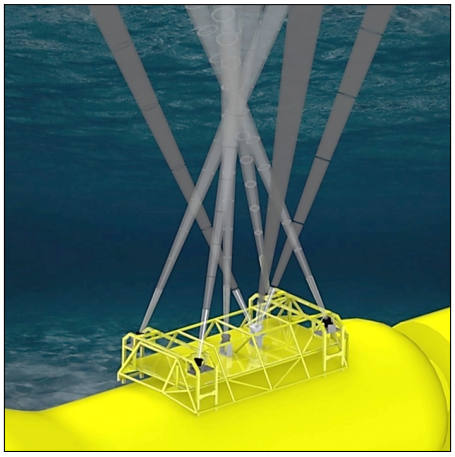

(b) ReDAPT Convergent Acoustic Doppler Profiler (C-ADP) concept render.

Figure 2.10: Divergent and Convergent Acoustic Doppler Profiler (C-ADP)

resolved into a single cell as shown in 2.8b. They can operate at high sample rates (up to 200Hz output with internal sampling above this rate) but are limited in range to $\sim 3-10$cm [71].

ADVs (both commercial and bespoke) have been used successfully in a range of laboratory and field applications including localised velocity measurements [72–76] and sediment transport studies [77, 78].

In recent studies, multiple ADVs were mounted on compliant moorings to achieve measurement locations at significant distance from the seabed [31, 79]. The velocity signal is corrected for instrument motion using the simultaneously measured instrument accelerations, with promising results. The measurement of high resolution velocity profiles has been achieved using a number of recent ADV designs [78, 80], however the range remains small for tidal application in the order of several tens of centimetres.

A large scale profiling C-ADV with baseline of three metres (C-ADP) was trialled during ReDAPT and is outlined in section 3.9.

In addition, single beam variants of these profilers have recently been released. These are designed for situations where they can be easily mounted in the centre of the water column such as on a tidal turbine. These sensors were widely used in this work.

Since 1991 Doppler sensors have utilised lower-signal-noise 'broadband' technology in many instruments, as supposed to the precursor 'narrowband'. A broadband pulse is composed of a repeated pattern of changing frequencies allowing a more accurate assessment of the Doppler shift compared with the single frequency narrowband pulse. This advancement allows the velocities to be resolved with greater accuracy. Device developer (RDI), claims that it reduces the variance in measurements by a factor of ~ 100 [5]. There is a third type of pulse processing which is called 'coherent' where two or more very short pulses are sent with silence between them to allow any 'ringing' of the transducer to dissipate before sending the next pulse or listening for the reflected pulse. Sensor manufacturer Nortek have suggested that this technique reduces sensor noise by up to 4 orders of magnitude compared with narrowband technology but it is limited to short ranges of ≤ 1m. An illustration of the different acoustic emission techniques is shown in Figure 2.11. A useful introduction to D-ADPs is provided by RDI's practical Primer [5].

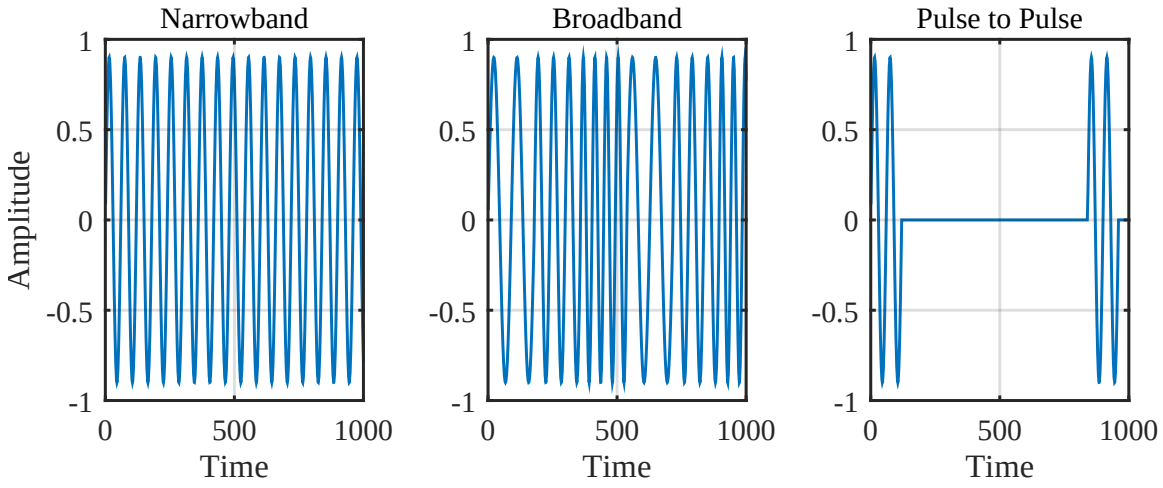

Figure 2.11: ADP pulse techniques: Narrowband, Broadband and Pulse to Pulse Coherent

2.7.4 Coordinate Transforms: Acoustic Beam to East, North and UP

D-ADPs measure the 'along-beam' velocities, i.e. those along the orientation of a given transducer. These velocities are of little use to TEC designers who are concerned with the flow onset to the rotor plane. It is therefore desirable is to define the flow in terms of the turbine orientation, thus metrics are usually defined in Cartesian coordinates, with x along the nacelle, y normal to this and horizontal and z as vertical. Further information on this coordinate transformation can be found in [81] and [82].

Two stages are required in order to achieve this velocity transform: the first is to transform the beam velocities into two pairs of one horizontal and one vertical velocity based on the planes of opposing D-ADP beams; the second is to rotate these to account for the heading, pitch and roll provided by the instruments on-board sensor (or potentially using external references where internal sensors are not fitted). The heading (yaw rotation around z) is normally adjusted such that two horizontal vectors are orientated to North and East, but can be aligned towards the primary flow direction.

The equations of this velocity transform are defined as:

$$u_{h1} = \frac{1}{2\sin(\beta)} \cdot (u_{B1} - vel_{B2}) \tag{2.24}$$

$$u_{h2} = \frac{1}{2\sin(\beta)} \cdot (u_{B4} - vel_{B3}) \tag{2.25}$$

$$u_z = -\frac{1}{4\cos(\beta)} \cdot (u_{B1} + u_{B2} + u_{B3} + u_{B4}) \tag{2.26}$$

where u is a velocity in either the horizontal axis of the plane of beams 1 and 2 ($h1$) or 3 and 4 ($h2$) and z is the vector equidistant from all the beams (but not necessarily exactly vertical) [82,83]. u_{B1} is the measured velocity along beam 1, etc. and β is the beam angle from vertical. In the case of the RDI 600 kHz Workhorse Sentinel ADCP instruments used for non-turbine connected velocimetry, β is 20°.

The rotation matrix to account for instantaneous (at sample rate) instrument yaw (heading), pitch and roll is defined as:

$$T = \begin{bmatrix} -\cos(\theta)\cos(\psi) - \sin(\theta)\sin(\phi)\sin(\psi) & \sin(\theta)\cos(\phi) & \sin(\theta)\sin(\phi)\cos(\psi) - \cos(\theta)\sin(\psi) \\ \sin(\theta)\cos(\psi) - \cos(\theta)\sin(\phi)\sin(\psi) & \cos(\theta)\cos(\phi) & \cos(\theta)\sin(\phi)\cos(\psi) + \sin(\theta)\sin(\psi) \\ \cos(\phi)\sin(\psi) & \sin(\phi) & -\cos(\phi)\cos(\psi) \end{bmatrix} \tag{2.27}$$

2.7.5 Relative Advantages and Limitations of Doppler Sensors

A key advantage of acoustic technology, in particular of D-ADPs, is the ability to take readings remotely and throughout the water column. Devices can be mounted on the seabed in a relatively fixed position and take three vector water measurements up to the surface. The uncertainty in position and velocity of constantly moving floating sensors can dominate measurements and typically gives a single point in the water column. As discussed in 2.7.3 work is ongoing in this area and it is expected that through integration of new and inexpensive technologies (including micro-electro-mechanical (MEM) motion sensors) floating arrays of sensors will provide previously unobtainable multi-point 3D velocities. Having a mid-depth fixed body is often impractical and (if large enough) will impede the flow. The challenges associated with acquiring in-situ mid-depth flow measurements has made D-ADP a standard technology for characterising potential tidal sites.

In order to deploy a D-ADP a solution for power and data storage must be devised. Most devices use batteries and memory cards, which limit deployment goals. Data readings must often be taken less frequently to maximise the deployment length, which is often desirable as the cost of deploying devices is high. Alternatively a higher data sample-rate can be used at the expense of longevity. The data capture set up along with the range and spatial resolution are decisions site surveyors face to get the most appropriate data for their requirements.

Co-ordinate Transformation and the Assumption of Flow Homogeneity

The transformation of the velocity components from the beam direction to the instrument coordinate system requires the assumption of flow homogeneity [82]. That is, the velocity vector transformation assumes that the velocities in sample bins at the same distance from the transducer are identical. This is often a reasonable assumption for mean flow velocities, which typically do not vary considerably within the spread of the acoustic beams.

In energetic tidal flows, the instantaneous flow velocity is seen to vary over a wide range of time and length scales. Coherent turbulent structures smaller than the distance separating the diverging beams of D-ADPs at a given elevation are unable to be resolved. Large scale eddies, although greater in scale than these beam separations, are misinterpreted through conventional D-ADP processing algorithms [84]. Furthermore, Doppler noise is an inherent feature of the measurements arising from this technique. While able to be removed in post-processing of bulk statistics [6,85], the contamination of the signal by this white noise limits the use of the instantaneous velocity time series acquired using existing D-ADP configurations.

Thus while D-ADPs remain a key tool in site characterisation, these limitations mean additional sensors are required to resolve the scales of turbulent motion.

2.8 Site Characterisation: Wind Generated Waves

2.8.1 Wave Parameters

A schematic of a water wave is seen in Figure 2.12. The wavelength, λ, is the distance from one wave peak to the next wave peak. Waveheight, **H**, is the difference from a wave's peak to its trough and wave amplitude, **A**, is the distance from the Mean Water Level (**MWL**) to the wave peak. The water depth, **d**, is the distance from the (**MWL**) to the sea bed (or floor of a wave basin/flume).

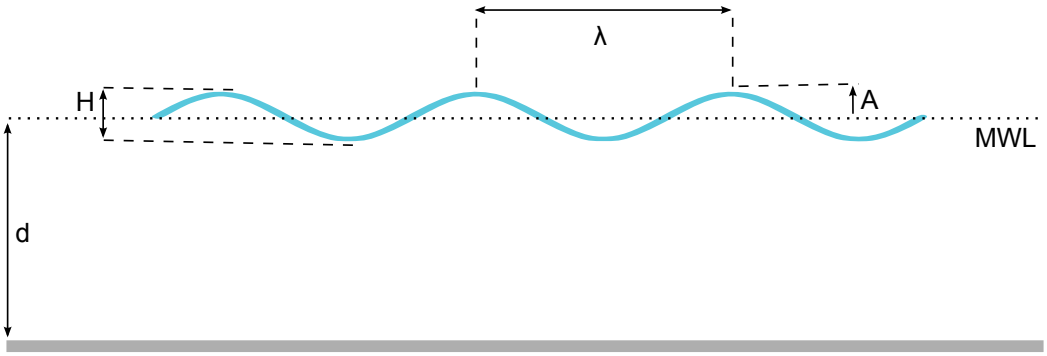

Figure 2.12: Schematic of water wave and associated parameters.

Other commonly used parameters:

- T , Wave period. The time required for two wave peaks to pass a fixed position. [s]
- η , Surface elevation. The height of the free water surface above or below (signified by a negative number) a specified MWL. [m]
- $\omega = 2\pi/T$, Angular frequency. [radians s^{-1}]
- $k = 2\pi/\lambda$, Wave number. [m^{-1}]
- $c = \lambda/T$, Phase velocity or celerity. [ms^{-1}]
- $s = H/\lambda$, Wave steepness.

where ρ is water density (taken as $1000kgm^{-3}$ for fresh water and $1020kgm^{-3}$ for sea water) and g is gravitational acceleration taken as $9.81ms^{-2}$.

2.8.2 Frequency Content Analysis: the Energy Spectrum

The distribution of energy as a function of frequency provides the energy spectrum which is traditionally also referred to as the wave spectrum. Two types of wave spectra are used: discrete spectra where Fourier analysis of a recorded time series gives the spectral density at discrete frequencies; and parametric spectra where the energy content is described as a function of frequency. Parametric spectra are used when only minimal global parameter statistics are known (no wave elevation time series for example) and an attempt is being made to obtain further characteristics based on the spectral shape governed by these basic inputs and also when a comparison between the two spectra has revealed similarities allowing the parametric spectra to be used as a representative model [86]. By recording wave elevations at many locations globally, deriving the discrete spectra and checking the fit of the observed spectra to a parametric model, the validity of the various parametric spectra have been assessed. Examples of parametric spectra include Bretschneider, JONSWAP, Pierson and Moskowitz, Mitsuyasu and Ochi and Hubble. These have been adjusted over the years to better fit experimental data and to include site specific factors such as wind fetch [87].

Symbol	Label	Description/Formula	Units
$S(\omega)$	Spectral (variance) density	$S(\omega) = \frac{1}{2}\frac{A^2(\omega)}{\delta\omega}$	m^2s
$S(f)$	Spectral (variance) density	$S(f) = 2\pi S(\omega)$	m^2s
S(f,θ)	Directional spectral density	$\mathbf{S}(f,\theta) = S(f)D(f,\theta)$	m^2 s deg^{-1}
H_{m0}	Significant wave height	$H_{m0} = 4\sqrt{m_0}$	m
T_{02}	Average wave period	$T_{02} = \sqrt{\frac{m_0}{m_2}}$	s
T_e	Energy period	$T_e = \frac{m_{-1}}{m_0}$	s
s	Wave steepness	$s = \frac{H}{\lambda}$	-
H_m	Mean wave height	Sum of zero-crossing-defined wave heights divided by number of waves	m
T_m	Mean wave period	Sum of zero-crossing-defined wave periods divided by number of waves	s

Table 2.1: Wave field parameters trialled as tidal current 'data filters'.

$S(\omega)$, the spectral variance density in m^2s is given by,

$$S(\omega) = \frac{1}{2}\frac{A^2(\omega)}{\delta\omega} \tag{2.28}$$

In terms of frequency, f, $S(f) = 2\pi S(\omega)$.

In practice the spectral variance density is found by performing a Fast Fourier Transform (FFT), the computationally optimised Discrete Fourier Transform (DFT), on a digitised, sampled signal. Fourier analysis requires that the wave elevation signal is periodic around it's length (in time) and thus modifications or taper windows are implemented at the beginning and end of the signal.

For a list of sea state parameters recommended for use in the wave energy field see table 2.1 and [88].

2.8.3 Wave by Wave Time Series Analysis

An alternative approach to quantifying wave elevation time histories is to analyse the signal on a wave by wave basis. This involves determining starting points and finishing points for regions of the signal and measuring their properties. The overall statistics are based on the aggregate of these individual wave events.

Figure 2.13 illustrates the method of identifying an individual wave based on the point in time at which the elevation crosses the mean water level (MWL) from a positive elevation to a negative elevation (zero down crossing). An alternative approach, zero up crossing, is to identify where a wave crosses the MWL with a positive gradient. The differences in overall statistics that these alternative

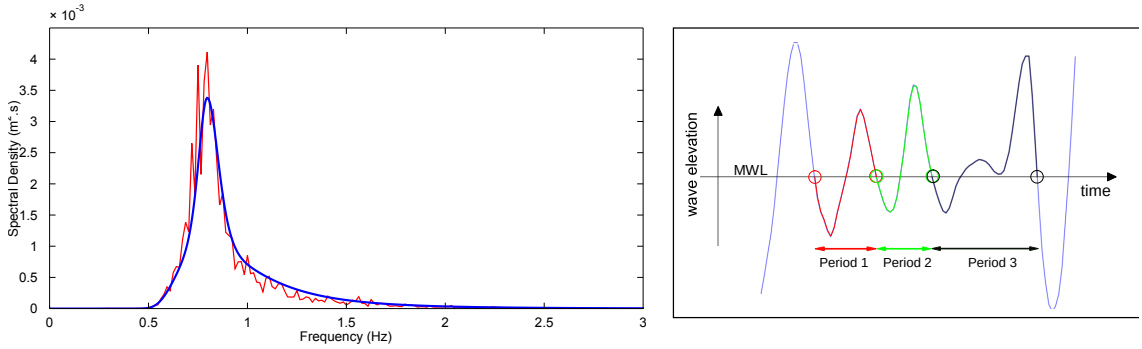

(a) Example discrete spectra from measured data (red) and corresponding parameterised JONSWAP spectra (blue) (with γ set to 3.3).

(b) Schematic showing wave zero-downcrossing method

Figure 2.13: Schematic showing spectral (a) and time-domain (b) representation of waves.

methods lead to are small and are not considered in this thesis. In practice, due to infrequent discretised sampling, the zero crossing point is determined by an interpolation scheme. Figure 2.13 also highlights the sensitivity of the process to small errors in elevation where wave number 3 may have been better described as a shorter period, small elevation wave as there is a turning point that almost exists below the MWL.

2.8.4 Directionality

A directional wave spectrum not only takes in to account the distribution of energy with respect to frequency but also the distribution of energy as a function of direction. In reality, most sea states (other than long-crested waves where the crest lines are straight and parallel) are composed of multi-directional waves thus the directional wave spectra offers the most comprehensive statistical wave field description. With full directional spectral analysis the drivers of a sea-state can be separated and identified. Good understanding of the directional spectrum is an important factor in the design and functioning of coastal and offshore structures and is critical in assessing the effects of reflected waves near structures [89], [90]. The directional spectrum is key in the field of wave modelling and air-sea interaction; and affects the forces experienced by piles and offshore structures including vessels and platforms; and plays a role in coastal erosion, sediment transport and polution dispersal. [91]

The directional spectral density, $\mathbf{S}(f,\theta)$, builds on equation 2.28,

$$\mathbf{S}(f,\theta) = S(f)D(f,\theta) \tag{2.29}$$

where $S(f)$ is the unidimensional spectrum (expressed as a function of frequency) and $D(f,\theta)$ is introduced as the angular spreading function. $D(f,\theta)$ is dimensionless and normalised by setting its integration, over angle, from 0 to 2π equal to 1,

$$\int_0^{2\pi} D(f,\theta)d\theta = 1 \tag{2.30}$$

Quantifying Directional Seas

The primary directional sea state parameters are the mean wave direction (at the peak of the spectrum) θ_{1p}, and the standard deviation of the directional distribution, the directional spreading (at the peak of the spectrum) σ_{1p}. The latter describes the distribution of wave energy around the mean

value. Unlike the more stable (in terms of analysis method) spectral parameters such as H_s and T_p, both θ_{1p} and σ_{1p} can be defined as functions of frequency.

There are several routes to identifying the key directions and frequencies contained in a wave field each with associated advantages and disadvantages and dependencies on the instruments used to supply the raw data. Ideally, to provide the full directional spectrum, without the use of prior information and assumptions, numerous high-resolution instruments would be deployed in an array over a wide area in order that all spatial scales of waves and their corresponding directions may be captured. Current technology remains well below the ideal specification for directional resolving of waves [91], and as such, methods are used (and assumptions are incorporated) which aim to maximise the use of sparse, and in some cases, low-resolution and noisy information.

Multiple methods exist to quantify directional seas including the Fourier expansion method, Extended Maximum Entropy Method (EMEP) and Bayesian Direct Method (BDM) [91–94]. Some studies including [95] show the EMEP method to be the best all-rounder providing high resolution, generally fast and error-tolerant results whilst [96] suggests a site and instrument-specific approach.

Within this work package preliminary wave spectral and directional analysis made use of the Wave Analysis for Fatigue and Oceanography (WAFO) and Directional Wave Spectra Toolbox (DIWASP) software packages [97, 98].

2.8.5 Non-Linearities

A disadvantage of the energy spectrum lies in its inability to provide information on parameters important to the design of marine structures, such as shock loads, which arise due to the *shape* of individual waves and wave groups [99].

One of the most obvious non-linearities in waves is the increasing asymmetry of the wave between trough height and crest depth, through the mean water level, as waves get larger in amplitude. Wave-wave interaction at a particular location causes non-linearities in addition to the non-linear evolution of a group of waves over time and wave breaking events [100].

Increasing effort is being directed to the effects of currents on wave characteristics and on the effects of wave motion to turbulent variation of mean current flow. These interactions are another source of non-linearity.

Significant Wave Height

The term significant wave height, H_s was traditionally determined by averaging the wave heights of the highest one third of waves in a wave time series, often labelled $H_{1/3}$. In addition it has been assigned to the variance of the wave time series. An alternative definition (and used in this work) stems from the frequency domain: H_{m0} - where the significant wave height is related to the zeroth spectral moment (or proportional to the square root of the area under the spectral graph).

$$H_{m0} = 4\sqrt{m_0} \tag{2.31}$$

Where the nth spectral moment is calculated from,

$$m_n = \int_0^\infty \omega^n S(\omega) d\omega \tag{2.32}$$

where $n = 0, 1, 2, 3, ...$

2.9 Site Characterisation: Wave Measurement

2.9.1 Wave buoys

Wave buoys have been deployed for monitoring the wave field and meteorology over the ocean since the 1960s [92]. Buoys provide good quality wave height, period and often direction measurements but suffer from poor spatial coverage. Whilst proven technology, wave buoys remain expensive to build, deploy and operate. In the case of large, offshore and long-term monitoring buoys deployment, maintenance and removal involves the use of expensive vessels. Being located on the surface, buoys are exposed to shipping, fishing and storm damage/loss.

Smaller wave buoys intended for shorter period deployments (months and years, not decades) can be lightly moored (compared to large diameter ocean weather monitoring platforms [101]) on elastic, compliant moorings. Incidents involving buoys becoming detached from their moorings are not uncommon.

Traditionally buoy generated timeseries are processed on board the buoy and the summary statistics of a selected period (typically 20 minutes to meet the requirement of psuedo-stationarity for spectral processing) are transmitted. This level of data may not be sufficient for the marine renewable sector where access to the raw time series is needed, either in near real-time or after a deployment for post processing. As is to be expected in the dynamic marine environment, the quality of these time series can be variable and can require extensive post processing [95].

Further advances in buoy technology may be required for the renewable sector leading to smaller and lighter buoys capable of supplying full raw data via high bandwidth telemetry. By residing on the surface and therefore having access to through-air telecommunication frequencies buoys have an advantage over their submerged competitors and can access cellular, radio or satellite communication networks.

At highly energetic tidal sites wave buoys may not be a viable option for reasons related to logistics, permitting and survivability.

2.9.2 X-Band radar

Commercially-available X-Band Radar can be installed on fixed (e.g. offshore oil installations, lighthouses) or moving (e.g. vessel-based) platforms. The ReDAPT project had access to the WaMOS II system installed on a tower on Eday, Orkney overlooking the EMEC tidal test site (see Figure 2.14b).

Operating on the principle of measuring the backscatter of radar energy from the ocean surface these systems offer massive spatial coverage improvements over Buoys with a typical system being able to cover a swept area of radius 2km at a spatial resolution down to 10m. Systems include Miros, WAVEX and OceanWaves WaMoS II. Shorter range, higher resolution set-ups exist, using a system covering an area of 20x20m with a resolution of 0.4m [102]. For spectral sea-state parameters H_{m0}, T_p , etc. X-Band Radar-based techniques have been shown to give good agreement (in trial conditions) with other measurement methods such as Buoys [103, 104]). However, these are averaged parameters and do not give information about individual waves. Software developments such as the DWFA algorithm in WaMoS II can identify individual waves from a radar image through linear wave theory as the basis of an inversion technique. Typical systems suffer from poor temporal resolution (Δt=2.5s) limited by the rate of rotation of the radar emitter and the number of images required for analysis and in addition may not be able to pick out wave heights below 0.5m [103]. In tests comparing time series of wave elevation, whilst there is general agreement, large errors are present particularly in wave amplitude [105]. For more robust results benchmark training data sets and improved calibrations are likely required. Other manufacturers include Nortek's SeaDarQ which whilst primarily used for oil spill detection will be undergoing trials (2015/2016) in wave measurement applications [106].

The ReDAPT radar measurement campaigns were conducted by EMEC in parallel - but outwith - the University of Edinburgh's MD site characterisation work and hence the results are not reported.

2.9.3 Acoustic Doppler Profilers

Previously introduced ADPs (see section 2.7) can also be used to measure wind waves. In terms of sensor positioning being situated on the seabed reduces the risk of shipping damage to an ADP but large forces remain which can lead to data loss and sensor damage [107]. Design and implementation of the locating frame are critical to an ADP's deployment and operation. Experiences such as during the Strangford narrows programme suggest that frames have to be extremely robust to survive prolonged deployment leading to installation difficulties for diver teams [108]. Figure 2.7 shows an RDI Teledyne "Workhorse Sentinel" ADCP 600kHz in the University of Edinburgh's custom (2000kg when submerged) gravity moorings with in-house extended battery-containing pressure vessels.

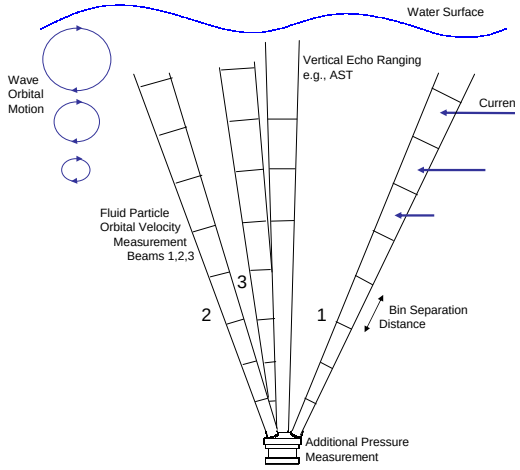

(a) Schematic showing principal of AWAC ADP in wave measurment mode.

(b) Screenshot of map of Fall of Warness showing WaMoS regions of measurement. EMEC 2015.

Figure 2.14: (a) - Schematic showing 3 slanted + 1 vertical beam D-ADP (AWAC). (b) - The radar coverage zones of the EMEC WaMoS II system installed at EDAY, Orkney.)

Some ADPs (e.g., RDI Workhorse Sentinel with "wave option") give directional wave data using software to convert orbital velocity measurements into wave frequency and directionality. The software makes use of linear wave theory to derive elevation. The Nyquist theorem dictates a maximum bed depth for a required surface wavelength resolution. At 50m depth and dependent on beam alignment an ADP can resolve only waves above approximately 3.5 seconds and,in terms of the directional spectrum are further limited to periods of approximately 6 to 9 seconds [109, 110].

The Nortek AWAC with Acoustice Surface Tracking (AST) measures wave direction, surface elevation (wave height). The AST echo-ranges to the surface using a vertically orientated (if the instrument is deployed level) transducer (see Figure 2.14a. This allows the measurement of short period, locally-generated waves and can output either time series histories of surface elevation or the summary statistics as produced by wave buoys. Via a co-installed pressure sensor the user has the ability to select to process wave time series through either the Pressure/U-velocity/V-velocity (PUV) method or Surface/U-velocity/V-velocity (SUV) method.

ADPs often store the data on-board with battery durations (depending on configuration) of the order of six months to a year. This data is retrieved at the end of the deployment after instrument recovery. If data is required on-the-fly there are several methods to achieve this including a cable

to shore (up to 5km using RS422 protocol) [111], acoustic modems to shore or acoustic modems or cables to either a hard-wired asset (e.g., tidal turbine) or a surface platform which can then relay via radio/satelitte/GSM.

2.9.4 Pressure gauges

Bottom mounted pressure transducers have been used for a long time (since around 1947) to measure surface elevation. A good example of their use is their configuration in bottom mounted directional-sensing arrays as part of the DUCK, USA instrumentation trials in the 1990s [112]. They benefit from being out of harms way regarding surface traffic and comprise relatively cheap components. As information from the surface is attenuated through the water column accuracy falls off with depth. However, non-linearity of the surface profile is stronger in shallow water and careful handling of the pressure data to reveal surface elevation is needed in this regime to maintain accuracy. [113]. Further consideration of the pressure to surface elevation transfer function is required in the presence of strong currents. The form of these frequency dependent transfer functions can lead to rapid increases in errors and can only be used reliably within defined wave frequency bands depending on installed depth. Pressure transducers are often used to provide complimentary data to other methods (such as acoustic surface tracking) where their disadvantages are offset by their reliability and insensitivity to sources of acoustic noise such as bubble formation from breaking waves. Figure 2.15 shows pressure data recorded during ReDAPT for a seabed mounted ADCP and a turbine-mounted high frequency pressure gauge during winter storms of 2014.

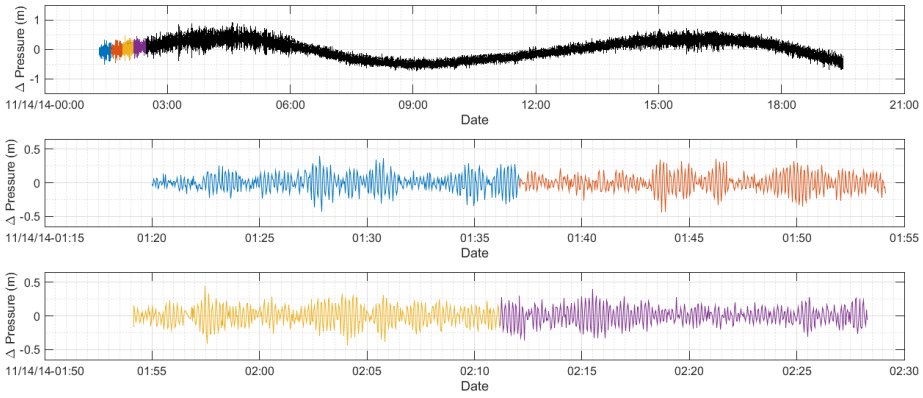

(a) Pressure time-series measured using seabed mounted ADCP.

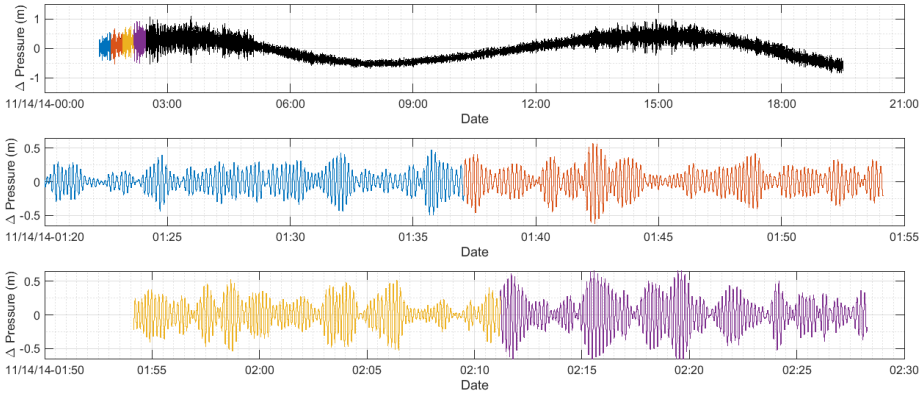

(b) Pressure time-series measured using turbine mounted gauge.

Figure 2.15: Variations in pressure measured from seabed-mounted ADCP pressure gauge sampling at 1Hz and mid-depth-mounted pressure gauge sampling at 10Hz during ReDAPT project in large storm waves, November 2014

2.9.5 Further Techniques

HF Radar

High Frequency (HF) Radar emits radio waves from ground base stations with wavelengths in the range 10-100m and can sense from 10km out to 200km with resolutions decreasing with range to a maximum of a few hundred metres for short range set-up [114]. Whilst it operates under the same principal as X-Band systems the longer electromagnetic wavelength explains the greater range but reduced spatial resolution. Accuracy of the directional spectrum and derived wave paramaters depends on radar power spectrum frequency resolution, temporal and spatial variability in the measurement cell, angle between two radar look directions, antenna sidelobe levels, and waveheight, noise, and interference levels [115]. Algorithms have been developed to process the radar images to extract sea-state parameters. HF Radar's use as a current measurement device is well established but there is some debate as to its ability to measure accurately these sea-state parameters. RF Licensing, interference and planning issues also affect the implementation of the technology [103, 105, 114, 115].

LIDAR

Light Detection and Ranging systems (LIDAR), whereby light of a choice of frequencies (from UV to near infra-red) is used to highlight a surface and report the range to that surface, have been used widely in atmospheric and terrain mapping fields. In the context of oceanography they were first developed for aerial surveying of coastal bathymetry and were later used in underwater obstacle detection tasks [116]. These lidars were operated at a near normal angle to the surface. A more practical installation for the use in measuring wave fields in the shipping, oil and gas and renewable sector would be vessel mounted lidar systems which would negate the inability of moving systems to continuously measure a fixed region. These would be able to monitor the vicinity around a vessel, rig or WEC but would be operating at much shallower angles (limited by the tower height). Difficulty arises in the signal processing of the very weakly returned and heavily scattered light. In one trial processing power is dynamically allocated depending on the distance from the optical radar and the condition of the signal [116]. This study used line scans where the wave field is sampled at various points in a line away from the radar. This technique can be expanded to planar scanning, where the emitter and receiver would sweep a field of view and build up a wave field from many line scans.

Evidence to support the utility of remote sensing technologies (both radar and laser systems) in the field and in the absence of absolute references comes from the WACSIS project [117] where good agreement was found between wave measurements taken via collocated laser and radar instruments - despite their varied measurement techniques [118].

Chapter 3

Site Characterisation at FoW

3.1 Overview of the Measurement Campaign

3.1.1 Phase I Activities

Preliminary work within MD3 involved discussion of the numerical modelling techniques proposed and subsequent identification of the fluid velocity measurement requirements of these numerical modelling activities. Thereafter the extent to which these measurement requirements could be met within ReDAPT was investigated and a prioritisation and scheduling of these measurements developed. Once complete, the instrumentation and measurement specification was used to design, procure and assemble instrumentation systems. This process was conducted in parallel with the design work of the Alstom 1MW DEEPGEN IV. Figure 3.1 shows the first batch of equipment arriving in Orkney for integration on the 1MW machine.

Figure 3.1: Equipment arriving on site at Hatston Quay, Kirkwall, Orkney for integration on the DEEPGEN IV.

3.1.2 Phase II Activities

In order to de-risk later deployments and gain some experience of the returned data limited, deployments were agreed, planned and conducted on the existing Alstom 500kW DEEPGEN III shown in Figure 3.3a.

Five Nortek single-beam ADPs (SBDs) were installed to brackets welded in-situ at the top rear of the turbine orientated to capture velocities in the streamwise, transverse and vertical directions. Figure

3.2 shows their locations and orientations. A Nortek AWAC 1Mhz D-ADP was installed to the top rear of the turbine orientated vertically (upwards) and a long range low frequency (192kHz) single-beam ADP Nortek Continental was installed at the top rear of the turbine orientated backwards along the streamwise direction. Table 3.1 summarises the instruments used and their electrical and communication protocol setup.

Instrument	Voltage (VDC)	Communications Protocol	Provided Via
SBD	24	TCP/IP Ethernet	Turbine Ethernet Switch
AWAC	12	Serial RS422	Vlinx Ethernet Serial Server
Continental	18.5	Serial RS422	Vlinx Ethernet Serial Server

Table 3.1: Instrument power and communications overview on the 500kW machine.

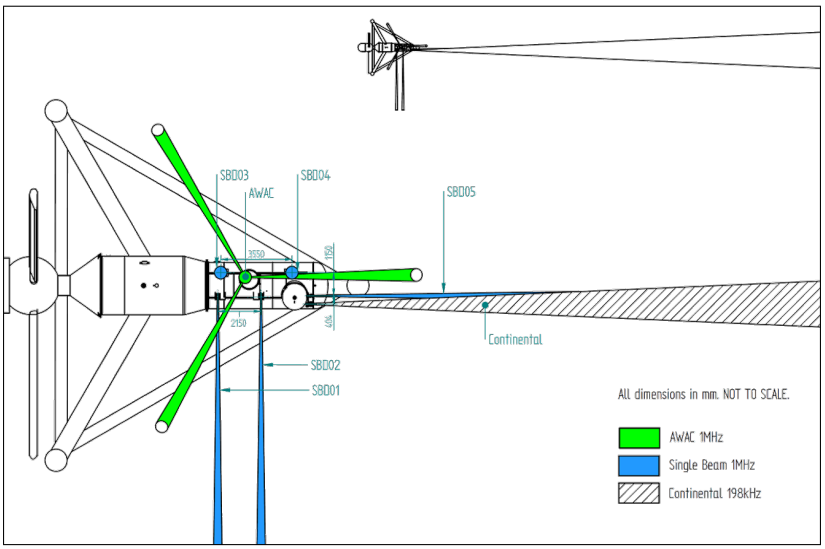

Figure 3.2: Instrumentation layout on the 500kW machine

3.1.3 Phase III Activities

In 2012 UoE instrumentation systems were installed and commissioned on the now available 1MW machine shown in Figure 3.3b.

The instrumentation methodology adopted involved two seabed mounted D-ADPs deployed either side of the turbine along the primary flow direction to provide depth profiles and um-impeded inflow (and reference) velocities to the turbine. On DEEPGEN IV three instrumentation mounting points were allocated: one on the top of the rear of the turbine nacelle - where the Edinburgh Subsea Instrumentation Platform 1 (ESIP-1) was installed, one on the rear of the turbine - where ESIP-2 was installed and a single sensor on the nose. Figure 3.6 highlights the locations of these platforms on DEEPGEN IV. ESIP-1 and ESIP-2 can be seen in Figures 3.5a and 3.5b. Figure 2.7 shows typical seabed mounted D-ADP campaigns photographs taken from on-board the deployment vessel the KML Severn Sea and from ROV footage.

(a) The 500KW DEEPGEN III being lifted by crane barge (not in scene).

(b) The 1MW DEEPGEN IV on stand.

Figure 3.3: The Alstom DEEPGEN turbines at Hatston Quay, Orkney

3.1.4 Deployment Site - Fall of Warness

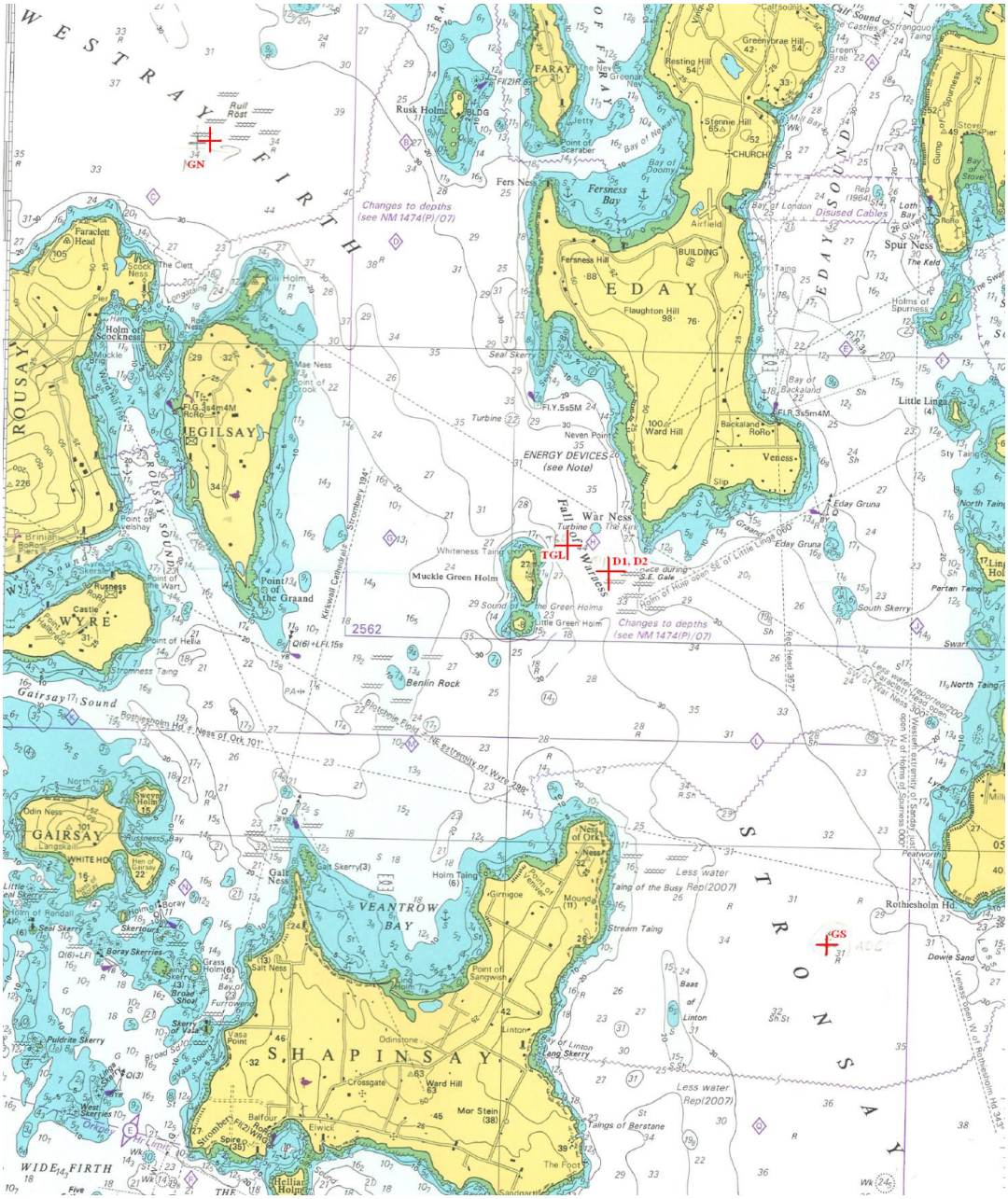

(a) Admiralty chart showing Westray Firth and Stronsay Firth. Device berth at EMEC tidal test site, Fall of Warness marked with red cross and labelled TGL.

(a) Photograph of ESIP-1 taken summer 2014 prior to deployment. Undergoing repair and maintenance and recently upgraded to allow mounting of C-ADP corner instruments.

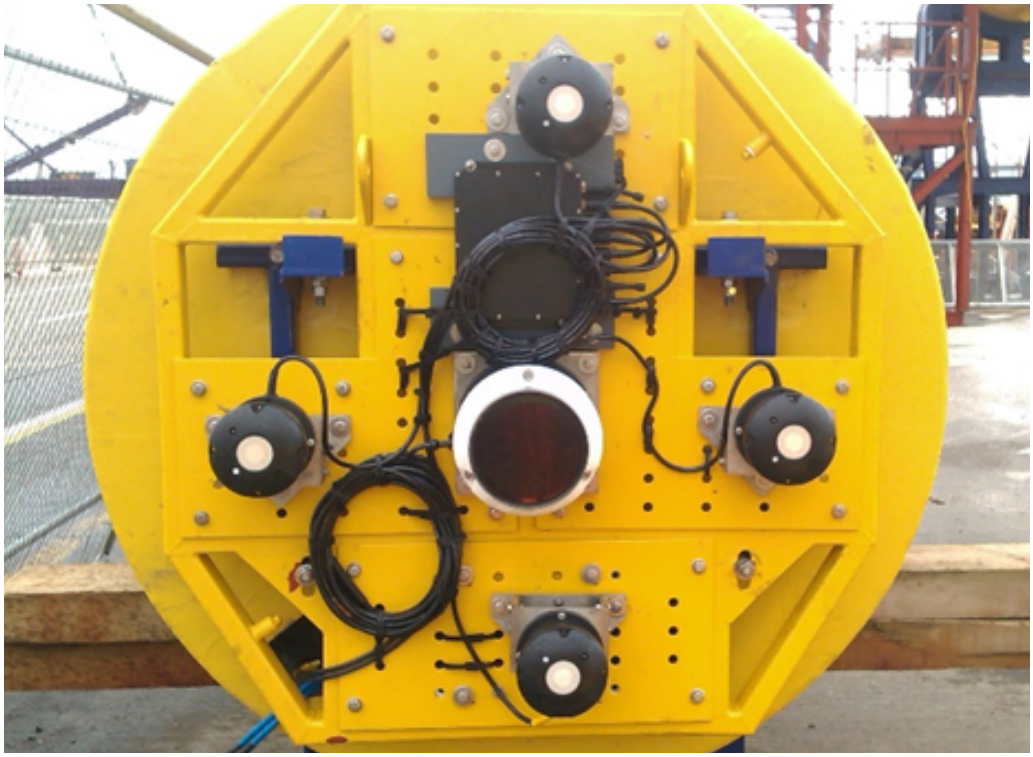

(b) Photograph of ESIP-2 taken summer 2014 ready for deployment.

Figure 3.5

Figure 3.6: Photograph of DEEPGEN IV being lifted by crane barge prior to deployment. Locations of the UoE instrument platforms, ESIP-1, ESIP-2 and the nose SBD identified.

3.1.5 Instrumentation Layout

ESIP-1

The following outline design specification for the Top Frame was developed:

- Tubular frame (originally S/S316 and later revised to glass-flake epoxy coated Carbon Steel)
- Dry Mass 600kg
- 6 mounting point system (M16 S/S A4 bolts)
- Instrumentation mounting plates (pre-drilled holes)
- Ability to remain electrically isolated from turbine if required
- Lifting eyes at four corners for easy removal for on-ground maintenance

Instrument layout varied between turbine deployments as instruments were replaced for maintenance or moved in order to complete specific tests. Hole patterns on ESIP-1 allowed instruments to be moved in 100 mm increments in the x or y directions. A representative instrument layout schematic is shown in Figure 3.7a. A standard configuration involved multiple SBDs (up to 4 on each axis) orientated in the transverse and vertical directions. Table 3.2 shows typical instrument positions and inter-instrument spacings on ESIP-1 for Turbine Deployment number 6.

ESIP-2

The following outline design specification for the Rear Frame was developed:

- Rectangular-section box frame (originally S/S316 and later revised to painted Carbon Steel)
- Dry Mass 215kg
- 4 mounting point system (M16 S/S A4 bolts)
- Instrumentation plates (pre-drilled holes)
- Ability to remain electrically isolated from turbine if required

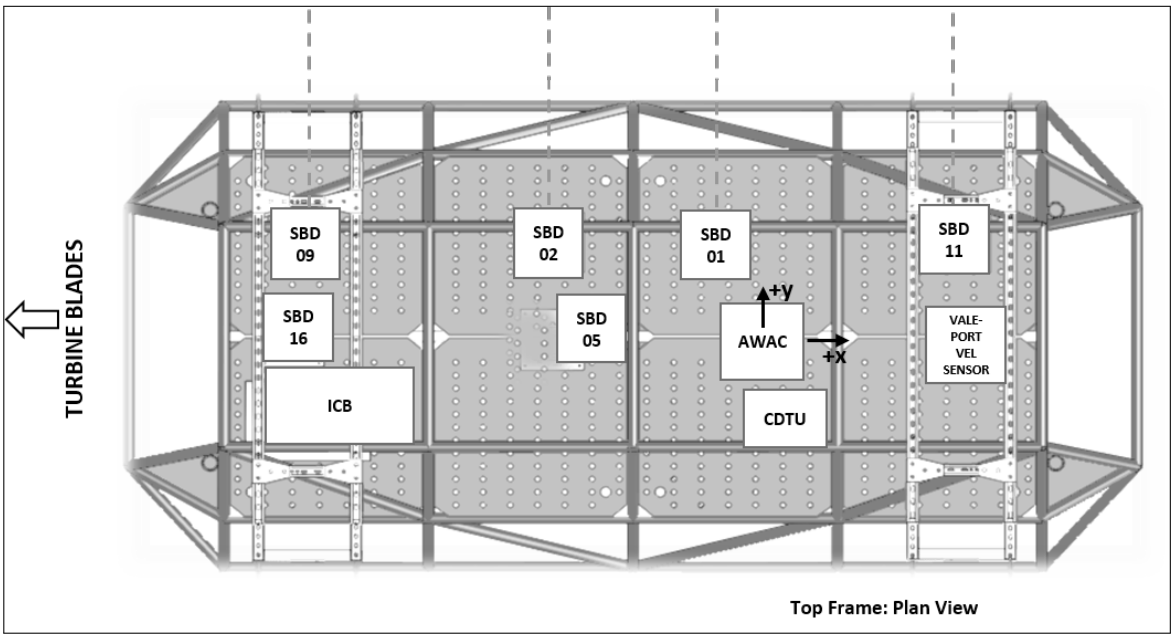

(a) Instrument layout on ESIP-1 during turbine deployment number 5.

Table 3.2: Table showing the position of instrumentation on ESIP-1 during turbine deployment number 6

Instrument	**X(mm)**	**Y (mm)**	**Z (mm)**	**Orientation**
AWAC	0	0	380	Up
SBD05	0	520	365	Up
SBD09	600	1565	105	Side
SBD02	600	765	105	Side
SBD01	600	-30	105	Side
SBD11	600	-840	105	Side
SBD15	-680	-870	495	Diagonally Up
SBD18	680	-870	495	Diagonally Up
SBD17	680	1650	495	Diagonally Up
SBD07	-680	1650	495	Diagonally Up
CDTU	-300	-130	-	-
VALEPORT	0	-980	900	-
ICB	-210	1370	-	-

- Lifting eyes at top 2 points for easy removal for on-ground maintenance

A CAD model of a candidate instrument configuration on the ESIP-2 is shown in Figure 3.8. The frame is positioned on the rear face of the turbine thruster housing.

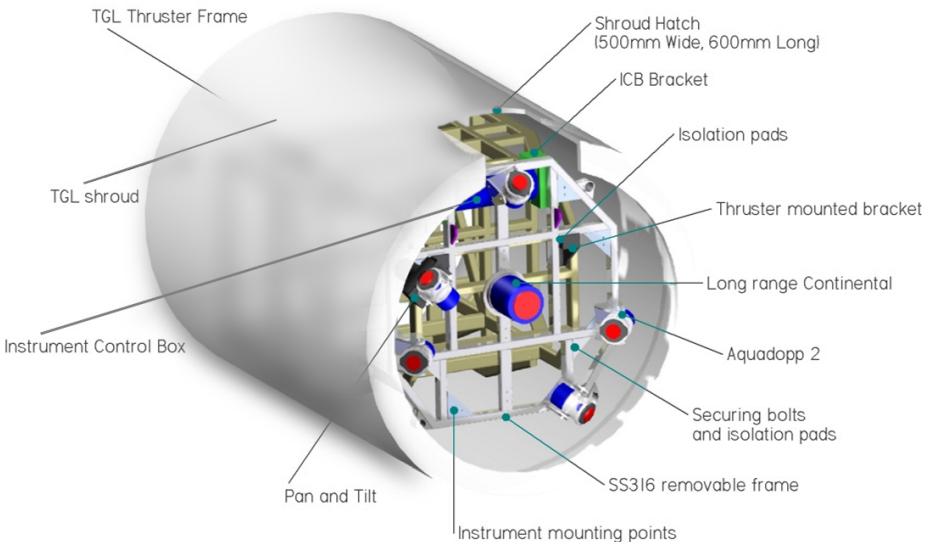

Figure 3.8: ESIP-2 (rear frame) positioning, outline instrumentation positioning and attachment method on 1MW turbine rear thruster unit.

3.1.6 Test Request Notices - Coordinating Multiple Measurement Campaigns

The entire ReDAPT test programme was conducted under the Test Request Notice (TRN) initiated whilst Rolls-Royce led the consortium. TRN's were used to track test specifications, test acceptance criteria and the interfaces between project partner's requirements and deliverables. Where the tests involved novel techniques the tests were updated iteratively as experience was gained targeting particular measurements.

An example of how UoE TRNs were logged, communicated to the team and updated is shown in Figure 3.9. Columns are shown which relate to top level detail (secondary level detail relates to the configuration of every instrument across the tests). Coordinating tests between the various sub-projects and project partners within a dynamic programme of work was a significant challenge.

Figure 3.10 shows an example of the visual aids created to help design tests within the consortium. Instrument/Turbine Coordinates are shown. Three dimensional models were also created and shared amongst the team. Figure 3.10a indicates lengthscales being targeted for ebb tides with the turbine reversed to flow; Figure 3.10b indicates lengthscales being targeted for ebb tides where the turbine has been yawed, broadside on to the incoming flow. In this scenario the instrument coordinate axis, Y (usually transverse), is aligned with the streamwise velocity. Figures 3.10c and 3.10d show similar scenarios for flood tides. These coordinate-system transforms: instrument (beam) to instrument/-turbine (Cartesian) to global (East, North, Up (ENU)) require careful consideration.

3.2 Data Analysis Methodology

This section outlines the processes applied to data from instrument to database. It includes a list of required software both proprietary and open-source. The following topics are covered:

- Data Acquisition and Conversion
- Data Transfer, Storage and Logistics
- Data Quality Control and Data Rejection
- Data Averaging
- Metric Production

3.2.1 Data Acquisition and Conversion

Data Time Synchronisation

A GPS driven Precision Time Protocol (PTP) master clock was installed on an antenna at EMEC's substation on Eday, Orkney. This connected via a matched RF cable to the Alstom servers and broadcast an extremely accurate timing signal to any PTP equipped application or hardware on the network. Timing accuracy was reduced local to the turbine due to the length of cable and multiple switches in the network but was stable to the microsecond level and appropriate for this application.

Data Acquisition from DEEPGEN IV

ESIP-1 and ESIP-2 were controlled in real-time remotely from UoE offices in Edinburgh over the internet. A server running a virtual machine with the Microsoft Windows XP operating system was installed within the Alstom equipment rack at the Eday substation. Via "remote desktop" connections could be made to the instrumentation on the turbine over the subsea fibre link. Hardware was communicated with via serial (AWAC, Continental) and TCP/IP (SBD) protocols through the use of MOXA serial servers over Ethernet and MOXA Ethernet unmanaged switches. The Nortek SBD instruments also made use of Nortek Ethernet switches contained in proprietary subsea enclosures. Data was logged to the virtual machine's HDD and routinely downloaded to UoE's secure servers.

Nortek SBD instruments were also controlled via bespoke Matlab code running on UoE servers across a Nortek supplied Application Program Interface (API). This feature enabled complex and semi-automated instrument configurations including time synchronisation to be executed.

Data Acquisition from Seabed

ADCP Workhorse Sentinel 600kHz deployments logged data to internal memory cards (4GB due to limits of the file system on these models). This data was downloaded using the PCMCIA slot in a legacy laptop running Windows ME (due to compatibility issues with all of the multiple modern Personal Computers (PCs) available. Multiple cards had either a) downloading issues or b) problems with subsequent data conversion. In this case the memory cards were reinserted into the ADCP units and the data downloaded over serial link from the instrument. This process could take up to 1 week.

/ CARRIED OUT	Acquired	Processed	WAITING ON ANALYSIS	#	TRN	TEST TYPE	CONFIG	CAN BE RUN OVERNIGHT?	TURBINE STATUS	TURBINE YAW
			WAIT	27	314,316	EBB PLANAR- LENGTHSCALE AND TI	FIXED	YES	OFF	R2E
			WAIT	28	314,316	FLOOD PLANAR - LENGTHSCALE AND TI	FIXED	YES	OFF	R2F
30/06/2014	DONE			29	339	AWAC POWER V SBD COUGH	FIXED	NO	LOWFLOW	
30/06/2014	DONE			30	339	AWAC POWER V SBD COUGH	FIXED	NO	LOWFLOW	
30/06/2014	DONE			31	339	AWAC POWER V SBD COUGH	FIXED	NO	LOWFLOW	
30/06/2014	DONE			32	339	WAWAC POWER V SBD COUGH	FIXED	NO	LOWFLOW	
30/06/2014	DONE			33	339	WAWAC POWER V SBD COUGH	FIXED	NO	LOWFLOW	
30/06/2014	DONE			34	339	WAWAC POWER V SBD COUGH	FIXED	NO	LOWFLOW	
01/07/2014	DONE			35	339	SBD(X) POWER VS AWAC HIGH	FIXED	NO	LOWFLOW	
01/07/2014	DONE			36	339	SBD(Y) POWER VS AWAC HIGH	FIXED	NO	LOWFLOW	
01/07/2014	DONE			37	339	SBD(Z) POWER VS AWAC HIGH	FIXED	NO	LOWFLOW	
03/07/2014	DONE			38	339	SBD(X) POWER VS WAWAC HIGH	FIXED	NO	LOWFLOW	
03/07/2014	DONE			39	339	SBD(Y) POWER VS WAWAC HIGH	FIXED	NO	LOWFLOW	
03/07/2014	DONE			40	339	SBD(Z) POWER VS WAWAC HIGH	FIXED	NO	LOWFLOW	
04/07/2014	DONE			41	334	PARALLEL WIDE SPACE	LOOP	NO	LOWFLOW	
04/07/2014	DONE			42	334	PARALLEL MULTI-COUGH	LOOP	NO	LOWFLOW	
01/07/2014	DONE			43	334	PARALLEL NARROW-MID-SPACED	LOOP	NO	LOWFLOW	
06/07/2014	DONE			44	334	PARALLEL WIDE SPACE	LOOP	NO	BROADSIDE	S2E
03/07/2014	DONE			45	334	PARALLEL MULTI-COUGH	LOOP	NO	BROADSIDE	S2E
06/07/2014	DONE			46	334	PARALLEL NARROW-MID-SPACED	LOOP	NO	BROADSIDE	S2E
			WAIT	47	314,316	EBB PLANAR- LENGTHSCALE AND TI	FIXED	YES	BROADSIDE	S2E
			WAIT	48	314,316	FLOOD PLANAR - LENGTHSCALE AND TI	FIXED	YES	BROADSIDE	S2F

Figure 3.9: A sample of the TRN methodology/spreadsheet and a small subset of combinations of instrumentation and turbine configurations.

Data Conversion

Data recorded in proprietary formats were converted to Matlab(multiple versions from 2011b onwards) either via custom scripts or supplied exporting features of the software. A summary of these processes is shown in Table 3.3.

Table 3.3: Overview of instrument file types and conversion software required.

Instrument	Mode	Software Used	Original Format	Converted to Matlab via
Nortek SBD	Current	Nortek MIDAS	.ntk, binary	Nortek MIDAS
Nortek AWAC	Current	Nortek AWAC	.wpr, binary	Nortek MIDAS
			.wpa, ASCII	Custom Matlab Code
Nortek AWAC	Wave	Nortek Quickwave	.wpr, binary	Nortek Quickwave & Custom Matlab Code
Nortek Continental	Current	Nortek Continental	.wpr, binary .wpa, ASCII	Custom Matlab Code
RDI Workhorse ADCP	Current	RDI .exe Tools RDI winADCP	.000, binary	Custom Matlab Code .
RDI Workhorse ADCP	Wave	Wavesmon	.000, binary	Custom Matlab Code

RDI ADCP to Matlab [1]

[1] RDI conversion to Matlab made us of R. Pawlowicz Matlab code, RDADCP from www.eos.ubc.ca/~rich/index.html#RDADCP

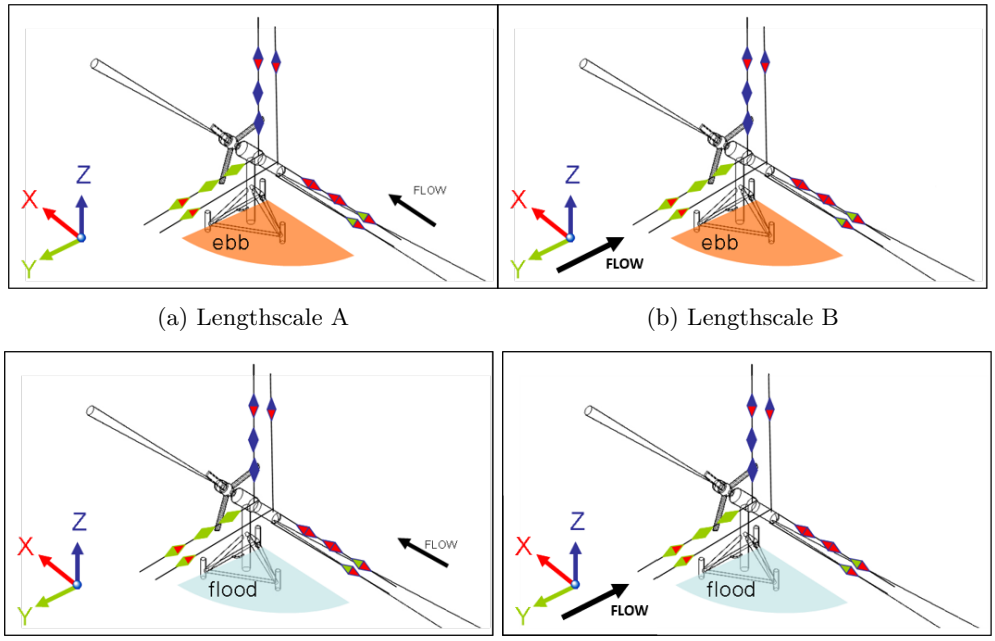

(a) Lengthscale A (b) Lengthscale B

(c) Lengthscale C (d) Lengthscale D

Figure 3.10: TRN Planning Schematics: Target Lengthscales

3.2.2 Coordinate Transformation

All instruments were set to collect data in the transducer beam coordinate system, i.e., without any on-board coordinate system transformations.

D-ADP (ADCP Workhorse Sentinel)

The coordinate transforms used to convert ADCP beam-measured velocities to velocities in E,N,U coordinates are provided in the RDI coordinate transform document, [119].

D-ADP (AWAC)

The coordinate transforms used to convert AWAC beam-measured velocities to velocities in E,N,U coordinates are provided in the Nortek coordinate transform note, [81].

SB-ADP (SBD and Continental)

No coordinate transformations were applied at the instrument level for single beam devices. However, a log of instrument orientation time-series (instruments were moved, repaired, replaced etc. throughout the campaigns) was produced. This information in addition to the turbine heading angle was applied in post-processing to filter data into streamwise, transverse and vertical directions.

3.2.3 Hardware Reported Error Code Rejection

Where instruments reported error values in the collected data this data was replaced by markers: 'Not-a-Number' (NaN) values. Where bad data points were isolated i.e., found between good neighbouring values, these data points were linearly interpolated.

3.2.4 Out of Range Velocity Rejection

Velocities of magnitude greater than 20 ms_{-1} were rejected and replaced with NaN values. Isolated rejected values were linearly interpolated.

3.2.5 Low Amplitude Rejection

Returned "amplitudes", the ADCPs returned echo Intensity and a measure of signal strength reflected to the acoustic transducer, below a value of 75 were rejected and replaced with NaN values. Isolated rejected values were linearly interpolated. Low amplitudes occur when insufficient scatterer density was present in a measurement volume or due to signal attenuation with range.

3.2.6 Median Absolute Deviation Rejection

A median absolute deviation (mad) routine [120] was applied to 5 minute detrended subsections of the velocity data. Velocities having a magnitude greater than 2.5 times this returned median absolute deviation value were rejected [121]. Isolated rejected values were linearly interpolated.

$$u_{mad} = \text{median}(abs(u - \widetilde{u})) \tag{3.1}$$

where u_{mad} is the median absolute deviation of the sub-set of velocity data, u, and $\widetilde{u}$ is the median of u.

3.2.7 Bad Value Combinations

Remaining NaN values are carried through to post-processing metric generation. At this stage, prior to any metric being evaluated, the percentage of NaN to real values is calculated. For mean velocity reporting and turbulence intensity a 95% threshold was applied. For lengthscale analysis and any spectral analysis any individual data 5 minute time series containing NaN were rejected.

3.2.8 QC Methodology Work is Ongoing

As of 2016, developing a standardised QC methodology across the various instrument types and many instrument configurations is ongoing.

3.2.9 Stationarity Period Selection

Detailed sensitivity studies are being undertaken in the area of stationarity period selection and its impact on returned metrics. Preliminary results agree with [48] and 5 minute ensemble averages have been used throughout.

3.2.10 Detrending Method Selection

The time series of velocity measurements and other relevant quantities display trends of multiple time scales. These may be seasonal, diurnal, wave-induced or turbulent, among others. Trends whose time scales do not pertain to the investigated phenomena are a cause of non-stationarity in signals, and have to be removed prior to analysis. This also allows for the analysis of other sources of variation in the signal. Here, detrending is used in the calculation of mean values and fluctuating time series, $\overline{u}$ and u.

Three detrending methods were compared; namely linear-fit, constant and moving average using sample data from seabed mounted D-ADP data sampled at 0.5 Hz and binned into subsets with length equal to the desired stationarity period. The constant detrending removes the mean value from the subset, while the linear-fit detrending removes the best straight-line fit. The moving-average applies a moving average filter with a defined span.

Firstly, the resulting mean velocities were compared. The stationarity period used is 5 minutes as presented in Section 3.2.9. The detrending method has an impact on the mean flow value. As the mean flow is widely used in the derivation of turbulent metrics these differences propagate to other metrics.

Secondly, the effect of detrending methods on impact on the turbulence intensities was investigated. Differences were computed for both ebb and flood flows, for three different ranges of streamwise velocity (namely [1:2] m/s, [2:2.7] m/s, and [2.7:max] m/s), for streamwise, transverse and vertical turbulence intensities. Results for the streamwise direction are reported in Table 3.4. TI values of a subset of this data is shown in Figure 3.11 which shows the differences decrease with increasing velocity. The negative signs indicate that the linear detrending gives lower turbulence intensities than the other methods.

In conclusion, it was found that the flow metrics depend on the chosen detrending method:

- The differences in turbulence intensity decrease with increasing velocity
- The differences depend on the investigated direction (streamwise, transverse or vertical)
- Linear detrending gives lower turbulence intensities than the other two detrending methods

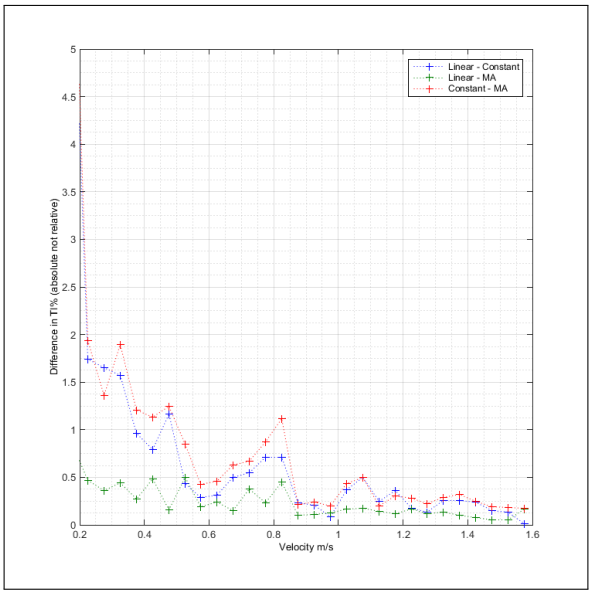

Figure 3.11: Differences seen in TI using varying detrending methods as a function of velocity

Table 3.4: Assessment of detrending impact on a flow metric, Streamwise Turbulence Intensity.

Streamwise		**Ebb**			**Flood**		
t stat =5 min **Detrending Method**	**Vel bin (m/s)**	**1<u<2**	**2<u<2.7**	**2.7<u**	**1<u<2**	**2<u<2.7**	**2.7 <u**
Constant	**TI (%) std**	11.3 3.2	8.9 1.3	8.7 1.0	9.91 2.1	9.5 1.1	9.4 1.1
	Δ TI (%)	-0.5	-0.2	-0.2	-0.5	-0.3	-0.3
	No. samples	2280.0	2665.0	670.0	2834.0	1828.0	254.0
Linear	**TI (%) std**	10.7 3.0	8.7 1.2	8.6 1.0	9.4 2.1	9.2 1.1	9.14 1.0
	Δ TI (%)	0.0	0.0	0.0	0.0	0.0	0.0
	No. samples	2280.0	2665.0	670.0	2834.0	1828.0	254.0
MA	**TI (%) std**	11.0 3.0	8.9 1.2	8.8 1.0	9.7 2.1	9.4 1.1	9.4 1.0
	Δ TI (%)	-0.3	-0.2	-0.2	-0.3	-0.3	0.2
	No. samples	2264.0	2670.0	656.0	2836.0	1833.0	256.0

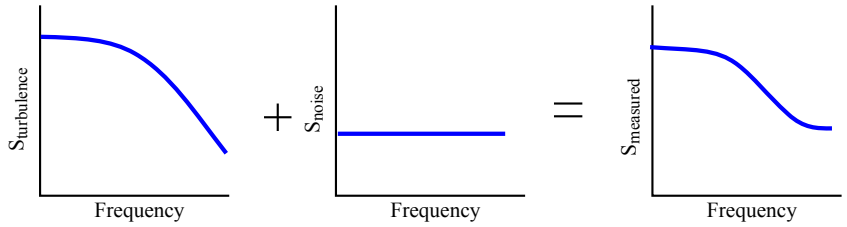

Figure 3.12: Illustration of the components of a measured spectrum. Adapted from [6].

3.2.11 Instrument Noise and Noise Correction Factors

In analysis of tidal sites, velocity metrics can be defined as being the sum of a mean value (that can be considered stationary over a period of minutes) and a fluctuating (turbulent) component [45, 48]:

$$u = \overline{u} + u' \tag{3.2}$$

where $\overline{u}$ is the mean velocity over a period of assumed stationarity (T_{stat}) as discussed in section 3.2.9, and u' is the velocity perturbation about this mean value.

Noise can be divided into two types: random error (increased signal variance), ϵ', and systematic error (bias), $\bar{\epsilon}$. This makes analysis of noise in turbulent flows particularly difficult as bias and mean velocity values are amalgamated, as are random error with turbulence induced fluctuations. Thus any given measurement of u can be described as a sum of four components, with both error and physical subdivisions having a mean and fluctuating element:

$$u = \overline{u} + u' + \bar{\epsilon} + \epsilon' \tag{3.3}$$

Spectral Slope Fitting Method

There are many factors that could introduce random error to a Doppler profiler. These include: density of back-scatterers in the flow, poorly correlated signal returns, uncertainty in measuring the Doppler-shift, high spatial variability of the flow and electrical noise [122]. **For more detailed information on the following processes and the relationship between the random error with instrument orientation, flow speed and electrical noise refer to the ReDAPT PhD thesis [123].**

In order to quantify the variance that is attributable to random error (σ^2_{noise}), a method developed by [124] and [6] was applied for the first time to the newly available SBD instruments. The technique uses spectral analysis and the principle that the variance of the measured velocity ($\sigma^2_{measured}$) can be sub-divided such that:

$$\sigma^2_{measured} = \sigma^2_{physical} + \sigma^2_{noise} \tag{3.4}$$

where $\sigma^2_{physical}$ is the physical (i.e. attributable to velocity perturbations) component and σ^2_{noise} is the noise component, as per the principle of Equation 3.3.

In order for this theoretical method to correctly fit the spectra of the measured data, two assumptions must be valid: That the noise is spread evenly across the frequency range and that the flow measured, and thus $\sigma^2_{physical}$, is turbulent.

In the turbulent flows of the Fall of Warness the frequency spectrum of the velocities should follow the energy cascade as detailed in Section 2.4.1. At the scales measured by these devices at this site, the kinetic energy of the fluctuations would be expected to show evidence of the inertial sub-range, i.e. the energy varying with frequency (f) with a $f^{-5/3}$ slope [3]. Thus the transition from the $f^{-5/3}$ slope to the 'noise-floor', where (as per the first assumption) the gradient is zero, can be easily identified. This is illustrated in Figure 3.12. The area under this noise floor represents the variance of the velocity due to noise as per Parseval's theorem, which can be used to correct turbulence intensity (I) measurements via the following equation [44]:

$$I_u = \frac{\sigma_{measured}}{\bar{u}} = \frac{\sqrt{\langle u'^2 \rangle - \sigma^2_{noise}}}{\bar{u}} \tag{3.5}$$

where $\sigma_{measured}$ is the standard deviation of the velocity u. Angled brackets denote the expected value over a period of stationarity (T_{stat}).

These two slopes for the theoretical sources of perturbation in the velocity time series can be summed together:

$$S_{measured}(f) = c_i \cdot f^{-5/3} + N \tag{3.6}$$

where $S_{measured}(f)$ is the Power Spectral Density (PSD) as a function of frequency (f), c_i is a constant (which is theoretically a function of the turbulent dissipation rate ϵ) and N is the PSD due to random error.

The theoretical two-line curve given in Equation 3.6 was fitted to the data by method of least squares linear regression. This is based on minimising the error (ΔS) based on the difference between the measured and fitted theoretical slope ($S_{theory}(f)$). This can then be solved numerically for c_i and N:

$$\Delta S = S_{measured}(f) - S_{theory}(f) \tag{3.7}$$

$$= S_{measured}(f) - c_i \cdot f^{-5/3} + N \tag{3.8}$$

$$E(N, c_i) = \sum_{i=1}^{f_n} \Delta S \tag{3.9}$$

The variance due to noise can be estimated by calculating the area under the N line across the frequency range:

$$\sigma^2_{noise} \approx N \cdot f_{Nyquist} \tag{3.10}$$

An example of this method for a single 256 second SBD data set collected at a sample rate of 2 Hz is given in Figure 3.13. It highlights the two individual curve components, the instrument noise and the turbulent slope, as well as the combined summation. The region used for the fit is highlighted between frequencies of 10^{-1} Hz and 1 Hz.

Noise Response to Velocity

Results are further binned by velocity range as users of Doppler sensors in tidal environments have reported random error increasing with flow velocity [6,48,73]. The relationship between mean streamwise velocity ($\overline{u}$) and σ^2_{noise} is assessed by calculating the mean PSD over a minimum of 20 sample sets for each 0.1 ms^{-1} velocity range as measured by an upstream D-ADP at equivalent depth in the channel.

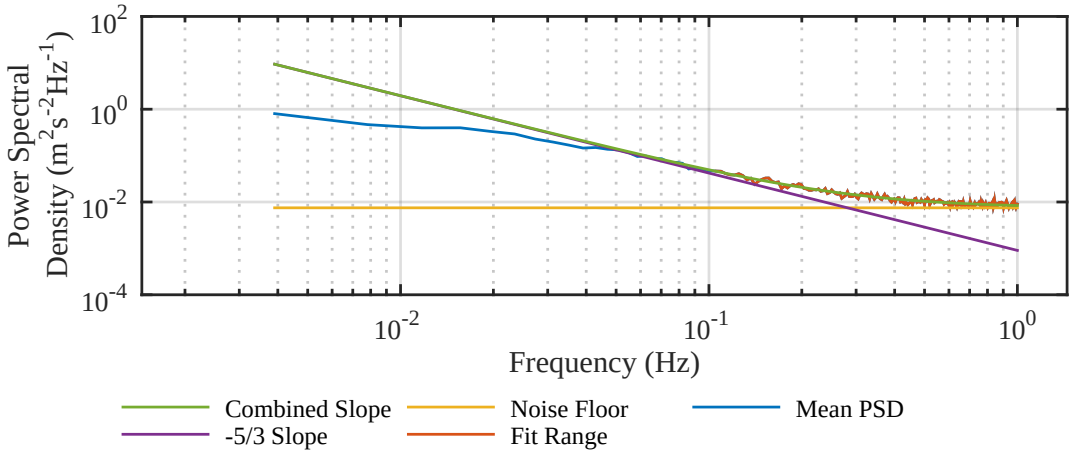

Figure 3.13: Example of the spectral curve fitting method of [6], highlighting the region used for the fit and the individual curve components.

Noise Response to Sensor Orientation

The process was repeated for three sensors: one mounted facing the onset flow, one normal to the flow oriented horizontally and one orientated vertically towards the surface.

Thus the relationship between σ^2_{noise} and flow velocity and sensor orientation can be assessed, producing an estimate for the noise correction factor, Equation 3.5, for a range of flow conditions.

Selected Noise Correction Factor

Given that the Doppler noise estimate plays a significant role in estimations of Turbulence Intensity, which manifests physically as fatigue inducing loading, conservative correction factors for the x,y,z directions were subsequently applied to data. Figure 3.46 shows the values used.

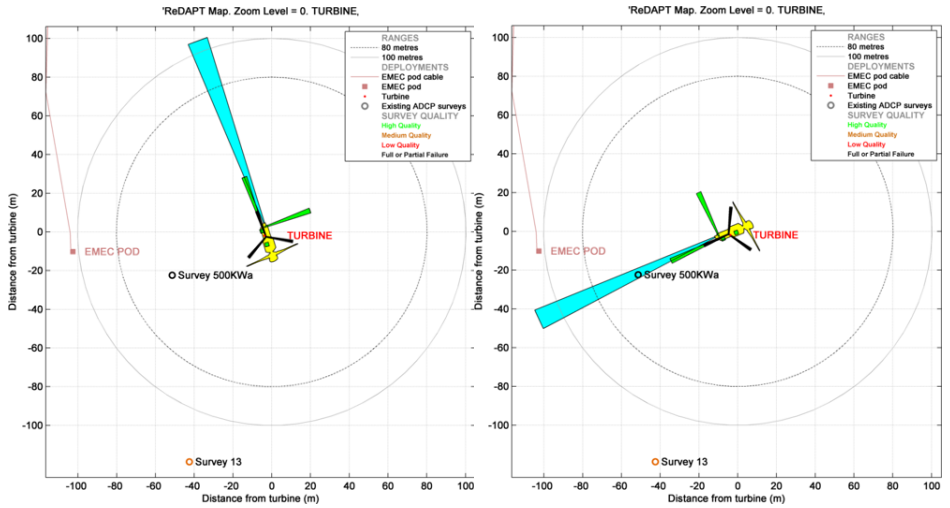

(a) Reversed to Flood

(b) Broadside to Flood

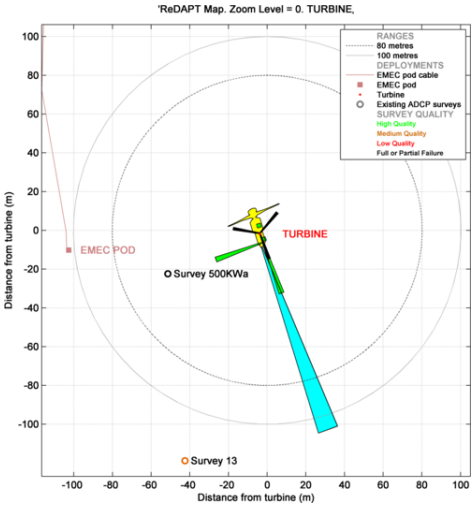

(c) Reversed to Ebb

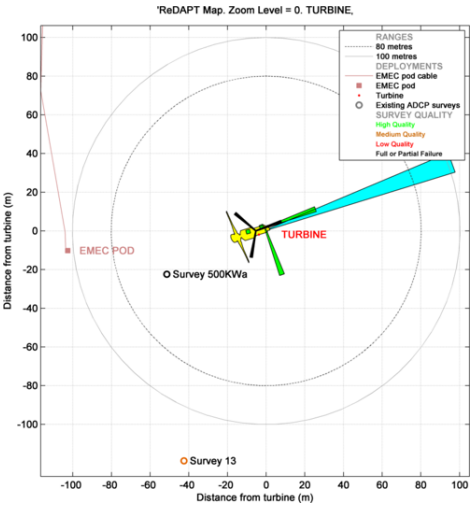

(d) Broadside to Ebb

Figure 3.14: Identified Test Orientations using Turbine's yaw capabilities to position ESIP-1 and ESIP-2 into desired tides.

3.3 Measuring Waves at the Fall of Warness

It was agreed at programme onset that wave measurement would form an auxiliary and non-core component of the ReDAPT measurement campaign. It transpired that a large proportion of early to mid-campaign data acquisition was carried out in the summer months due to programme schedule, logistics and technical issues. Following completion of core current data collection in October 2014, supplementary data was acquired in volume in the subsequent winter months through to January 2015. During these months several storms were observed for the first time and the impact of waves in these conditions on the data set became apparent.

Due to the non-continuous acquisition of wave data and low prioritisation of analysis previous to this deployment and the requirement to re-analyse the data set including wave data, significant resource has been expended assimilating an auxiliary and in places patchy data stream with the core tidal current data. The following section describes this process of assimilation.

For clarity, much of the following activity goes beyond the scope of the original report and will be continued by the authors in 2015.

Table 3.5: Summary of wave measurement methods.

Instrument	**Measurement Principle**	**Description**
SB-ADP (SBD) Direct	Surface detection via high amplitude return	Instrument vertically orientated on Turbine Fast sample rates for waves (4Hz) Real-Time Data Low Spatial Resolution (0.4m) Point source (no directional data).
Div-ADP Vertical Beam (AWAC) Direct	Surface detection via high amplitude return	Instrument vertically orientated on Turbine Fast sample rates for waves (2Hz) Low-Delay Data Good Spatial Resolution (0.1m) Point source (no directional data)
Div-ADP Array (AWAC) Combination	Surface detection via high amplitude return inc. Array based processing to give full directional spectra	Instrument vertically orientated on Turbine Fast sample rates for waves (2Hz) Low-Delay Data Use of this mode affects ability to gather current data. Good Spatial Resolution (0.1m) Array gives directional data
Div-ADP Array (ADCP) Indirect	Array based processing to give full directional spectra	Instrument vertically orientated on Seabed Fast sample rates for waves (2Hz) No Real-Time Data (unless hard wired) Use of this mode affects ability to gather current data.

Continued from previous page

WAMOS Indirect	Radar backscatter transformed to surface elevation maps	Radar located on land (Eday) overlooking deployment site. Preliminary use of instrument (not calibrated) Wide area coverage Long-term data set
SB-ADP mounted Pressure Gauge (SBD) Indirect	Surface detection via transform from pressure to surface elevation via linear wave theory.	Less complex measurement principal than velocimetry. Fast sample rates for waves (2Hz) Real-Time Data High resolution (cm) Point source (no directional data) Highly sensitive to depth via wave orbital velocity attenuation.
ADCP mounted Pressure Gauge (SBD) Indirect	Surface detection via transform from pressure to surface elevation via linear wave theory.	Less complex measurement principal than velocimetry. Fast sample rates for waves (2Hz) No Real-Time Data (unless hard wired) High resolution (cm) Point source (no directional data) Highly sensitive to depth via wave orbital velocity attenuation.
HF Turbine mounted Pressure Gauge Indirect	Surface detection via transform from pressure to surface elevation via linear wave theory.	Less complex measurement principal than velocimetry. Very fast sample rates for waves (10Hz) High resolution (¡cm) Real-Time Data Point source (no directional data) Highly sensitive to depth via wave orbital velocity attenuation.

3.3.1 Acoustic Surface Tracking with Vertical ADP

Multiple SBDs were installed on both the 500KW and 1MW via ESIP-1 in a vertical orientation wrt turbine on quayside stand. Initially these instruments were solely used for flow measurement in the vertical direction. Inspection of the data later revealed a strong correlation between large gradients in amplitude return and the air-water interface (sea surface). Thereafter, where possible within a specific test programme, vertically mounted SBDs were programmed to have an extended listening range tp provide sufficient head-room of range in order to pick up the acoustic surface return from the surface. An example of SBD AST is shown in figure 3.15.

Outline Processing Steps

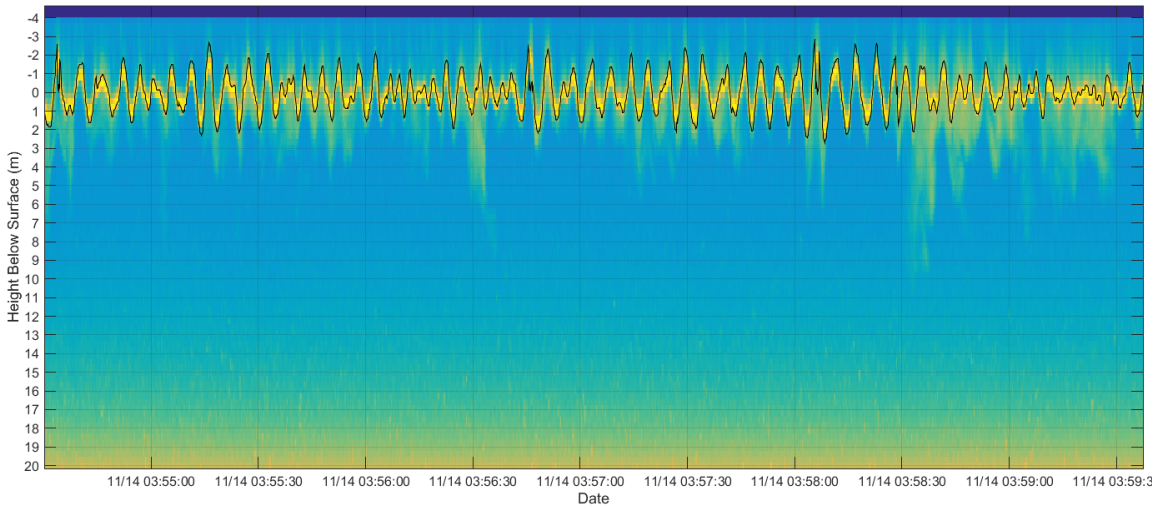

Figure 3.15: Signal Amplitude with post-processed surface elevation overlaid (black).

- Raw instrument data of one hour duration converted from proprietary format to MATLAB format.
- Data collated to 24 hour sections.
- 24 hour sections QC'd.
- Data re-categorised by instrument configuration (varying bin size, sample rate etc.).
- Image processing routines used to select best local fit to air-water interface.
- Time series extracted.
- Spectral analysis conducted.
- Data collated and interpolated onto standard database 5 minute grid.

3.3.2 Combined Mode - Acoustic Surface Tracking with Vertical ADP and Wave Velocities

A multi-beam D-ADP (Nortek AWAC 1MHz) was installed on to the 500KW turbine and the ESIP-1 on the 1MW turbine. This was remotely controlled over the internet via serial over ethernet extenders. Once high priority tidal current tests were complete this instrument became available to conduct wave studies.

Whilst wave data is updated and available visually on the instrument's software GUI, post-processing of recording files is required to extract wave data for further analysis. The software is a separate purchase. Data shown in 3.21 is the direct output from the Nortek software using their proprietary routines [125,126]. Custom algorithms have been developed in MATLAB to post-process Nortek wave software outputs and indeed to produce wave parameters from the raw data itself, thus circumventing the proprietary method. This work is outside of the scope of this document and is not reported herein.

3.3.3 Pressure Gauge

Alstom installed a pressure gauge to the 1MW turbine at a depth of 21.5m and following the winter storms of 2014/2015 supplied this long-running and robust data set. Data was supplied at a sample rate of 10Hz.

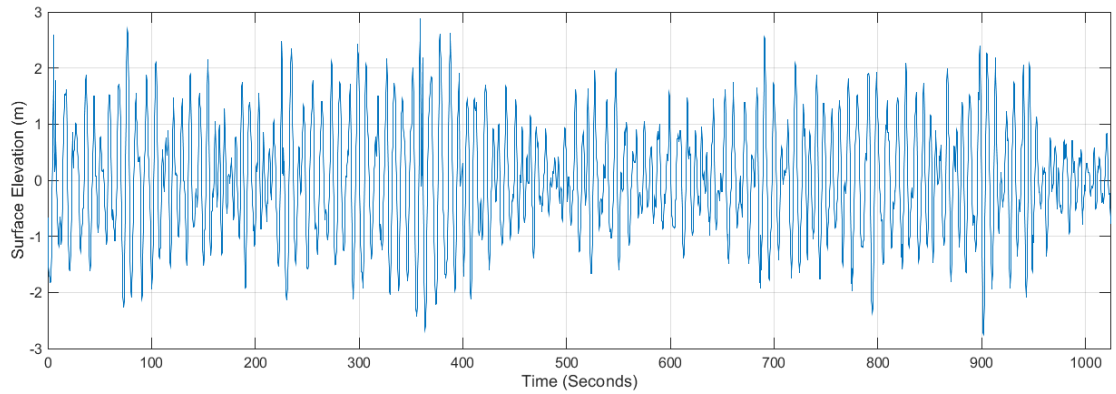

(a) Result of image processing: moving surface tracking, edge detection, filtering

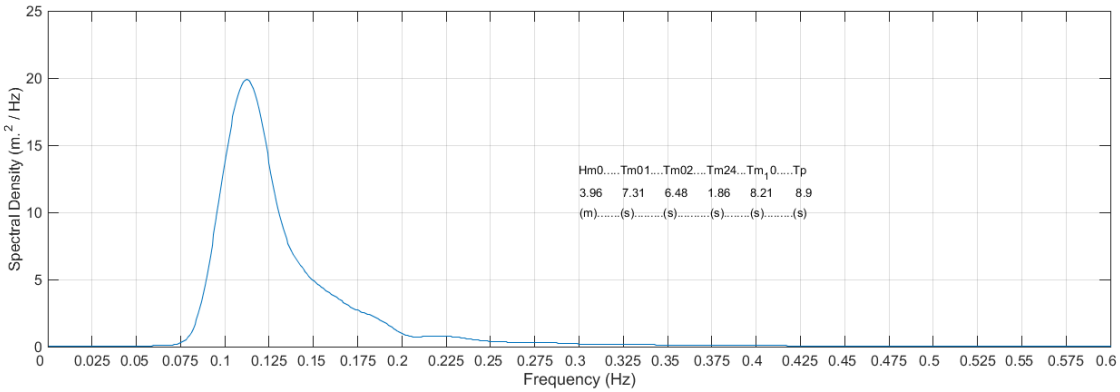

(b) Spectral Analysis to provide wave spectral parameters.

Figure 3.16: A figure

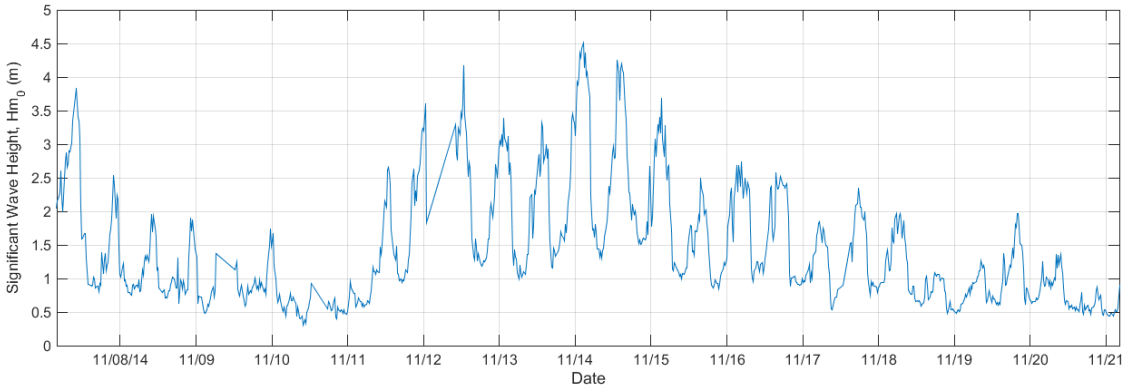

(a) Individual spectral analysis collated into database signal time-series of Hm_0.

Figure 3.17: A figure

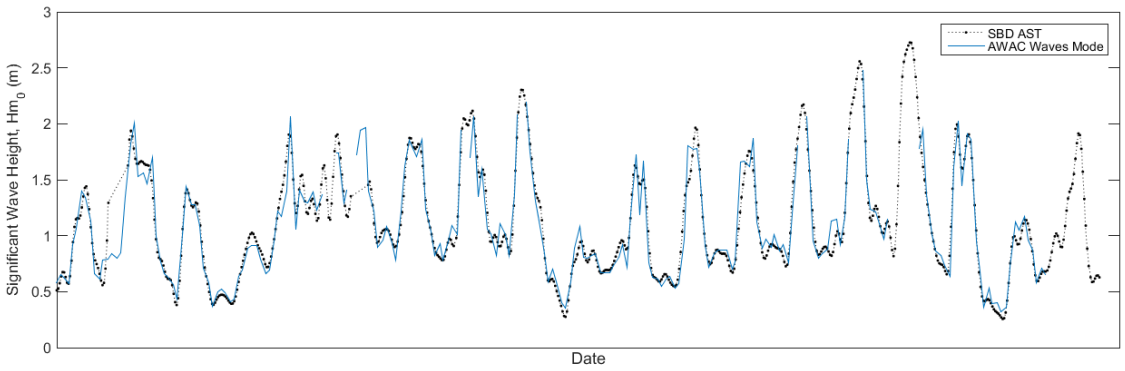

(a) Time series of W-AWAC vs SBD-AST significant wave height, H_m0

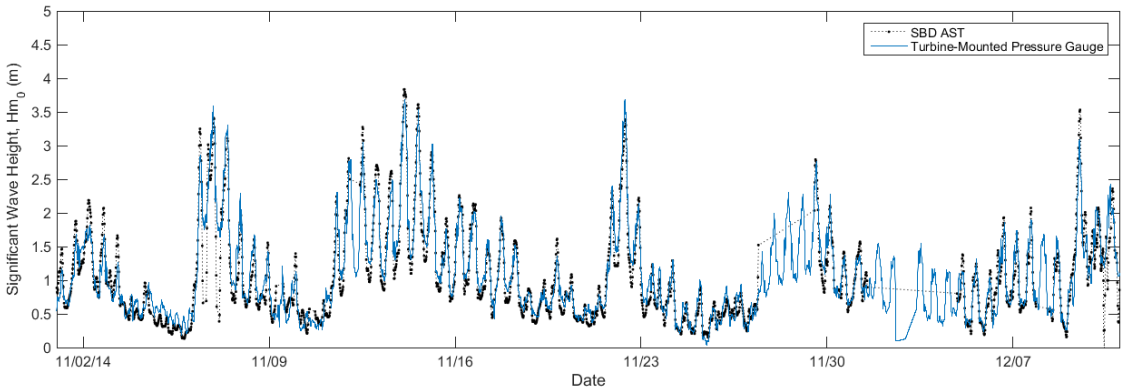

(b) Time series of Pressure Gauge vs SBD-AST significant wave height, H_m0

Figure 3.18: Comparison of W-AWAC and SBD-AST measurements of significant wave height

Outline Processing Steps:

- Alstom supplied time-stamp-corrected pressure gauge data at sampling rate of 10Hz.
- Transfer function applied to pressure data to correct for varying attenuation of pressure rates with depth and frequency.
- Additional transfer function applied to correct for local time-averaged site parameters i.e., wave direction and swell, tide direction and current velocity.
- Constant gain and offset applied across entire set calibrated against SBD-AST.

Equation 3.11 was used to transform pressure spectra to wave spectra.

$$T = \left(\frac{cosh(kd)}{cosh(kd_{pg})} \right)^2 \tag{3.11}$$

where d is the total water depth in metres, d_{pg} is the depth of the pressure gauge in metres and k is the wavenumber in rad/m calculated through an iterative approximation of the dispersion relation [127] shown in 3.12.

$$w^2 = gk\, tanh(kd) \tag{3.12}$$

where w is the wave frequency in rads/s and g is acceleration due to gravity.

An experimental additional transfer function which takes into account local instantaneous and local averaged wave and current parameters is under development. The difference in agreement between un-corrected and corrected wave spectra obtained via pressure gauges is shown in figure 3.27.

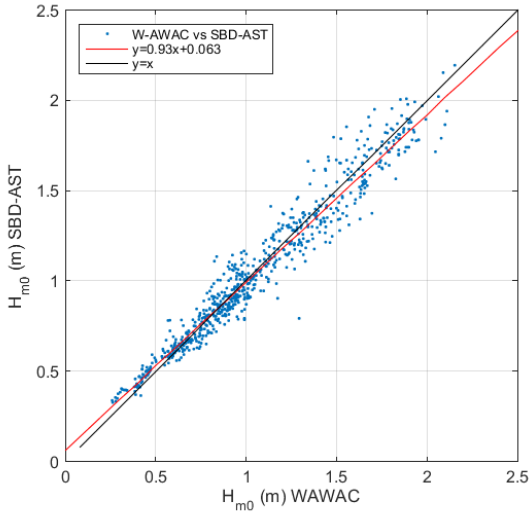

(a) Comparison of W-AWAC vs SBD-AST significant wave height, H_m0 and best-fit

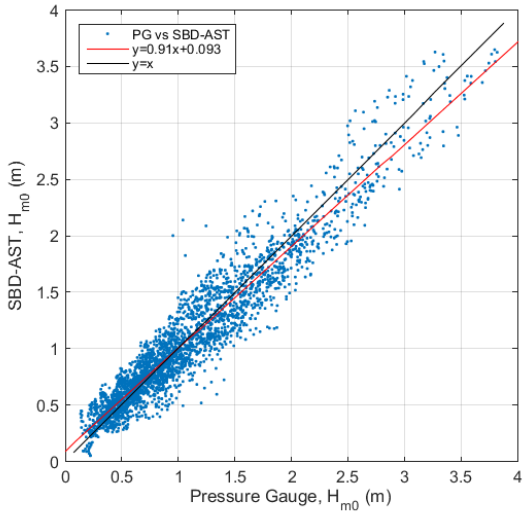

(b) Comparison of Pressure Gauge vs SBD-AST significant wave height, H_m0 and best-fit

Figure 3.19: Comparison of W-AWAC and SBD-AST measurements of significant wave height

3.4 Velocimetry: Wave Orbital Velocity to Wave Spectra

Outline Processing Steps

- Hourly to 24 Hour
- QC
- Upsampling (Interpolation) and Filtering
- Low Frequency Surface Tracker Applied
- Velocity Bin Selection (moving in time)
- Velocity to Wave Spectra via DIWASP
- Transfer Function as per PG

An ADCP sampling rate of 0.5Hz was the primary configuration for most of the turbine-proximal deployments. This resulted from a trade-off between deployment duration and the battery consumption and on-board storage capacity of the instrument. Given how difficult it proved to align turbine operating point, tide and wave system point and the CFD simulations this low sampling rate, whilst sub-optimal for turbulence and wave studies, proved necessary in other components of the ReDAPT test programme. It was unknown if this minimal sampling rate could provide wave information.

3.5 Combined Wave Measurements

Wave measurements extracted from available instrumentation between 2013 and 2015 are assigned to 5-minute average values within the ReDAPT database with the following ranking:

- 1) AWAC in Waves Mode
- 2) Vertically Orientated SBD
- 3) Wave Orbital Velocity from turbine-upstream and turbine-downstream ADCP.
- 4) Calibrated Pressure Gauge
- Transfer Function as per PG

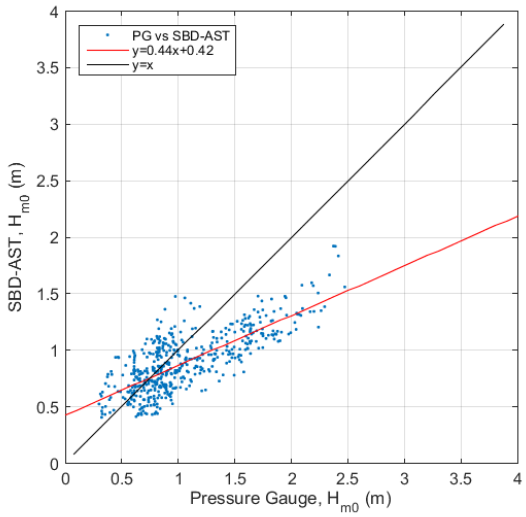

(a) Comparison of W-AWAC vs SBD-AST significant wave height, H_m0 and best-fit

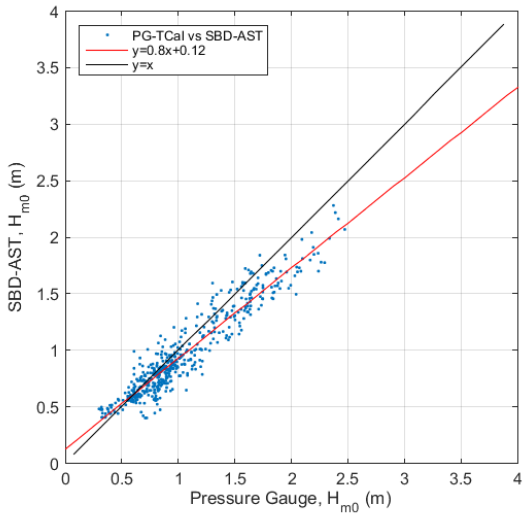

(b) Comparison of Pressure Gauge vs SBD-AST significant wave height, H_m0 and best-fit

Figure 3.20: Comparison of Pressure Gauge and SBD-AST measurements of significant wave height under different pressure gauge calibration routines.

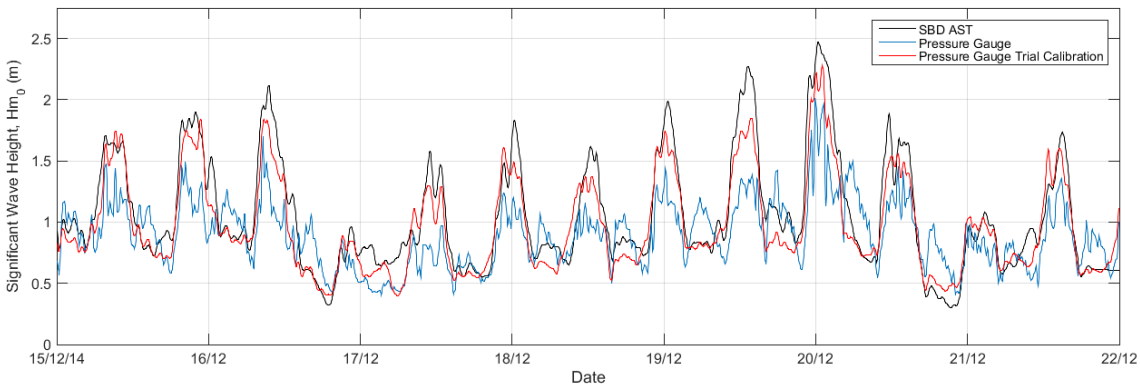

(a) Time series of Pressure Gauge vs SBD-AST significant wave height, H_m0

Figure 3.21: Comparison (time-series) of Pressure Gauge and SBD-AST measurements of significant wave height under different pressure gauge calibration routines.

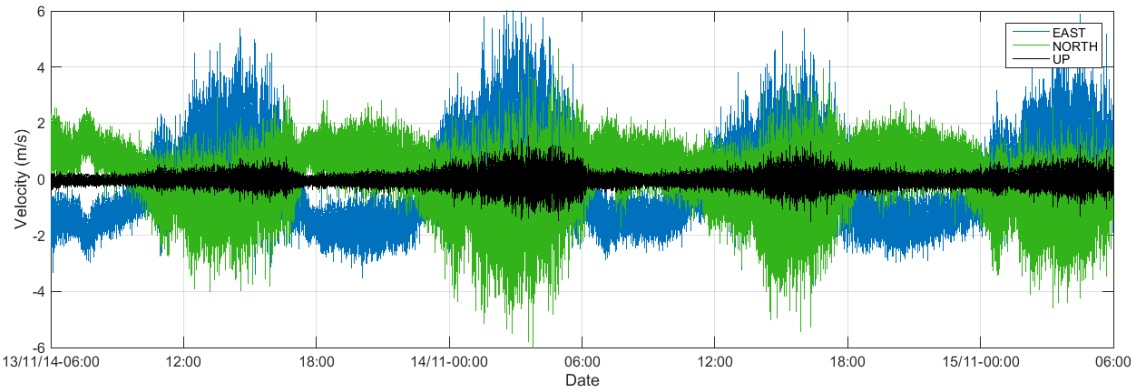

(a) Time series of Pressure Gauge vs SBD-AST significant wave height, H_m0

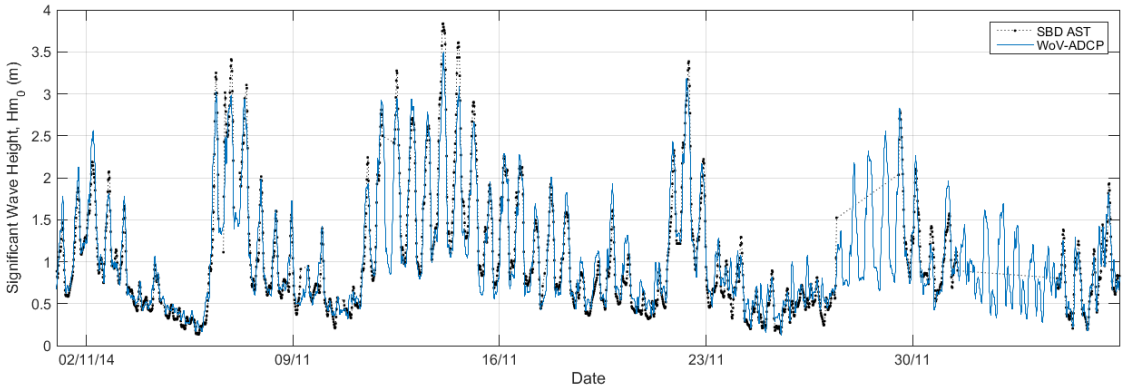

(a) Comparison of WoV-ADCP vs SBD-AST significant wave height, H_m0

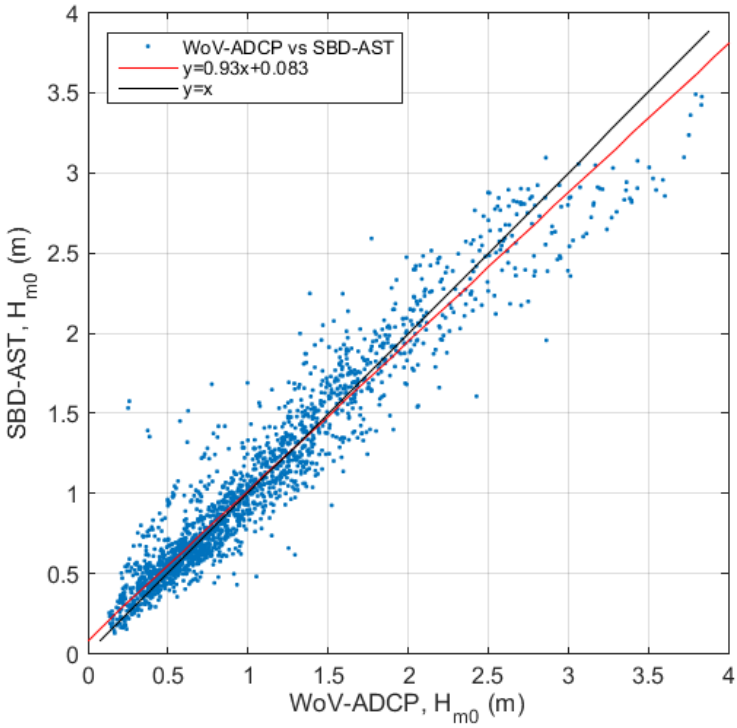

(b) Comparison of WoV-ADCP vs SBD-AST significant wave height, H_m0 and best-fit

Figure 3.23: Comparison of WoV-ADCP and SBD-AST measurements of significant wave height.

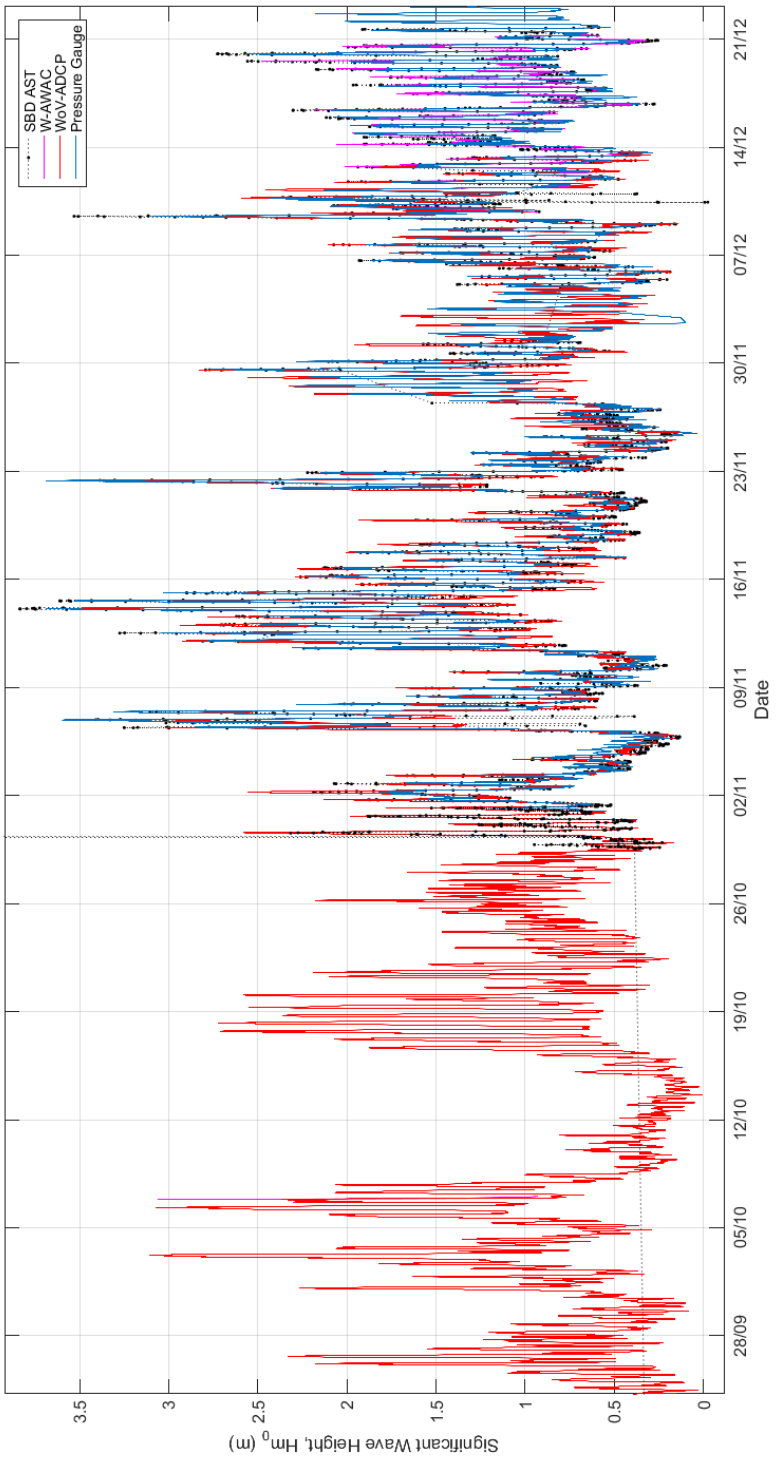

(a) Comparison of all wave measurement signals' significant wave height, H_m0 and best-fit

3.6 Site Characterisation: Results

The following section shows selected analysis of flow measurement at the turbine berth within the Fall of Warness during Flood and Ebb Tides using data acquired and post-processed between March 2013 and December 2014. Subsections are arranged as follows:

- Section 3.7 concerns **turbine-mounted instrumentation**.
- Sections 3.7.1 and 3.7.2 discuss lengthscale results for turbine-mounted instrumentation for Flood and Ebb tides respectively.
- Sections 3.7.4 and 3.7.5 discuss turbulence intensity results for turbine-mounted instrumentation for Flood and Ebb tides respectively.
- Section 3.8 concerns **seabed-mounted instrumentation** deployed predominantly upstream and downstream of the turbine.
- Sections 3.8.1 and 3.8.4 presents velocity depth profiles for stand-alone D-ADP instrumentation for Flood and Ebb tides respectively.
- Sections 3.8.2 and 3.8.5 presents turbulence intensity results for stand-alone D-ADP instrumentation for Flood and Ebb tides respectively.
- Sections 3.8.3 and 3.8.6 presents Reynolds Stress results for stand-alone D-ADP instrumentation for Flood and Ebb tides respectively.
- Sections 3.8.7 and 3.8.8 presents deviation of flow in direction both horizontally and vertically for stand-alone D-ADP instrumentation for Flood and Ebb tides respectively.

3.6.1 Data Collection Searching

Data Filtering: Flow Velocity

All results have been segmented to 5 minute duration ensembles and binned by velocity of increments of either $0.2ms^{-1}$ or $0.4ms^{-1}$ where data volume is low as indicated by greater standard deviation than neighbouring data subsets.

Data Filtering: Wave Height

A wave reference filter using H_m0 estimated across the entire data set (see Figure 3.24a) has been applied to the velocity binned. Thresholds were chosen to reflect the various precision of multiple measurement systems used. Additionally, an initial trial was conducted to observe the effect of H_m0 threshold on a) the number of data points returned in typical conditions and b) the trends of the turbulence or flow metrics returned. Work is ongoing to extend this wave filter to include other wave parameters including:

- T_p , the peak period
- s, the wave steepness
- θ_{1p} , the mean wave direction (at the peak of the spectrum)
- σ_{1p} , the directional spreading (at the peak of the spectrum)

Table 3.6: Table showing the ranges of significant wave height assigned to each of the three wave bands: *small*, *medium* and *large*.

Wave Band Label	**H_{m0} Range (m)**
Small Waves	$0.0 < H_{m0} < 0.8$
Medium Waves	$0.8 < H_{m0} < 1.6$
Large Waves	$1.6 < H_{m0} < 4.0$

Data Filtering: Flow Acceleration

Following sensitivity studies flow acceleration filters are implemented. The output of a particular data query e.g.,

is shown in Figure 3.26.The impact of additional acceleration filtering can be seen in Figure 3.26b where significant quantities of data are removed (compared to Figure 3.26a), despite having met velocity binning thresholds, due to the tides being in an accelerating or decelerating system state and thus exhibiting different behaviours in terms of e.g., turbulence and flow direction.

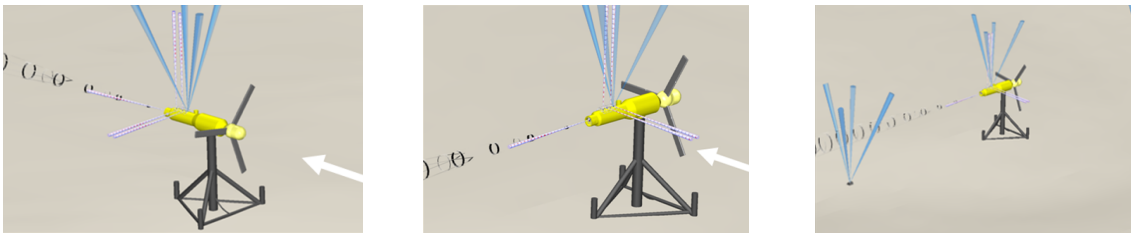

(a) Turbine Facing Flow (b) Turbine Broadside to Flow (c) Turbine & ADCP to rear visible

Figure 3.25: Visualisation of database querying: selecting turbine and instrumentation orientations wrt flood/ebb

3.6.2 Returned Metrics

Analysis of data is reported for the metrics listed and outlined in Table 3.7. The subset of lengthscales that are reported are highlighted in bold in Table 3.8.

Turbulence Intensity

Turbulence Intensities for streamwise, transverse and vertical directions were calculated as described in Section 2.5.2. Equation 2.11 is repeated below for convenience:

$$I_i = \frac{\sqrt{\langle u_i'^2 \rangle}}{\overline{u_x}} \times 100 \tag{2.11 revisited}$$

Where u_i' for the i^{th} Cartesian vector (i.e. $u_y' = v'$) with I normalised by the mean streamwise velocity component $\overline{u_x}$.

Table 3.7: Table of Reported Flow and Turbulence Metrics.

Metric	Description		Location	Instrument Platform/Data Used			
	Direction	Metric		SBD Nose	SBD ESIP-1	SBD ESIP-2	ADCP Seabed
U_x	Streamwise	Velocity	z=hh	TF	TB	TR	for comparison
U_y	Transverse	Velocity	z=hh	TF	TB	TR	for comparison
U_z	Vertical	Velocity	z=hh	TF	TB	TR	for comparison
TI_x	Streamwise	Turb. Intensity	z=hh	TF	TB	TR	for comparison
TI_y	Transverse	Turb. Intensity	z=hh	TF	TB	TR	for comparison
TI_z	Vertical	Turb. Intensity	z=hh	TF	TB	TR	for comparison
Lx	Streamwise	Lengthscale	z=hh	TF	TB	TR	for comparison
Ly	Transverse	Lengthscale	z=hh	TF	TB	TR	for comparison
Lz	Vertical	Lengthscale	z=hh	TF	TB	TR	for comparison
U_x	Streamwise	Velocity	z*=sb-s	.	.	.	UT
U_y	Transverse	Velocity	z*=sb-s	.	.	.	UT
U_z	Vertical	Velocity	z*=sb-s	.	.	.	UT
TI_x	Streamwise	Turb. Intensity	z*=sb-s	.	.	.	UT
TI_y	Transverse	Turb. Intensity	z*=sb-s	.	.	.	UT
TI_z	Vertical	Turb. Intensity	z*=sb-s	.	.	.	UT
τ_{uw}	Streamwise	Reynolds Stress	z*=sb-s	.	.	.	UT
τ_{vw}	Transverse	Reynolds Stress	z*=sb-s	.	.	.	UT

Turbine not generating. TF=Turbine Facing Flow, TB=Turbine Broadside to Flow, TR=Turbine Reversed to Flow.
hh=hub-height, sb-s=seabed to sea surface, UT=Upstream of Turbine
* at range from turbine (x=0,y=0) between 40m and 110m

Table 3.8: Description of the set of lengthscales combinations

Symbol		Description
[2]		
L_u	≡ xLu	the change of streamwise velocity in the streamwise direction
	xLv	the change of lateral velocity in the streamwise direction
	xLw	the change of vertical velocity in the streamwise direction
	yLu	the change of streamwise velocity in the lateral direction
L_v	≡ yLv	the change of lateral velocity in the lateral direction
	yLw	the change of vertical velocity in the lateral direction
	zLu	the change of streamwise velocity in the vertical direction
	zLv	the change of lateral velocity in the vertical direction
L_w	≡ zLw	the change of vertical velocity in the vertical direction

1. simplified two-term notation used here since other lengthscales not reported.

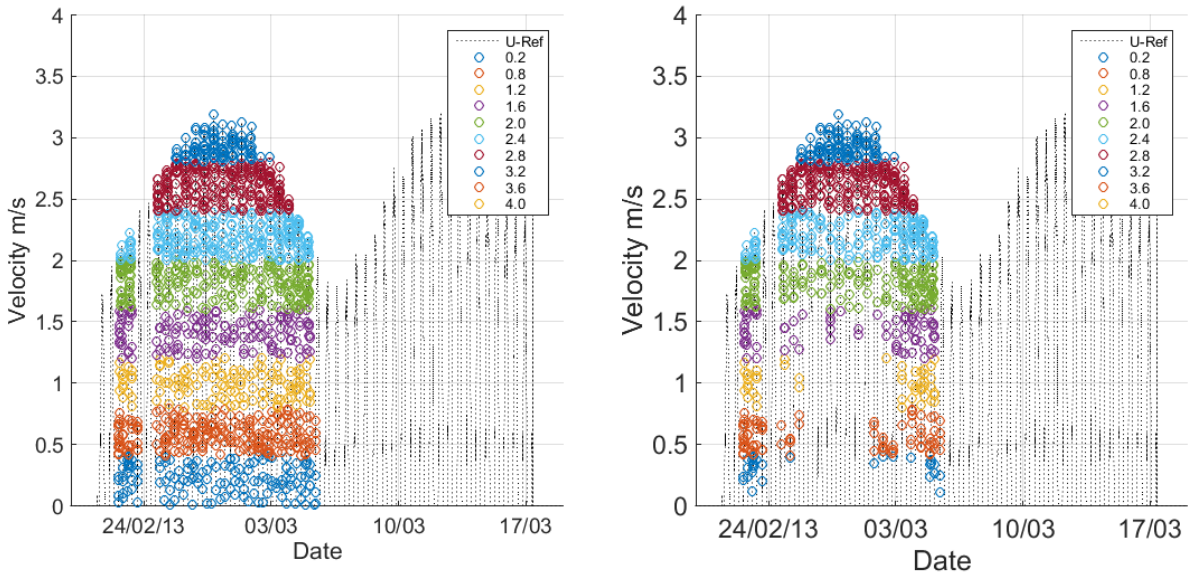

(a) Timestamps returned following a database query based on velocity bins of width 0.4 m/s. With acceleration filters applied.

(b) Timestamps returned following a database query based on velocity bins of width 0.4 m/s. With acceleration filters applied.

Figure 3.26: Example of velocity binning and the effect of acceleration threshold on the returned data sets prior to flow metric analysis.

Integral Lengthscale

Integral lengthscales were calculated using time auto-correlation techniques as described in Section 2.5.2. Equations 2.15 and 2.16 are repeated below for convenience:

$$R(\tau) = \frac{\langle (u_t - \overline{u})(u_{t+\tau} - \overline{u}) \rangle}{\sigma_u^2} \qquad \text{(2.15 revisited)}$$

$$\ell_x = \overline{u} \cdot \Im = \overline{u} \cdot \sum_{\tau=0}^{R(\tau)=0} R(\tau)\, \mathrm{d}\tau \qquad \text{(2.16 revisited)}$$

Assuming the largest turbulent structures are frozen as proposed by [32] the timescale multiplied by the mean velocity advecting the structures will yield the lengthscale as given in equation 2.16.

3.6.3 Reference Velocities

Reference velocity, u_{ref} is constructed by taking the time-stamp corrected non-power-weighted depth average of the section of upstream D-ADP (ADCP model) depth profile which coincides with the vertical extent of the turbine blades. An algorithm detects flood and ebb tidal cycles and through comparison to the position of the ADCP relative to the turbine selects the appropriate ADCP which can provide undisturbed incident flow. Resultant (maximum) velocity is used throughout for u_{ref}. An example of u_{ref} integrated with the site measurements can be seen in Figure 3.27b.

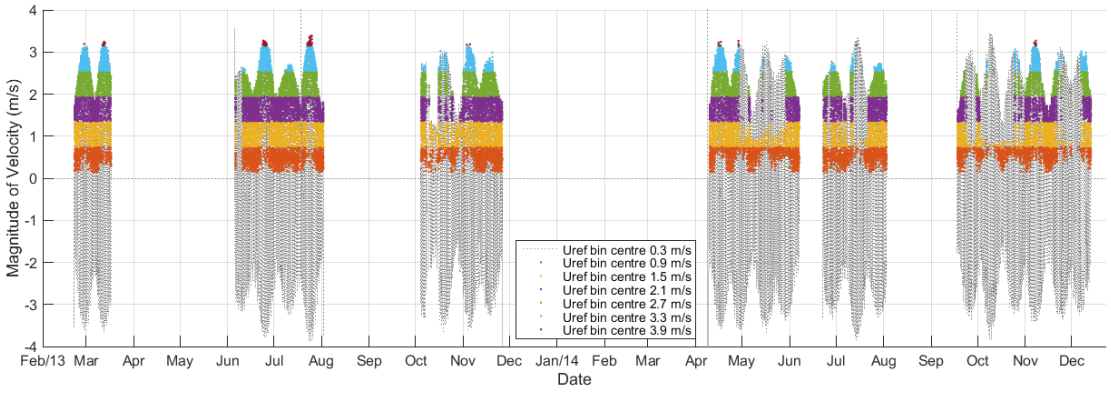

(a) Returned ADCP data for non-generating times. Flood tides.

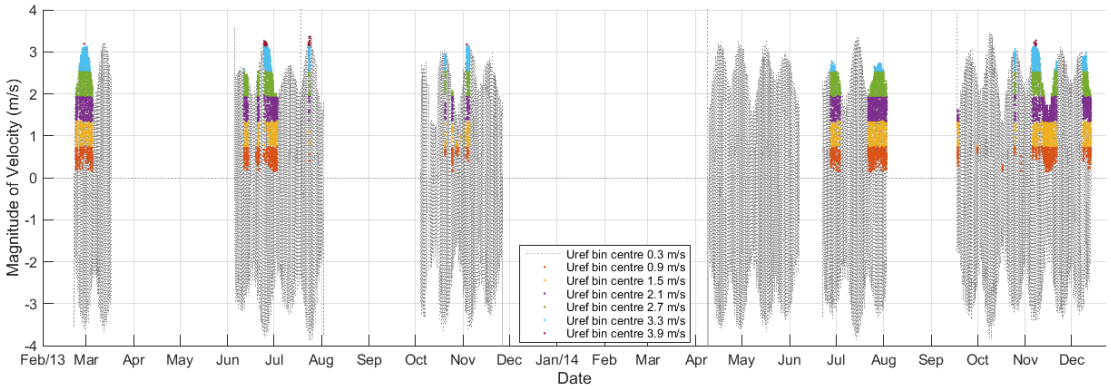

(b) Returned ADCP data for specific turbine conditions: Turbine reversed to Flood tide

Figure 3.27: Example of database querying

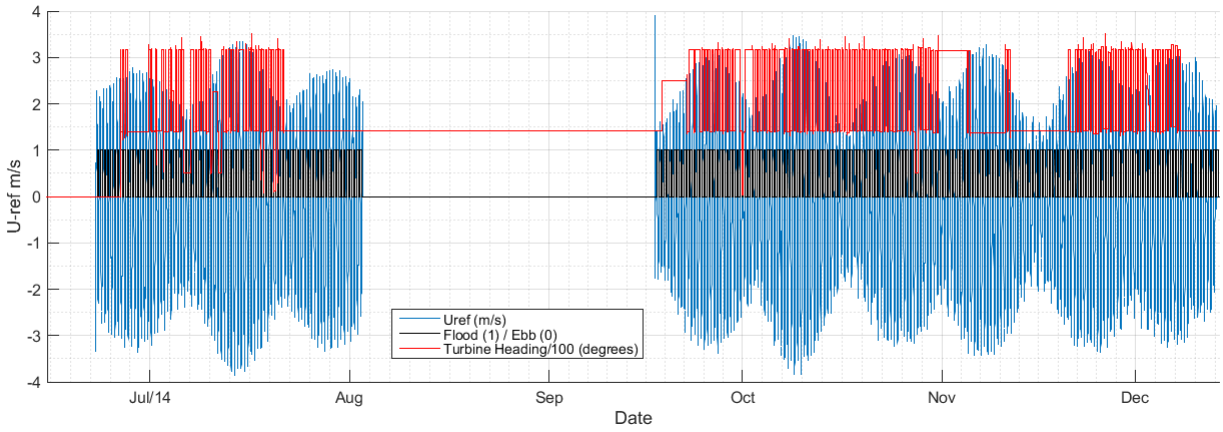

(a) Database reference signals showing date range June 2014 to December 2014

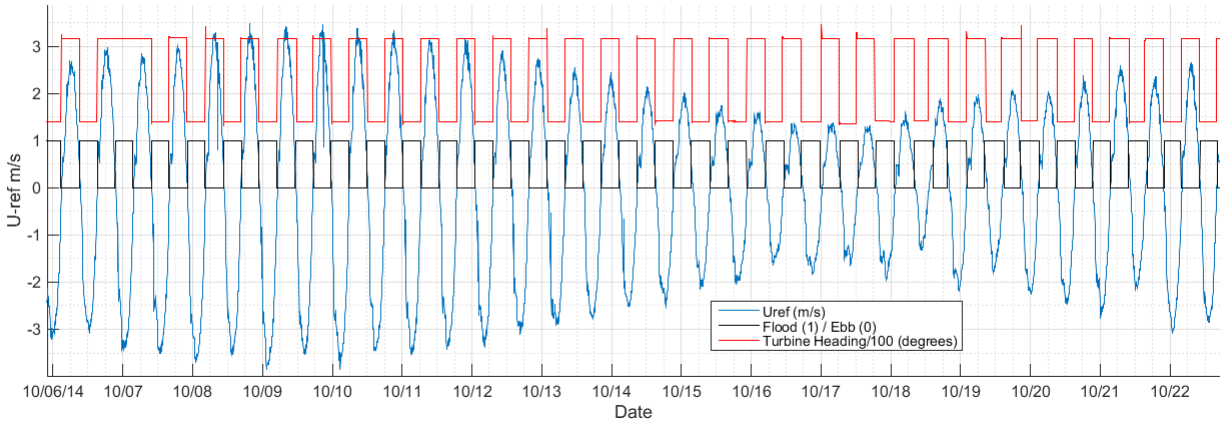

(b) Database reference signals showing more detail: date range October 2014

Figure 3.28: Database reference signals. Blue trace shows u_{ref}. Black shows tidal state: 1 = ebb, 0 = flood and red shows the turbine heading (/100). Further signals are added as required and form the building blocks of data queries (e.g., return all data corresponding to tide=flood, turbine heading <300 degrees and u_{ref} >2.5 m/s.)

3.7 Analysis: Turbine-Mounted Instrumentation

The following section shows results for turbine mounted SBD instrumentation acquired from ESIP-1, ESIP-2 and the nose of the turbine.

- Sections 3.7.1 discusses **lengthscale** results for Flood tides
- Sections 3.7.2 discusses **lengthscale** results for Ebb tides
- Sections 3.7.4 discusses **turbulence intensity** results for Flood tides
- Sections 3.7.5 discusses **turbulence intensity** results for Ebb tides

3.7.1 Lengthscales - Flood Tide

Summary of Flood Lengthscales

Figure 3.29a and 3.29b show streamwise lengthscales returned with the turbine orientated reversed to Flood flow for post processing involving constant-mean detrended and linear-fit detrended velocity signals respectively under the influence of small, medium and large wave field conditions as specified in Table 3.6.

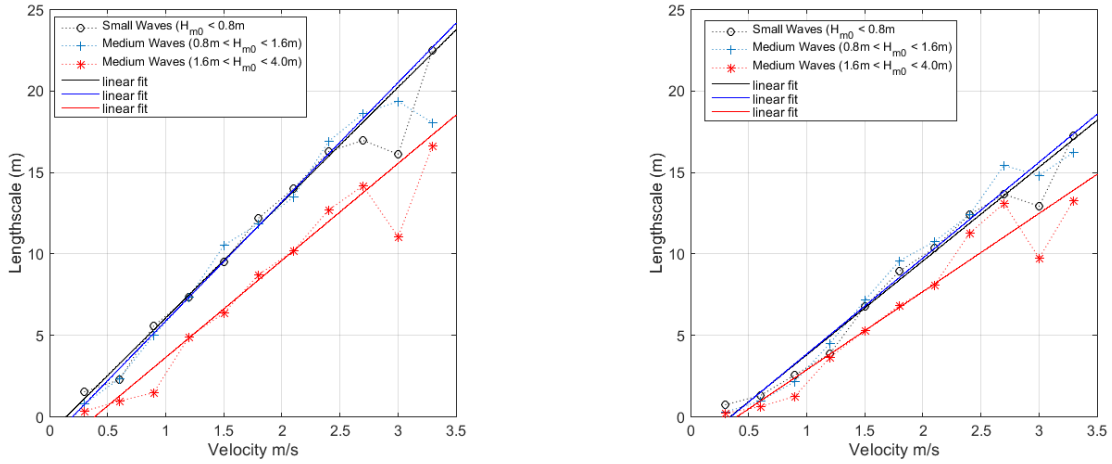

(a) Lengthscales resulting from the constant mean detrending method

(b) Lengthscales resulting from the linear-fit detrending method

Figure 3.29: Streamwise Lengthscale as a function of tidal reference velocity.

It can be seen in Figure 3.29b that linear detrending results in lower streamwise lengthscales and produces smaller variations between varying wave conditions (as defined by significant wave height).

Figures 3.30, 3.31 and 3.32 show the detail behind Figure 3.29 for the **streamwise** direction at small, medium and large wave heights respectively. Lengthscale versus binned velocity is shown under the three detrending methods applied: constant mean, linear-fit and moving average (from top to bottom). The number of ensembles with a T_{stat}=300 s (5 minutes) for each filtered subset is shown in grey at the top of the graphs. Modifications to the standard box-plot algorithm were applied to account for the distribution of the lengthscale values appearing to be better described by a log-normal distribution as opposed to the traditionally applicable normal distribution. The red circle indicates the mean value for each subset of data; the red line representing the median.

In Figure 3.30 linear detrending shows closer agreement between the median and the mean values (produced by more narrow distributions). Again lower lengthscales are reported by the linear-fit method. Moving-average detrending produces significantly reduced lengthscales. This would be expected using an aggressive moving average but with values set to 150 seconds is unexpected. Further investigation will be carried out on the datasets to investigate the sensitivity to the moving-average window size.

The presence of waves with H_m0 >0.8m (Figures 3.31 and 3.32) appears to reduce the quantity of large lengthscales and reduces median and mean values. Whilst smaller volume sample sets are available and thus uncertainties are higher, there also appears to be a reduction in lengthscale at high velocities (as seen in the graphs at U_{ref} $>2.6ms^{-1}$).

Transverse lengthscales, as shown in Figure 3.33, exhibit closer agreement between the detrending methods, particularly evident in the moving-average set where the reduced physical size of the turbulent structures are further removed from the filtering effect of the moving-average.

Vertical lengthscales, as shown in Figure 3.34, exhibit even closer agreement between the detrending methods, again evident in the moving-average set where the further reduced physical size of the turbulent structures are less effected by the filtering effect of the moving-average.

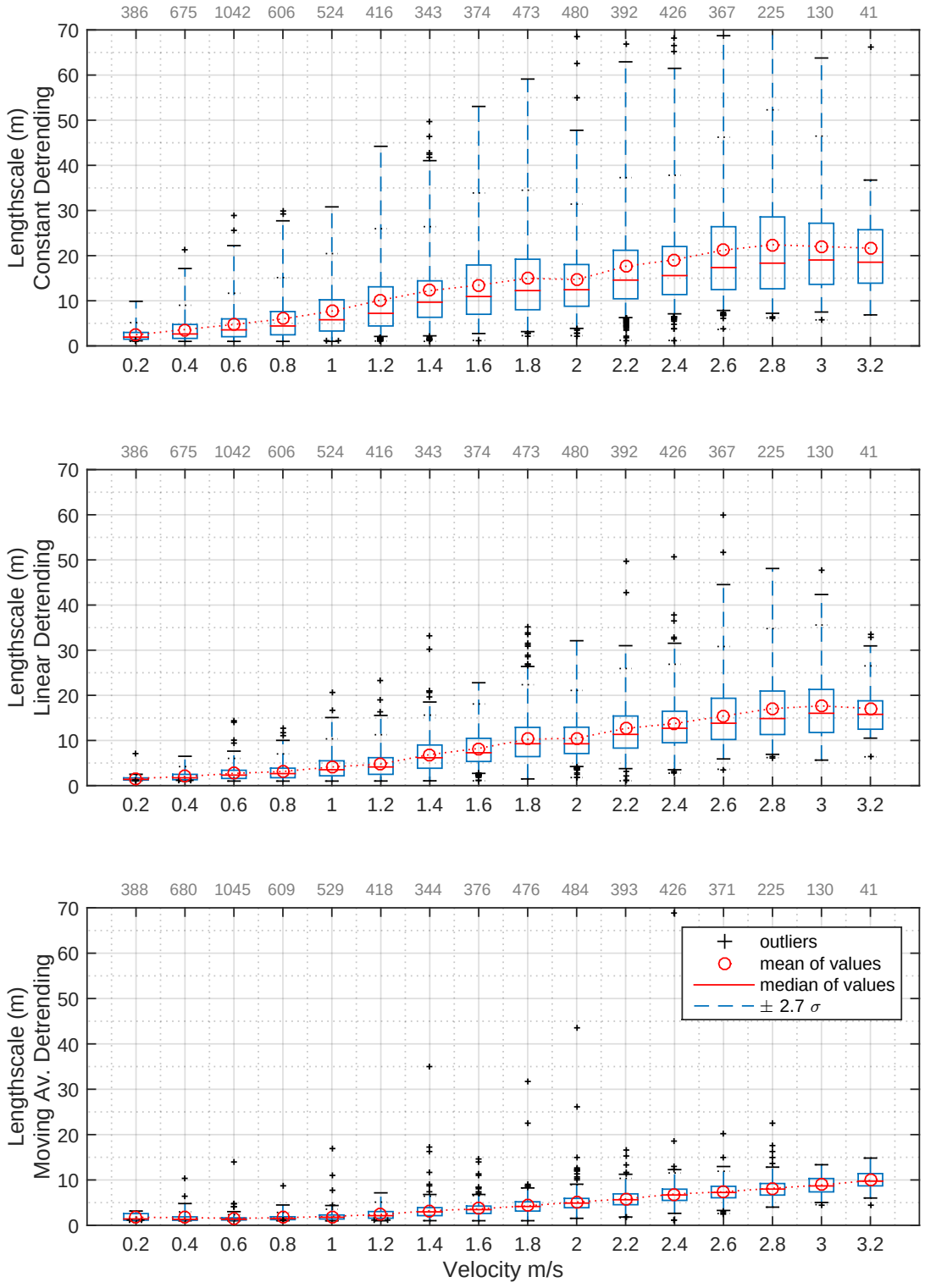

Figure 3.30: **Streamwise Lengthscale** - Ambient Flow, Flood Tide. **Small Waves**. Number of 5 minute ensembles are shown in grey at top outer edge of each plot.

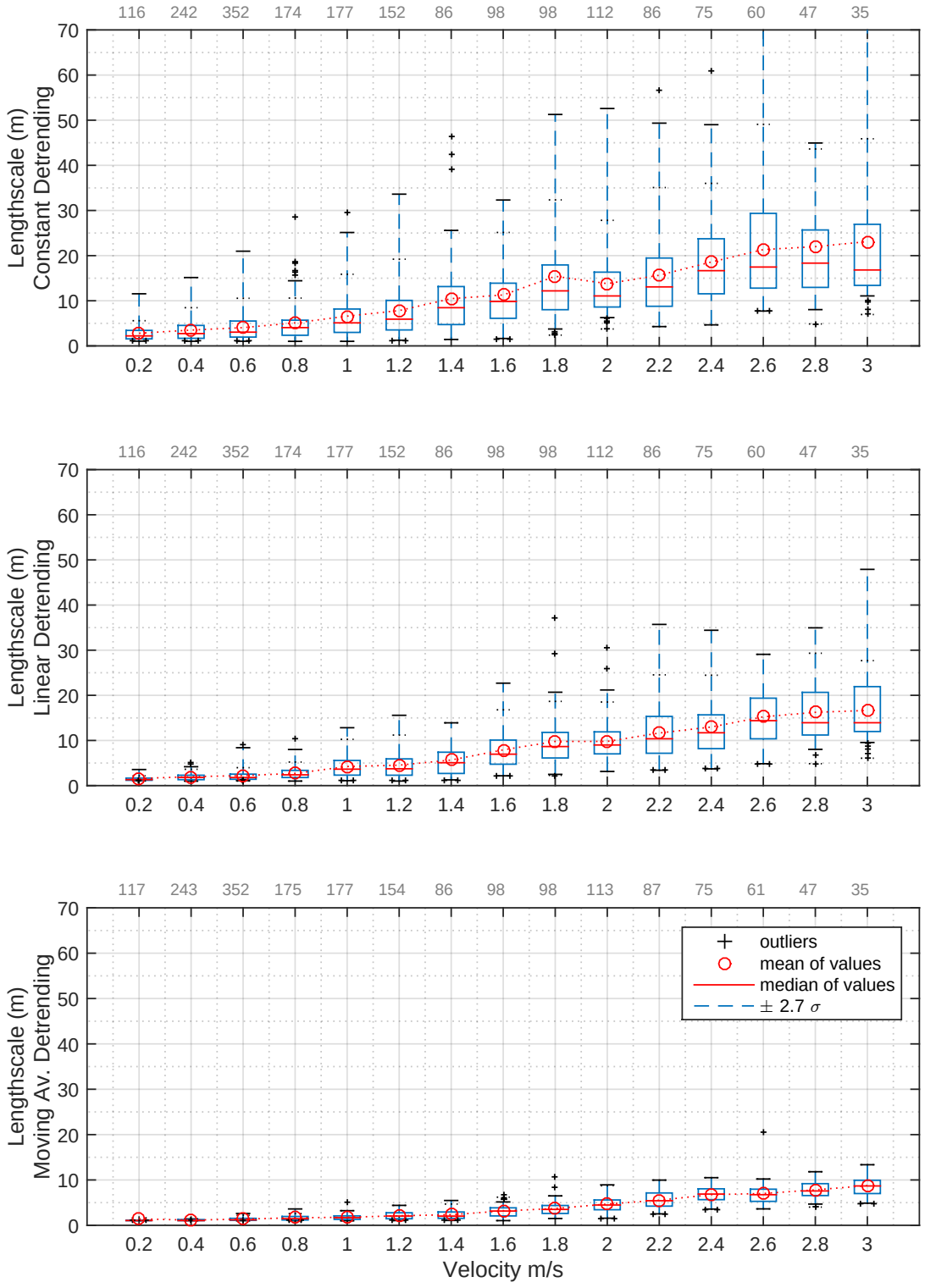

Figure 3.31: **Streamwise Lengthscale** - Ambient Flow, Flood Tide. **Medium Waves**. Number of 5 minute ensembles are shown in grey at top outer edge of each plot.

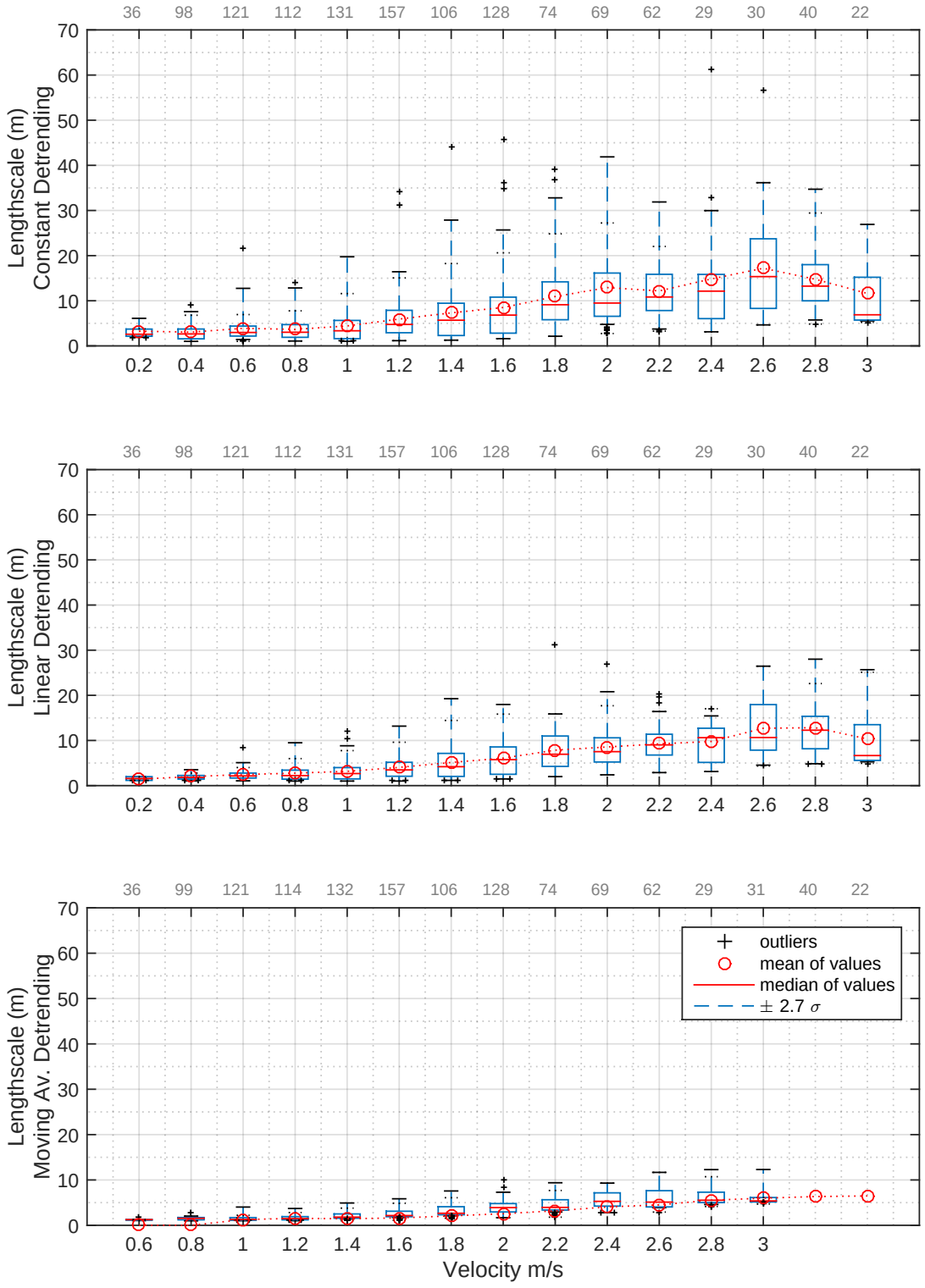

Figure 3.32: **Streamwise Lengthscale** - Ambient Flow, Flood Tide. **Large Waves**. Number of 5 minute ensembles are shown in grey at top outer edge of each plot.

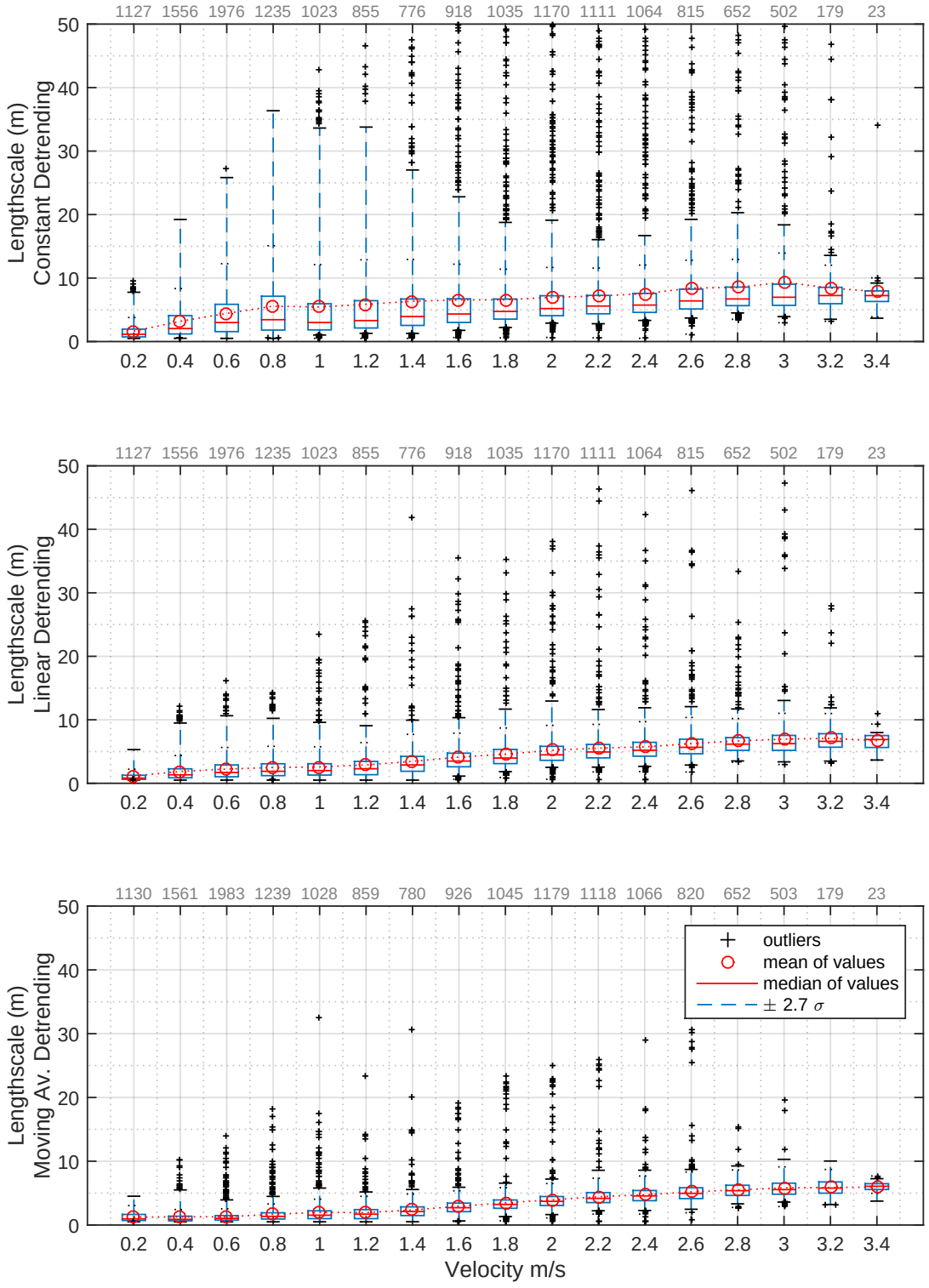

Figure 3.33: **Transverse Lengthscale** - Ambient Flow, Flood Tide. **Small Waves**. Number of 5 minute ensembles are shown in grey at top outer edge of each plot.

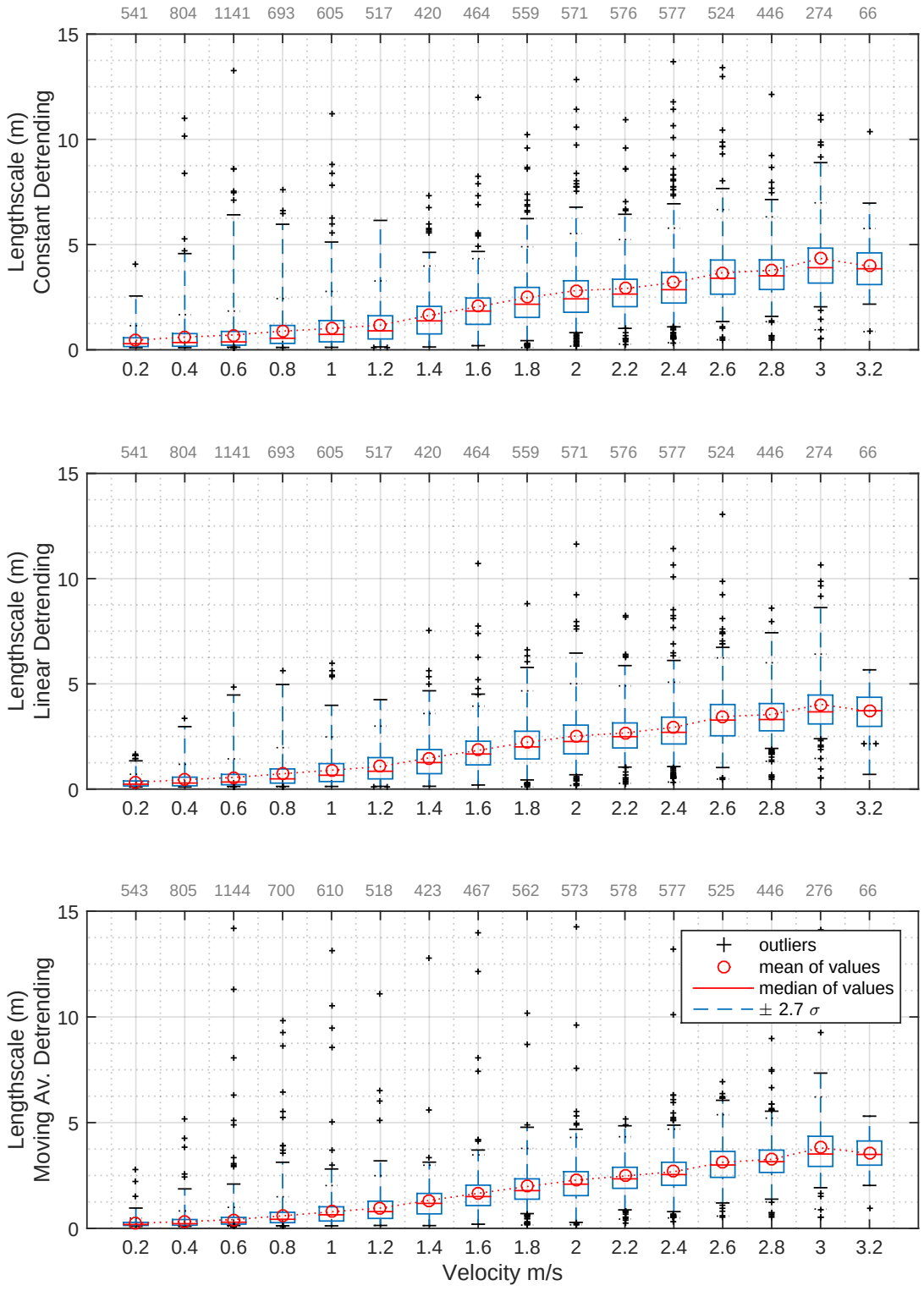

Figure 3.34: **Vertical Lengthscale** - Ambient Flow, Flood Tide. **Small Waves**. Number of 5 minute ensembles are shown in grey at top outer edge of each plot.

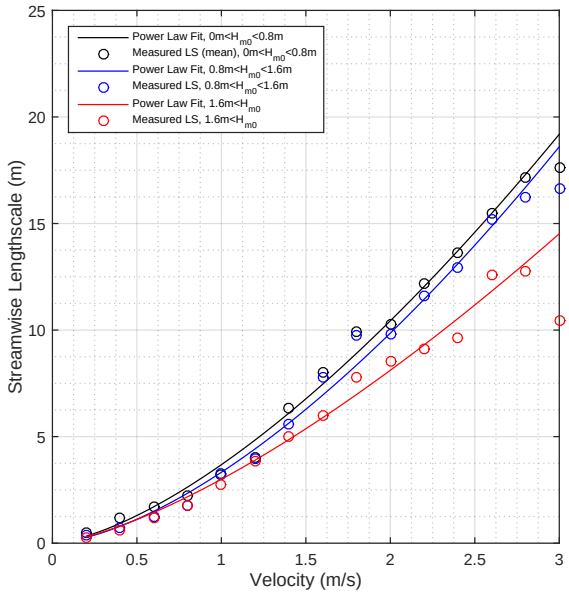

Figure 3.35: **Streamwise Lengthscale** - Ambient Flow, Flood Tide. No Doppler noise correction.

Streamwise lengthscales with linear-fit detrending for small, medium and large wave conditions are shown in Figure 3.35. Power law fits were applied to the data points. It can clearly be seen that in this circumstance streamwise lengthscale has been significantly diminished in magnitude under the influence of waves with of H_m0 >1.6m.

This trend is repeated in the **Transverse** direction as shown in Figure 3.36. The trend is more complex in the **Vertical** directions as shown in Figure 3.37 with lengthscales during large wave conditions fluctuating around the lengthscales present in small wave conditions. There is a reduction in lengthscale for moderate wave conditions however.

Summary

Table 3.9 shows the mean values of lengthscales as measured by turbine-mounted, mid-channel depth SBD instruments in the streamwise, transverse and vertical directions. Values were averaged at flow speeds above U_{ref} >2.0ms^{-1}) as these are the flow speeds of most relevance to the installed turbine. The choice of this averaging range is not robustly defined.

Table 3.9: Flood Tide. Orthogonal Lengthscales mean and standard deviation

Detrend	**0m<H_{m0}<0.8m**			**0.8m<H_{m0}<1.6m**			**1.6m<H_{m0}**		
Method	X	Y	Z	X	Y	Z	X	Y	Z
Constant	**21.3 ± 12.1**	9.0 ± 9.8	3.7 ± 1.7	**21.5 ± 13.2**	7.6 ± 4.6	3.6 ± 3.2	**16.9 ± 11.7**	10.1 ± 10.2	3.5 ± 0.5
Linear	**15.5 ± 6.9**	6.3 ± 3.8	3.4 ± 1.3	**15.2 ± 5.8**	5.8 ± 2.1	3.2 ± 2.1	**12.6 ± 6.9**	5.8 ± 1.9	3.5 ± 0.5
MA	**7.4 ± 2.8**	5.2 ± 2.4	3.1 ± 1.4	**7.0 ± 3.6**	4.6 ± 1.1	3.2 ± 3.4	**6.0 ± 4.5**	5.1 ± 1.6	4.2 ± 4.7

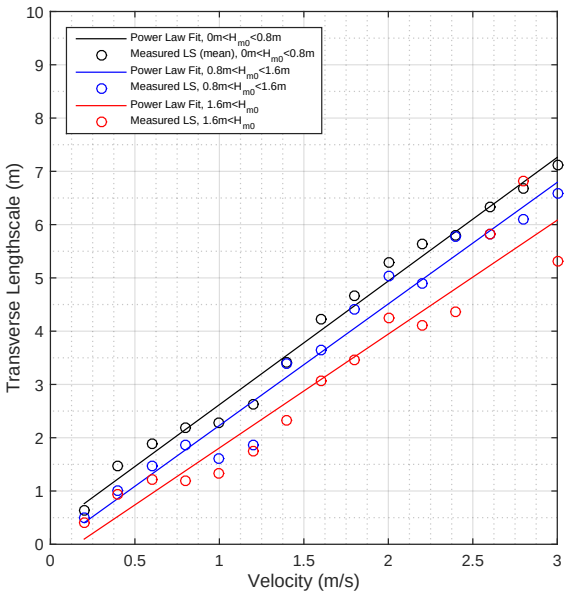

Figure 3.36: **Transverse Lengthscale** - Ambient Flow, Flood Tide. No Doppler noise correction.

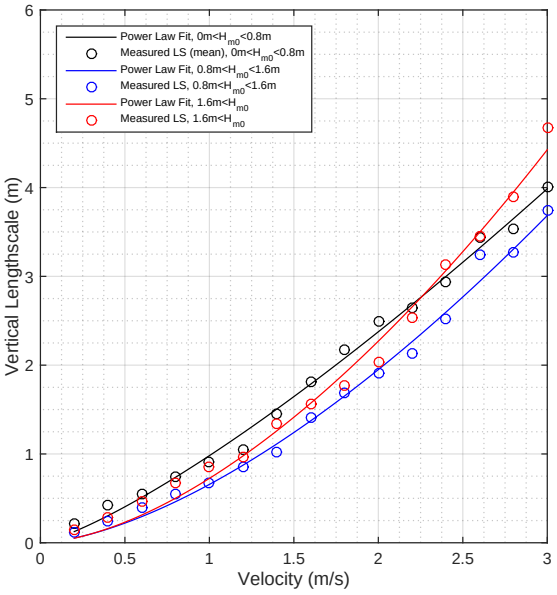

Figure 3.37: **Vertical Lengthscale** - Ambient Flow, Flood Tide. No Doppler noise correction.

3.7.2 Lengthscales - Ebb Tide

Figures 3.38, 3.39 and 3.40 show lengthscales for the **streamwise** direction at small, medium and large wave heights respectively. Lengthscale versus binned velocity is shown under the three detrending methods applied: constant mean, linear-fit and moving average (from top to bottom). The number of ensembles with a T_{stat}=300 s (5 minutes) for each filtered subset is shown in grey at the top of the graphs.

In Figure 3.38 linear detrending shows closer agreement between the median and the mean values (produced by more narrow distributions). Again lower lengthscales are reported by the linear-fit method with a large reduction in the number of lengthscales reported of magnitude greater half of the channel depth. Moving-average detrending produces significantly reduced lengthscales. This would be expected using an aggressive moving average but with values set to 150 seconds is unexpected. Further investigation will be carried out on the datasets to investigate the sensitivity to the moving-average window size.

The rate of change with velocity of the streamwise lengthscale is also very different in Ebb compared to Flood. There is a rapid increase up to 1 ms^{-1} followed by a plateau-like feature. Overall streamwise lengthscales in Ebb are approximately 50% of the magnitude of the Flood streamwise lengthscales.

The presence of waves with H_m0 >0.8m as shown in Figure 3.39 reduces the quantity of large lengthscales and reduces median and mean values.

The presence of waves with H_m0 >1.6m as shown in Figure 3.40 significantly reduce the magnitude of the lengthscales although there is limited data quantity in this system state. For example, in small wave conditions at 2.2 ms^{-1} x samples were present compared with 77 for large wave conditions.

Transverse lengthscales, as shown in Figure 3.41, unlike their Flood counterparts, do no exhibit closer agreement (compared to streamwise) between the constant and linear detrending methods. At flow speeds between 0.4 ms^{-1} and 1 ms^{-1} they differ markedly. Both methods on average do show closer agreement with moving-average method when compared to streamwise differences.

Vertical lengthscales, as shown in Figure 3.42, exhibit even closer agreement between the detrending methods, again evident in the moving-average set where the further reduced physical size of the turbulent structures are less effected by the filtering effect of the moving-average.

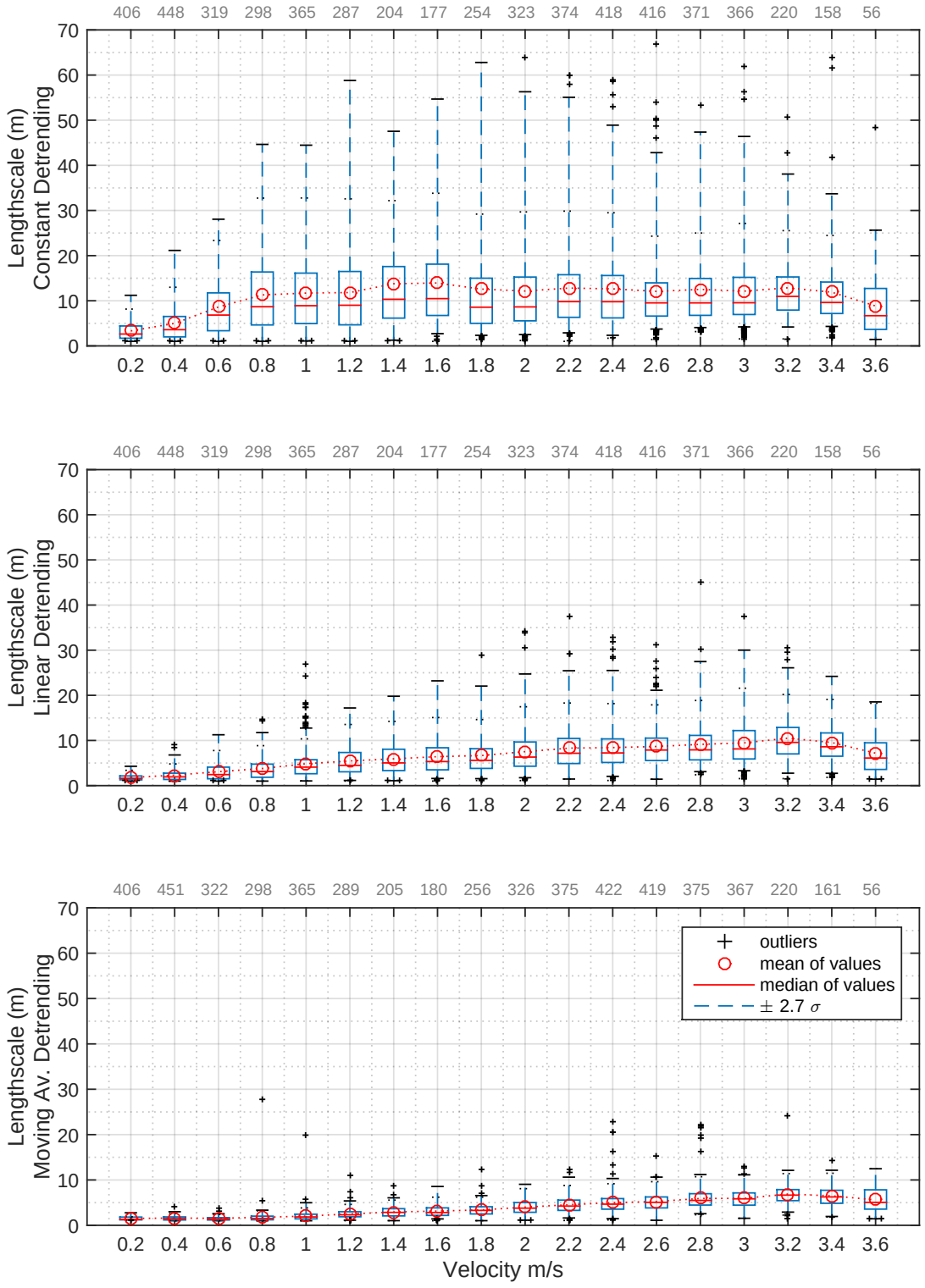

Figure 3.38: **Streamwise Lengthscale** - Ambient Flow, Ebb Tide. **Small Waves**. Number of 5 minute ensembles are shown in grey at top outer edge of each plot.

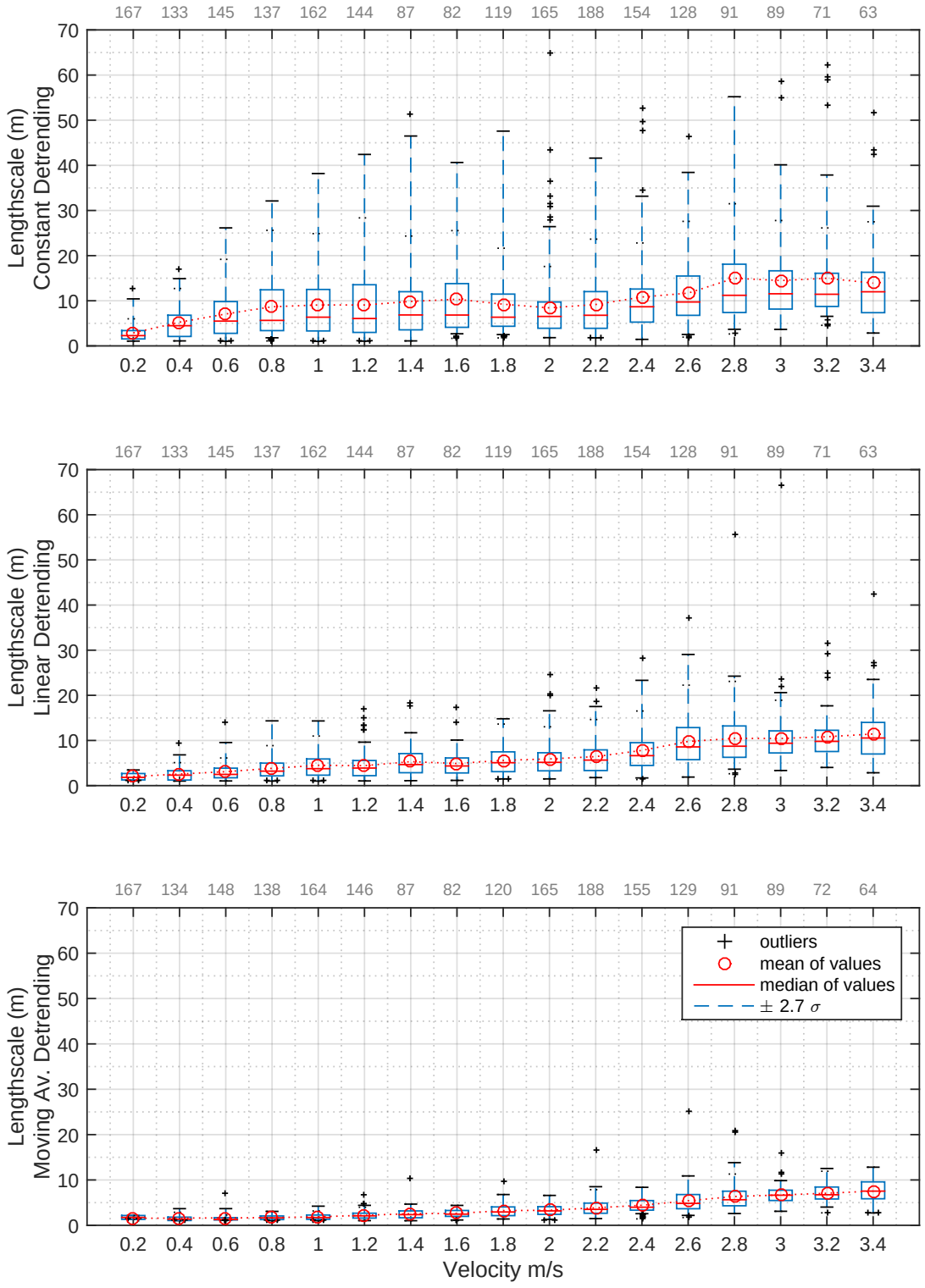

Figure 3.39: **Streamwise Lengthscale** - Ambient Flow, Ebb Tide. **Medium Waves**. Number of 5 minute ensembles are shown in grey at top outer edge of each plot.

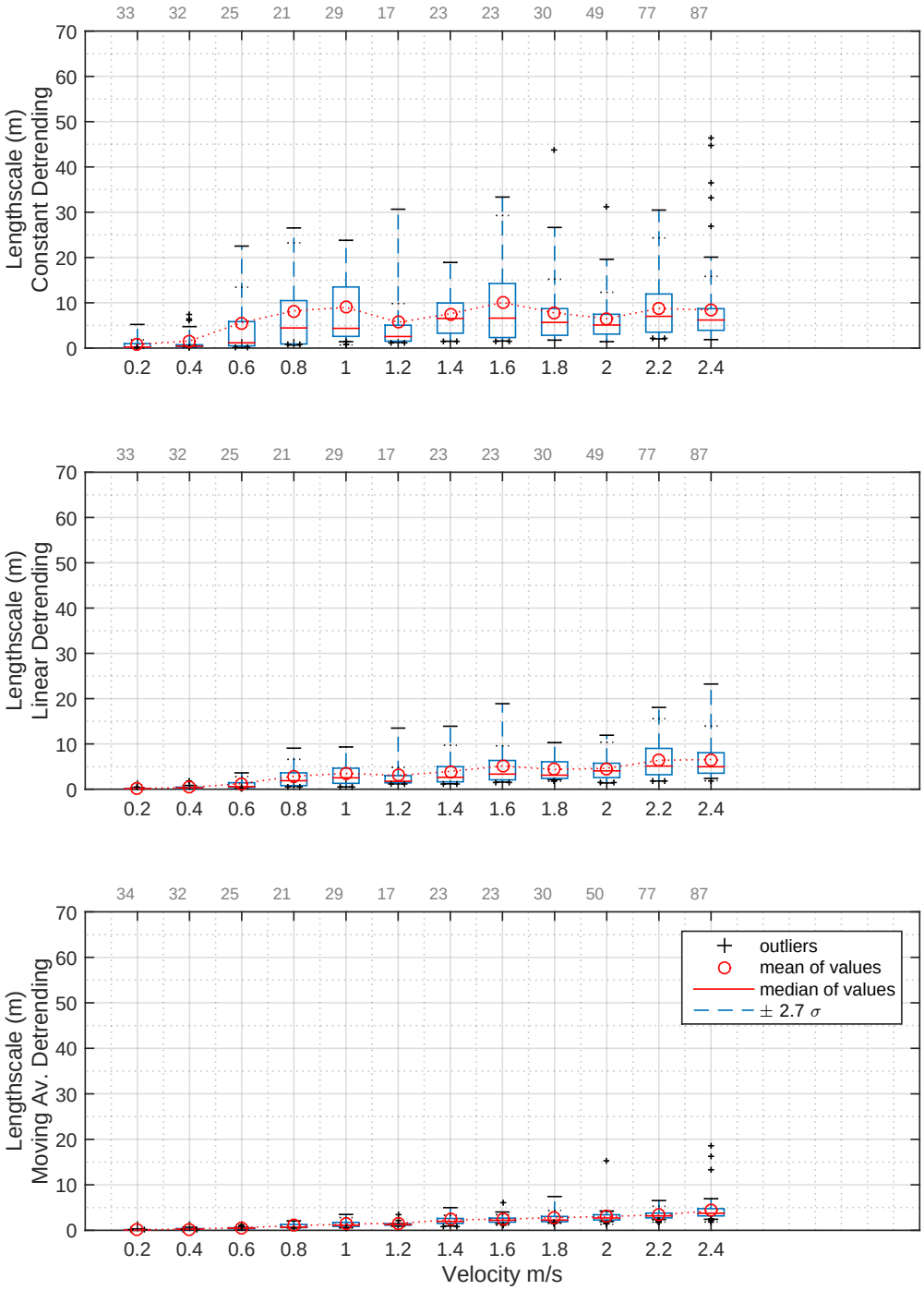

Figure 3.40: **Streamwise Lengthscale** - Ambient Flow, Ebb Tide. **Large Waves**. Number of 5 minute ensembles are shown in grey at top outer edge of each plot.

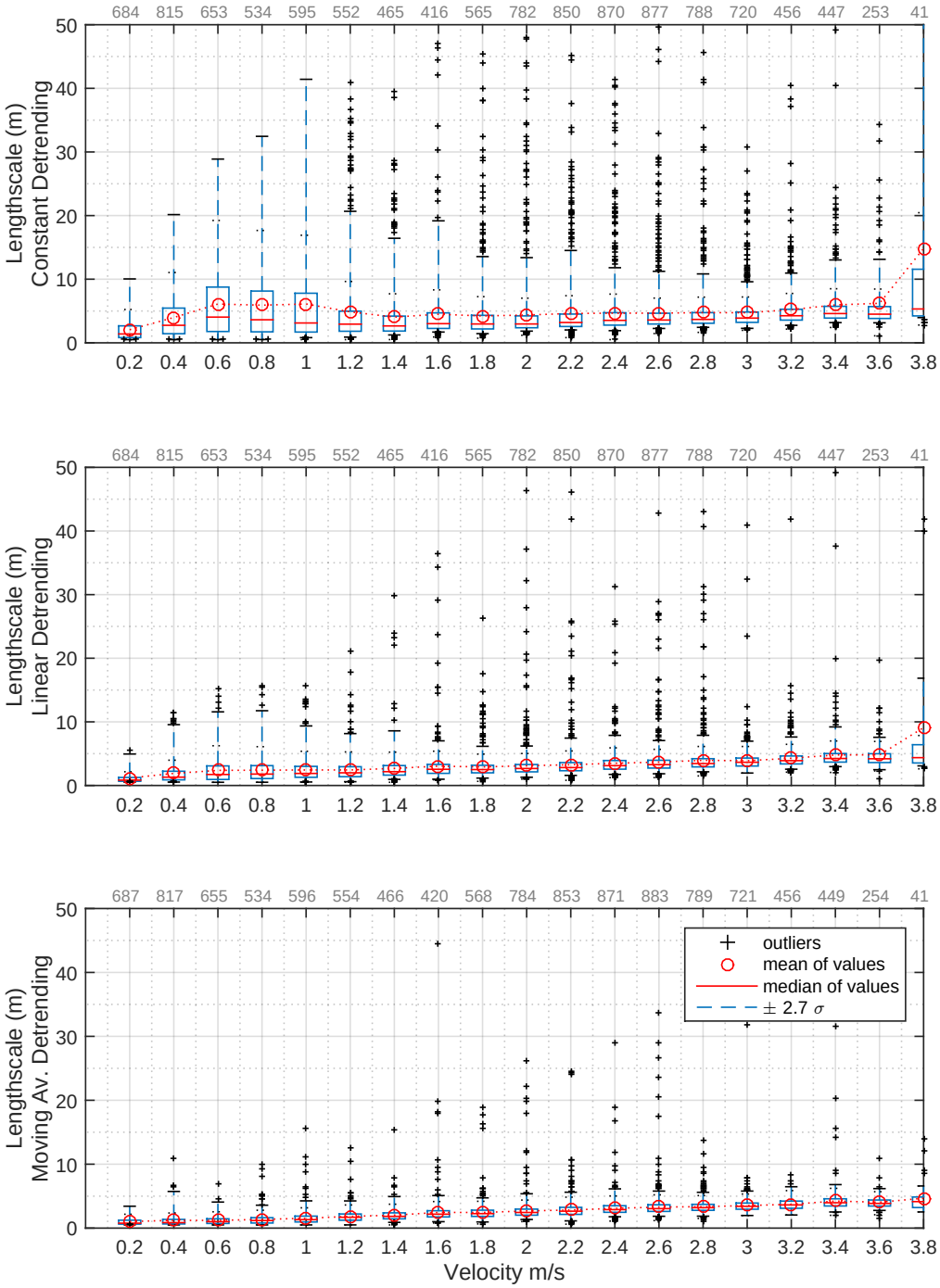

Figure 3.41: **Transverse Lengthscale** - Ambient Flow, Ebb Tide. **Small Waves**. Number of 5 minute ensembles are shown in grey at top outer edge of each plot.

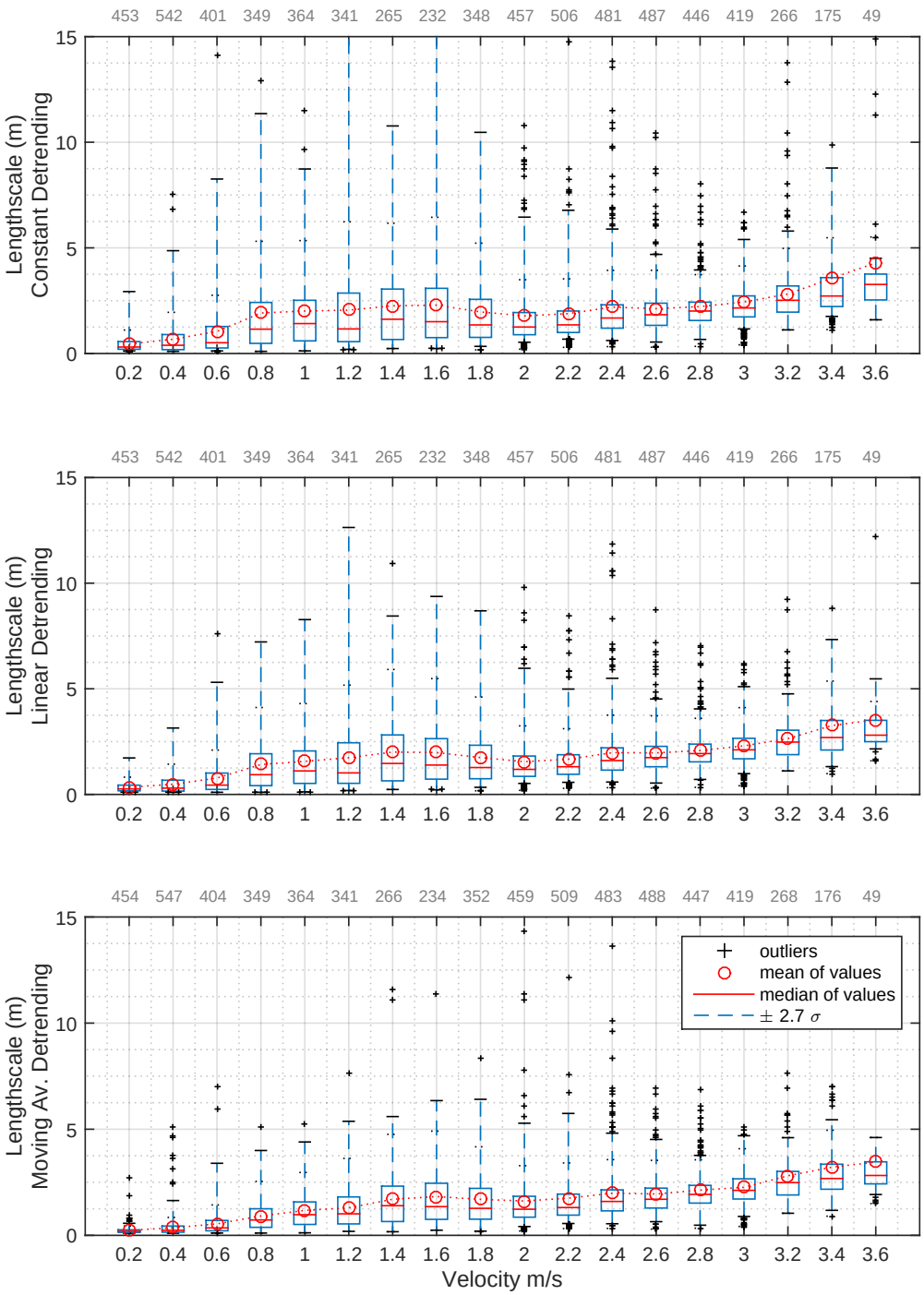

Figure 3.42: **Vertical Lengthscale** - Ambient Flow, Ebb Tide. **Small Waves**. Number of 5 minute ensembles are shown in grey at top outer edge of each plot.

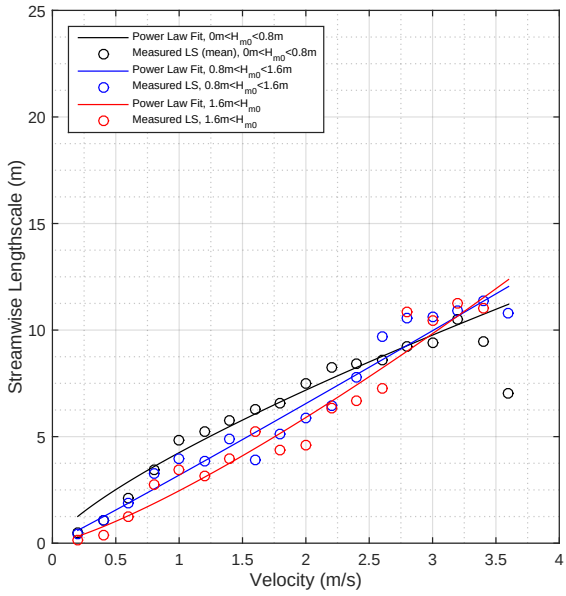

Figure 3.43: **Streamwise Lengthscale** - Ambient Flow, Ebb Tide. No Doppler noise correction.

Streamwise lengthscales with linear-fit detrending for small, medium and large wave conditions are shown in Figure 3.43. Power law fits were applied to the data points. These trends show different overall behaviour to those in the Flood tidal direction. Streamwise lengthscale remain diminished in magnitude under the influence of waves with of H_m0 >0.8m and more so under the influence of waves with H_m0 >1.6m. Trends are more difficult to assess at flow speeds greater than $\approx$ 2.5 ms^{-1}

This increased-complexity-trend is repeated in the **Transverse** direction as shown in Figure 3.44 with lengthscales during large wave conditions fluctuating around the lengthscales present in small wave conditions. The graphs suggest a reduction in lengthscale for moderate wave conditions at higher flow speeds and show an increase in lengthscale in the mid-velocity range under large wave conditions.

The trend is more complex in the **Vertical** direction as shown in Figure 3.45. It appears that there is an increase in lengthscale above $\approx$ 0.6 ms^{-1} and below $\approx$ 1.8 ms^{-1} for small wave conditions.

Summary

Table 3.10 shows the mean values of lengthscales as measured by turbine-mounted, mid-channel depth SBD instruments in the streamwise, transverse and vertical directions. Values were averaged at flow speeds above U_{ref} >2.0ms^{-1}) as these are the flow speeds of most relevance to the installed turbine. As with Flood analysis (above) the choice of this range over which to average varying parameters is not robustly defined.

3.7.3 Turbulence Intensity

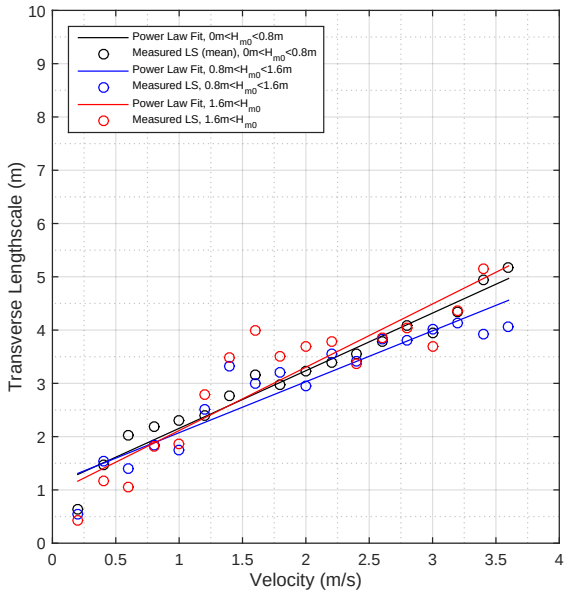

Figure 3.44: **Transverse Lengthscale** - Ambient Flow, Ebb Tide. No Doppler noise correction. .

Table 3.10: Ebb Tide. Orthogonal Lengthscales mean and standard deviation

Detrend	**0m<H_{m0}<0.8m**			**0.8m<H_{m0}<1.6m**			**1.6m<H_{m0}**		
Method	X	Y	Z	X	Y	Z	X	Y	Z
Constant	**12.2 ± 9.1**	5.1 ± 6.4	2.2 ± 2.3	**11.6 ± 7.4**	4.9 ± 6.3	2.2 ± 1.0	**10.6 ± 8.1**	5.2 ± 3.7	2.7 ± 0.4
Linear	**8.6 ± 4.4**	3.8 ± 2.8	2.0 ± 1.5	**9.7 ± 5.5**	3.8 ± 4.2	2.1 ± 0.8	**7.3 ± 3.6**	3.9 ± 1.6	2.7 ± 0.4
MA	**5.2 ± 2.7**	3.4 ± 2.1	2.0 ± 2.5	**5.4 ± 3.3**	3.1 ± 1.3	2.2 ± 1.8	**5.0 ± 4.5**	3.8 ± 3.8	3.2 ± 3.6

Time Series Detrending

Since the turbulence intensity metric is derived from the decomposition of the representative underlying tidal flow and the fluctuating flow elements the method of separating these constituents impacts metric value. As with the previous Lengthscale section, multiple methods of "detrending" the time varying signal were used.

The effects of detrending method are shown in Figures 3.47 , 3.48. Differences are small between constant and linear-fit methods. However, larger differences of the order of several % (final absolute % not relative e.g., TI= 6.5% as opposed to TI= 8.3% as opposed to) exist between the moving-average detrended data.

Correction of Doppler Noise

For more detailed information on Doppler Noise correction refer to Section 3.2.11. A brief summary is included here for convenience.

- Multiple techniques were used to ascertain the noise-floor from spectra produced by turbine-mounted single beam instruments.
- Most recently the method of [6] was implemented which features an automated approach.

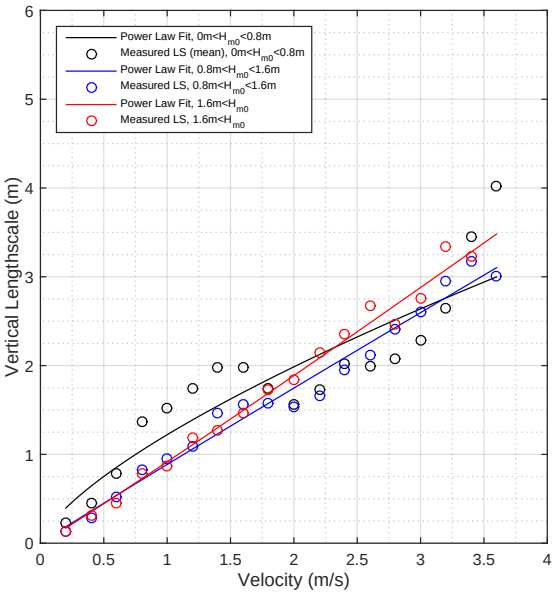

Figure 3.45: **Vertical Lengthscale** - Ambient Flow, Ebb Tide. No Doppler noise correction.

- Recent work by [123] shows the measurement data to have an instrument noise level featuring velocity dependency.
- Once determined, knowledge of instrument noise can be used to "correct" data using the method shown in equation 3.5 [128].
- In setting a noise-correction factor a conservative approach was taken: whilst work continues in this area instrument noise variance has been selected low so as to reduce the removal of real turbulent fluctuations (see figure 3.46).
- The mean value of this velocity dependent correction factor matches with previous preliminary methods (non automated) giving further confidence in this more robust and automated routine.

$$I_u = \frac{\sigma_u}{< u >} = \frac{\sqrt{< u'^2 > - n^2}}{\overline{u}} \qquad \text{(3.5 revisited)}$$

where I_u is the turbulence intensity, σ_u is the standard deviation of the fluctuations and n is the standard deviation of the noise component in m/s).

3.7.4 Turbulence Intensity - Flood Tide

Figure 3.47 shows TI versus velocity for flood tides in ambient conditions from multiple turbine mounted single-beam instruments. Moving average detrending produces the smallest TI values whilst constant mean detrending produces the largest.

Figure 3.48 shows TI versus velocity for flood tides in ambient conditions from multiple turbine mounted single-beam instruments with Doppler noise correction applied to the data using equation 3.5.

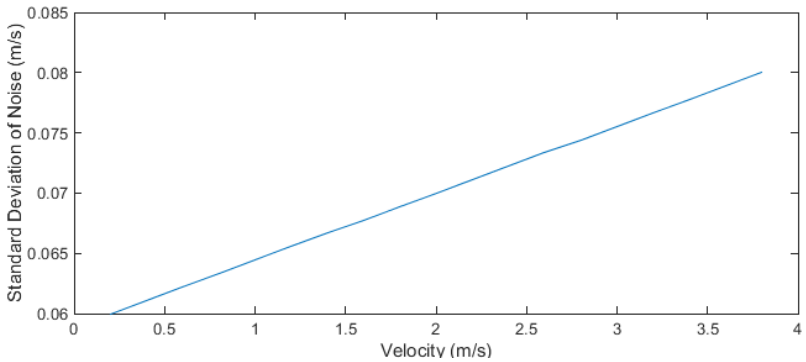

Figure 3.46: Doppler noise correction values for Mark I, Nortek SBD AD2CP 1MHz integrated in DEEPGen IV

Figure 3.49 shows **streamwise** Turbulence Intensities returned with the turbine orientated reversed to the flood tide. The linear-fit method of detrending was applied to the velocity time series under the influence of small, medium and large wave field conditions as previously defined. I_u in these plots are corrected for Doppler noise.

Whilst I_u increases under large wave conditions it decreases under conditions where waves were moderately sized (at velocities above approximately 1.2 ms^{-1}).

Figure 3.50 shows **transverse** Turbulence Intensities returned with the turbine orientated reversed to the flood tides under the influence of small, medium and large wave field conditions. I_v in these plots are corrected for Doppler noise.

I_v clearly increase as significant wave heights increase.

Figure 3.50 shows **vertical** Turbulence Intensities.

I_w shows very large increase as significant wave heights increase.

Table 3.11 provides summary data for I_u, I_v, and I_w in Flood tides featuring small, medium and large waves for both uncorrected and Doppler noise-corrected post-processing.

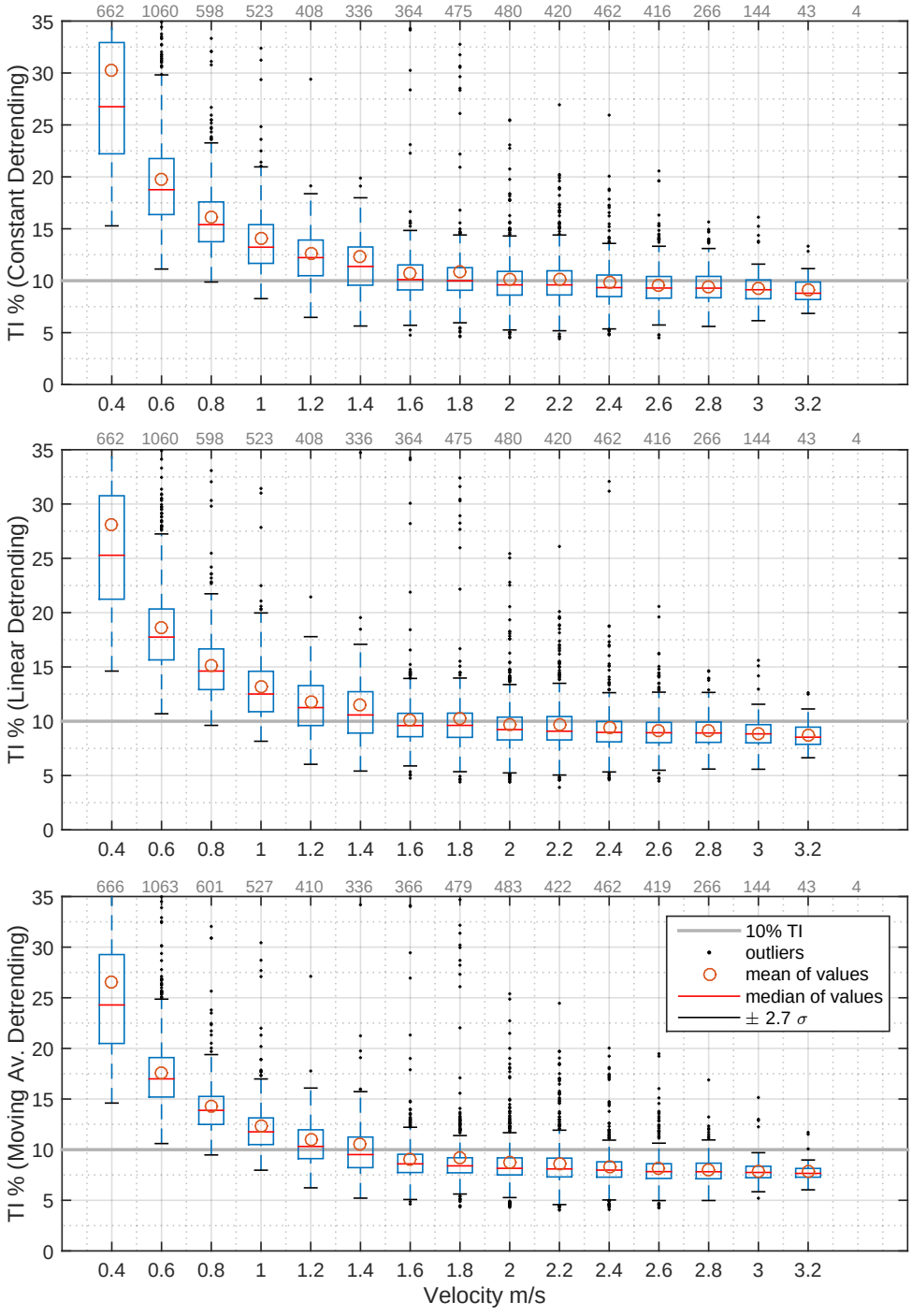

Figure 3.47: Streamwise TI - Ambient Flow, Flood Tide. No Doppler noise correction. Number of 5 minute ensembles are shown in grey at top outer edge of each plot.

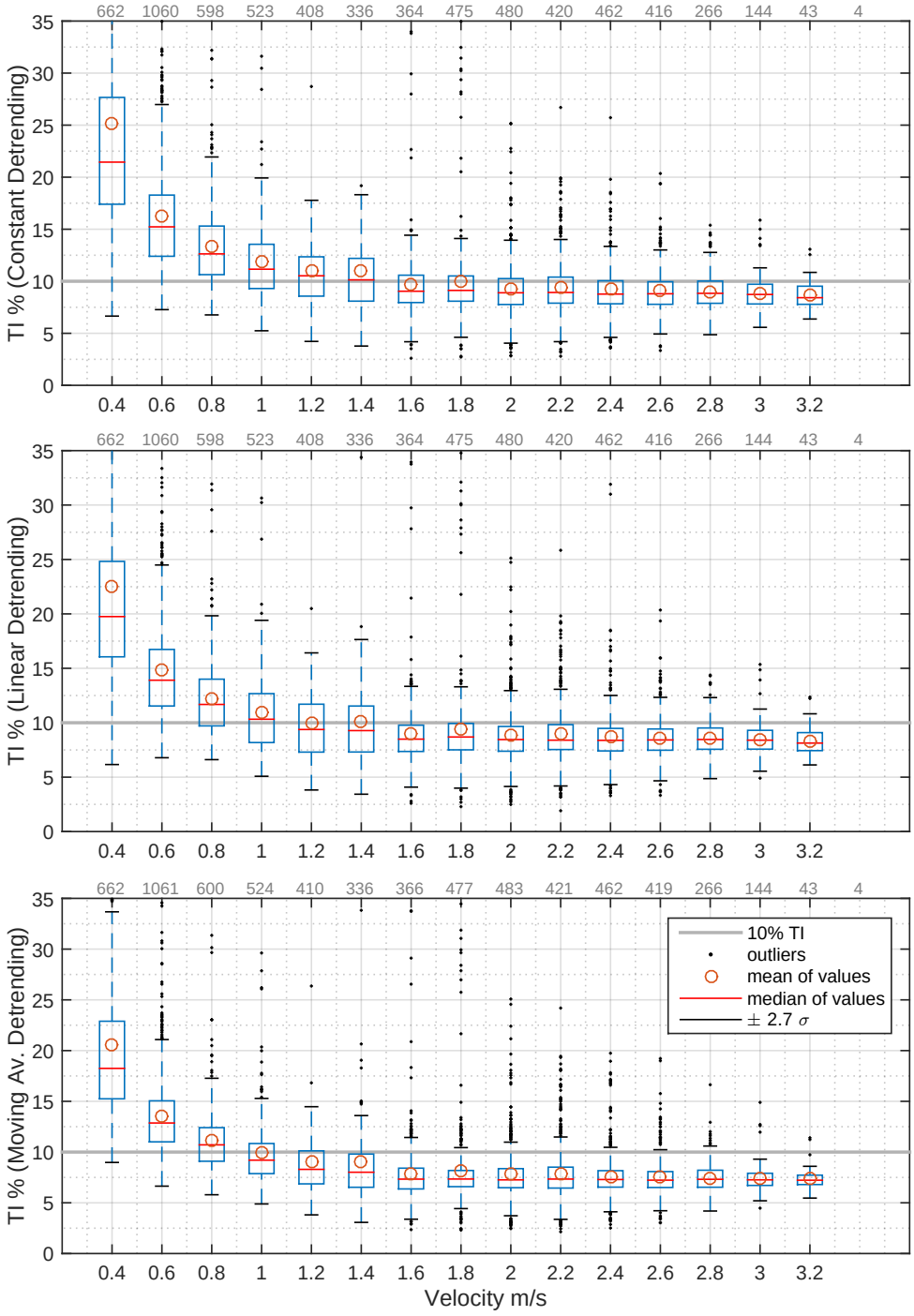

Figure 3.48: Streamwise TI - Ambient Flow, Flood Tide. Doppler noise correction applied.

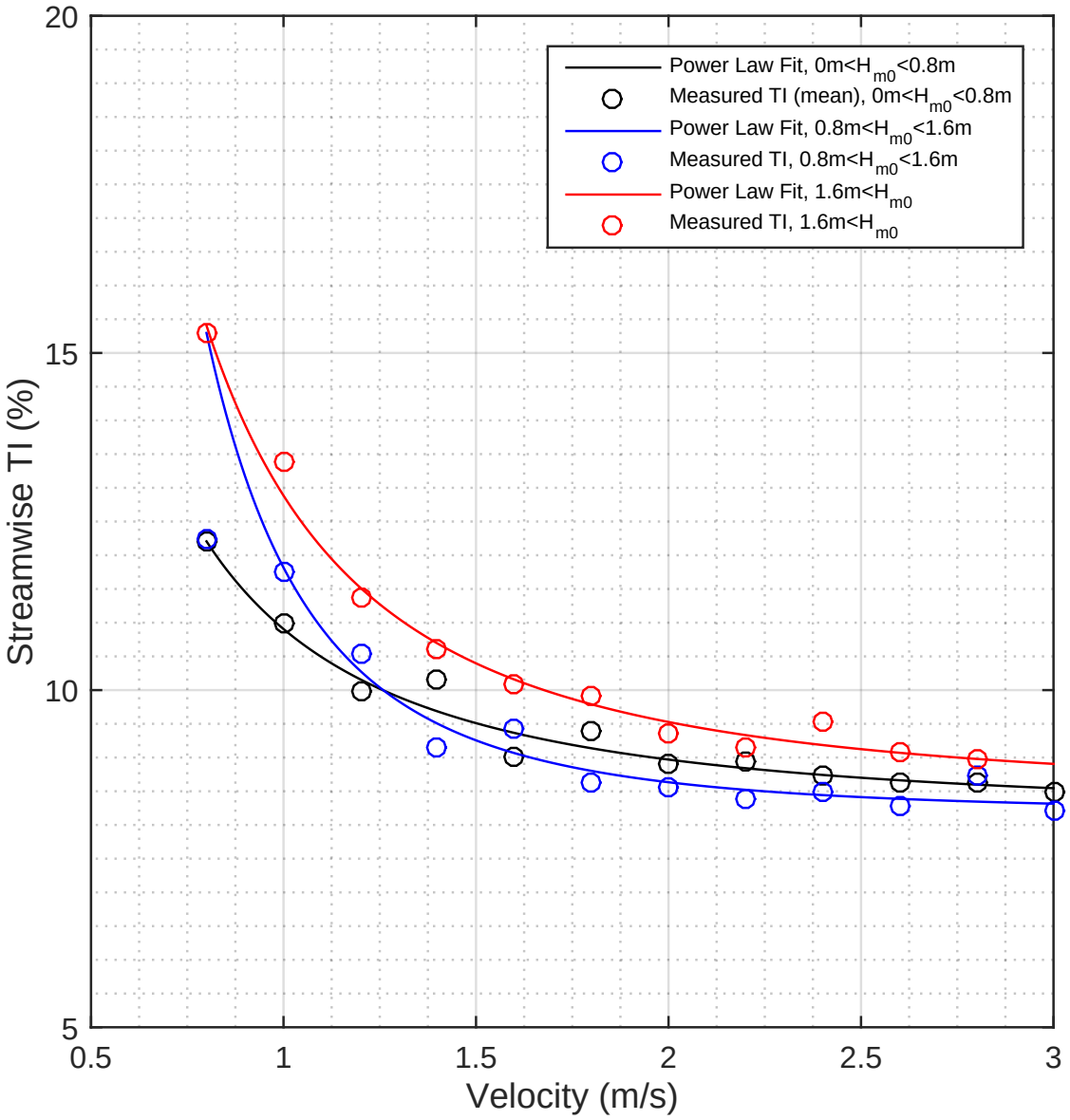

Figure 3.49: Streamwise TI - Ambient Flow, Flood Tide. Doppler noise correction applied.

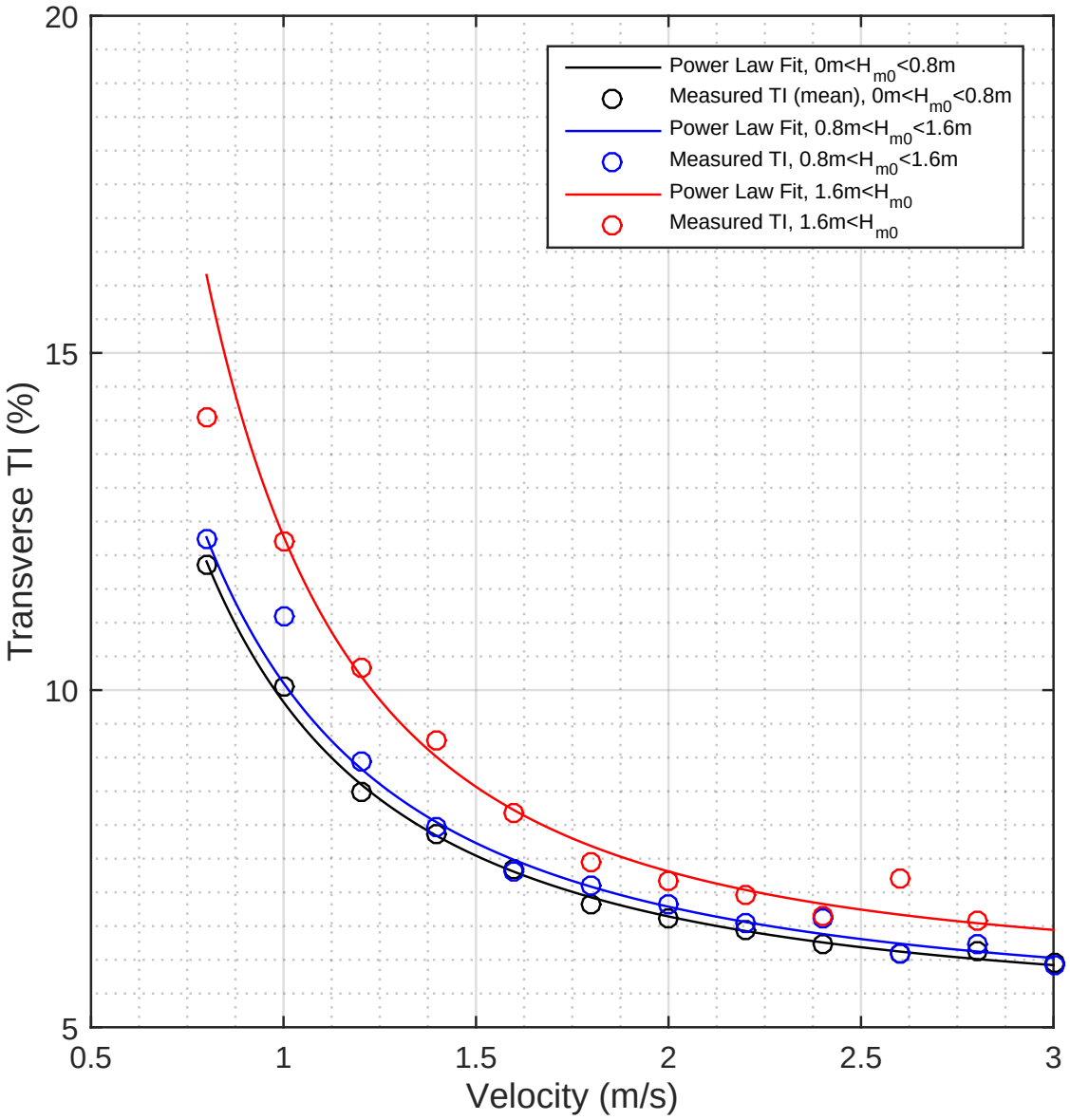

Figure 3.50: Transverse TI - Ambient Flow, Flood Tide. Doppler noise correction applied.

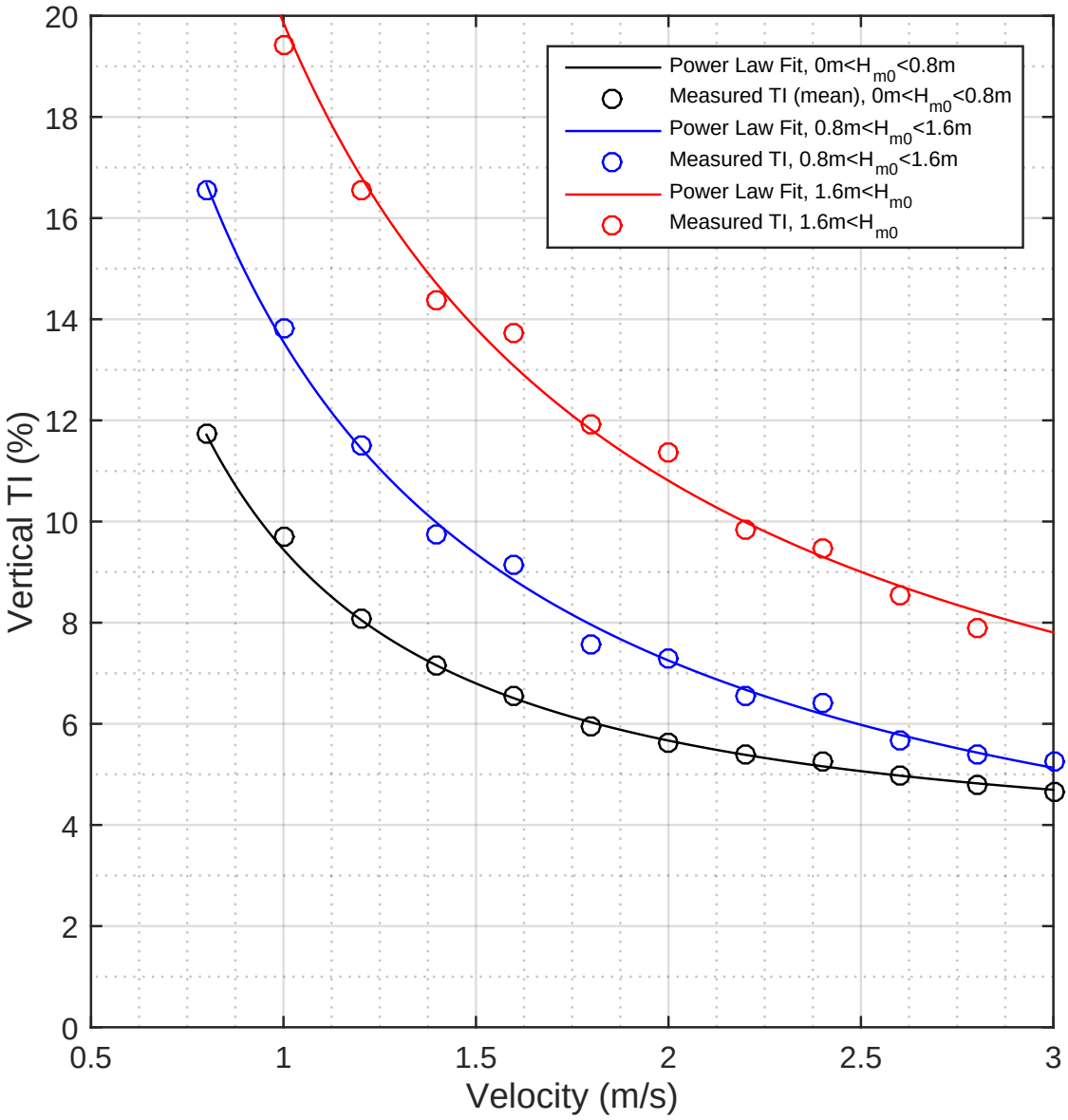

Figure 3.51: Vertical TI - Ambient Flow, Flood Tide. Doppler noise correction applied.

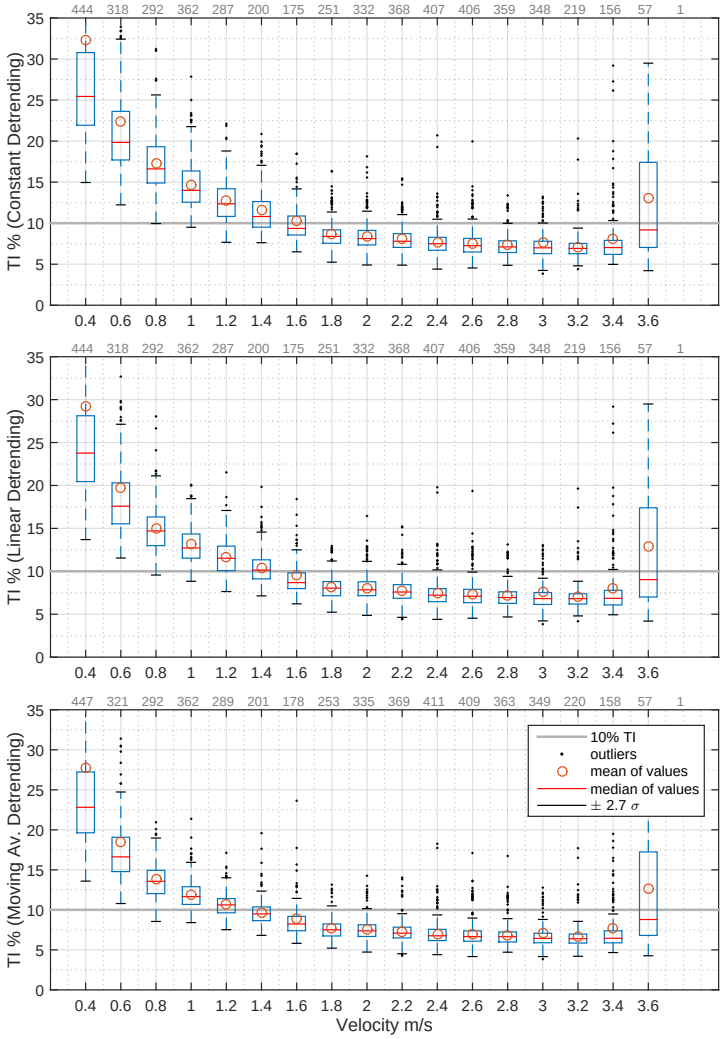

Figure 3.52: Streamwise TI - Ambient Flow, Ebb Tide. No Doppler noise correction. Number of 5 minute ensembles are shown in grey at top outer edge of each plot.

3.7.5 Turbulence Intensity - Ebb Tide

Figure 3.52 shows TI versus velocity for ebb tides in ambient conditions from multiple turbine mounted single-beam instruments. Moving average detrending produces the smallest TI values whilst constant mean detrending produces the largest.

Figure 3.53 shows TI versus velocity for flood tides in ambient conditions from multiple turbine mounted single-beam instruments with Doppler noise correction applied to the data using equation 3.5.

Figure 3.54 shows **streamwise** Turbulence Intensities returned with the turbine orientated reversed to the flood tide. The linear-fit method of detrending was applied to the velocity time series under the influence of small, medium and large wave field conditions as previously defined. I_u in these plots are corrected for Doppler noise.

I_u increases under wave conditions above the smallest band for low velocities below approximately 2 ms^{-1}).

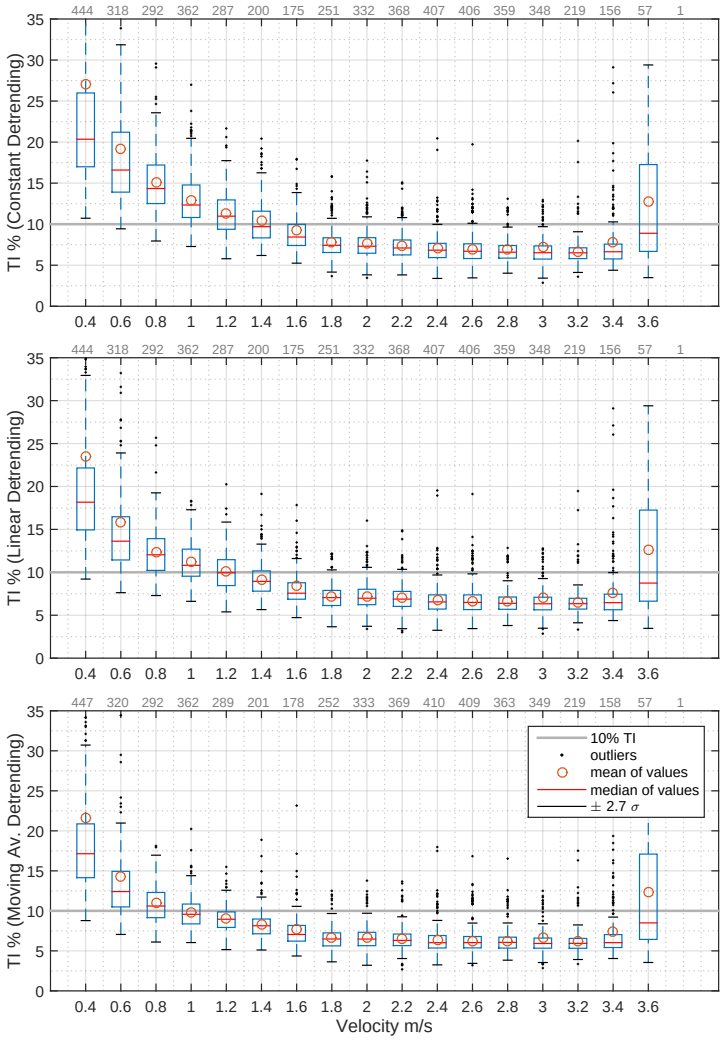

Figure 3.53: Streamwise TI - Ambient Flow, Ebb Tide. Doppler noise correction applied.

Table 3.11 provides summary data for I_u, I_v, and I_w in Flood tides featuring small, medium and large waves for both uncorrected and Doppler noise-corrected post-processing.

Summary Table. Turbulence Intensity for Flood and Ebb Tides

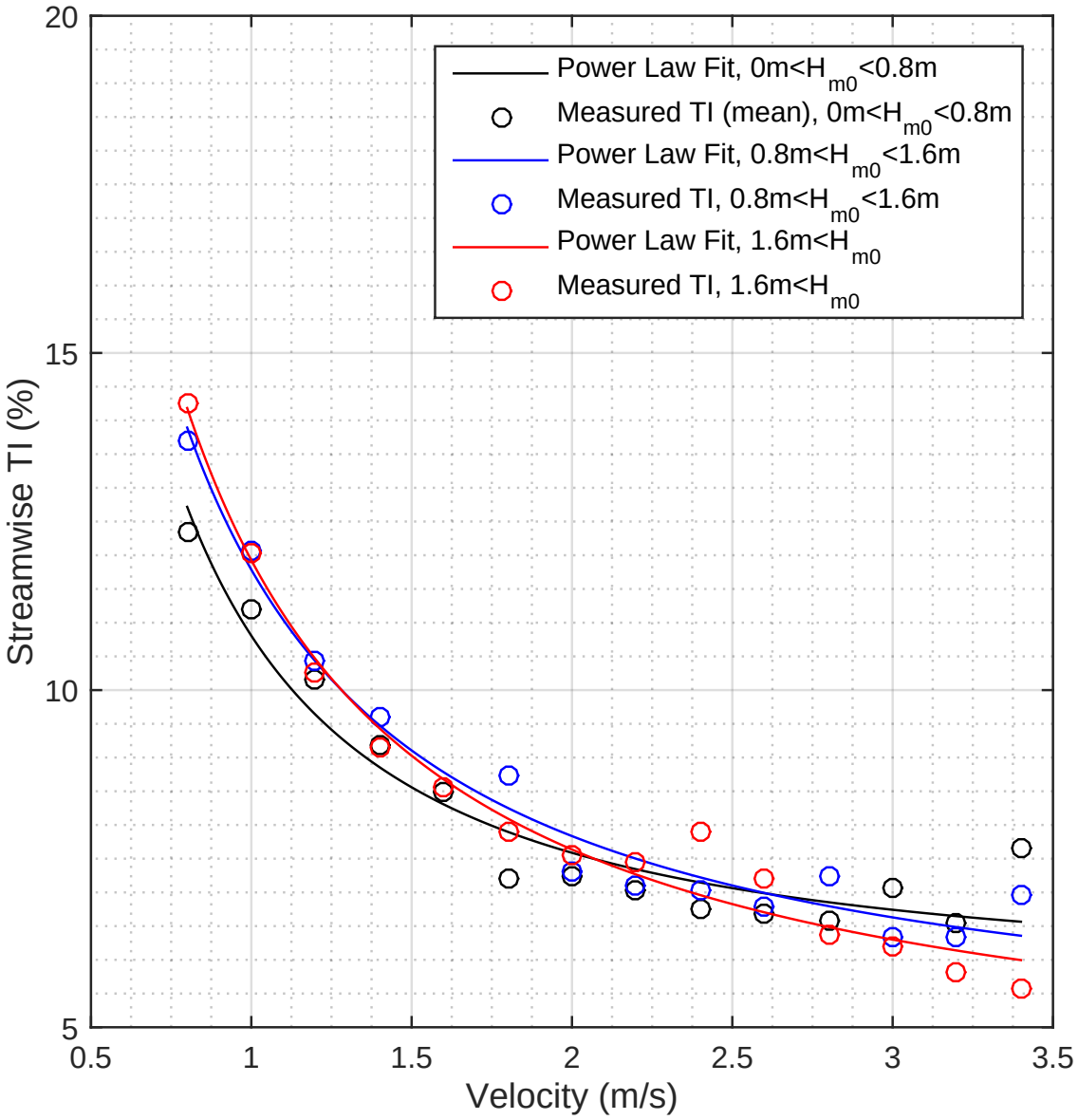

Figure 3.54: Streamwise TI - Ambient Flow, Ebb Tide. Doppler noise correction applied.

Table 3.11: Flood Tide. Component TI mean and standard deviation

Detrending	**X** **0m<H_{m0}<0.8m**			**Y** **0.8m<H_{m0}<1.6m**			**Z** **1.6m<H_{m0}**		
Constant	**9.6 ± 2.0**	6.8 ± 0.9	5.7 ± 0.7	**9.2 ± 1.3**	6.8 ± 0.6	6.3 ± 1.2	**10.0 ± 1.5**	8.0 ± 1.0	9.0 ± 2.1
Linear	**9.1 ± 1.9**	6.7 ± 0.9	5.7 ± 0.6	**8.8 ± 1.2**	6.7 ± 0.6	6.3 ± 1.2	**9.6 ± 1.5**	7.7 ± 1.0	9.0 ± 2.1
MA	**8.1 ± 1.8**	6.5 ± 1.0	5.6 ± 0.6	**7.8 ± 1.3**	6.5 ± 0.5	6.3 ± 1.2	**8.6 ± 1.5**	7.6 ± 1.0	9.0 ± 2.2

Table 3.12: Flood Tide. Component TI mean and standard deviation with noise correction

Detrending	**X** **0m<H_{m0}<0.8m**			**Y** **0.8m<H_{m0}<1.6m**			**Z** **1.6m<H_{m0}**		
Constant	**9.1 ± 2.1**	6.3 ± 1.0	5.0 ± 0.7	**8.7 ± 1.4**	6.2 ± 0.6	5.7 ± 1.3	**9.5 ± 1.5**	7.5 ± 1.1	8.6 ± 2.2
Linear	**8.6 ± 2.0**	6.1 ± 1.0	5.0 ± 0.7	**8.3 ± 1.3**	6.1 ± 0.6	5.7 ± 1.3	**9.1 ± 1.6**	7.2 ± 1.0	8.5 ± 2.3
MA	**7.5 ± 1.9**	5.9 ± 1.1	5.0 ± 0.7	**7.2 ± 1.4**	5.9 ± 0.6	5.6 ± 1.3	**8.1 ± 1.6**	7.1 ± 1.0	8.5 ± 2.3

Table 3.13: Ebb Tide. Component TI mean and standard deviation.

Detrending	**X** **0m<H_{m0}<0.8m**			**Y** **0.8m<H_{m0}<1.6m**			**Z** **1.6m<H_{m0}**		
Constant	**7.5 ± 1.6**	6.3 ± 1.0	5.1 ± 1.3	**7.5 ± 1.1**	6.2 ± 1.7	5.7 ± 1.3	**8.0 ± 1.2**	6.2 ± 0.9	6.2 ± 0.9
Linear	**7.3 ± 1.6**	6.2 ± 1.0	5.0 ± 1.3	**7.4 ± 1.0**	6.1 ± 1.4	5.7 ± 1.3	**7.8 ± 1.2**	6.1 ± 0.9	6.2 ± 0.9
MA	**6.9 ± 1.5**	6.1 ± 1.1	5.0 ± 1.3	**6.9 ± 1.0**	6.0 ± 1.0	5.7 ± 1.3	**7.5 ± 1.2**	6.0 ± 1.2	6.2 ± 0.9

Table 3.14: Ebb Tide. Component TI mean and standard deviation with noise correction.

Detrending	**X** **0m<H_{m0}<0.8m**			**Y** **0.8m<H_{m0}<1.6m**			**Z** **1.6m<H_{m0}**		
Constant	**6.9 ± 1.8**	5.7 ± 1.1	4.2 ± 1.5	**6.9 ± 1.1**	5.6 ± 1.8	5.0 ± 1.5	**7.4 ± 1.3**	5.6 ± 1.0	5.6 ± 1.0
Linear	**6.7 ± 1.7**	5.6 ± 1.1	4.2 ± 1.4	**6.8 ± 1.1**	5.5 ± 1.5	5.0 ± 1.5	**7.2 ± 1.3**	5.5 ± 1.0	5.6 ± 1.0
MA	**6.2 ± 1.6**	5.5 ± 1.2	4.2 ± 1.4	**6.3 ± 1.1**	5.3 ± 1.1	5.0 ± 1.5	**6.9 ± 1.3**	5.3 ± 1.2	5.6 ± 1.0

3.8 Analysis: Seabed Mounted Instrumentation

This section provides summary results for seabed deployed D-ADP (ADCPs) installed predominantly upstream and downstream of the DEEPGEN IV tidal turbine. Depth profiles of velocity are shown in sections 3.8.1 and 3.8.4 for flood and ebb tides. Depth profiles of turbulence intensity are shown in sections 3.8.2 (flood) and 3.8.5 (ebb). Depth profiles of Reynolds stress, τ_{uw}, are shown in sections 3.8.3 (flood) and 3.8.6 (ebb).

3.8.1 Depth Profiles of Velocity - Flood Tide

Figures 3.55 and 3.56 present the Flood tide velocity as a function of depth for each of the NW D-ADP deployments, representing the uninterrupted inflow to the turbine. Each sub-plot is subdivided into velocity bins of $\pm$ 0.2ms^{-1}. The effect of the surface can be seen near the Mean Water Line (MWL) in each sub-figure. The presence of medium and high wave conditions are marked by crosses and circles respectively.

Seasonal variations can be seen in Figures 3.56 through the differences in maximum velocities with sub-figure (b) showing maximum values of $\overline{u}$ of < 3 ms^{-1}, while sub-figure (e) shows maximum values of up to 3.4ms^{-1} near the surface for a similar deployment location. As can be seen the velocity as a function of depth follows a power law [12] with velocity increasing with increased separation from the boundary.

In the majority of results, the presence of waves has little effect on the shape of the profile, with slight variations in magnitude compared with the low wave case, this is particularly noticeable at higher flow speeds. There is one significant exception in Figure 3.56 sub-figure (f) for the ADCP02-NW-Dep5, where large waves can be seen to cause a significant slowing of the flow near the surface. This is most likely due to the wave direction in this case being opposed to the flow direction, while for the other medium and high wave cases presented, the wave direction is likely closely aligned with the flow.

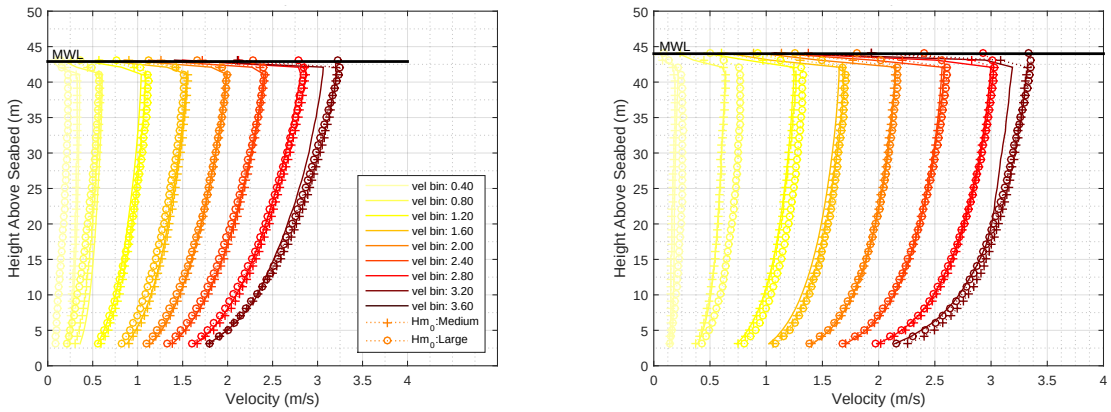

(a) ADCPTD7-01-Dep1

(b) ADCPTD7-02-Dep1

Figure 3.55: Depth profiles of velocity (m/s) for seabed ADCPs upstream of flood tidal flow

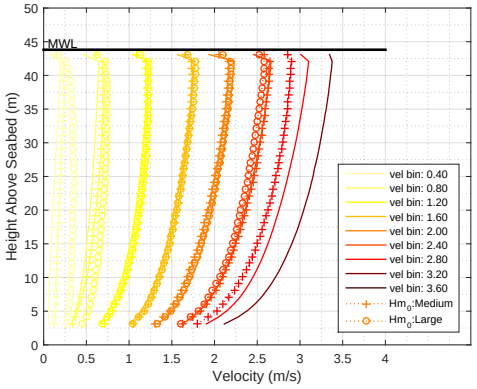

(a) ADCP01-NW-Dep0

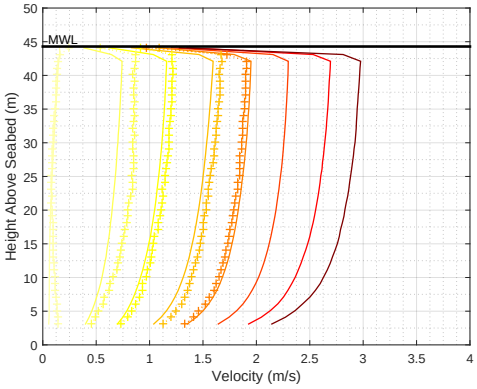

(b) ADCP01-NW-Dep1

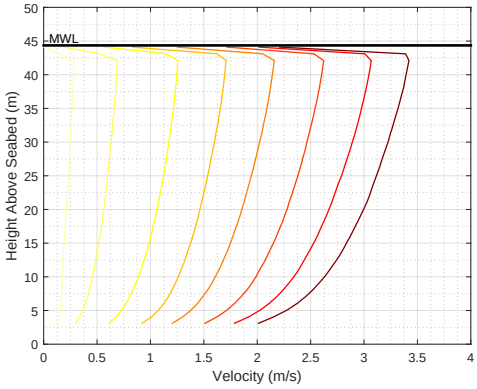

(c) ADCP01-NW-Dep2

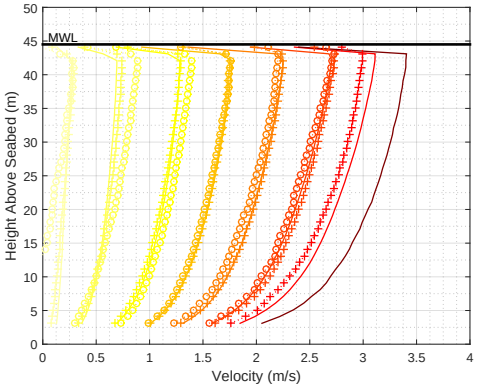

(d) ADCP01-NW-Dep3

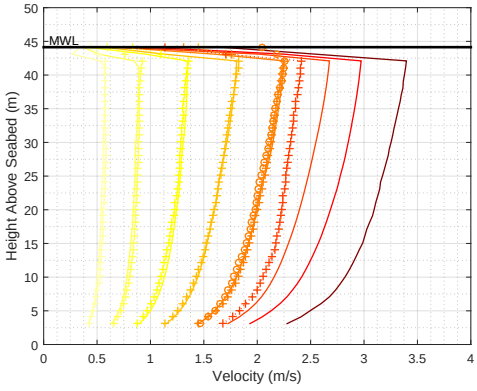

(e) ADCP01-NW-Dep5

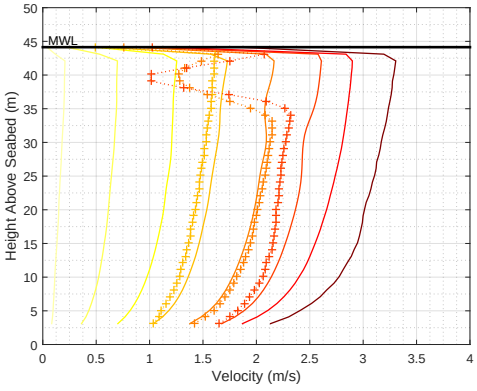

(f) ADCP02-NW-Dep5

Figure 3.56: Depth profiles of velocity (m/s) for seabed ADCPs upstream of turbine on flood tidal flow

3.8.2 Depth Profiles of Turbulence Intensity - Flood Tide

Figures 3.57 and 3.58 present the flood tide turbulence intensity as a function of depth for each of the NW D-ADP deployments representing the uninterrupted inflow to the turbine. Each sub-plot is subdivided into velocity bins of $\pm$ 0.2ms^{-1}. The effect of the surface can be seen near the Mean Water Line (MWL) in each sub-figure.

Deployments featuring medium-band wave fields (crosses) and large-band wave conditions (circles) e.g., as shown Figures 3.58a, 3.58c, 3.58d and particularly Figures 3.57a and 3.57b show clear and significant increases in reported TI under these conditions.

If site characterisation was conducted without considering wave conditions then reported TI values could, on the evidence of these plots, be drastically over estimated.

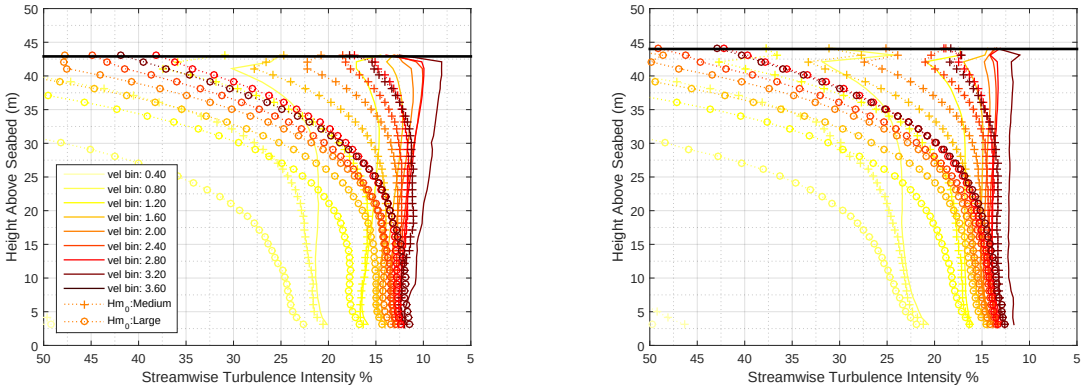

(a) ADCPTD7-01-Dep1

(b) ADCPTD7-02-Dep1

Figure 3.57: Depth profiles of streamwise turbulence intensity for seabed ADCPs upstream of flood tidal flow

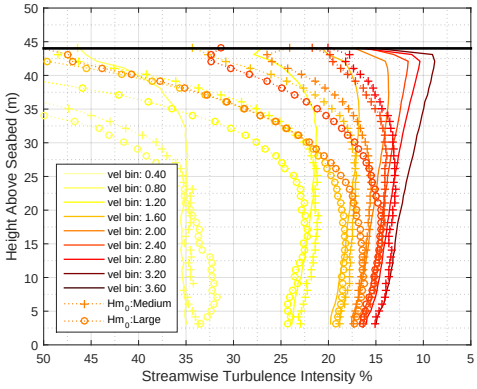

(a) ADCP01-NW-Dep0

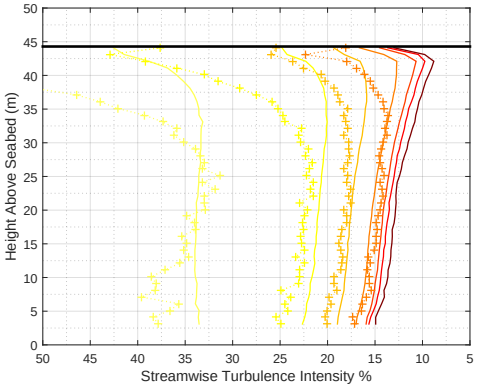

(b) ADCP01-NW-Dep1

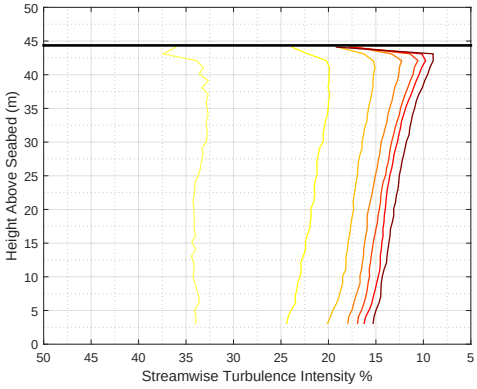

(c) ADCP01-NW-Dep2

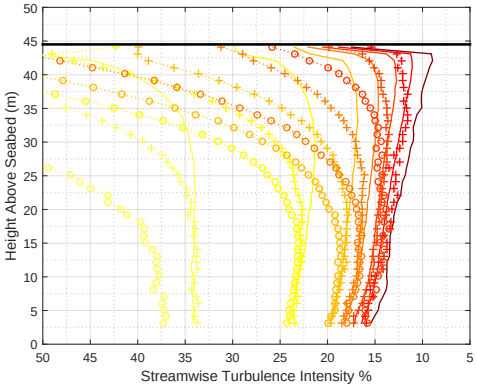

(d) ADCP01-NW-Dep3

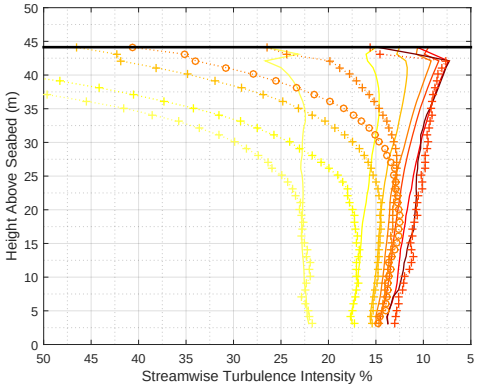

(e) ADCP01-NW-Dep5

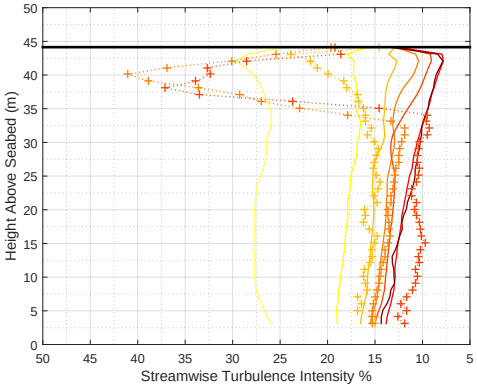

(f) ADCP02-NW-Dep5

Figure 3.58: Depth profiles of streamwise turbulence intensity for seabed ADCPs upstream of flood tidal flow

3.8.3 Depth Profiles of Reynolds Stress - Flood Tide

Figures 3.59 and 3.60 show the results of the streamwise-vertical Reynolds stress tensor for flood tides as measured by the NW D-ADP for all deployments representing the uninterrupted inflow to the turbine. Each sub-plot is subdivided into velocity bins of ± 0.2 ms^{-1}. As with previous sections the presence of medium and high wave conditions are marked by crosses and circles.

For all deployments τ_{uw} can be seen to decrease with height above the seabed, with values near the surface showing significantly less variation with flow-speed than at the bottom boundary. The Reynolds stresses in the presented data sets follow a roughly linear trend, with the greatest deviation from this near (< 10 m) the seabed. The results for a given velocity bin appear relatively constant across the deployments. The exception being the Deployment 7 results (presented in Figures 3.59a and 3.59b) which show different trends and lower mean values for a given velocity range, pointing to the effect of spatial variation at the site. Spurious results near the surface in sub-figure (b) are likely the result of higher ($> 3°$) tilt angles of the D-ADP.

Waves appear to have a minimal effect of the gradient of the Reynolds stresses with depth while biasing the magnitude lower by a small amount. Exceptions to this only exist for highest flow speed cases where limited data was available and thus results have a higher associate uncertainty.

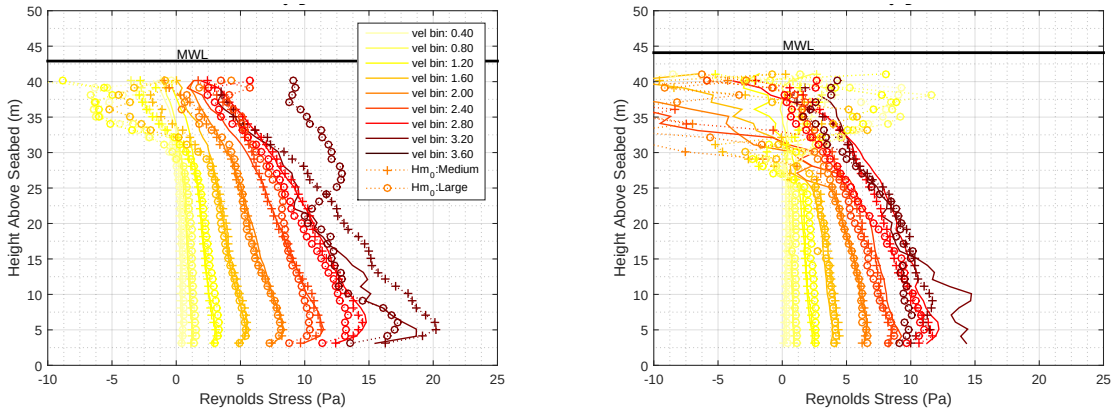

(a) ADCPTD7-01-Dep1

(b) ADCPTD7-02-Dep1

Figure 3.59: Depth profiles of Reynolds Stress (uw) for seabed ADCPs upstream of flood tidal flow

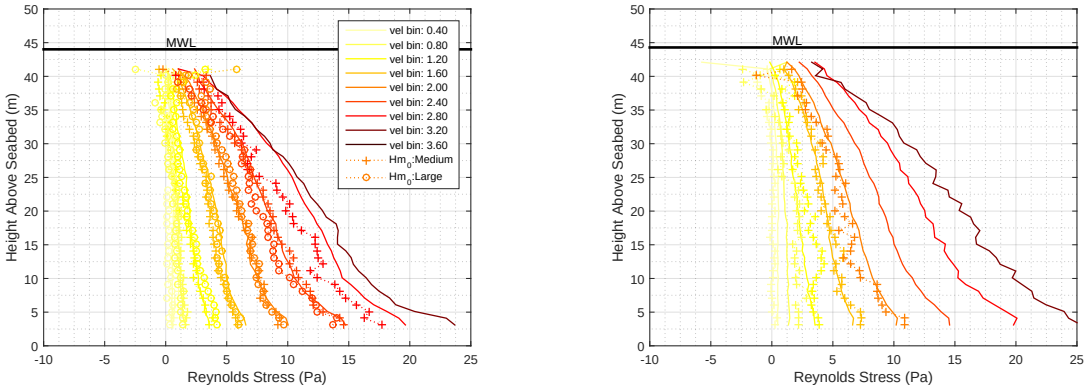

(a) ADCP01-NW-Dep0

(b) ADCP01-NW-Dep1

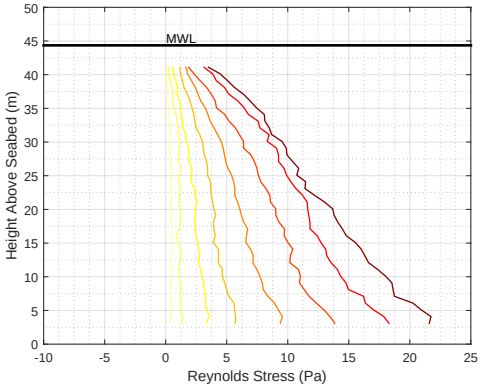

(c) ADCP01-NW-Dep2

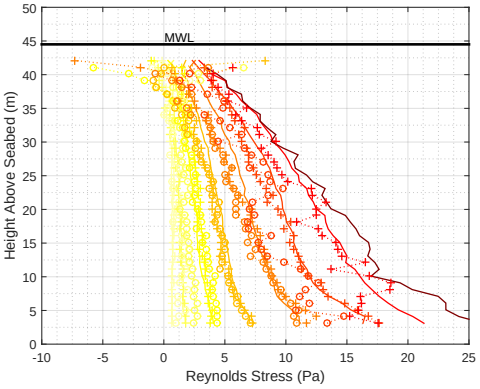

(d) ADCP01-NW-Dep3

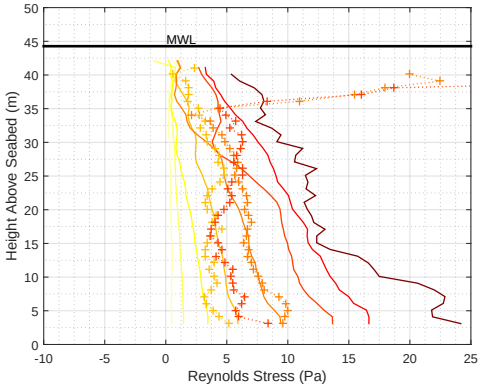

(e) ADCP02-NW-Dep5

Figure 3.60: Depth profiles of Reynolds Stress (uw) for seabed ADCPs upstream of flood tidal flow

3.8.4 Depth Profiles of Velocity - Ebb Tide

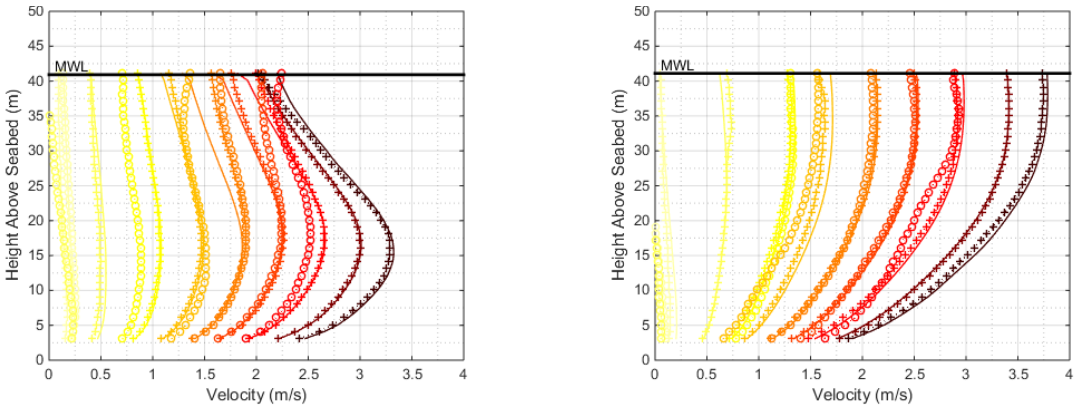

(a) ADCPTD7-01-Dep1

(b) ADCPTD7-02-Dep1

Figure 3.61: Depth profiles of velocity (m/s) for seabed ADCPs upstream of ebb tidal flow

Figures 3.61 and 3.62 present the Ebb tide velocity as a function of depth for each of the SE D-ADP deployments representing the uninterrupted inflow to the turbine. Each sub-plot is subdivided into velocity bins of $\pm$ 0.2ms^{-1}. The effect of the surface can be seen near the Mean water Line (MWL) in each sub-figure. The presence of medium and high wave conditions are marked by crosses and circles.

The flow velocities for ebb at mid-depth are greater than in the flood case across all deployments, reaching maximum values of 3.7 ms^{-1} in several deployments. A significant difference in shape can be seen in all deployments compared with those measured for the Flood tide. The flow increases with separation from the seabed up until a height of $\sim$22 m, where the flow starts to slow as it approaches the surface. The presence of medium and high waves (see Figures 3.62c and 3.62d) show an exaggeration of this effect. This suggests that the phenomenon is due at least in part to surface waves and currents which are opposed to the flow direction. The last two deployments presented in Figure 3.61 show an exception to this, with Figure 3.61a showing the maximum velocity value only 15 m above the seabed and 3.61b showing a profile more closely aligned with the power law as seen in the Flood tide results. This suggests that spatial variability is high at the site and highlights the importance of ADCP placement for both resource analysis and power curve definition.

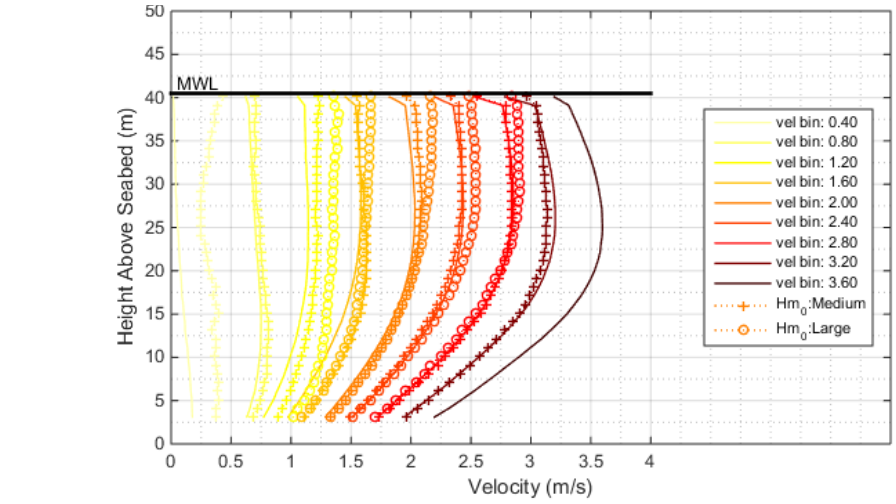

(a) ADCP02-SE-Dep1

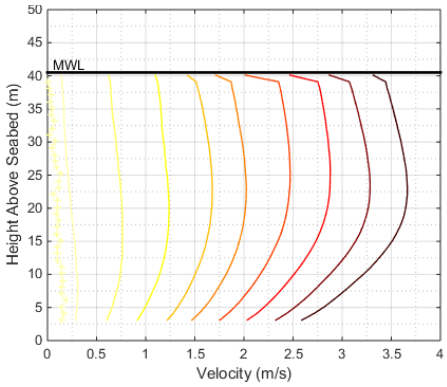

(b) ADCP02-SE-Dep2

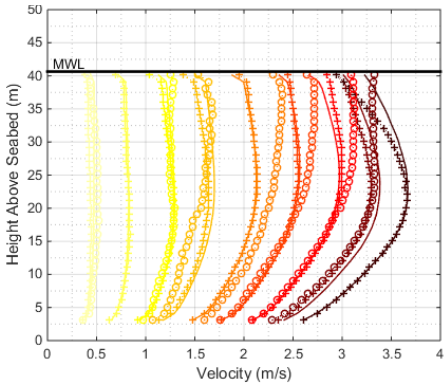

(c) ADCP02-SE-Dep3

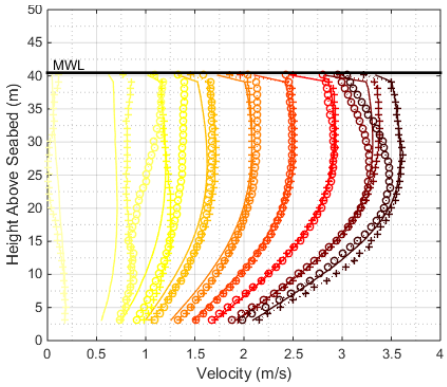

(d) ADCP02-SE-Dep4

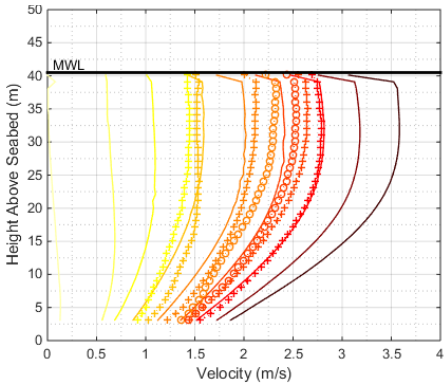

(e) ADCP03-SE-Dep1

Figure 3.62: Depth profiles of velocity (m/s) for seabed ADCPs upstream of ebb tidal flow

3.8.5 Depth Profiles of Turbulence Intensity - Ebb Tide

Figures 3.63 and 3.64 present the flood tide turbulence intensity as a function of depth for each of the NW D-ADP deployments representing the uninterrupted inflow to the turbine. Each sub-plot is subdivided into velocity bins of $\pm$ 0.2ms^{-1}. The effect of the surface can be seen near the Mean Water Line (MWL) in each sub-figure.

Deployments featuring medium-band wave fields (crosses) and large-band wave conditions (circles) e.g., as shown Figures 3.58a, 3.58c, 3.58d and particularly Figures 3.57a and 3.57b show clear and significant increases in reported TI under these conditions.

If site characterisation was conducted without considering wave conditions then reported TI values could, on the evidence of these plots, be drastically over estimated.

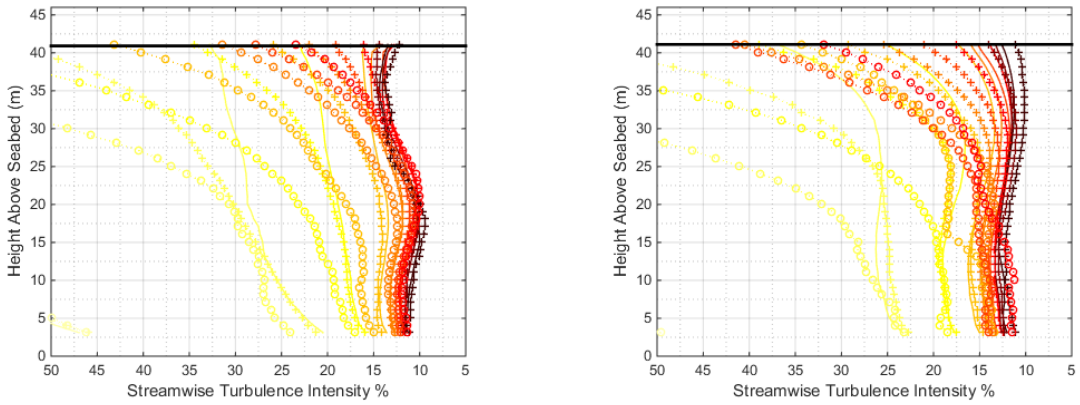

(a) ADCPTD7-01-Dep1

(b) ADCPTD7-02-Dep1

Figure 3.63: Depth profiles of streamwise turbulence intensity for seabed ADCPs upstream of ebb tidal flow

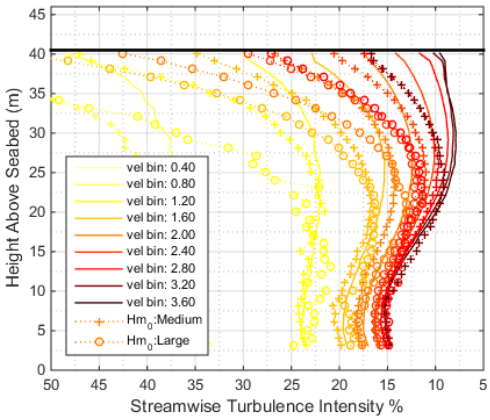

(a) ADCP02-SE-Dep1

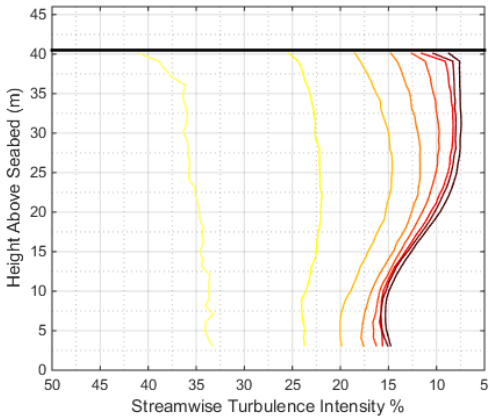

(b) ADCP02-SE-Dep2

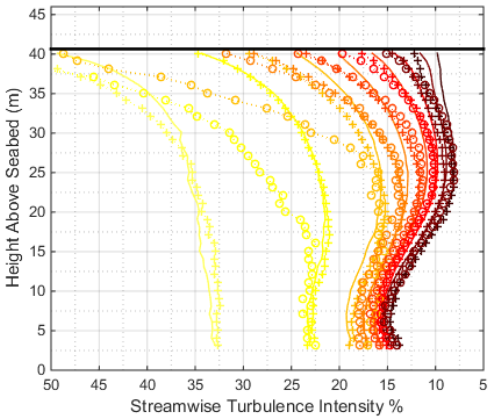

(c) ADCP02-SE-Dep3

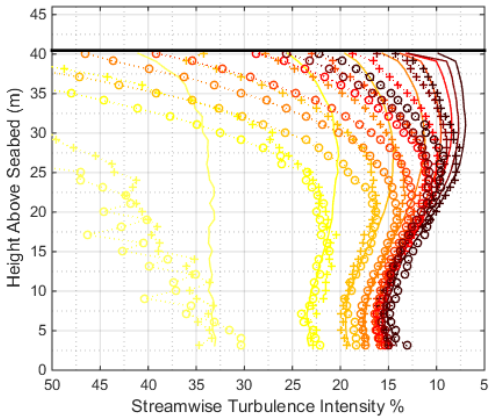

(d) ADCP02-SE-Dep4

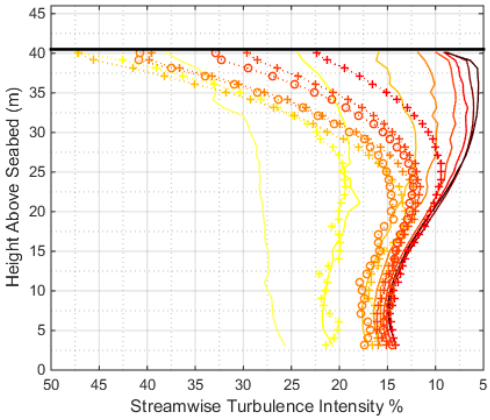

(e) ADCP03-SE-Dep1

Figure 3.64: Depth profiles of streamwise turbulence intensity for seabed ADCPs upstream of ebb tidal flow

3.8.6 Depth Profiles of Reynolds Stress - Ebb Tide

Figures 3.65 and 3.66 show the results of the streamwise-vertical Reynolds stress tensor for Ebb tides as measured by the SE D-ADP for all deployments representing the uninterrupted inflow to the turbine. Each sub-plot is subdivided into velocity bins of $\pm$ 0.2 ms^{-1}.

Figure 3.66c represents spurious results due to significantly high and dynamic tilt angles while Figure 3.66e also presents spurious results the cause of which is not clear. The remaining sub-figures in Figure 3.66c show similar trends across the three deployments. Ebb tide Reynold stresses differ to those for the flood tide, exhibiting higher maximum values and non-linear and steeper gradients of τ_{uw} with depth. Values increase from the seabed to a maximum at $\sim$ 7 m, then decrease to zero at $\sim$ 25 m. Values above this height swap sign for the highest flow speeds, indicating a change of shear direction near the surface.

Figure 3.65 gives the results for Deployment 7 which (as with the flood tide results for this instrument) highlight the high spatial variation at the site. Figure 3.65a shows an exaggerated version of the other Ebb results with a extreme change of sign from the seabed to values at $\sim$ 25 m height. Figure 3.65b shows similar values as the same sensor for the Flood tide results.

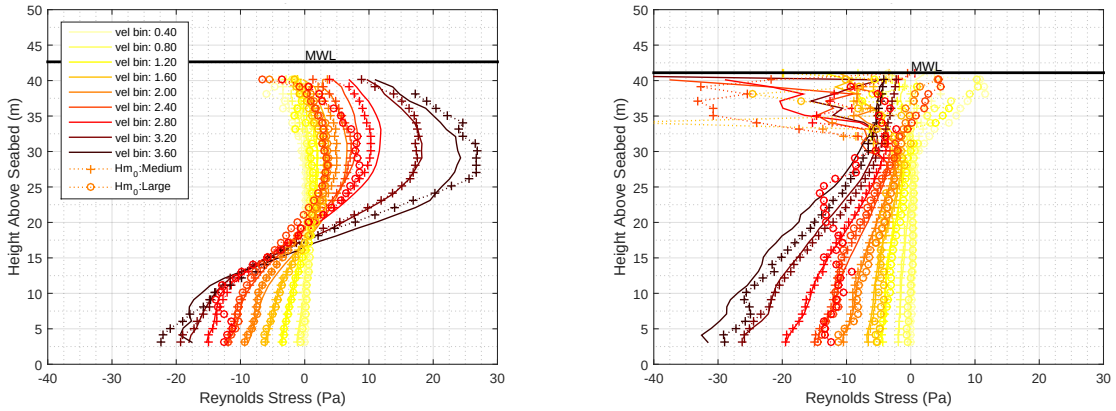

(a) ADCPTD7-01-Dep1

(b) ADCPTD7-02-Dep1

Figure 3.65: Depth profiles of Reynolds Stress (uw) for seabed ADCPs upstream of ebb tidal flow

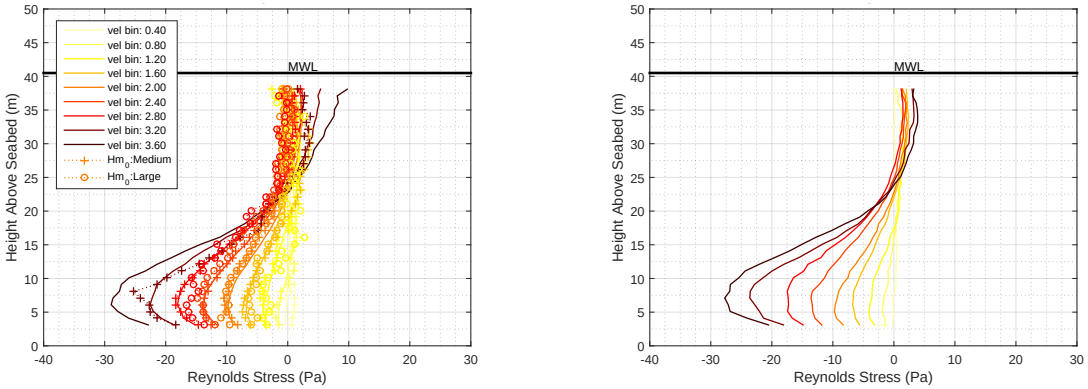

(a) ADCP02-SE-Dep1

(b) ADCP02-SE-Dep2

(c) ADCP02-SE-Dep3

(d) ADCP02-SE-Dep4

(e) ADCP03-SE-Dep1

Figure 3.66: Depth profiles of Reynolds Stress (uw) for seabed ADCPs upstream of ebb tidal flow

3.8.7 Flow Direction Variation - Flood Tide

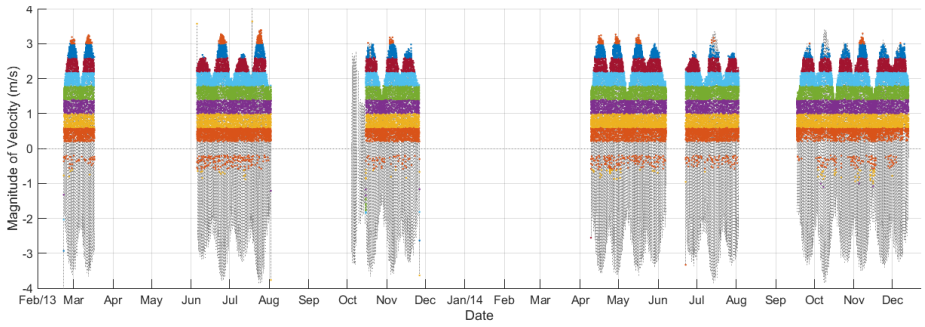

(a) Flood Tide

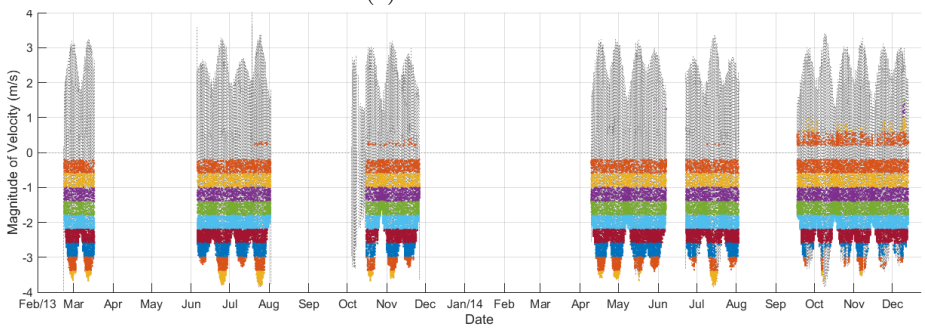

(b) Ebb Tide

Figure 3.67: Data Query:flood and ebb flows; all waves; no acceleration filter applied

Analysis was carried out on the level of variation in the horizontal and vertical directions from mean flow directions derived at hub height from the D-ADP data in both Flood and Ebb Tides.

Figure 3.67a shows the returned data sets for Flood tides. Figure 3.67b shows the returned data sets for Ebb tides. Wave filtering is removed in these instances.

Figure 3.68 shows the *horizontal* deviation of the hub-height flow from the mean flow direction as a function of binned flow velocity for Flood tides. Velocity bins are of width 0.4ms^{-1}. It can be seen that as the tide becomes fully established directional spread reduces from levels of approximately 30° at 0.8ms^{-1} to 5° at 2.0ms^{-1}. At velocities below 2.0ms^{-1} the increase in directional spread is marked is bifurcated (by either tidal ramp up, tidal ramp down). Figure 3.69 shows the same data set plotted in the form of box-plots. These are a useful tool for showing how consistent the directional variation is at higher flow speeds but do remove the information about the split directionality at lower speeds. This information could be maintained by binning the flow data into positive and negative acceleration regions.

Similarly structured results are shown in Figure 3.70 and 3.71. Here, the maximum range of deviation in direction across the *vertical* extent of the rotor plane is shown. Data is in good agreement across the ADCP deployments with mean values below 5° for all flow speeds above 1.6ms^{-1}

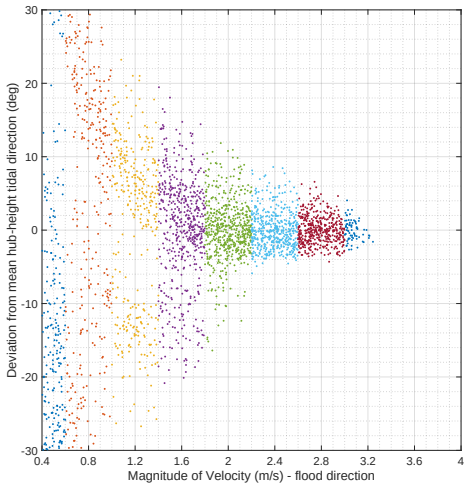

(a) ADCP01-NW-Dep0

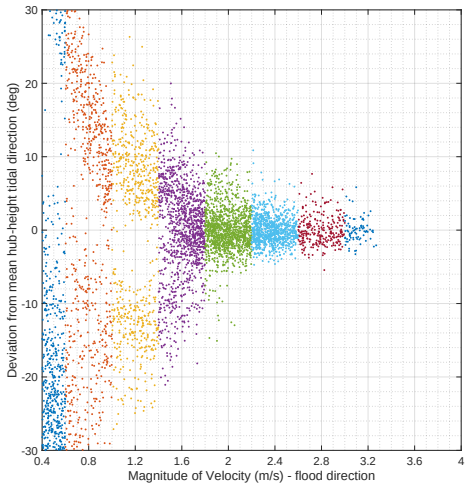

(b) ADCP01-NW-Dep1

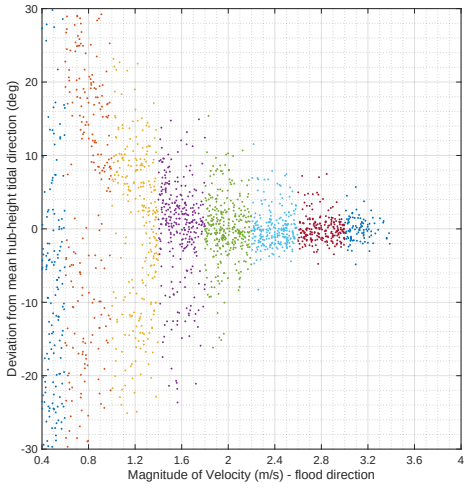

(c) ADCP01-NW-Dep2

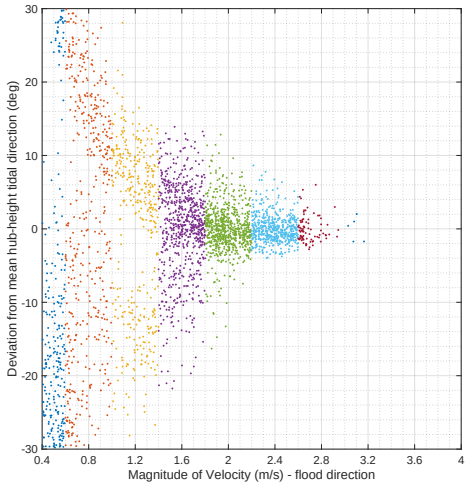

(d) ADCP02-NW-Dep5

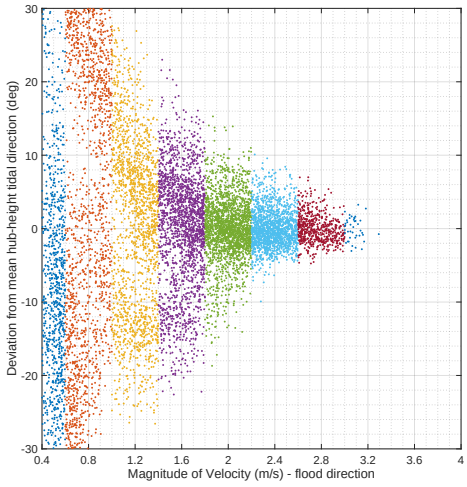

(e) ADCPTD7-01-Dep1

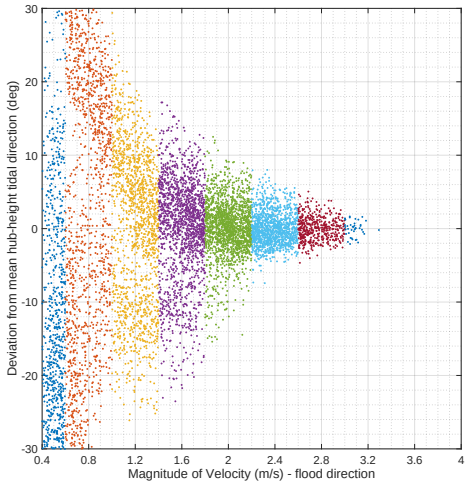

(f) ADCPTD7-02-Dep1

Figure 3.68: Deviation from mean hub-height tidal direction (degrees) for seabed ADCPs upstream of turbine on flood tidal flow

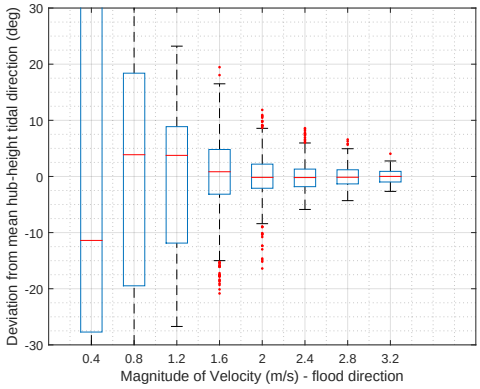

(a) ADCP01-NW-Dep0

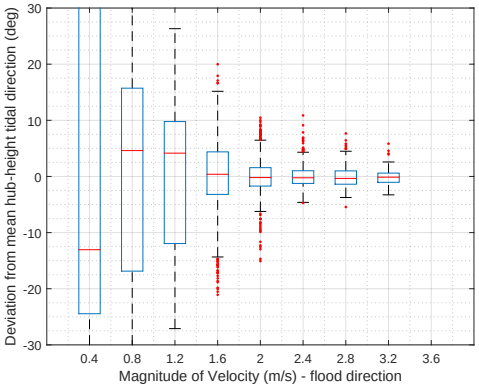

(b) ADCP01-NW-Dep1

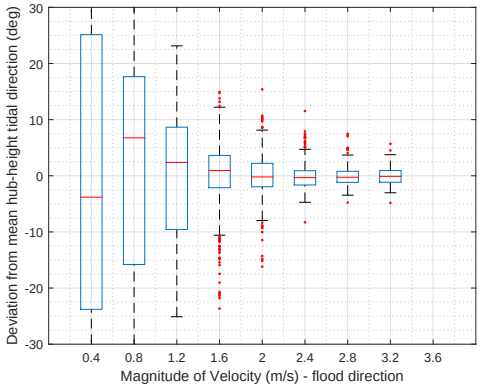

(c) ADCP01-NW-Dep2

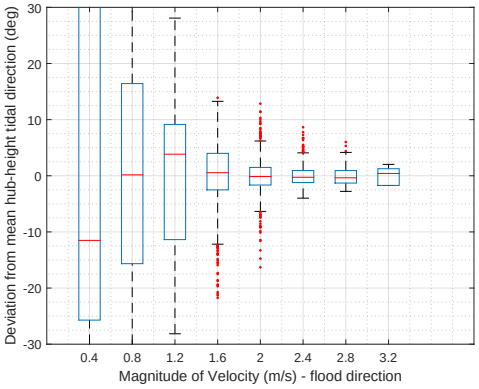

(d) ADCPTD7-01-Dep1

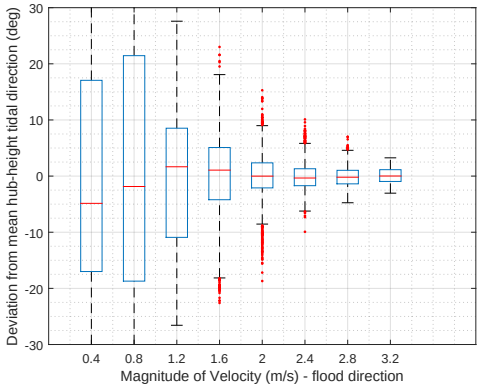

(e) ADCPTD7-02-Dep1

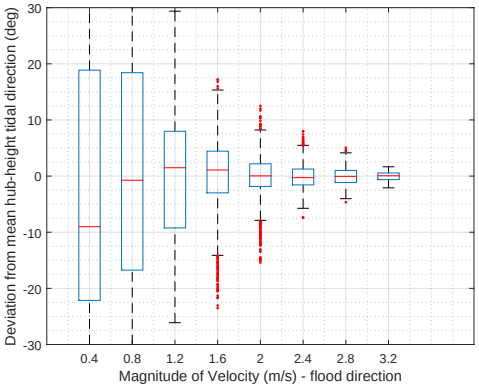

(f) CCombination (inline ADCPs)

Figure 3.69: Deviation from mean hub-height tidal direction (degrees) for seabed ADCPs upstream of turbine on flood tidal flow

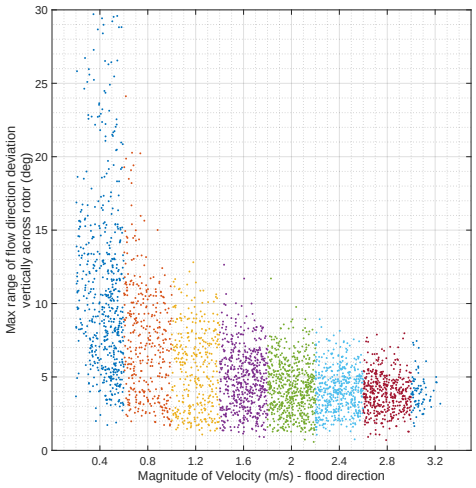

(a) ADCP01-NW-Dep0

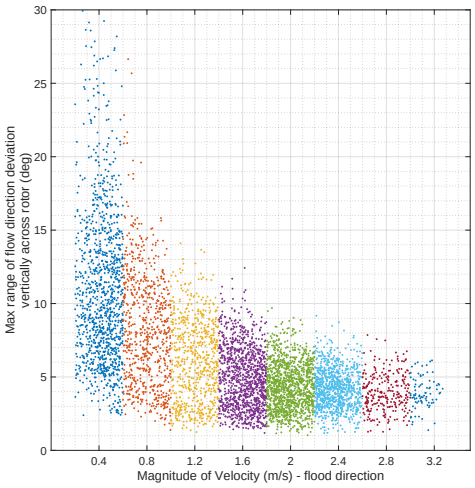

(b) ADCP01-NW-Dep1

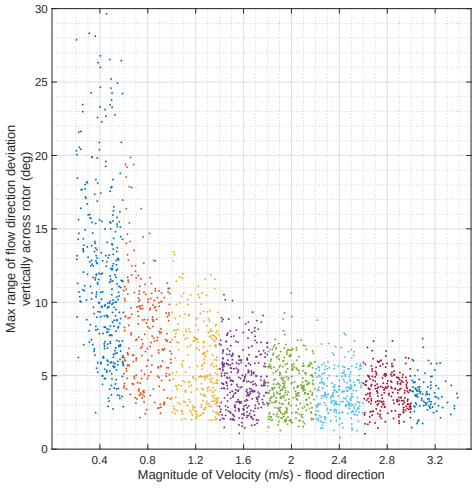

(c) ADCP01-NW-Dep2

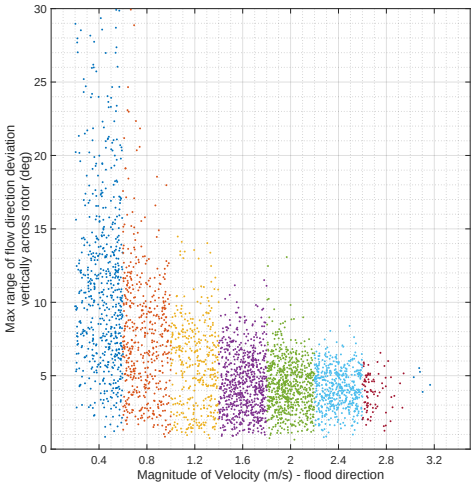

(d) ADCP02-NW-Dep5

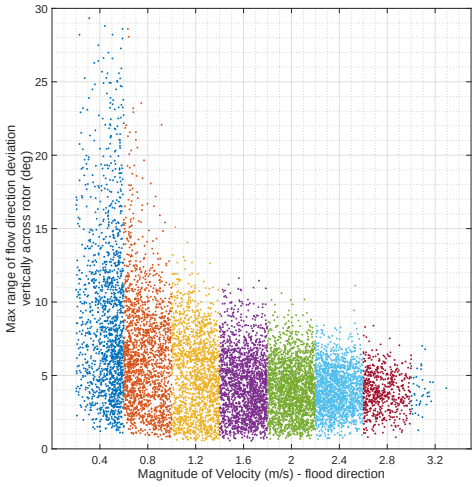

(e) ADCPTD7-01-Dep1

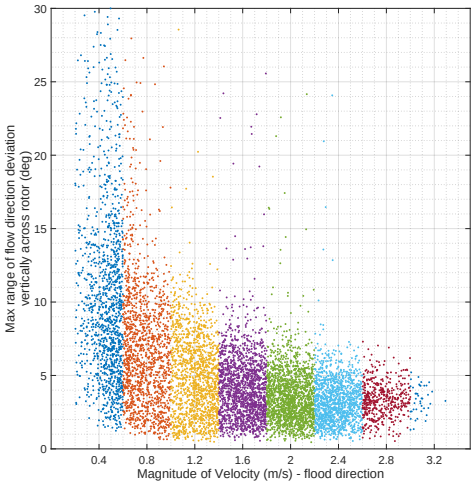

(f) ADCPTD7-02-Dep1

Figure 3.70: Max range of flow direction deviation vertically across rotor (deg)

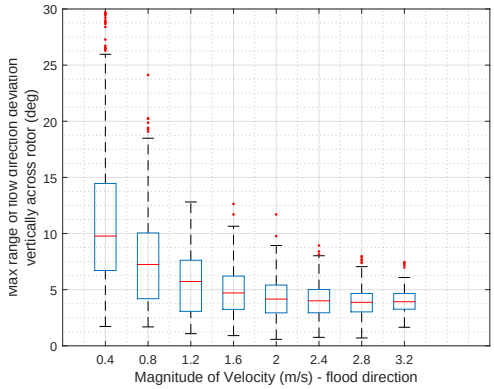

(a) ADCP01-NW-Dep0

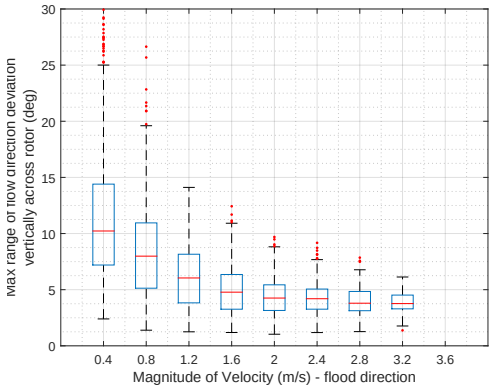

(b) ADCP01-NW-Dep1

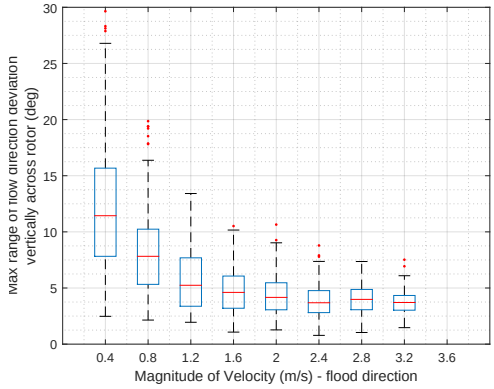

(c) ADCP01-NW-Dep2

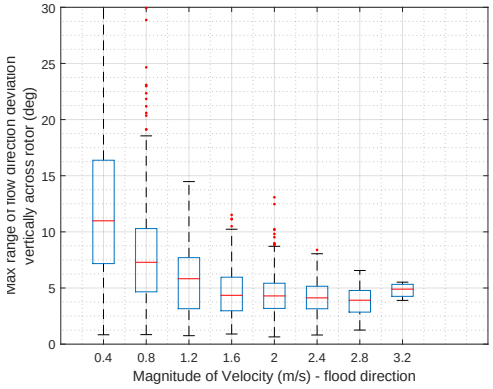

(d) ADCP02-NW-Dep5

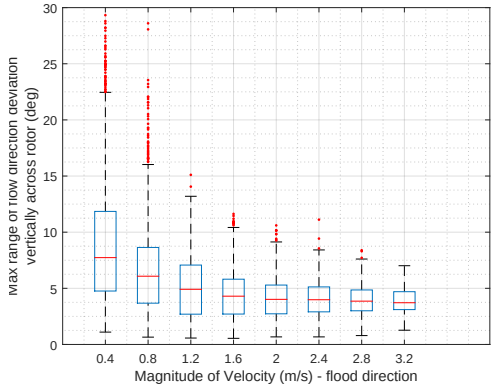

(e) ADCPTD7-01-Dep1

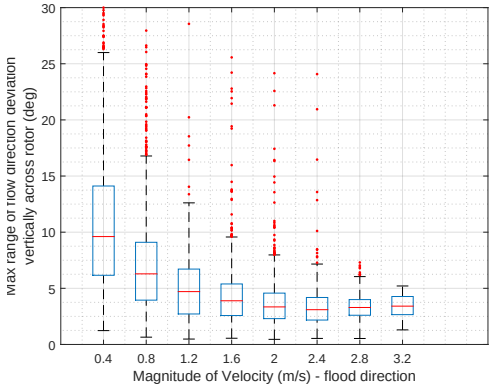

(f) ADCPTD7-02-Dep1

Figure 3.71: Max range of flow direction deviation vertically across rotor (deg)

3.8.8 Flow Direction - Ebb Tide

Figure 3.72 shows the *horizontal* deviation of the hub-height flow from the mean flow direction as a function of binned flow velocity for Ebb tides. Velocity bins are of width 0.4ms^{-1}. It can be seen that as with Flood tides, as the Ebb tide becomes fully established directional spread reduces. The level of low-flow-speed spread is lower, however, and varies from levels of approximately 15° at 0.8ms^{-1} to 5° at 2.0ms^{-1}. At velocities below 2.0ms^{-1} the increase in directional spread is marked is bifurcated (by either tidal ramp up, tidal ramp down).

Figure 3.73 shows the same data set plotted in the form of box-plots.

As with Flood tide data, similarly structured results are shown in Figure 3.74 and 3.75. Here, the maximum range of deviation in direction across the *vertical* extent of the rotor plane is shown. Data is in good agreement across the ADCP deployments with mean values for Ebb higher than those of Flood: approximately between 7° and 8° for flow speeds above 1.6ms^{-1}

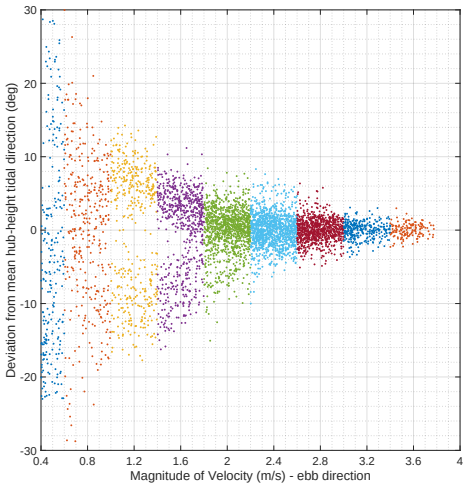

(a) ADCP02-SE-Dep1

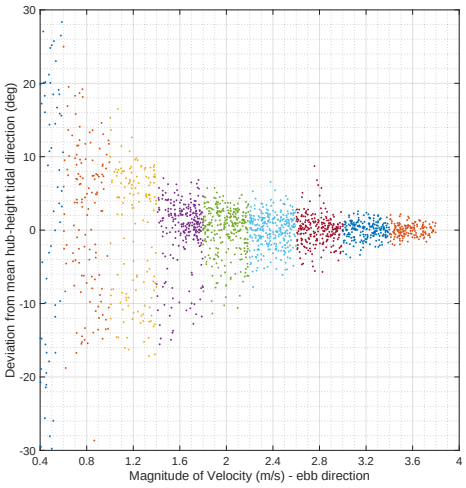

(b) ADCP02-SE-Dep2

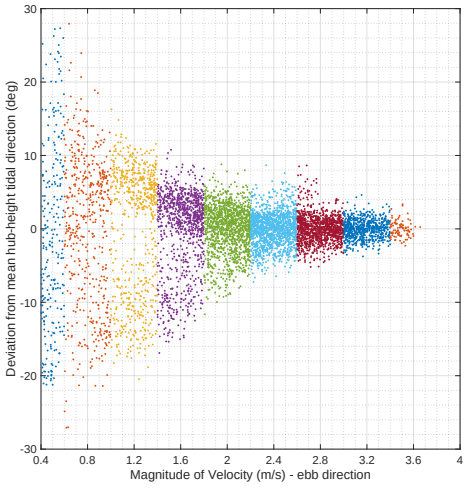

(c) ADCP02-SE-Dep4

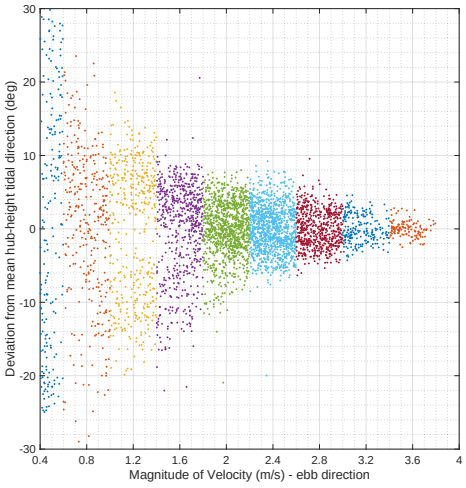

(d) ADCP03-SE-Dep1

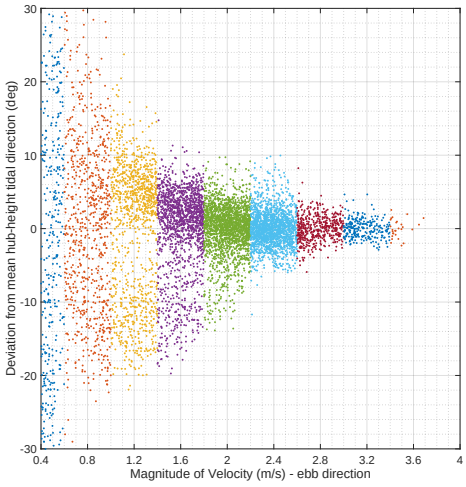

(e) ADCPTD7-01-Dep1

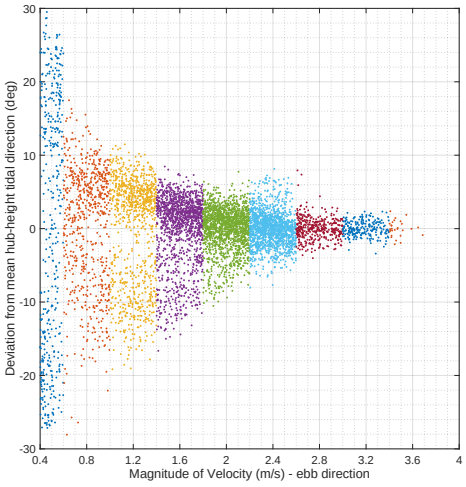

(f) ADCPTD7-02-Dep1

Figure 3.72: Deviation from mean hub-height tidal direction (degrees) for seabed ADCPs upstream of turbine on ebb tidal flow

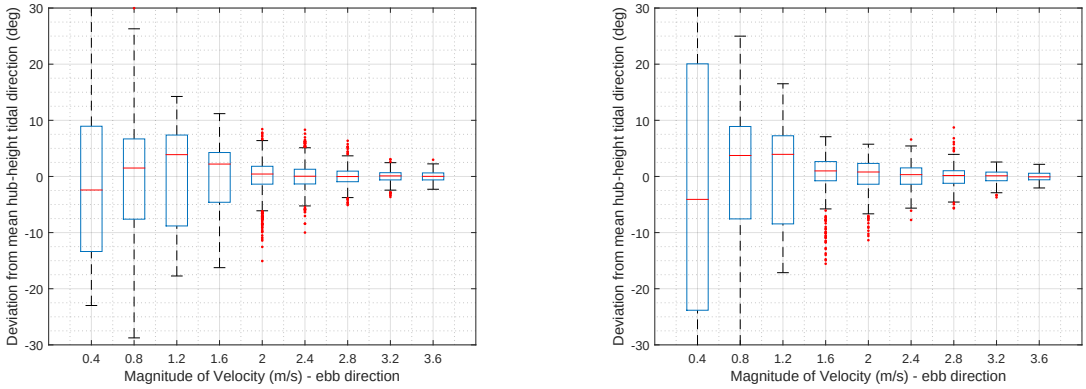

(a) ADCP02-SE-Dep1

(b) ADCP02-SE-Dep2

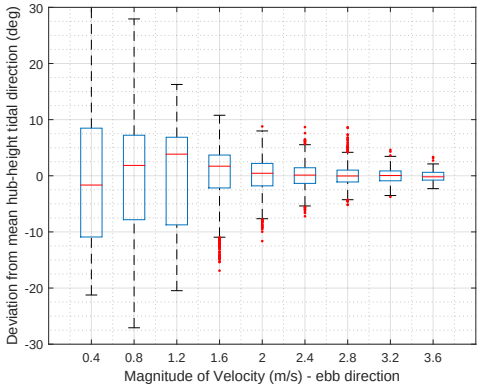

(c) ADCP02-SE-Dep4

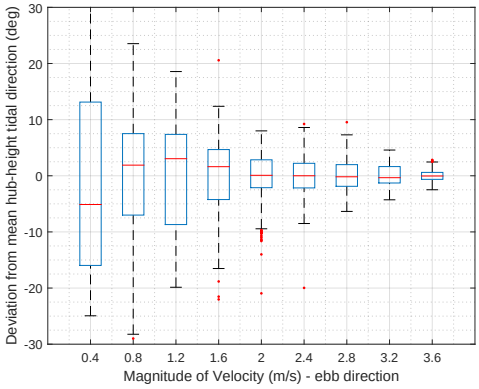

(d) ADCP03-SE-Dep1

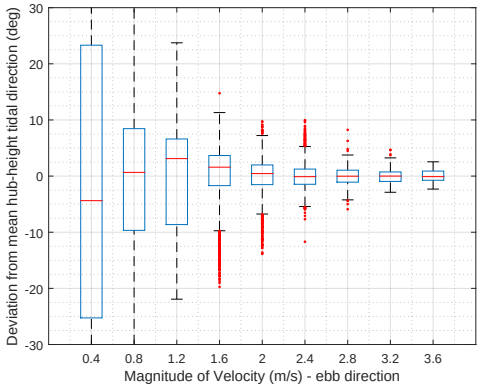

(e) ADCPTD7-01-Dep1

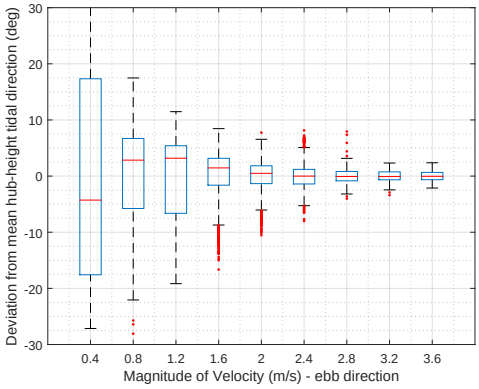

(f) ADCPTD7-02-Dep1

Figure 3.73: Deviation from mean hub-height tidal direction (degrees) for seabed ADCPs upstream of turbine on ebb tidal flow

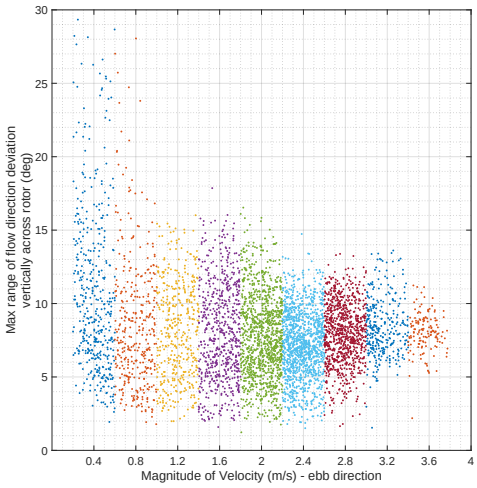

(a) ADCP02-SE-Dep1

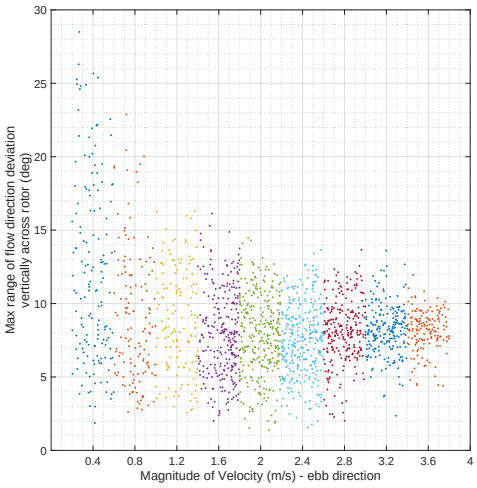

(b) ADCP02-SE-Dep2

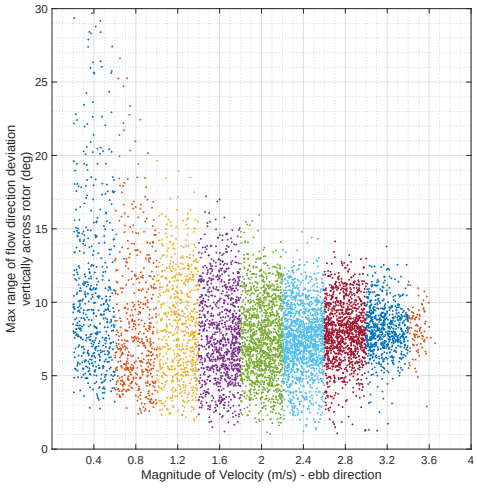

(c) ADCP02-SE-Dep4

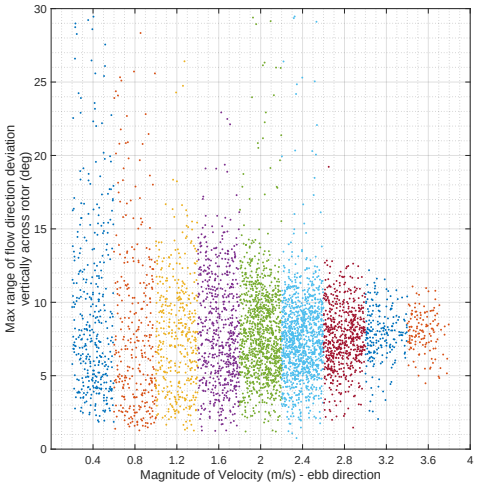

(d) ADCP03-SE-Dep1

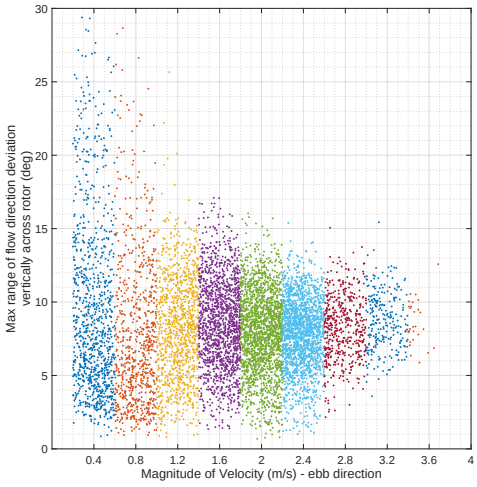

(e) ADCPTD7-01-Dep1

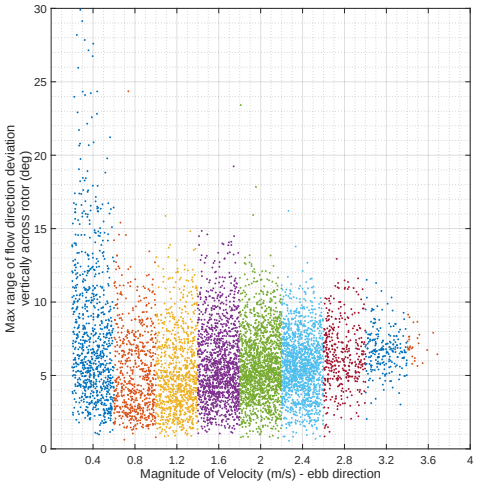

(f) ADCPTD7-02-Dep1

Figure 3.74: Max range of flow direction deviation vertically across rotor (deg)

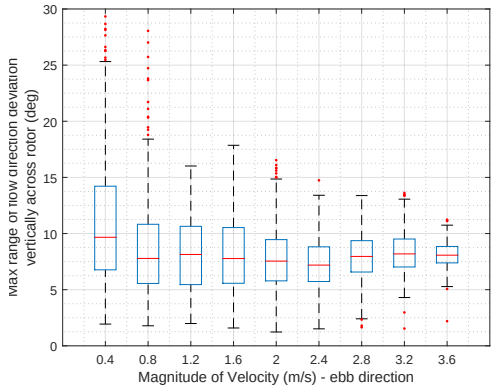

(a) ADCP02-SE-Dep1

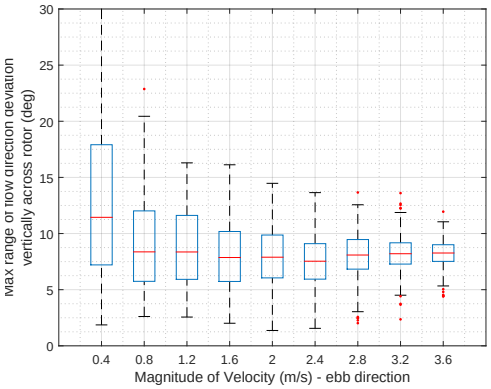

(b) ADCP02-SE-Dep2

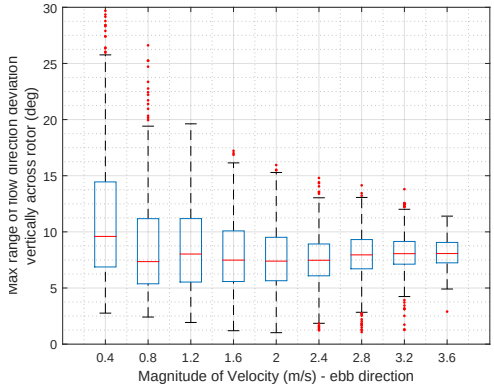

(c) ADCP02-SE-Dep4

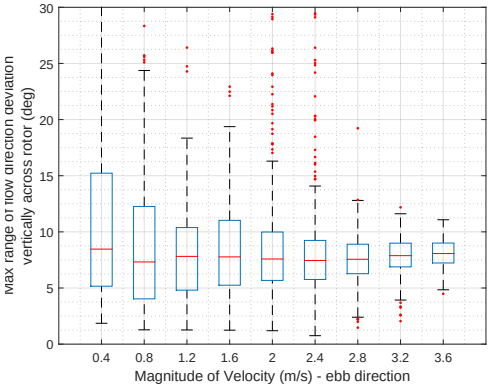

(d) ADCP03-SE-Dep1

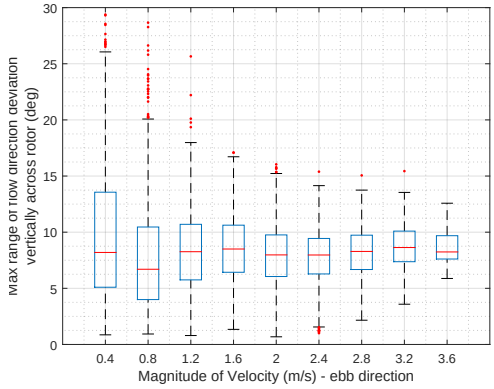

(e) ADCPTD7-01-Dep1

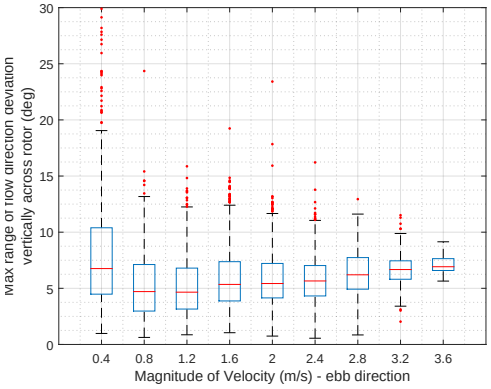

(f) ADCPTD7-02-Dep1

Figure 3.75: Max range of flow direction deviation vertically across rotor (deg)

3.9 Advanced Measurement Techniques (C-ADP vs D-ADP)

The following section is derived from a recently published **open-access** paper by Sellar et al, 2015 [4]. Content has been condensed for use in this MD3.8 report.

3.9.1 Introduction

During a turbine inspection window in summer 2014 an array of geometrically converging single-beam acoustic Doppler profilers was developed for the high resolution measurement of three-dimensional tidal flow velocities and subsequently deployed in September 2014. This configuration was developed to increase spatial resolution of velocity measurements in comparison to D-ADPs. This was achieved using geometrically convergent acoustic beams creating a sample volume at the focal point of 0.03 m^3. Away from the focal point, the array is also able to simultaneously reconstruct three-dimensional velocity components in a profile throughout the water column. This configuration of ADP is referred to as a convergent-beam acoustic Doppler profiler (C-ADP). Figure 3.76b (repeated for convenience) illustrates the differences in beam geometry between C-ADP and D-ADP systems. The proof-of-concept is summarised below and described in more detail (in open-access format) in [4].

C-ADP vs D-ADP

In energetic tidal flows, the instantaneous flow velocity is seen to vary over a wide range of time and length scales. Coherent turbulent structures smaller than the distance separating the divergent beams of D-ADPs at a given elevation are unable to be resolved. Large scale eddies, although greater in scale than these beam separations, are misinterpreted through conventional D-ADP processing algorithms [84, 129].

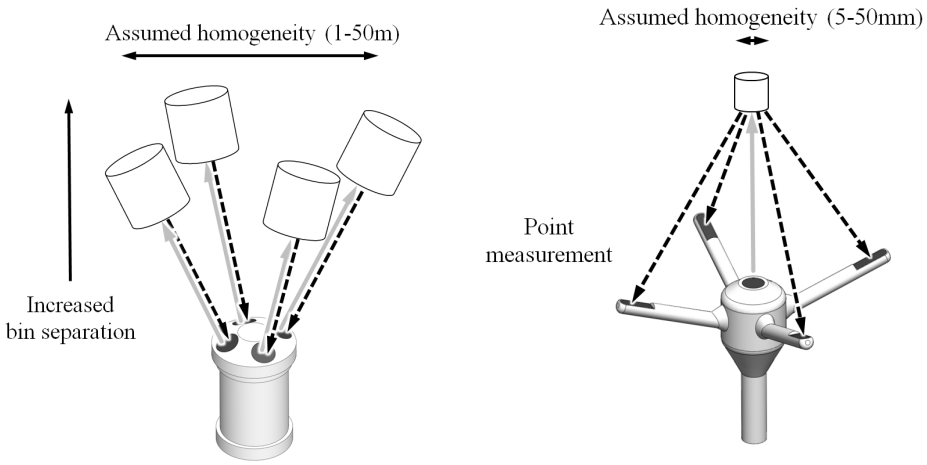

(a) d (b)

Figure 3.76: Comparison of beam directions for representative a) D-ADP and b) ADV instruments. The grey arrow in the direction of the sample volume represents the transmitted acoustic signal, and the dashed black arrow in the direction of the receiver represents the reflected signal.

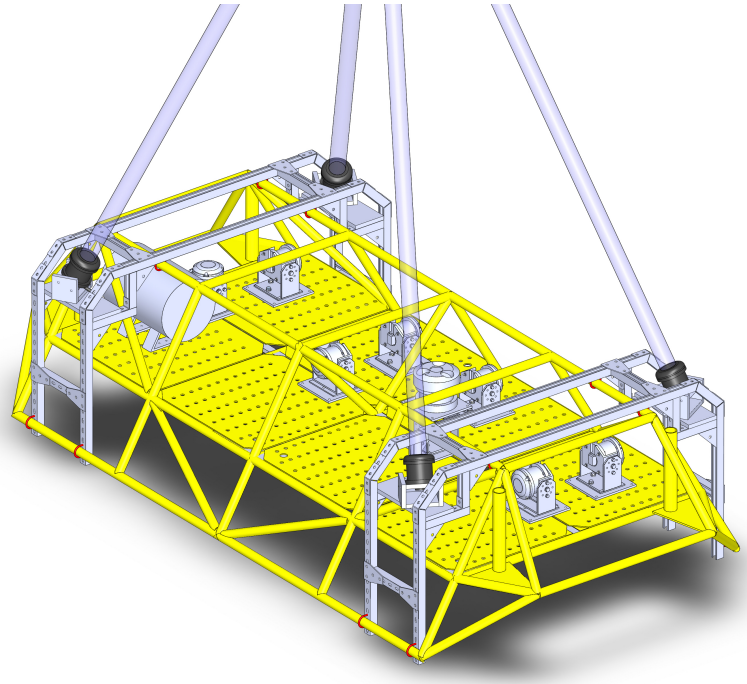

(a) CAD model of modifications to ESIP-1 to enable a Convergent-ADP trial

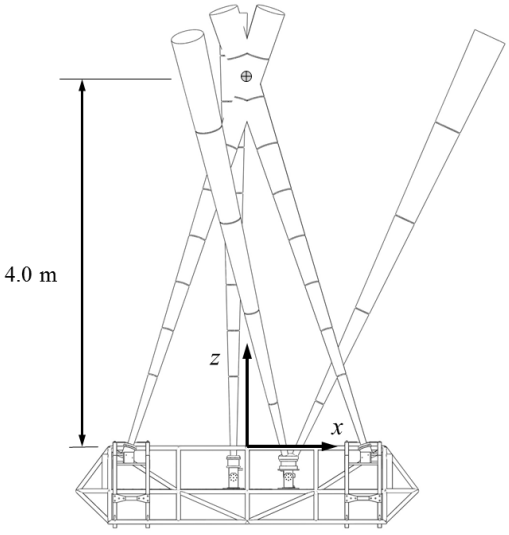

(b) Elevation view of C-ADP system

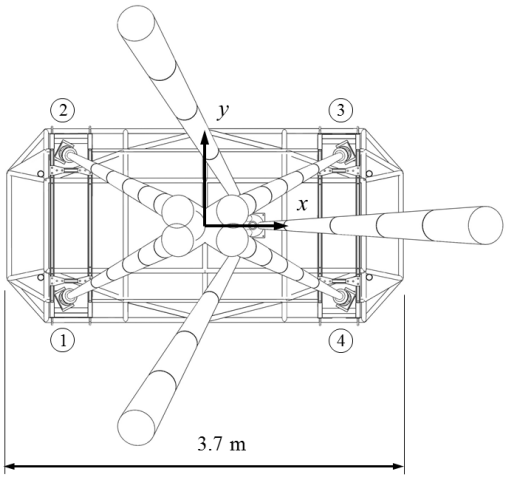

(c) Plan view of C-ADP system

Figure 3.77: CAD visualisation of the C-ADP modifications to ESIP-1 (a) and elevation and plan dimensioned sketches (b) and (c)

Table 3.15: Summary comparison of acoustic Doppler velocimetry instrument configurations.

	D-ADP	ADV	C-ADP
Acoustic beam directions	Divergent	Convergent	Convergent
Sample volumes	Multiple	Single	Multiple
Transmitter-receiver configuration	Mono-static	Bi-static	Either
Spatial resolution (m^3)	$0.4 - 20$	2×10^{-6}	0.03
Temporal resolution (Hz)	2*	200	4

* Recently available instruments feature faster sampling rates of up to 16 Hz for specific modes of operation

Being installed on the turbine, the coordinate system of the each instrument was defined in terms of the turbine coordinate system, with the x-direction along the turbine axis in the principal flow direction, the y-direction in the cross-flow direction, and the z-direction as upwards to the water surface.

By adjusting the blanking distance and profiling bin size of each instrument measurements were achieved at comparable vertical separations. The convergence of the acoustic beams at the focal point of the C-ADP obscures the reflected signal to each of the respective instruments if the acoustic signals are fired concurrently - termed synchronous operation. Instrument offset times were varied and the resulting influence on the measurements (signal return amplitude and velocity) were observed in mono-static mode. In this mode, each instrument operates independently to receive the reflected acoustic signal that was transmitted from itself. Bi-static sampling is available by using the vertically orientated s-ADP as the transmitter and the C-ADP (comprising four convergent s-ADP instruments) as receivers. Bi-static modes of operation involving a large test-matrix of configuration settings were also tested. Analysis is ongoing and results are not presented.

3.9.2 Results

Agreement between C-ADP and D-ADP

At the focal point, $z = 4$ m, the mean velocity components measured by the C-ADP show good agreement with those of the divergent-beam reference instrument. This is shown by Figure 3.78, where the mean velocity component measured by the C-ADP is plotted against that of the D-ADP at the focal point elevation. These results show 36-hours of 5-minute mean velocity with the turbine aligned with the flow direction.

Cross-correlation of vertical velocity

Cross-correlation can be used as a measure of the similarity between two signals. In this case, the maximum cross-correlation coefficient of the vertical velocity measured by the s-ADP and C-ADP is calculated to indicate the comparability of two instrument measurements with varying durations of temporal averaging [130]. Figure 3.79 shows this result. An averaging period of $t_a = 0.25$ s corresponds to the raw 4 Hz data.

Again, a peak in the maximum cross-correlation coefficient was observed near the focal point of the convergent beam system ($z = 4$ m). The beam separation of the C-ADP increases with distance from this focal point and the correlation is seen to decrease as a result. The width of the correlation peak increases with averaging period, as the magnitude of flow perturbations with length scales less than the beam separation are reduced. The peak cross-correlation of 0.8 is calculated at the focal point using the raw 4 Hz data, which increases to 0.96 when a moving average of $t_a = 4$ s is applied.

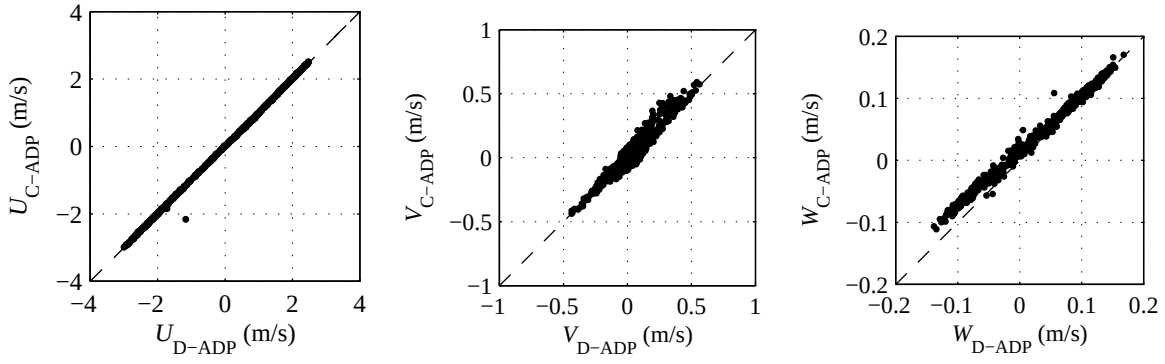

(a) d (b) (c)

Figure 3.78: Comparison of 662 mean Cartesian velocity measurements, comparing velocity components of the C-ADP and reference D-ADP instrument at $z = 4$ m.

Discussion

Results from these trials demonstrate the ability of the C-ADP to resolve velocity perturbations with a relatively high spatial and temporal resolution. The results at the focal point are evidence of the importance of using an instrument with a reduced spatial resolution, compared to existing divergent beam configurations, when high-frequency velocity measurements are required.

Conclusion

The array of convergent acoustic Doppler velocity profilers has been shown to improve the spatial and temporal resolution of underwater velocimetry.

The convergent-beam acoustic Doppler profiler (C-ADP) has been initially validated through a series of comparative experiments with reference instrumentation including a divergent-beam ADP and a vertical acoustic Doppler profiler. Cross-correlation coefficients of 0.80 was calculated for the raw vertical velocity component and cross-correlation of 0.96 in frequency ranges relevant to wave analyses in a direct comparison with a vertically orientated instrument are encouraging. A peak in measurement accuracy was observed at the focal point of $z = 4$ m for this comparison.

The asynchronous timing control of each profiling instrument was found to be critical to avoid acoustic signal interference at the focal point when the array was operated in mono-static sampling mode. Further optimisation of both mono-static and bi-static modes of operation are currently being undertaken in addition to the analysis of higher order flow metrics and an assessment of the impact of highly energetic wave conditions resulting from recent storms.

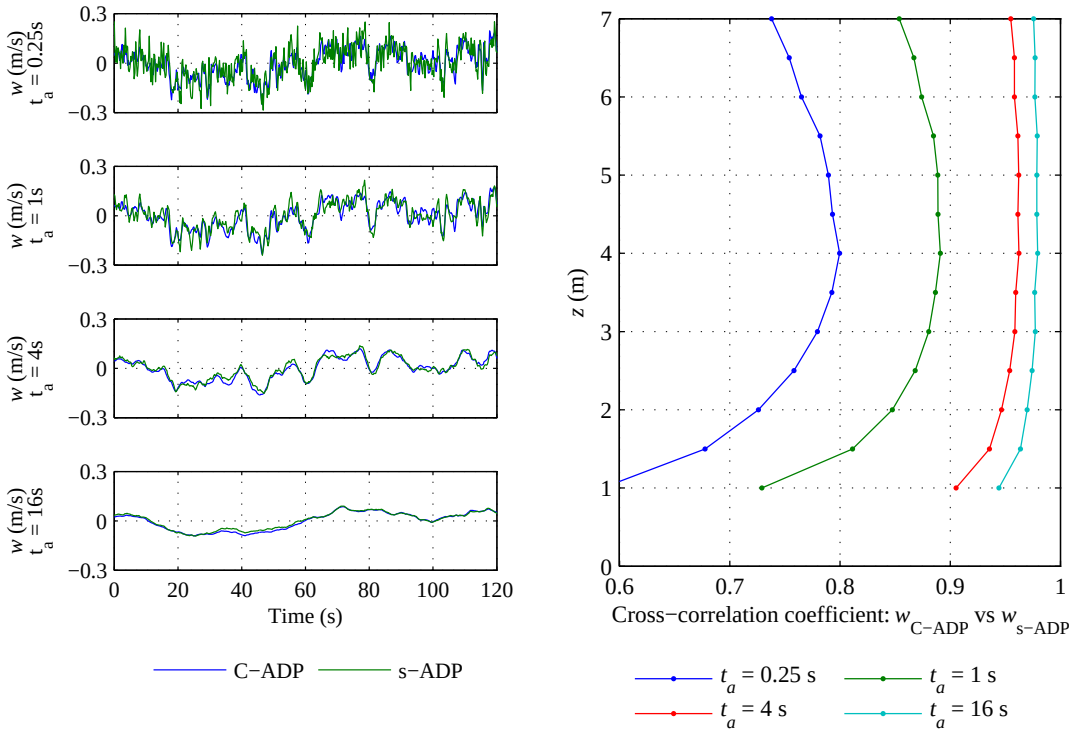

(a) Representative time series at $z = 4$ m for range of averaging periods

(b) Depth profile of cross-correlation coefficients for range of averaging periods

Figure 3.79: Cross-correlation of vertical velocity signals between the C-ADP and vertical SBD showing depth and averaging periods effects.

3.10 Conclusions on Site Characterisation

3.10.1 Summary

Measurements were acquired at the EMEC tidal test site, berth six in the Fall of Warness, Orkney between March 2012 and October 2014 from turbine-mounted and seabed-mounted velocity profilers comprising SB-ADP, D-ADP and in experimental form C-ADP. A targeted set of metrics (Section 3.6 and Table 3.7) was developed within the Project. This included Turbulence Intensity, Lengthscales associated with the change of along-axis velocity in that same axis direction (see Table 3.8), velocity and Reynolds stress τ_{uw} and τ_{vw}.

Turbine-mounted measurement analysis and results are outlined in Section 3.6.

Seabed-mounted measurement analysis and results are outlined in Section 3.8.

Main findings specific to Fall of Warness:

- The flood and ebb tides vary markedly in most parameters measured or derived with the exception of

  ratios of primary lengthscale L_u:L_v:L_w.

  divergence around mean heading at established (low acceleration) tidal phases.

- Turbulence Intensity and Lengthscales - derived with reduced uncertainty levels - are lower in ebb than flood whilst mean velocities are higher.
- Depth profiles of streamwise velocity show ebb tide to have parabolic form with reduction in flow speeds from mid-depth to the surface.
- Depth profiles of streamwise velocity show flood tide to have power-law form.
- The presence and form of surface waves play a significant role in the values of turbulence metrics returned.
- Most recently analysed data indicates that spatial variation may be high as measurements are acquired off-axis (across channel) from the principal flow direction, potentially at distances of 50m-100m

Main findings applicable to broader industry:

- Velocimetry using acoustic Doppler techniques is a powerful tool for the tidal sector.
- The measurement of waves will at many sites need to be fully integrated into measurement programmes both for design work and ongoing control and extreme event damage mitigation.
- The prevalence of "non-standard" shear profiles at other tidal sites should be assessed.
- Using combinations of diverging, converging and single-beam ADPs provides large reductions in uncertainty around measured metrics.
- Turbine-installed ADPs proved highly useful due to their controllability, real-time data access and close proximity to volumes of flow incident to the rotor plane. A rationalised set of recommended equipment is listed below.
- Newly available technologies will likely offer improved data for turbulence studies due to their five-beam configurations and higher sampling rates (up to 16Hz which is 4 x faster than available at Project commencement).
- Instruments which individually or in combination can provide continuous flow data whilst measuring wave properties would be beneficial.

- Fundamental studies using new technologies or existing technologies in novel ways are required to enable the capture of fully three dimensional high frequency turbulence.

For many of the metrics listed below a further sub-division of the description of the wave field is required in order to investigate the relationship between the presence of a particular wave state and the increasing or decreasing of magnitude of that metric.

3.10.2 Mean Flow Speeds

Ebb tides are faster than flood tides at this site. This was shown in Section 3.8.1 and 3.8.4. These mean flow speeds and the relative differences between a flood tide and the nex ebb tide vary across the month, seasonally and yearly. Long term tidal elevation and velocity predictions using *harmonic* analysis is not within the scope of this report. For reference and summary, mean flow speeds using *time-domain* analysis for all flood and ebb tides measured during the 1MW Turbine deployment campaigns are shown in Table 3.16 and found to be 2.45 ms^{-1} for flood and 2.77ms^{-1} for ebb, equating to $\approx$ 13% increase in ebb tides relative to flood tides. As can be seen in Figure 3.80 inter tidal velocity variation changes periodically at differing frequency.

Table 3.16: Add caption

Tide Direction	Flow Speed (ms^{-1})	
	Mean	Standard Deviation
Flood	2.45	0.57
Ebb	2.77	0.67

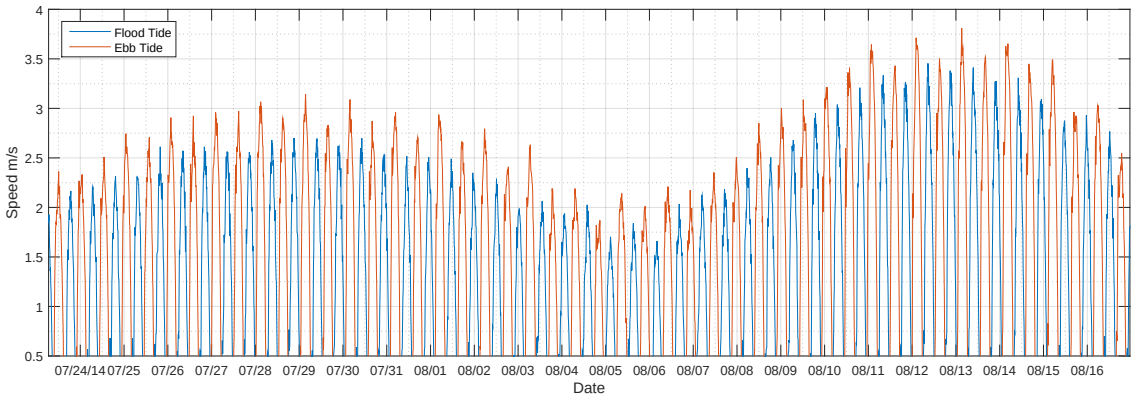

Figure 3.80: Histogram of mid-depth flood and ebb velocities

3.10.3 Depth Profiles of Flow Speeds

Velocity depth profiles showed significant differences between flood and ebb tides. Whilst flood tides exhibit power-law behaviour ebb tides diverge from this behaviour at approximately 20m above the seabed. The effect is more pronounced in the presence of waves (waves also effect the velocity profiles for flood tides) and further work is needed on sub-dividing wave conditions further into a more detailed characterisation e.g., including wave direction. More broadly an assessment is also required as to the prevalence at other locations in the Fall of Warness and at other sites of these type of "surface-slow" tidal profiles.

The final D-ADP campaign positioned off to the sides of the turbine (as opposed to in-line with the principal tidal directions) revels a different depth profile from the others. Here divergence from a power-law fit occurs deep in the water column, between 10-15m above seabed and shows a pronounced reduction in flow speed. The cause and prevalence of these strongly surface-slowed tides needs further investigation.

3.10.4 Turbulence Intensity

As shown in Sections 3.7.4 and 3.7.5 for mid-depth measurements acquired from the turbine and Sections 3.8.2 and 3.8.5 for measurements acquired by seabed mounted instrumentation, Turbulence Intensity varies between flood and ebb tides, with depth and in the presence of surface waves.

Mid-Depth Turbulence Intensity

Streamwise Turbulence Intensity in the **flood tide** and without the presence of any significant wave action was found to be 9.1% ± 1.9%. Applying noise correction techniques brings this value to 8.6% ± 2.0%. Streamwise Turbulence Intensity in the **ebb tide** and without the presence of any significant wave action was found to be 7.3% ± 1.6%. Applying noise correction techniques brings this value to 6.7% ± 1.7%. Summaries of these and their transverse and vertical counterparts were presented in Table 3.11.

Depth Profiles of Turbulence Intensity

As shown in Section 3.8.2 and 3.8.5 depth profiles of Turbulence Intensity on flood tides show I_u decreasing with distance from the seabed. By mid-depth, magnitudes have fallen by ≈ 15%. Ebb profiles show a far larger decrease in TI, ≈ 30% by mid-depth elevations. However, both systems are dominated by wave action, where very large increases in I_u are evident particularly in the top 50% of the water column as shown in Figures 3.58 and 3.64.

D-ADPs (ADCPs) report higher TI values (in comparable regions of the flow i.e., at mid-depth) to those values measured by turbine-mounted instruments. Methods to establish a correction value to account for instrument Doppler noise have been applied to the SB-ADPs and these should be used as the benchmark data. Estimations (non varying with velocity) for the level of correction applicable to D-ADPs, of approximately 15cm$^-$1, bring the D-ADP turbulence intensity values into agreement with D-ADP.

3.10.5 Lengthscale

As shown in Sections 3.7.4 and 3.7.5 - for mid-depth measurements acquired from the turbine - streamwise, transverse and vertical lengthscales vary between flood and ebb tides and in the presence of surface waves. Figure 3.81, repeated here for convenience and to allow side-by-side comparison, shows the clear difference in turbulent structure between flood and ebb tides.

The level of difference between the ebb and flood tides, and moreover the difference between ebb measured streamwise lengthscale and that predicted from theory of approximately half the channel depth is significant. This difference would impact on the results generated by numerical models where assumed inflow conditions would be non representative of the site.

Averaged streamwise Lengthscale in the **flood tide** and without the presence of any significant wave action was found to be $15.5m \pm 6.9m$ and displaying a log-normal distribution. Values were averaged at flow speeds $U_{ref} > 2.0 ms^{-1}$. Under large wave conditions (featuring H_{m0} >1.6m) measured in storms of 2014 these values are shown to diminish to $12.6m \pm 6.9m$.

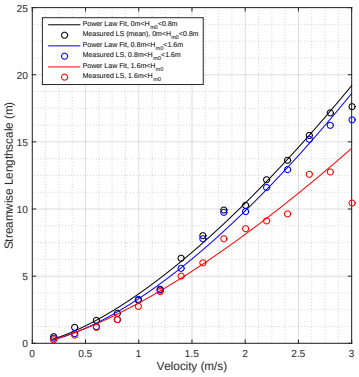

(a) **Flood** Streamwise Lengthscale

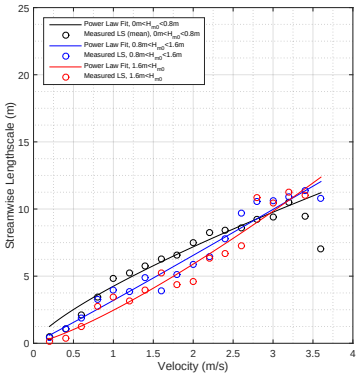

(b) **Ebb** Streamwise Lengthscale

Figure 3.81: Flood (a) and ebb (b) tide streamwise lengthscale (mid-depth) as a function of velocity and under the influence of waves.

Averaged streamwise Lengthscale in the **ebb tide** and without the presence of any significant wave action was found to be $8.6m \pm 4.4m$ and displaying a log-normal distribution. Under the large wave conditions (featuring H_{m0} >1.6m) measured in storms of 2014 these values are shown to diminish to $7.3m \pm 3.6m$.

In terms of the relative magnitude of directional lengthscales within a tide, both the flood and ebb tides, despite their differing individual lengthscales, exhibit the same ratios of L_u:L_v:L_w of approximately 1:0.4:0.2 changing to 1:0.5:0.4 in the presence of large waves (as previously defined by the wave filtering method).

Efforts are ongoing to improve understanding of the influence of waves (and other site parameters) on these lengthscales.

3.10.6 Flow Direction and Variation

Analysis was carried out on the change in flow direction with tidal phase and the level of horizontal and vertical variation from the mean flow directions derived at hub height from the D-ADP (ADCP) data across flood and ebb tides.

Flow direction when reported from uncorrected ADCP instrument headings shows large variation between deployments of up to 20°. A major proportion of heading error (which leads to flow direction misrepresentations) can be attributed to non-ideal instrument compass calibrations being carried out. Where instrument alignment has either been verified as being below $2degree$ after compass calibration or by other means (e.g., through heading readings supplied by "docked" ROVs to the frames) differences in flow headings remain - but are reduced - across the range of instrument separation of 100-200m. Where required, ADCPs displaying large variation were "corrected" in post-processing via an alignment technique referencing fixed instrumentation installed on the turbine (which has a known and changeable orientation in yaw). Again, differences in flow direction remain between deployments - but at reduced variation.

Average results across all ADCP data sets and including corrected headings for the **flood tide** are found to be $137° \pm 4°$.

Average results across all ADCP data sets and including corrected headings for the **ebb tide** are found to be $318° \pm 5°$.

Horizontal variation in flow varies as the tides accelerate and decelerate. At this site flood tides ramp up along a different heading from their ramp-down direction, separated by $\approx 30degree$ at flow speeds

of $1ms^{-1}$. These values are around 50% lower in the ebb tide. In both tides standard deviations in heading within a single deployment campaign typically converge to 3-4° above flow speeds of $2.4ms^{-1}$.

Vertical "twist" levels were found to vary between flood and ebb tides: with ebb displaying greater levels of differences in flow direction across the rotor plane. On both tides twist remained below 5 ° for flow speeds above $1ms^{-1}$. As a parameter, however, it should be assessed at other sites.

3.10.7 Waves

Methodology

Waves were measured by multiple methods both direct and inferred. On the turbine, SBD instruments orientated vertically measured the large signal return when the acoustic signal meets the sea surface at 4Hz with coarse (minimum bin-size available at the time) of 0.4m. An AWAC D-ADP measured combined current and wave orbital velocities when in "current" mode and combined a selection of these velocities with acoustic surface tracking and pressure gauge readings when operating in "wave" mode. Pressure gauges were also used at various sampling frequencies from 1Hz to 10Hz. On the seabed ADCP D-ADP's measuring in "current" mode measured combined current and wave orbital velocities. Due to programme and technical constraints, as discussed in Section 3.3, these seabed deployments typically ran at 0.5Hz or 1Hz, below that recommended for wave analysis.

From these multiple data streams through instrument-instrument calibration a waves signal was generated that could be applied to the entire pseudo-database (operating within Matlab). Spectral parameters H_{m0} and T_p along with time-domain parameters H_m and T_m were extracted and available in a look-up table to permit filtering of tidal flow data under various sea-states. Wave directionality and its impact was not available in time to be included in this report.

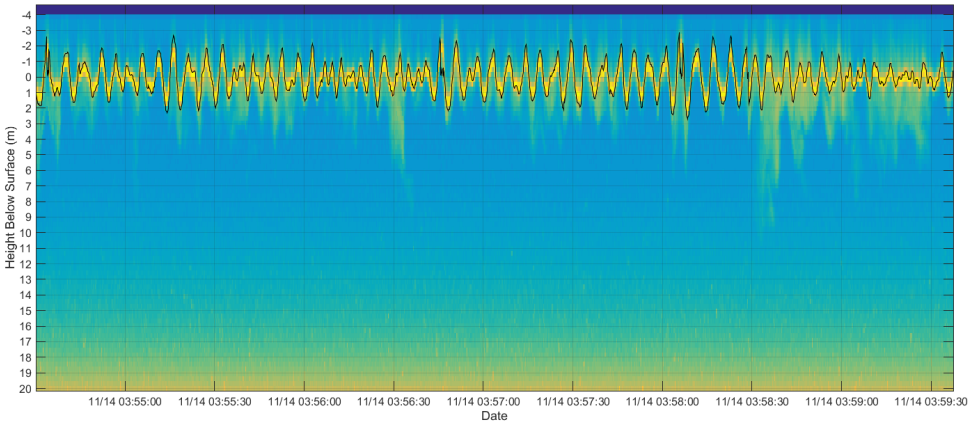

Figure 3.82: Signal Amplitude with post-processed surface elevation overlaid (black). (Repeated)

Confidence in the wave calibrations for H_{m0} comes from the good agreement seen between both the upward orientated SBD data and the transformed pressure data with the benchmark instrument, the turbine installed Nortek 1MHz AWAC, operating in "waves" mode as shown in Section 3.3, Figure 3.18b. This section revealed how sensitive measured wave climate is to the tidal cycles with marked oscillations at tidal frequencies. Without corrections being applied to the measured wave data (indirect methods) taking into account the underlying tidal flow, error in e.g., significant wave height regularly exceeds 100%. More work is needed to assess the accuracy of the inferred wave periods. A

sensitivity study was conducted to assess the effect of the H_{m0}-derived waves filter on returned data sub-sets and from this three wave bands were selected.

Once wave period and directional information is available more detailed sub-division of the data sets will be enabled which will aid identification of causality across the tidal and wave systems.

Impact on Tidal Flow

As discussed previously the presence of waves strongly effects the values of measured tidal metrics. Without taking into account waves the uncertainty levels in Turbulence Intensities and Lengthscales (and to a lesser extent Reynolds stresses) would be significantly higher. Significant reductions in lengthscales and increases in TI were seen for the data presented here. This will be re-analysed as wave information fidelity is increased to assess the link between wave field and the sign and magnitude of the resulting effect.

Going forward it is recommended that full integration of waves measurement is included in any tidal site characterisation. It is recognised, however, that where sites are sheltered from long period swell waves or where there is limited fetch for local winds to bring about significant wave fields such focus of waves may not be necessary. This would need to be assessed early in characterisation works.

3.10.8 Flow Characterisation: Recommended Rationalised Equipment Set

Tidal turbine developers and project operators will clearly not want to implement the array of instrumentation and analysis presented here for reasons of cost, time and prioritisation. Listed below is a recommended rationalised set of equipment based on the experiences of UoE within ReDAPT. These recommendations would be altered to take into account any special feature of the tidal site, for example one which features particularly high changes in tidal elevation, and where arrays of turbines were being installed to take advantage of the machine layout.

A recommended instrument set would include:

- ADP installed on horizontal axis TEC, forward facing.
- D-ADP installed on top of TEC to allow assessment of ambient flow including headings and waves
- Pressure gauges are reliable and represent good value for money and could play a useful role in the measurement of large wave conditions.[3]
- Upstream and downstream-positioned D-ADPs provide full-depth data which provides a description of inflow conditions for any numerical modelling activities as well as data that can be used for turbine control (if connected to the turbine either physically or with through-water communications). Where necessary their specification should be upgraded for use in the tidal energy industry.

As a final note, given the large number of "moving parts" when considering a system comprising off-the-shelf and bespoke instrumentation, tidal turbine machinery and the dynamic marine environment it is recommended to involve multiple analysts with various skills in (i) the planning and execution of measurement campaigns and (ii) the analysis of the data. It is the experience of the authors that working closely (daily, weekly, monthly) with the turbine developers and the numerical modellers provided many benefits to the process as a whole.

[3] If only large, long wavelength waves are a concern a calibrated and properly post-processed pressure gauge system may suffice for wave measurement. This could be particularly useful if volume TEC arrays were implemented where multiple ADP units could prove too expensive and where wave directionality was important (due to the advantages of physical array-based measurements for wave directionalityy studies)

Chapter 4

Lessons Learned and Industry Guidance

4.1 Introduction and Overview

The University of Edinburgh measurement campaigns of the ReDAPT project are briefly summarised in the sections below, covering sensor system integration with the Alstom 500kW and 1MW tidal turbines as well as seabed-located sensor deployments. Lessons learned of both a technical and programme administrative nature are discussed. The report authors would encourage correspondence to discuss this overview further.

4.2 Timeline and Project Duration

Less Data, More Staff

Background: Measurement campaigns were conducted by the University of Edinburgh from March 2012 using the 500kW machine and beginning February 2013 through to October 2014 were conducted on the 1MW machine. Following completion of core activities, data collection continued in an ad-hoc manner up to January 2015 with a priority of collecting previously unattained winter storm measurements. Table 4.1 and Figure 4.2 provide an overview and time-line of deployments. The target deployment strategy was based upon stand-alone ADCP deployments upstream and downstream of the tidal turbine with simultaneous acquisition of turbine-mounted instrumentation in real-time.

(a) The 500kW DEEPGEN III being lifted.

(b) The 1MW DEEPGEN IV on stand.

Figure 4.1: The Alstom DEEPGEN turbines at Hatston Quay, Orkney

Issues: Targeting such a broad range of measurements and maintaining a data collection campaign over this duration was expensive and time consuming. Equipment maintenance issues arose due to the number and durations of deployments putting pressure on budget. Dozens of field trips during coordinated activities with turbine deployments and retrievals also increased project cost. Overly restrictive project administrative mechanisms played a role in delays in the first year of work.

1. More time should have been allocated at project kick-off to assess changes on the ground between contract signing and project commencement.
2. Flexibility was gradually added to the programme (essential given the nature of the project). This had a positive impact on planning and resourcing and allowed the hiring of additional resource (on an opportunistic basis) when experienced staff became available.
3. Having access to flexible staffing resource would have helped enormously. Solutions were sought throughout the project (visiting students, interns etc.) but a feeling of being ever-late on project deliverables has been prevalent throughout.
4. The compartmentalised analysis of acquired data should have been a higher priority at various stages, perhaps even deciding to "skip" a deployment in order to "catch-up".

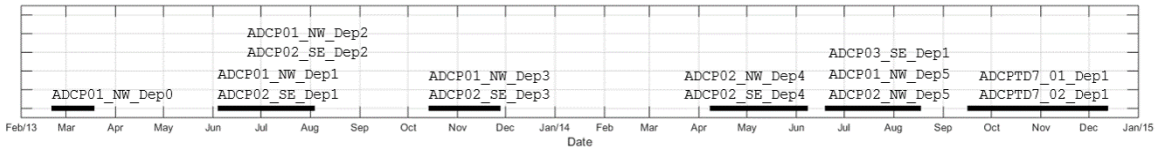

Figure 4.2: ADCP deployment time-line

4.3 Test Design, Methodology and Performance Tracking

Pick a System (preferably a tried-and-tested system)

Background: Measurement campaigns were carried out under the "Test Request Notice" system (TRN) operated by the Project Lead, Alstom (*previously Rolls-Royce*).

TRNs were produced to:

- provide data at appropriate timings to project partners for their parallel works, namely numerical modelling validation and turbine operation monitoring and turbine performance assessment
- provide sufficient data for Fall of Warness site characterisation work (see chapter 3)

Turbine performance assessment and machine control required acquisition during periods of turbine generation. Site characterisation tests involved the scheduled (or opportunistic) acquisition of data during periods of turbine non-generation.

Issue: Coordination of multiple tests across multi-partner work scope was complex a major project challenge.

1. TRNs - when controlled pro-actively - proved a useful tool to coordinate activities.
2. Combining TRNs with in-house daily/weekly data collection completion forms (in Microsoft Excel) made a positive difference in being able to communicate progress, highlight problems and to aid negotiations on the scheduling of competing tests.
3. Once established procedures were in place and routine communication was taking place (brief daily phone-calls for example) test scheduling efficiency improved significantly

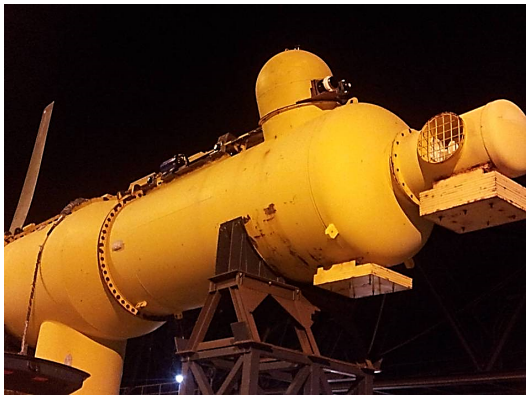

(a) Installing instrumentation to the 500kW turbine on site at Hatston Quay, Orkney

(b) Instrumentation and instrumentation control-box installed on the 500kW machine

Figure 4.3: Instrumentation integration on the 500kW DEEPGEN III

4.4 Turbine System Integration: Mechanical Interfacing on the 500kW turbine

Early Testing of Equipment

Due to UoE velocimetry instrumentation being available prior to the completion of commissioning of the 1MW machine the decision was taken to conduct a deployment of the 500kW machine (see Figure 4.3a). A subset of available instrumentation was attached to the 500kW to de-risk later deployments by: providing earlier access to data for analysis; trial UoE-Alstom testing coordination and use of the TRN process; test the electrical and communications interfaces and assess instrument performance.

1. Staggered procurement would have provided more benefit from early testing by allowing more flexible decision making as the project developed. Early trialling of equipment revealed issues which required resources to mitigate.
2. Further data analysis on this early data set would have been beneficial. However, due to the time and resources invested in this campaign and alignment with other project deliverables focus had to return to the upcoming 1MW commissioning.

4.5 Turbine System Integration: Electrical and Communication on the 500kW turbine

Troubleshooting instrument integration across complex "third party" systems is time consuming

Background:

AWAC and SBD power and comms were pre-routed through the Instrument Control Box 1 [1] (ICB1) as shown (blue cylinder) in Figure 4.3b. This allowed control over re-wiring, in-line fuse placement

[1] Zinc anodes were fitted to the all-welded body and were changed during maintenance periods. The condition of this enclosure remained excellent throughout seven deployments (across the 500kW and 1MW) and totalling approximately 12 months of submersion.

and independent remote power cycling. The AWAC and Continental instruments operate over RS422 protocol and the SBDs over TCP/IP. Both systems had problems when taken out of the laboratory environment.

Issues: Despite having individually working sub-systems, reliably communicating with the integrated system took weeks of troubleshooting - which had knock on effect on schedule and budget. Suppliers find it difficult to assist with hardware or software clashes due to multiple third party conversion/routing/switching hardware in the loop since their equipment is "working" on the bench. Often instrumentation was functional on the turbine (from within the turbine control cabinets) but not across the additional connection of the turbine to the on site maintenance control room.

1. Using third party equipment which partner staff members have knowledge and experience of provides significant benefits. Whilst potentially more expensive, complex to procure or involving changing configurations the standardising of sub-systems proved highly useful throughout the project.
2. Increased time for initial commissioning was required.
3. New pre-deployment commissioning TRNs were generated and followed.
4. IT/network problems were anticipated with any changes to server settings, firewalls etc. and were subsequently notified in advance and probed early.

4.6 Mechanical Interfacing on the 1MW turbine

Make use of partners' experience at the design stage and in the field

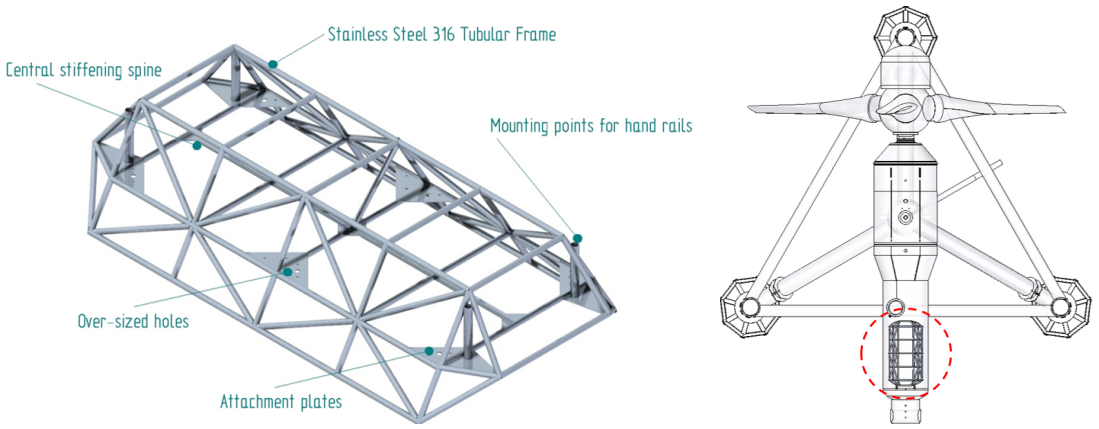

(a) Top Frame early design option post preliminary design review

(b) 1MW turbine in plan showing top frame mounted at turbine top rear.

Figure 4.4: Top frame (ESIP-1) early design option and positioning on 1MW turbine

Background: Integration of UoE instrumentation systems with the 1MW turbine was managed through a single document which in turn was produced by a three stage design review process featuring: Preliminary Design Review (PDR), Critical Design Review (CDR) and Installation Readiness Review (IRR). The integration process, "Interface Agreement and Outline Installation and Removal Plan for UoE ADP Instrumentation and ReDAPT 1MW Tidal Turbine" took approximately 6 months to finalise. An overview of some of the design work required is shown in the Figures 4.4 to **??**.

Given that the 1MW machine features a buoyant nacelle both the mass and displacement of instrumentation systems had to be considered and revised iteratively. Multiple design options for frames

were proposed.

Issues: Despite group planning and the Three Stage Review procedure some problems arose mainly around first attempts at installation and removal of equipment. Taking a pragmatic approach and with coordination these issues were sorted out Quayside with little time lost. Maintenance and access to certain components was made more difficult by lack of foresight and modifications to other sub-systems which over the long duration of the project caused delays.

1. Things will change on site but can be worked around under coordinated mitigation.
2. Designing and building the 1MW instrumentation frames, ESIP-1 and ESIP-2 in a conservative manner, whilst time consuming and expensive was worthwhile. The frames performed well and survived one year deployment in Orkney waters with little maintenance required.
3. Design in flexibility, modularity and ease of access (including when operating upside down in snow).
4. Redundancy of fasteners and fastening mechanisms proved worthwhile including the use of all stainless fasteners (A4), Nyloc nuts and heavy-duty nylon 66 cable ties frequently laid down over cables.

4.7 Electrical and Communication Interfacing on the 1MW turbine

Design-in and test instrumentation grounding and power supply quality

Background: AWAC and SBD power and comms were pre-routed through the Instrument Control Box 1 (ICB1) as shown (blue cylinder) in Figure 4.3b. An ethernet switch located inside ICB1 routed ethernet communications from the turbine to the ICB's internal CPU and sub-systems and the SBDs externally distributed hub. The ICB contained multiple fuses to prevent individual instrument failure (e.g., flooding of units) from disabling the entire array.

Issues: Electrical noise was suspected to be affecting several of the instruments on the ESIP-1. This was intermittent and difficult to assess. By turbine deployment 6 there was sufficient time available to produce a modification. Additionally, cable failure rates were high: approximately one or two cables per 2 month deployment. The suspected cause was grounding issues on the DC supplies but tests could not be carried out in a controlled manner.

1. New DC grounding was implemented in a user-selectable way to assess the impact of different grounding schemes on sensor performance.
2. Increased program flexibility allowed resource to be shifted into maintenance allowing swap out of cables sets prior to failure (as opposed to replacing failed units).
3. Redundancy was increased by supplying the two Nortek ethernet switch boxes, EB1 and EB2, with separate power and ethernet connection via the ICB. This parallel set-up enabled ongoing operation of up to 7 SBDs in the event of a failure of one ethernet box.

4.8 Maintenance of Instrumentation

Develop Spares Budget

Background: A large number of components were required to install and operate the instrumentation array on the 1MW machine. Over seven turbine deployments and relatively prolonged immersion

times parts failed due to corrosion issues likely due to sub-optimal electrical grounding. Other failures occurred due to individual problems with manufacture or improper servicing.

Issues: Lead times for some parts, including replacement cables, was at times up to 8 weeks. Replacement connectors could take more than two weeks to arrive by which time the turbine may have been due for turn-around and redeployment. Delivery to Island areas can add additional time on to component delivery in some cases also.

1. A dedicated set of spare units, whilst costly initially, would have saved a lot of time developing layers of "work-arounds" based on alternative system configurations or suppliers.
2. For seabed deployments (or turbine installed equipment where you have fixed - depending on weather - retrieval points) use of rental equipment should be considered in parallel to purchased equipment to increase flexibility and enable maintenance time between deployments.

4.9 Seabed Mounted Instrumentation

(a) Type B (top centre) and Type C (others) ADP frames with RDI Workhorse Sentinel ADCP installed (bottom centre) and Nortek Signature 500 installed (right). Positioned on a crane barge at Hatson Quay, Kirkwall prior to uplift by the deployment vessel.

4.10 ADCP Gravity Foundations

Suitability of mooring frame varies with test specification and vessel logistics

For deployments outwith immediate proximity to the turbine stand i.e., ranges >approximately 200m, ADCP foundations of the type commonly deployed by EMEC - designated Type A - were used. For deployments in close proximity to the turbine an existing Alstom foundation (Type B) was initially used and was later augmented with a UoE design (Type C). All three designs can be seen in Figure 4.6. Outline descriptions can be found in table 4.2.

Type-B and Type-C foundations were selected to increase the level of force required to move or overturn the foundations post deployment and moreover to be deployed and recovered with the assistance

Turbine Deployment	ADCP Code	Date Deployed	Date Recovered	Duration (Days)
500kW	ADCP01_NW_Dep0	2013-02-21	2013-03-17	24
2	ADCP01_NW_Dep1	2013-06-05	2013-07-17	42
2	ADCP02_SE_Dep1	2013-06-05	2013-07-17	42
3	ADCP01_NW_Dep2	2013-07-18	2013-08-02	15
3	ADCP02_SE_Dep2	2013-07-18	2013-08-02	15
4	ADCP01_NW_Dep3	2013-10-15	2013-11-26	42
4	ADCP02_SE_Dep3	2013-10-15	2013-11-24	40
5	ADCP02_NW_Dep4	FAILED	FAILED	N/A
5	ADCP02_SE_Dep4	2014-04-09	2014-06-06	58
6	ADCP03_SE_Dep1	2014-06-20	2014-08-05	46
6	ADCP01_NW_Dep5	2014-06-22	2014-08-02	41
6	ADCP02_NW_Dep5	2014-07-07	2014-08-16	40
7	ADCPTD7_01_Dep1	2014-09-17	2014-12-11	85
7	ADCPTD7_02_Dep1	2014-09-17	2014-11-27	71

Table 4.1: ADCP Turbine-Proximal Deployments

Frame Type	Description	Approx. Dimensions (m)	Main Materials	Approx. Mass (Dry) (kg)	Approx. Mass (Wet) (kg)
Type A	S/S welded frame with S/S sheet panelling Lead weights attached to bottom frame section. Single lifting point.	1.5x1.0x1.5	Stainless Steel Lead	300	260
Type B	Concrete-filled S/S sheeted shell Single lifting point Patented ROV docking feature 3 reinforced feet	1.8x1.3x0.7x1.3	Concrete Stainless Steel	2200	1400
Type C	Concrete (from UoE mould) S/S reinforcing elements Single lifting point 3 feet	1.8x1.3x0.8	Concrete Stainless Steel	3000	2000

Table 4.2: ADCP frame Types A to C. Dimensions and construction type.

of a remotely operated underwater vehicle (ROV). UoE designed Type-C featured deliberately enlarged equipment bays to allow modification after initial use. This feature proved useful following the requirement to install enhanced-duration battery packs.

1. Both Alstom's Type B and UoE's Type C gravity moorings performed well in close proximity to the turbine and foundation. The level position that the Type C's assume upon lifting and deployment and retrieval was noted as beneficial by vessel operators.
2. Their increased volume provides space for upgrades and auxiliary equipment.
3. UoE are investigating new designs of gravity mooring based on these experiences.

Deployment Methods

Background: Instrumentation housed in Type A frames were deployed at positions D1,D2,GN and GS (see Figure 3.4a). Due to being relatively low in weight these frames were deployed with small vessels (see Figure 4.3). Due to being sufficiently remote from other seabed assets within EMEC's site polymer side-lines were laid out either side of the gravity frame to approximately 100m which were terminated and held down with clump weights. Attached to one end of these side-lines was a

(a) Type A ADP frame.

(b) RDI ADCP in Type B ADP frame being deployed

(c) Type B ADP frame.

(d) Type C ADP frame.

Figure 4.6: Multiple instrumentation frames used during ReDAPT

buoy marker which would breach the surface around slack-tide and enable retrieval. The presence of the side-lines both removes the buoy marker from the acoustic path of the profiling instrument and provides a contingency method for retrieval whereby the frame's side-lines can be grappled with the vessel conducting a series of transects perpendicular to the path of the laid out lines. On each occasion the frames were retrieved with no requirement for the contingency method. An additional benefit of this method is in the simplicity of lowering equipment required i.e., there is no need for a hydraulically or acoustically operated release: the deployment is conducted on a single loop of rope that is pulled through and back up upon deployment.

Type B and C frames, due to their larger weight, required more powerful vessel-mounted hydraulically powered lifting equipment (often referred to as HIABs) in order to manoeuvre the frames into position on the vessels and for lifting over the side. Figure 4.6b shows a typical deployment including ROV assisted location on the SEABED. The presence of an ROV provides confirmation of the seabed positioning of the deployed frame, allowing the frames to be repositioned in the frequently occurring event of having been deployed on boulders or loose slabs of rock. Additionally, ROV assisted deployments have access to the ROV on-board sensor systems which feature acoustic positioning (relative to the vessel which is base-lined via GPS), depth gauges and heading sensors.

An alternative (hybrid) method of deployment was also successfully carried out whereby a sub-sea remotely operated camera was simultaneously lowered with the frame and used to enable fine-tuning

of the deployment location and obstacle avoidance. In this case and in the absence of an ROV a hydraulically operated latch was used.

1. Large heavy frames are good for having confidence that equipment won't move, are robust and can be readily modified. However, they can reduce the number of vessels that can be used to deploy and retrieve them due to their mass and bulk.
2. Lighter stainless steel frames featuring side-positioned buoys functioned well for far-field data gathering.
3. ROVs provide excellent functionality at the cost of introducing expense and additional lines to the operation.
4. A hybrid solution worked well during a deployment trial.

Multiple vessels were used to deploy and recover ADCPs over the course of the ReDAPT project as shown in table 4.3.

Vessel Operator	Vessel Name	Vessel Description	ADCP Frame-Type Deployed/Recovered
Leask Marine Ltd.	MV Uskmoor	16m Workboat Class 2	Type A
Leask Marine Ltd.	MV Challenge	14.4m Workboat Class 3	Type A
Leask Marine Ltd.	MV C-Odyssey	26m Workboat Class 1	Type B / C
Keynvor MorLift Ltd.	Severn Sea	30m Workboat Class 1	Type B / C

Table 4.3: Vessels used in ADCP deployments and recoveries

Instrumentation Configuration

Background: The Teledyne RDI Workhorse Sentinel 600kHz Acoustic Doppler Current Profiler (ADCP) was selected to provide seabed acquired velocity profiles. This instrument has been used successfully worldwide and at the EMEC site over many years.

Issue: Whilst the electronics and software of the instrument are tried-and-tested and robust this leads to a disadvantage: restrictive memory due to the file allocation table (FAT) system in use leads to a limited data storage capacity of 4GB through the use of two 2GB PCMCIA SATA memory cards. This in turn limits the sampling frequency of the instrument in order to provide a sufficiently long deployment duration which is required to a) coordinate with other deployed assets b) measure sufficient data for long term flow prediction e.g., via harmonic analysis. In terms of coordinating with other deployments given that opportunities to deploy occur generally every 14 days (in summer) and during this period slack water typically lasts between 30 minutes and 1 hour (at the Fall of Warness) a failed deployment of either another ADCP unit or, more importantly, a tidal turbine could lead to an instrument deployment producing data that doesn't meet the test requirements. Activating a write-over-data-once-full feature brings similar problems since the retrieval schedule is inherently uncertain due to tides, performance of axillary equipment, boat availability and of course site weather conditions.

A trade-off between sampling frequency, power consumption and deployment duration was required. This had to be optimised depending on each turbine deployment taking into account multiple factors e.g., the stage of turbine commissioning, critical test schedules, season and weather windows. Our designed modification to allow retrofitted Workhorse Sentinels to collect data beyond their internal 4Gb limit was not completed due to time pressures in the lead up to the last two deployments.

1. Low instrument sample rates (0.5Hz) were necessary in order to ensure operational longevity and the availability of data overlapping with turbine operational states. This configuration enabled an 85 day deployment and was satisfactory for mean flow velocity analysis.
2. Slow sample rates prevent off-the-shelf operation of the RDI software for waves analysis.
3. Modifications should be implemented to overcome the 4Gb data limit to allow continuous 2Hz sampling.

Wave/Current Mixed Duty Cycle

Background: A specific goal of the ReDAPT project involved the validation of cutting edge CFD which was conducted by EDF and the University of Manchester. Ambient flow conditions were measured and provided to the CFD modellers. The loads from the modelled turbine subjected to these characterised flows were compared to the actual loads as measured by the 1MW machine.

Issue: As anticipated it proved challenging to build up a large volume of measurement points where the 1MW tidal turbine was operating within an environmental system state sufficiently similar to that modelled. For this reason it was decided at preliminary stages of the project to not operate the ADCPs in a split Wave/Current mode whereby the instruments would measure waves for 17-20 minutes then switch back to current mode (reducing raw high frequency flow data duty cycle to as low as 0.66).

Whilst it was appropriate in summer months lack of direct and in-situ wave measurements makes more difficult (and time consuming) the advanced analysis of highly wave affected flows.

1. The decision to prioritise waves and currents within instrument sets that cannot operate in dual-mode should have been reviewed at each deployment.
2. A separate seabed-mounted ADCP waves monitoring TRN should have been implemented. This could have been deployed away from the turbine thus allowing flexible (less expensive) deployments and retrievals.

Custom Peripherals

Background: Following recovery of an early ADCP deployment and analysis of the data very high rates of instrument pitching and rolling were observed. At low velocity data was usable but at speeds relevant to power production (e.g., U_{ref} >1ms^{-1} the data was dominated by noise.

Issue: As ROV/camera confirmation of the resting location was not carried out at this time it is believed that the cause was one or a combination of too light ballasting of the ADCP unit, overly compliant gimbal set or frame coming to rest on even ground.

Custom components were designed, tested and integrated into existing and new ADCP gravity frames following this deployment:

- High stability polymer gimbals (with variable damping levels)
- Use of ROV or moveable camera systems upon deployment to check for uneven placement
- Ballasting of the ADCP units was increased to the maximum permissible in the working depth of the Type C frame.

1. Following changes to the deployment methodologies listed above this problem did not re-occur.

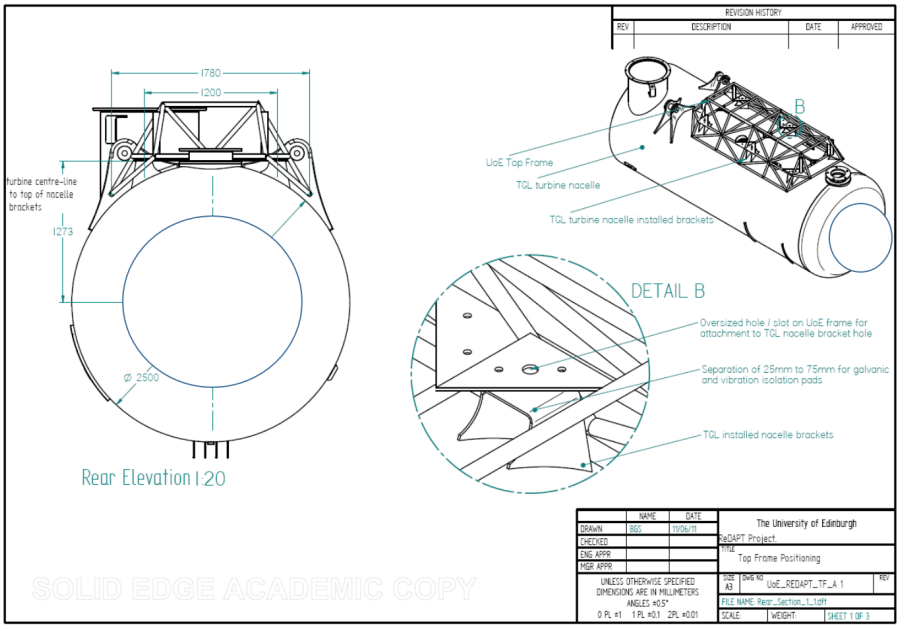

(a) Top Frame positioning and attachment method on 1MW turbine (some turbine features have been masked)

Bibliography

[1] TeraWatt project consortium, "Large scale interactive coupled 3d modelling for wave and tidal energy resource and environmental impact,ep/j010170/1," TeraWatt project consortium, Tech. Rep., 2014.

[2] V. Venugopal and N. Reddy, "Marine energy resource assessment for orkney and pentland waters with a coupled wave and tidal flow," in *Proc. 7th European Wave and Tidal Energy Conference (Oporto).*, 2014.

[3] S. Pope, *Tubulent Flows*, 1st ed. Cambridge University Press,, 2000.

[4] B. Sellar, S. Harding, and M. Richmond, "High-resolution velocimetry in energetic tidal currents using a convergent-beam acoustic doppler profiler," *Measurement Science and Technology*, vol. 26, no. 8, p. 085801, 2015. [Online]. Available: http://stacks.iop.org/0957-0233/26/i=8/a=085801

[5] RDI, *Acoustic doppler current profilers principles of operation: A practical primer*, 1989.

[6] J.-B. Richard, J. Thomson, B. Polagye, and J. Bard, "Method for identification of Doppler noise levels in turbulent flow measurements dedicated to tidal energy," *International Journal of Marine Energy*, vol. 3-4, pp. 52–64, Dec. 2013.

[7] I. Afgan, U. Ahmed, D. Apsley1, T. Stallard, and P. Stansby, "Cfd simulations of a full-scale tidal stream turbine: Comparison between large-eddy simulations and field measurements: ETI REDAPT MA1001 MD1.4," School of MACE, University of Manchester, Tech. Rep., 2014.

[8] I. Afgan, U. Ahmed, D. Apsley1, T. Stallard, and P. Stansby, "Cfd simulations of a full-scale tidal stream turbine: Comparison between large-eddy simulations and field measurements: ETI REDAPT MA1001 MD1.5," School of MACE, University of Manchester, Tech. Rep., 2014.

[9] K. Gunn and C. Stock-Williams, "Fall of Warness 3D model validation report: ETI REDAPT MA1001 PM14 MD5.2," E.ON New Build & Technology, Tech. Rep., 2012.

[10] K. Gunn and C. Stock-Williams, "On validating numerical hydrodynamic models of complex tidal flow," *International Journal of Marine Energy*, vol. 34, pp. 82 – 97, 2013. [Online]. Available: http://www.sciencedirect.com/science/article/pii/S2214166913000398

[11] S. Way and M. Thomson, "Site characterisation and design basis report ETI REDAPT MA1001 MD6.1," GL Garrad Hassan, Tech. Rep., 2011.

[12] S. Way and M. Thomson, "Site characterisation and design basis report ETI REDAPT MA1001 MD6.2," GL Garrad Hassan, Tech. Rep., 2011.

[13] S. Way and M. Thomson, "Site characterisation and design basis report ETI REDAPT MA1001 MD6.3," GL Garrad Hassan, Tech. Rep., 2011.

[14] B. Sellar, "An introduction to the redapt tidal project environmental data set," University of Edinburgh, Tech. Rep., 2016.

[15] T. H. E. Clark, "Turbulence in Marine Environments (TiME): A framework for understanding turbulence and its effects on tidal devices." *In review*, 2015.

[16] Andritz Hydro Hammerfest, "08.02.2012: Tidal Turbine getting ready to feed the grid," 2012. [Online]. Available: http://www.hammerfeststrom.com/news/08-02-2012-tidal-turbine-getting-ready-to-feed-the-grid/

[17] MCT, "Project Background — SeaGeneration." [Online]. Available: http://www.seageneration.co.uk/background.php

[18] T. Burton, N. Jenkins, D. Sharpe, and E. Bossanyi, *Wind Energy Handbook*. JOHN WILEY & SONS, LTD, 2011.

[19] H. Homann, J. Bec, and R. Grauer, "Effect of turbulent fluctuations on the drag and lift forces on a towed sphere and its boundary layer," *Journal of Fluid Mechanics*, vol. 721, pp. 155–179, 2013. [Online]. Available: http://journals.cambridge.org/abstract_S0022112013000669

[20] P. Evans, S. Armstrong, C. Wilson, I. Fairley, C. Wooldridge, and I. Masters, "Characterisation of a Highly Energetic Tidal Energy Site with Specific Reference to Hydrodynamics and Bathymetry," 2013.

[21] J. A. Knauss, *Indtroduction to Physical Oceanography*. Prentice-Hall, 1978.

[22] I. Fairley, P. Evans, C. Wooldridge, M. Willis, and I. Masters, "Evaluation of tidal stream resource in a potential array area via direct measurements," *Renewable Energy*, vol. 57, pp. 70–78, Sep. 2013.

[23] J. Anderson, *Fundamentals of Aerodynamics*, 5th ed. McGraw-Hill Education, 2010.

[24] J. G. Leishman, "Challenges in modelling the unsteady aerodynamics of wind turbines," *Wind Energy*, vol. 5, no. 2-3, pp. 85–132, Apr. 2002. [Online]. Available: http://doi.wiley.com/10.1002/we.62

[25] C. Garrett and P. Cummins, "The efficiency of a turbine in a tidal channel," *Journal of Fluid Mechanics*, vol. 588, pp. 243–251, 2007.

[26] T. Nishino and R. H. J. Willden, "The efficiency of an array of tidal turbines partially blocking a wide channel," *Journal of Fluid Mechanics*, vol. 708, pp. 596–606, 2012.

[27] R. Vennell, "Exceeding the Betz limit with tidal turbines," *Renewable Energy*, vol. 55, pp. 277–285, 2013. [Online]. Available: http://dx.doi.org/10.1016/j.renene.2012.12.016

[28] Y. Çengel and R. Turner, *Fundamentals of thermal-fluid sciences*, 2nd ed. McGraw-Hill, 2005.

[29] A. Kolmogorov, "A refinement of previous hypotheses concerning the local structure of turbulence in a viscous incompressible fluid at high Reynolds number," *J. Fluid Mech*, vol. 13, no. 01, pp. 82–85, 1962. [Online]. Available: http://journals.cambridge.org/production/action/cjoGetFulltext?fulltextid=368739

[30] T. Blackmore, W. Batten, M. Harrison, and A. Bahaj, "The Sensitivity of Actuator-Disc RANS Simulations to Turbulence Length Scale Assumptions," *European Wave and Tidal Energy Conference*, pp. 390–399, 2011.

[31] L. Kilcher, J. Thomson, and J. Colby, "Determining the spatial coherence of turbulence at MHK sites," in *2nd Marine Energy Technology Symposium*, Seattle, WA, 2014.

[32] G. Taylor, "Spectrum of turbulence," *Proceedings of the Royal Society of London. Series A, Mathematical and Physical Sciences*, vol. 164, no. 919, pp. 476–490, Febuary 1938.

[33] M. Topper, "Supergen marine: Guidance for numerical modelling in wave and tidal energy," University of Edinburgh, Tech. Rep., 2010.

[34] T. A. Adcock, S. Draper, and T. Nishino, "Tidal power generation a review of hydrodynamic modelling," *Proceedings of the Institution of Mechanical Engineers, Part A: Journal of Power and Energy*, 2015. [Online]. Available: http://pia.sagepub.com/content/early/2015/03/24/0957650915570349.abstract

[35] S. Gant and T. Stallard, "Modelling a tidal turbine in unsteady flow," in *Proc. 18th ISOPE (Vancouver).*, 2008.

[36] W. Rodi, *Turbulence Models and Their Applications in Hydraulics A state-of-the-art review*, 3rd ed. A.A. Balkema, 1993.

[37] F. Archambeau, N. M chitoua, and M. Sakiz, "Code_saturne A finite volume code for the computation of turbulent incompressible flows industrial applications." *Int. J. Finite*, pp. 1 – 62, 2003.

[38] N. J. (a), b. S. Benhamadouche, a. D. Laurence, and a. R. Prosser, "A synthetic-eddy-method for generating inflow conditions for large-eddy simulations." *International Journal of Heat and Fluid Flow*, vol. 27, no. Special Issue of The Fourth International Symposium on Turbulence and Shear Flow Phenomena - 2005, pp. 585 – 593, 2006.

[39] G. McCann, G. Rawlinson-Smith, and K. Argyriadis, "2006 load simulation for tidal turbines using wind turbine experience," in *ICOE*, 2006.

[40] H. Tennekes and J. L. Lumley, *A First Course in Turbulence*. the MIT press, 1972.

[41] A. Lohrmann, B. Hackett, and L. P. Rø ed, "High Resolution Measurements of Turbulence, Velocity and Stress Using a Pulse-to-Pulse Coherent Sonar," *Journal of Atmospheric and Oceanic Technology*, vol. 7, no. 1, pp. 19–37, 1990.

[42] Y. Lu and R. G. Lueck, "Using a Broadband ADCP in a Tidal Channel. Part I: Mean Flow and Shear," *Journal of Atmospheric and Oceanic Technology*, vol. 16, pp. 1556–1567, 1999.

[43] Y. Lu and R. Lueck, "Using a broadband ADCP in a tidal channel. Part II: Turbulence." *Journal of Atmospheric & Oceanic ...*, pp. 1568–1579, 1999.

[44] J. Thomson, B. Polagye, M. Richmond, and V. Durgesh, "Quantifying turbulence for tidal power applications," in *MTS/IEEE Seattle, OCEANS 2010*, no. 4, 2010. [Online]. Available: http://ieeexplore.ieee.org/xpls/abs_all.jsp?arnumber=5664600

[45] I. A. Milne, R. N. Sharma, R. G. J. Flay, and S. Bickerton, "Characteristics of the turbulence in the flow at a tidal stream power site Characteristics of the turbulence in the flow at a tidal stream power site," *The Royal Society A*, 2013.

[46] M. Togneri and I. Masters, "Comparison of marine turbulence characteristics for some potential turbine installation sites," in *4th International Conference on Ocean Energy*, 2012, pp. 6–11.

[47] C. Legrand, Black and Veatch, and Emec, *Assessment of Tidal Energy Resource*, 2009.

[48] J. Thomson, B. Polagye, V. Durgesh, and M. C. Richmond, "Measurements of Turbulence at Two Tidal Energy Sites in Puget Sound, WA," *IEEE Journal of Oceanic Engineering*, vol. 37, no. 3, pp. 363–374, 2012.

[49] O. Reynolds, "On the Dynamical Theory of Incompressible Viscous Fluids and the Determination of the Criterion," pp. 123–164, 1895.

[50] S. Thorpe, *The Turbulent Ocean*. Cambridge University Press, 2007.

[51] H. Grant, "The Large Eddies of Turbulent Motion," *J. Fluid Mech*, vol. 4, no. 02, pp. 149–190, 1958. [Online]. Available: http://journals.cambridge.org/production/action/cjoGetFulltext?fulltextid=367456

[52] E. Osalusi, J. Side, and R. Harris, "Structure of turbulent flow in EMEC's tidal energy test site," *International Communications in Heat and Mass Transfer*, vol. 36, no. 5, pp. 422–431, May 2009.

[53] P. O'Neill, D. Nicolaides, D. Honnery, and J. Soria, "Autocorrelation Functions and the Determination of Integral Length with Reference to Experimental and Numerical Data," in *15th Australasian Fluid Mechanics Conference*, vol. 1, no. December, 2004, pp. 1–4.

[54] M. T. Stacey, G. Monismith, and J. R. Burau, "of Reynolds stress profiles in unstratified," *JOURNAL OF GEOPHYSICAL RESEARCH*, vol. 104, pp. 933–949, 1999.

[55] W. Emery and R. Thomson, *Data analysis methods in physical oceanography*, 2nd ed., 2001.

[56] P. J. Wiles, T. P. Rippeth, J. H. Simpson, and P. J. Hendricks, "A novel technique for measuring the rate of turbulent dissipation in the marine environment," *Geophysical Research Letters*, vol. 33, no. 21, p. L21608, Nov. 2006. [Online]. Available: http://www.agu.org/pubs/crossref/2006/2006GL027050.shtml

[57] Rockland Scientific, "rocklandscientific.com," 2015. [Online]. Available: http://rocklandscientific.com/

[58] J. H. Simpson, J. a. M. Green, T. P. Rippeth, T. R. Osborn, and W. A. M. Nimmo-Smith, "The structure of dissipation in the western Irish Sea front," *Journal of Marine Systems*, vol. 77, no. 4, pp. 428–440, 2009.

[59] F. Wolk, R. G. Lueck, and L. S. Laurent, "Turbulence Measurements from a Glider Turbulence Package and Glider," in *13th Workshop on Physical Processes in Natural Waters, Palermo*, no. September, 2009, pp. 1–4.

[60] I. Fer and M. Bakhoday Paskyabi, "Autonomous ocean turbulence measurements using shear probes on a moored instrument," *Journal of Atmospheric and Oceanic Technology*, vol. 31, no. 2, pp. 474–490, 2014.

[61] "Conductivity, Salinity & Total Dissolved Solids - Environmental Measurement Systems," 2015. [Online]. Available: http://www.fondriest.com/environmental-measurements/parameters/water-quality/conductivity-salinity-tds/

[62] Valeport, *Model 803 Operating Manual*, 2001.

[63] B. Dargahi, "The turbulent flow field around a circular cylinder," *Experiments in Fluids*, vol. 8, no. 1-2, pp. 1–12, 1989.

[64] M. Detert, V. Weitbrecht, and G. H. Jirka, "Laboratory Measurements on Turbulent Pressure Fluctuations in and above Gravel Beds," *Journal of Hydraulic Engineering*, vol. 136, no. 10, pp. 779–789, 2010.

[65] L. Goddijn-Murphy, D. K. Woolf, and M. C. Easton, "Current Patterns in the Inner Sound (Pentland Firth) from Underway ADCP Data," *Journal of Atmospheric and Oceanic Technology*, vol. 30, no. 1, pp. 96–111, Jan. 2013.

[66] T. Rippeth, E. Williams, and J. Simpson, "Reynolds Stress and Turbulent Energy Production in a Tidal Channel," *Journal of Physical Oceanography*, vol. 32, pp. 1242–1251, 2002.

[67] E. A. Nystrom, C. R. Rehmann, and K. A. Oberg, "Evaluation of Mean Velocity and Turbulence Measurements with ADCPs," *Journal of Hydraulic Engineering*, vol. 133, no. 12, pp. 1310–1318, 2007.

[68] B. Gunawan and V. S. Neary, "ORNL ADCP Post-Processing Guide and MATLAB Algorithms for MHK Site Flow and Turbulence Analysis," Oak Ridge National Laboratory, Tech. Rep. September, 2011.

[69] Nortek-AS, "Aquadopp HR-Profiler," 2015. [Online]. Available: http://www.nortek-as.com/en/products/current-profilers/aquadopp-hr-profiler

[70] Nortek-AS, "Continental 3D Current Profiler Datasheet," 2015.

[71] Nortek-AS, "Vectrino Data Sheet," 2015.

[72] A. Lohrmann, R. Cabrera, and N. C. Kraus, "Acoustic-Doppler Velocimeter (ADV) for Laboratory Use," in *Fundamentals and Advancements in Hydraulic Measurements and Experimentation*, Buffalo, New York, 1994, pp. 351–365.

[73] G. Voulgaris and J. H. Trowbridge, "Evaluation of the Acoustic Doppler Velocimeter (ADV) for Turbulence Measurements," *Journal of Atmospheric and Oceanic Technology*, vol. 15, pp. 272–289, 1998.

[74] D. Hurther and U. Lemmin, "A Correction Method for Turbulence Measurements with a 3D Acoustic Doppler Velocity Profiler," *Journal of Atmospheric and Oceanic Technology*, vol. 18, pp. 446–458, 2001.

[75] C. M. García, M. I. Cantero, Y. Niño, and M. H. García, "Turbulence Measurements with Acoustic Doppler Velocimeters," *Journal of Hydraulic Engineering*, vol. 131, no. 12, pp. 1062–1073, 2005.

[76] H. Chanson, M. Threvethan, and C. Koch, "Discussion of "Turbulence Measurements with Acoustic Doppler Velocimeters" by Carlos M. García, Mariano I. Cantero, Yarko Niño, and Marcelo H. García," *Journal of Hydraulic Engineering*, vol. 133, no. 11, pp. 1283–1286, 2007.

[77] R. Cooke, "Design and Implementation of a 3-Axis Coherent Doppler Velocity Profiler," in *2nd International Conference & Exhibition on Underwater Acoustic Measurements: Technologies & Results*, 2007, pp. 1019–1026.

[78] H. D, T. P. D, B. M, L. U, and B. J. M, "A multi-frequency acoustic concentration and velocity profiler (ACVP) for boundary layer measurements of fine-scale flow and sediment transport processes." *Coastal Engineering*, vol. 58, pp. 594–605, 2011.

[79] J. Thomson, L. Kilcher, M. Richmond, J. Talbert, A. DeKlerk, B. Polagye, M. Guerra, and R. Cienfuegos, "Tidal turbulence spectra from a compliant mooring," in *1st Marine Energy Technology Symposium (METS)*, Washington, D.C., 2013.

[80] R. Craig, C. Loadman, B. Clement, P. Rusello, and E. Siegel, "Characterization and testing of a new bistatic profiling acoustic doppler velocimeter: The vectrino-ii," in *Current, Waves and Turbulence Measurements (CWTM), 2011 IEEE/OES 10th*, March 2011, pp. 246–252.

[81] Nortek AS, "Nortek coordinate transform, MATLAB script," 2016. [Online]. Available: http://www.nortek-as.com/lib/forum-attachments/coordinate-transformation/view

[82] . . RD Instruments, "ADCP Coordinate Transformation: Formulas and Calculations," RDI Instruments, Tech. Rep. July, 1998.

[83] *Acoustic Doppler Current Profiler Principles of Operation A Practical Primer*, 2nd ed., 1996.

[84] J. A. Boldt, "Use of numerical simulations to investigate the performance of a virtual acoustic Doppler current profiler in characterizing flow," Masters, University of Illinois, 2013.

[85] V. Durgesh, J. Thomson, M. C. Richmond, and B. L. Polagye, "Noise correction of turbulent spectra obtained from acoustic doppler velocimeters," *Flow Measurement and Instrumentation*, vol. 37, pp. 29–41, Jun. 2014.

[86] D. Ingram, "EQUIMAR, Equitable Testing and Evaluation of Marine Energy Extraction Devices in terms of Performance, Cost and Environmental Impact: D2.7 Protocols for wave and tidal resource assessment," The Equimar Consortium, Tech. Rep., 2011.

[87] Y. Goda, *Random Seas and Design of Maritime Structures*, 2nd ed., ser. Advanced series on Ocean Engineering, P. L. F. Liu, Ed. World Scientific, 2000, vol. 15.

[88] G. Smith, "Preliminary wave energy device performance protocol, annex ii report," International Energy Agency, Tech. Rep., 2007.

[89] H. N., "Analysis of the directional wave spectra from field data." in *Advances in Coastal and Ocean Engineering*, P.-F. Liu, Ed., vol. 3. World Scientific, Singapore, 1997, pp. 103–143.

[90] M. A. Davidson, D. A. Huntley, and P. A. D. Bird, "A practical method for the estimation of directional wave spectra in reflective wave fields," *Coastal Engineering*, vol. 33, no.

2-3, pp. 91 – 116, 1998. [Online]. Available: http://www.sciencedirect.com/science/article/B6VCX-3VNHBPD-2/2/34248cc06774bb4e4ba78b0f40fe7d60

[91] K. Kahma, D. Hauser, H. Krogstad, S. Lehner, J. Monbaliu, and L. Wyatt, "Measuring and analysing directional spectra of ocean waves - COST action 714, eur 21367," European Union, Tech. Rep., 2005.

[92] M. Longuet-Higgins, D. Cartwright, and N. Smith, "Observations of the directional spectrum of sea waves using the motions of a floating buoy." in *Ocean Wave Spectra*. Prentice-Hall, Englewood Cliffs, NJ, USA, 1963, p. 111136.

[93] G. G. Benoit M., "Comparative evaluation of directional wave analysis techniques applied to field measurements," in *Proceedings of the Ninth International Offshore and Polar Engineering Conference (ISOPE) Brest, France*, vol. III, 1999.

[94] T. Pedersen, J. Goldberg, A. Lohrmann, and E. Siegel, "Resolving transformed wave directions near coastalstructures," in *International Conference on Coastal Engineering (ICCE), 2006*, 2006.

[95] J. Cruz, E. Mackay, and T. Martins, "Advances in wave resource estimation measurements and data processing." in *Proc. 7th European Wave and Tidal Energy Conference (Oporto).*, 2007.

[96] M. D. Earle, K. E. Steele, and D. W. C. Wang, "Use of advanced directional wave spectra analysis methods," *Ocean Engineering*, vol. 26, no. 12, pp. 1421 – 1434, 1999.

[97] P. Brodtkorb, P. Johannesson, G. Lindgren, I. Rychlik, J. Rydén, and E. Sjö, "WAFO - a Matlab toolbox for the analysis of random waves and loads," in *Proc. 10'th Int. Offshore and Polar Eng. Conf., ISOPE, Seattle, USA*, vol. 3, 2000, pp. 343–350.

[98] D. Johnson, "Directional wave spectra toolbox (diwasp) user manual," MetOcean Solutions Ltd., Tech. Rep., 2010.

[99] P. Nielsen, "Analysis of natural waves by local approximations," *Journal of Waterway, Port, Coastal, and Ocean Engineering*, vol. 115, no. 3, pp. 384–396, 1989.

[100] T. B. Johannessen and C. Swan, "On the nonlinear dynamics of wave groups produced by the focusing of surfacewater waves," vol. 459, no. 2032, pp. 1021–1052, 2003.

[101] C.-C. Teng, T. Mettlach, J. Chaffin, R. Bass, C. Bond, C. Carpenter, R. Dinoso, M. Hellenschmidt, and L. Bernard, "National data buoy center 1.8-meter discus buoy, directional wave system," 29 2007-oct. 4 2007, pp. 1 –9.

[102] J. Eshbaugh and S. Frasier, "Measurement of sea surface displacement with interferometric radar," *J. Atmos. Ocean. Technol. (USA)*, vol. 19, no. 7, pp. 1087 – 95, July 2002.

[103] K. Hessner, K. Reichert, J. Dittmer, and J. C. N. Borge, "Ocean wave measurements by x-band radar - from spectral wave parameters to single wave detection," OceanWaveS GmbH, Tech. Rep., 2003.

[104] Ocean Waves GMBH, "Wamos II data comparison and error statistics," 2007. [Online]. Available: http://www.oceanwaves.org/download/PDF/E_STAT2007.pdf

[105] K. Reichert, K. Hessner, I. Trankmann, and B. Lund, "X-band radar as a tool to determine spectral and single wave properties," OceanWaveS GmbH, Luneburg, Germany, Tech. Rep., 2004.

[106] "An overview of work by lews castle college (LCC)," 2015. [Online]. Available: http://www.nortek-as.com/lib/user-seminars/donald-armstrong-uhi

[107] K. Rorbaek and H. Andersen, "Evaluation of wave measurements with an acoustic doppler current profiler," *OCEANS 2000 MTS/IEEE Conference and Exhibition. Conference Proceedings*, vol. vol.2, pp. 1181 – 1187, 2000.

[108] C. Boake, Nortek User Symposium, France, 2008.

[109] T. RDI, ADCP Deployment Planning Software, 2011.

[110] SonTek, Tech. Rep.

[111] Nortek AS, "Datasheet: Awac / real time systems."

[112] W. A. Birkemeier and E. B. Thornton, "The DUCK94 Nearshore Field Experiment," in *Proceedings of the Conference on Coastal Dynamics '94*, 1994, pp. 815–821.

[113] C.-H. Tsai, M.-C. Huang, F.-J. Young, Y.-C. Lin, and H.-W. Li, "On the recovery of surface wave by pressure transfer function," *Ocean Engineering*, vol. 32, no. 10, pp. 1247 – 1259, 2005.

[114] L. Wyatt, J. Green, and A. Middleditch, "Wave, current and wind monitoring using hf radar," june 2005, pp. 53 – 57.

[115] L. R. Wyatt, J. J. Green, A. Middleditch, M. D. Moorhead, J. Howarth, M. Holt, and S. Keogh, "Operational wave, current, and wind measurements with the pisces hf radar," *Oceanic Engineering, IEEE Journal of*, vol. 31, no. 4, pp. 819 –834, oct. 2006.

[116] M. Belmont, J. Horwood, R. Thurley, and J. Baker, "Shallow angle wave profiling lidar," *J. Atmos. Oceanic Technol.*, vol. 24, pp. 1150 – 1156, 2007.

[117] R. van Unen, A. van Beuzekom, G. Forristall, J. Mathisen, and J. Starke, "Wacsis-wave crest sensor intercomparison study at the meetpost noordwijk measurement platform," in *OCEANS '98 Conference Proceedings*, vol. 3, sep-1 oct 1998, pp. 1757 –1761 vol.3.

[118] S. F. Barstow, H. E. Krogstad, L. Lonseth, J. P. Mathisen, G. Mork, and P. Schjolberg, "Intercomparison of sea-state and zero-crossing parameters from the wacsis field experiment and interpretation using video evidence," *Journal of Offshore Mechanics and Arctic Engineering*, vol. 126, no. 1, pp. 35–42, 2004. [Online]. Available: http://link.aip.org/link/?JOM/126/35/1

[119] RDI, "ADCP Coordinate Transformation," 2010.

[120] F. Mosteller and J. Tukey, *Data Analysis and Regression: A Second Course in Statistics*, ser. Addison-Wesley series in behavioral science. Addison-Wesley Publishing Company, 1977. [Online]. Available: https://books.google.co.uk/books?id=pGlHAAAAMAAJ

[121] C. Leys, C. Ley, O. Klein, P. Bernard, and L. Licata, "Detecting outliers: Do not use standard deviation around the mean, use absolute deviation around the median," *Journal of Experimental Social Psychology*, vol. 49, no. 4, pp. 764 – 766, 2013. [Online]. Available: http://www.sciencedirect.com/science/article/pii/S0022103113000668

[122] E. A. Nystrom, K. A. Oberg, and C. R. Rehmann, ""measurement of turbulence with acoustic doppler current profilers sources of error and laboratory results," in *Proc., Hydraulic Measurements & Experimental Methods*, Reston, VA, 2002.

[123] D. Sutherland, "Assessment of mid-depth arrays of single beam acoustic doppler velocity sensors to characterise tidal energy sites: In review," Ph.D. dissertation, The University of Edinburgh, 2015.

[124] V. Durgesh, J. Thomson, M. C. Richmond, and B. L. Polagye, "Noise correction of turbulent spectra obtained from acoustic doppler velocimeters," *Flow Measurement and Instrumentation*, vol. 37, pp. 29–41, 2014. [Online]. Available: http://dx.doi.org/10.1016/j.flowmeasinst.2014.03.001

[125] Nortek AS, "Comprehensive Manual," Nortek, Tech. Rep., 2013.

[126] *Nortek AS, (2005): AWAC Acoustic Wave And Current Meter User Guide. Document. No: n3000-126. First Edition.*

[127] H. Lamb, "'hydrodynamics'," *'Cambridge, England: Cambridge University Press, 6th ed.*, 1932.

[128] J. Thomson, B. Polagye, M. Richmond, and V. Durgesh, "Quantifying turbulence for tidal power applications," in *OCEANS 2010*, 2010, pp. 1–8.

[129] M. Richmond, S. Harding, and P. Romero-Gomez, "Numerical performance analysis of acoustic doppler velocity profilers in the wake of an axial-flow marine hydrokinetic turbine," *International Journal of Marine Energy*, vol. 11, pp. 50 – 70, 2015. [Online]. Available: http://www.sciencedirect.com/science/article/pii/S2214166915000211

[130] R. K. R. Yarlagadda, *Analog and Digital Signals and Systems*. Boston, MA: Springer US, 2010.